UNIVERSITY OF SOUTHAMPTON

FACULTY OF NATURAL AND ENVIRONMENTAL SCIENCES

Department of chemistry

Cyclic peptide inhibitors of the eukaryotic translation initiation factor 4E and 4G interaction

Volume 1 of 1

Alex Hoose

Doctorate of Philosophy

April 2016

ABSTRACT
FACULTY OF NATURAL AND ENVIRONMENTAL SCIENCES

Department of chemistry

Doctorate of Philosophy

CYCLIC PEPTIDE INHIBITORS OF THE EUKARYOTIC TRANSLATION INITIATION FACTOR 4E AND 4G INTERACTION

Alex Hoose

1 Abstract

Cancerous tumors require a range of oncogenic proteins to promote cellular proliferation and inhibit apoptotic signals. The effective cap-dependent translation of oncogenic mRNA displays an absolute requirement for certain eukaryotic translation initiation factors (eIF). In particular the interaction of eukaryotic translation initiation factor 4E (eIF4E) with eukaryotic initiation factor 4G (eIF4G) is absolutely required to maintain the malignant phenotype. By contrast the eIF4E / eIF4G interaction is not required for the cap-independent translation of mRNAs that encode homeostatic proteins within healthy cells. As such, the inhibition of cap-dependent translation via disruption of the eIF4E / eIF4G interaction has become an attractive strategy towards the development of novel cancer drugs.

A reverse two-hybrid system was constructed with binding fragments of eIF4E and eIF4G within *Escherichia coli*, in order to mimic the oncogenic PPI found within malignant tissue. Split intein circularization of peptides and protein technology was then utilized to screen a library of DNA encoded cyclic peptides against the eIF4E / eIF4G interaction. Screening isolated four potential cyclic peptide inhibitors of the oncogenic protein-protein interaction that disrupted the eIF4E / eIF4G interaction in *Escherichia coli*. Putative cyclic peptide inhibitors of the eIF4E / eIF4G interaction were subsequently synthesized by 9-fluorenylmethoxycarbonyl solid phase peptide synthesis in preparation for testing against immortalized cancerous cell lines.

A series of assays were devised to determine the effect of compound treatment on translation. Screening of cyclic peptides by MTT cell viability assay determined that two putative inhibitors of the eIF4E / eIF4G interaction elicited a dose-dependent response in MCF7 cells. Further testing of cyclic peptides by a luciferase reporter assay suggested that cyclic peptide treatment had little effect on cap-dependent or cap-independent translation in HeLa cells. This finding was confirmed by ^{35}S labelled methioinine/ cysteine incorporation, which suggested that cyclic peptide treatment had little effect on global translation rates in HeLa cells. m^7 GTP pull-down experiments subsequently revealed that cyclic peptides did not disrupt the eIF4E / eIF4G interaction within HeLa cells or within HeLa cell lysate. It is therefore probable that SICLOPPS screening failed to isolate cyclic peptide inhibitors of this oncogenic PPI.

2 Contents

3 List of Tables

4 List of Figures

5 Declaration of Authorship

I, Alex Hoose declare that this thesis and the work presented in it are my own and has been generated by me as the result of my own original research.

Cyclic peptide inhibitors of eukaryotic translation initiation factor 4E and 4G interaction

I confirm that:

1. This work was done wholly or mainly while in candidature for a research degree at this University;
2. Where any part of this thesis has previously been submitted for a degree or any other qualification at this University or any other institution, this has been clearly stated;
3. Where I have consulted the published work of others, this is always clearly attributed;
4. Where I have quoted from the work of others, the source is always given. With the exception of such quotations, this thesis is entirely my own work;
5. I have acknowledged all main sources of help;
6. Where the thesis is based on work done by myself jointly with others, I have made clear exactly what was done by others and what I have contributed myself;
7. None of this work has been published before submission.

Signed: .....

Date: April 2016

6 Acknowledgements

As a chemist prior to the commencement of this degree, I had never considered that by the end of the program I could diversify towards in vitro cell biology. As such I am extremely grateful to Dr. Daniel Asby, Dr. Hannah Pendergraff and Ishna Mistry for tutoring and assistance with tissue culture. The testing of potential inhibitors of the Eukaryotic Translation Initiation Factor 4E (eIF4E) and 4G (eIF4G) interaction would have simply been impossible without your help. I would also like to thank Eliot Osher, Dr. Daniel Asby, Dr. Hannah Pendergraff and Dr. Mark Coldwell who helped to proof read this thesis and provided advice on structure and content.

I would like to thank Dr. Mark Willet, Dr. Joanne Cowan and Dr. Mark Coldwell for assistance and advice with regards to luciferase assays, pull-down experiments and ^{35}S methionine incorporation studies. Your invaluable assistance enabled the rapid validation of inhibitors of the eIF4E / eIF4G interaction and the completion of the project could not have happened without you. In addition I would like to thank the Coldwell group for their advice, assistance and guidance during my transition from chemistry to cell biology.

The diversification from my undergraduate chemistry background to the biochemist that I am today has been a significant challenge and one that I would not have thought possible without the support of my family. Their emotional support has been invaluable to the successful completion of the project.

I would like to thank my supervisor for his advice on my project, in addition to his proof reading of my thesis. I would also like to thank all the members of the Tavassoli group for their advice and guidance throughout the program.

I would like to express my gratitude to Dr. Mike Waring and Astrazeneca for advice and funding of laboratory consumables. I would also like to express my thanks to the EPSRC for providing funding to enable this research.

7 Abbreviations

- $\Delta G_{binding}$: Gibbs free energy of binding
- ^{1}H 1D: One-dimensional proton spectroscopy
- ^{1}H COSY: Two-dimensional proton correlation spectroscopy
- ^{1}H TOCSY: Two-dimensional proton total correlation spectroscopy
- 3-AT: 3-Amino-1, 2, 4-triazole
- 3' UTR: 3' untranslated region
- 434: DNA binding domain of the bacteriophage 434 repressor protein
- *434 / P22:* Chimeric DNA operator with 434 / 'P22' specificity
- 43S PIC: 43S pre-initiation complex
- 48S PIC: 48S pre-initiation complex
- 4EBP: eIF4E binding protein
- 4E-SE: eIF4E sensitivity element
- 4E-T: eIF4E nuclear transporter protein
- 5' UTR: 5' untranslated region
- A: Adenosine
- 'A': Acceptor site of 80S ribosome
- AA: Amino acid
- AMP: Adenosine monophosphate
- AMPK: Adenosine monophosphate activated protein kinase
- AmpR: Ampicillin resistance gene
- Apaf-1: Apoptotic protease activating factor 1
- APS: Ammonium persulfate
- AraBAD: Arabinose promoter
- AraC: Protein repressor of the arabinose operon
- Arg: Arginine
- Asp: Aspartic acid
- ATP: Adenosine triphosphate
- AttB: Bacterial attachment site
- AttP: Phage attachment site
- BME: β-mercaptoethanol
- bp: Base pair

- BSA: Bovine serum albumin
- C: Cytosine
- CAT: Chloramphenicol acetyl transferase
- CBD: Chitin binding domain
- CIEEL: Chemically induced electron exchange luminescence
- c-Myc: Myelocytomatosis oncogenic transcription factor
- CP: Cyclic peptide
- CRIM: Conditional replication, integration and modular
- CtBP: C-terminal binding protein
- CTD: C-terminal domain
- Cys: Cysteine
- Da: Dalton
- DCM: Dichloromethane
- DIC: *N*,*N*'-Diisopropylcarbodiimide
- DIPEA: *N*,*N*-Diisopropylethylamine
- Dmab: 4-(*N*-(1-(4,4-dimethyl-2,6-dioxocyclohexylidene)-3-methylbutyl)-amino) benzyl ester
- DMEM: Dulbecco's modified eagle medium
- DMF: *N*,*N*-Dimethylformamide
- DMSO: Dimethyl sulfoxide
- DNA: Deoxyribonucleic acid
- dNTPs: 2'-Deoxynucleotide 5'-triphosphates
- DTT: Dithiothreitol
- 'E': Exit site of 80S ribosome
- *E. coli*: Escherichia coli bacterium
- EDC: *N*-(3-Dimethylaminopropyl)-*N*'-ethylcarbodiimide
- EDTA: Ethylenediaminetetraacetic acid
- eEF1: Eukaryotic translation elongation factor 1
- eEF2: Eukaryotic translation elongation factor 2
- EGFR: Extracellular growth factor receptor
- eIF: Eukaryotic translation initiation factor
- eIF1: Eukaryotic translation initiation factor 1

- eIF1A: Eukaryotic translation initiation factor 1A
- eIF2: Eukaryotic translation initiation factor 2
- eIF3: Eukaryotic translation initiation factor 3
- eIF4A: Eukaryotic translation initiation factor 4A
- eIF4E: Eukaryotic translation initiation factor 4E
- eIF4F: Eukaryotic translation initiation complex F
- eIF4G: Eukaryotic translation initiation factor 4G
- eIF5: Eukaryotic translation initiation factor 5
- eIF5B: Eukaryotic translation initiation factor 5B
- ELISA: Enzyme linked immunosorbent assay
- EMCV: Encephalomyocarditis virus
- eq.: Equivalents
- eRF1: Eukaryotic release factor 1
- eRF3: Eukaryotic release factor 3
- ESI+: Electrospray ionization, positive ion mode
- Et_2O: Diethyl ether
- FAG: Fragment of apoptotic cleavage of eIF4G
- FBS: Fetal bovine serum
- FGF: Basic fibroblast growth factor
- Fluc: Firefly luciferase from *Phontinus pyralis*
- Fmoc: 9-Fluorenylmethoxycarbonyl protecting group
- G: Guanosine
- GDP: Guanosine diphosphate
- Gln: Glutamine
- Glu: Glutamic acid
- GTP: Guanosine triphosphate
- h: Hours
- HF: High fidelity
- His: Histidine
- *His-3*: Imidazoleglycerol phosphate dehydratase gene
- HIV: Human immunodeficiency virus
- HOAt: 1-Hydroxy-7-azabenzotraizole

- HOBt: Hydroxybenzotriazole
- HRV: Human rhinovirus
- I_C: C-terminal intein
- I_N: N-terminal intein
- inc.: Inclusive
- inteins: Internal protein sequences
- IPA: Isopropyl alcohol
- IPTG: Isopropyl β-D-thiogalactopyranoside
- IR: Infrared spectroscopy
- IRES: Internal ribosomal entry site
- *Kan*: Neomycin phosphotransferase II gene
- kb: Kilobase
- kDa: Kilodalton
- LacI: Repressor protein of the lactose operon
- *LacZ*: β-galactosidase gene
- LB agar: Luria Bertani agar media
- LB broth: Luria Bertani broth
- LD_{50}: Median lethal dose
- Leu: Leucine
- Lys: Lysine
- m^7 GTP: 7-methyl guanosine triphosphate
- MAPK: Mitogen activated protein kinase
- MeCN: Acetonitrile
- MEK: Mitogen activated protein kinase kinase
- MeOH: Methanol
- Met: Methionine
- $^{Met}tRNA_i$: Initiator methionine transfer ribonucleic acid
- min: Minutes
- MnK: Mitogen activated protein kinase interacting kinase
- MOPS: 4-morpholinepropanesulfonic acid
- MPER: Mammalian protein extraction reagent
- mRNA: Messenger ribonucleic acid

- MS: Mass spectrometry
- mTOR: Mammalian target of rapamycin
- mTORC1: Mammalian target of rapamycin complex 1
- mTORC2: Mammalian target of rapamycin complex 2
- MTT: Thiazolyl blue tetrazolium bromide
- NEB: New England biolabs
- NMR: Nuclear magnetic resonance
- Npu: *Nostoc punctiforme*
- NTD: N-terminal domain
- OD: Optical density
- ODC: Ornithine decarboxylase
- ONPG: Ortho-nitrophenyl- β-galactoside
- 'P': Peptidyl site of 80S ribosome
- 'P22': Chimeric repressor protein based on the N-terminus of 434
- PABP: Poly adenosine binding protein
- PAGE: Polyacrylamide gel electrophoresis
- Pbf: 2, 2, 4, 6, 7-pentamethyldihydrobenzofuran-5-sulfonyl protecting group
- PBS: Phosphate buffered saline
- PCR: Polymerase chain reaction
- PDB ID: Protein data bank identifier
- PG1: Protecting group 1
- PG2: Protecting group 2
- Phe: Phenylalanine
- Pi: Inorganic phosphate
- PI3K: Phospho inositol 3-kinase
- PKB: Protein kinase B
- PLac: Promoter of the lactose operon
- PLB: Passive lysis buffer
- PPI: Protein-protein interaction
- Pro: Proline
- P/S Penicillin / Streptomycin
- PTac: Mutant promoter of the lactose / tryptophan operon

- PyBOP: (Benzotriazol-1yloxy)tripyrrolidinophosphonium hexafluorophosphate
- R: Purine (adenosine or guanosine)
- Raf: Proto-oncogene serine / threonine protein kinase
- Ras: Rat sarcoma kinase
- REN: Restriction endonuclease
- Rluc: Renilla luciferase from *Renilla reniformis*
- RNA: Ribonucleic acid
- RP-HPLC: Reverse phase high performance liquid chromatography
- rpm: Rotations per minute
- RT: Room temperature
- RTHS: Reverse two-hybrid system
- s: Seconds
- SDS: Sodium dodecyl sulfate
- Ser: Serine
- SICLOPPS: Split intein circular ligation of peptides and proteins
- SOC: Super optimal culture
- SPPS: Solid phase peptide synthesis
- Ssp: *Synechocystis sp. PCC6803*
- StBu: Tert-Butylthio protecting group
- TBST: Tris buffered saline tween
- tBu: Tert-butyl protecting group
- TC: Ternary complex
- TCA: Trichloroacetic acid
- TCEP: tris(2-carboxyethyl)phosphine hydrochloride
- TEMED: *N, N, N', N'*-Tetramethylethylenediamine
- TFA: Trifluoroacetic acid
- THS: Two-hybrid system
- TIS: Triisopropylsilane
- TNBS: Trinitrobenzene sulfonic acid
- Tris: Tris(hydroxymethyl)aminomethane
- tRNA: Transfer RNA
- Trp: Tryptophan

- Trt: Trityl protecting group
- TSAP: Thermostable alkaline phosphatase
- TSC: Tuberous sclerosis complex
- Tyr: Tyrosine
- Val: Valine
- VEGF: Vascular endothelial growth factor
- U: Uracil
- UV: Ultra violet
- UV-vis: Ultra violet visible spectroscopy

8 Project aims

The transformation of healthy cells into malignant tissue requires the overexpression of certain oncogenic proteins that promote angiogenesis, stimulate cell cycle progression and inhibit apoptosis. The translation of these oncogenic proteins within healthy cells can be repressed by the secondary structure present within the 5' untranslated region of the coding mRNA strand. Cancerous tumors may bypass this regulatory feature by displaying elevated levels of cap-dependent translation, which melts mRNA secondary structure and induces oncogenic protein expression.

Eukaryotic translation initiation factors are a vital determinant of the efficient translation of oncogenic mRNAs and hence represent a tempting therapeutic target. In particular the interaction of eukaryotic translation initiation factor 4E (eIF4E) with eukaryotic translation initiation factor 4G (eIF4G) is indispensible to the effective cap-dependent translation of oncogenic mRNAs. However the eIF4E / eIF4G interaction is not absolutely required for the effective cap-independent translation of housekeeping genes that are necessary for healthy cell survival. Therefore the targeted disruption of the eIF4E / eIF4G interaction represents a method to selectively inhibit cap-dependent translation of oncogenic proteins within malignant tissue, without toxic off target effects on healthy tissue.

This project therefore aimed to develop therapeutics that disrupt the eIF4E / eIF4G interaction, with concomitant inhibition of the translation of oncogenic mRNAs. A key milestone of the project was the construction of a 'two-hybrid' system in *Escherichia coli* to permit the *in vivo* interrogation of the eIF4E / eIF4G interaction. The construction of this bacterial model system would then allow the screening of DNA encoded cyclic peptide libraries for potential inhibitors of the eIF4E / eIF4G interaction. Putative inhibitors of the oncogenic protein-protein interaction would then be synthesized via solid phase peptide synthesis for *in cellulo* validation studies. A range of assays would then be performed to determine the effect of putative cyclic peptide inhibitors on the eIF4E / eIF4G interaction within the malignant environment.

9 Introduction

9.1 Drug discovery and protein-protein interactions

The drug development process has classically relied on the fragment based or high throughput screening of small molecule inhibitors that are complient with Lipinski's rule of five parameters. [1] [2] [3] The presence of deep surface pockets within enzymes and kinases, when combined with X-ray diffraction has enabled the rational design of substrate mimics via structure activity relationships and provided a convenient route to new therapeutic classes. Over recent years the pharmaceutical industry has exhausted the supply of readily druggable targets with defined small molecule binding clefts. The current scarcity of this 'low hanging fruit' has forced biochemists to re-consider strategies towards hit compound identification. As such the focus of therapeutic research has shifted towards macromoleculer biological therapeutics such as polypeptides and antibodies derived from phage display. [4]

The disruption of protein-protein interactions (PPIs) represents an appealing yet challenging approach towards therapeutic development. PPIs are typically large and flat interfaces with a typical surface area of 1600 (±400) $Å^2$, but with a defined minimum area of at least 600 $Å^2$. [5] [6] The disruption of the extensive network of intermolecular interactions between two protein binding partners represents a significant challenge to the development of small molecule inhibitors and is more suitable to the development of macromolcular inhibitors such as peptides and antibodies.

The identification of certain residues within PPIs that contribute a large percentage of the free energy of binding (>75 % of $\Delta G_{binding}$ in the case of the human growth hormone and its receptor), marked a significant advance towards therapeutic intervention at these interfaces. [7] Point mutations of certain residues with alanine revealed that these 'hot spots' contributed up to 4.5 kcal mol^{-1} of $\Delta G_{binding}$. [7] [8] A distinct amino acid bias was also observed among key binding residues at hot spots in PPIs. Tryptophan (21 %), arginine (13.3 %) and tyrosine (12.3 %) residues were all frequently observed as hot spot binding residues. [9] The hydrophobic steric bulk of tyrosine and tryptophan, combined with their ability to form hydrogen bonds and π-π stacking interactions may contribute to the exclusion of solvent and the formation of stabilized interactions between protein binding partners. It was also noted that phenylalanine occurs three

times less frequently at hot spots than tyrosine, which would seem to indicate the importance of directional hydrogen bonding to the stabilization of PPIs. Arginine is capable of forming multiple directional hydrogen bonds and ionic interactions and it is therefore not surprising that this residue is capable of contributing a significant percentage of $\Delta G_{binding}$ to a PPI. [9] The presence of the arginine side chain as a guanidinium salt at physiological pH presents an additional obstacle that must be overcome for the formation of a stable interface. The solvation of hot spot residues by water molecules generates an energetic de-solvation cost that must be paid prior to PPI formation. Analysis of the X-ray crystal structures of known PPIs revealed that hot spots are surrounded by bordering residues that contribute little to $\Delta G_{binding}$, but help to exclude the bulk solvent from hot spot residues. This 'O-ring motif' therefore shields hot spots from solvation by water and functions to reduce or eliminate the free energy cost of de-solvation, thereby stabilizing the protein dimer interface with respect to two free protein monomers in solution. [7 9] The combination of 'O-ring' and hot spot theory has permitted the development of small molecule PPI inhibitors that bind to hot spot residues within interfaces. [10 11] The ability of pre-organized macromolecular compounds such as constrained peptides to bind to extended flat interfaces has also made these therapeutic classes an appealing approach to the development of PPI inhibitors. [12]

Malignant tumors rely on the aberrant activation or deactivation of signaling cascades to stimulate angiogenesis, avoid apoptosis and stimulate proliferation. [13] Signalling pathways within mammalian cells rely on the integrity of PPIs to stimulate transcription and translation, enhancing proliferation and cell survival. [14 15] As such the targeting of PPIs with cyclic peptides has become a valuable strategy for the development of novel chemo-therapeutics. [16] This work is focused on the development of cyclic peptide inhibitors of a PPI involved in the assembly of the cap-dependent translation initiation complex, which is a vital pre-requisite for the survival and proliferation of malignant tissue. [17]

9.2 Eukaryotic translation

Eukaryotic messenger ribonucleic acids (mRNAs) are modified at both the 5' and 3' termini to facilitate nuclear export, enhance translation and increase resistance to intracellular exonucleases. The 5' end of eukaryotic mRNA is modified with a 7-methyl guanosine triphosphate (m^7 GTP) cap, whereas the 3' end of the mRNA is elongated by poly (A) polymerase. [18] [19] [20] Both the 5' cap and the 3' polyadenylated (poly A) tail of mRNA are vital recognition sites for proteins that facilitate polypeptide synthesis. Eukaryotic translation can be divided into three stages. Translational initiation requires a wide range of eukaryotic translation initiation factors (eIF) to localize the 40S ribosomal subunit to the mRNA strand and to recruit the 60S subunit to form the competent 80S ribosome. Translational elongation then extends the peptide chain from the amino (N) terminal residue, by adding amino acids sequentially to the carboxyl (C) terminus of the growing polypeptide strand until the final protein is assembled. The translational termination stage subsequently cleaves the polypeptide from the ribosomal complex and dissociates the translation apparatus for recycling.

9.2.1 Eukaryotic translation initiation

The initial step of translational initiation is the formation of the ternary complex (TC, **Figure 1:** A), consisting of eukaryotic translation initiation factor 2 (eIF2) with initiator methionine transfer ribonucleic acid ($^{Met}tRNA_i$) and guanosine triphosphate (GTP). [21] [22] [23] [24] [25] The TC then recruits a complex involving the 40S ribosomal subunit, eukaryotic translation initiation factor 3 (eIF3), eukaryotic translation initiation factor 1 (eIF1) and eukaryotic translation initiation factor 1A (eIF1A) to form the 43S pre-initiation complex (43S PIC, **Figure 1:** B). [26] [27] [28] [29] [30] [31] [32] At this point, cytoplasmic recruitment of the 43S PIC to the 5' untranslated region (5' UTR) of the mRNA strand proceeds via one of two distinct mechanisms. eIF3 can interact with the cap-dependent translation complex termed eukaryotic translation initiation complex 4F (eIF4F), to form the 48S pre-initiation complex (48S PIC, **Figure 1:** C). Alternatively the 43S PIC may be directly recruited in a cap-independent manner, to an internal ribosomal entry site (IRES) within the mRNA 5' UTR. [33] [34]

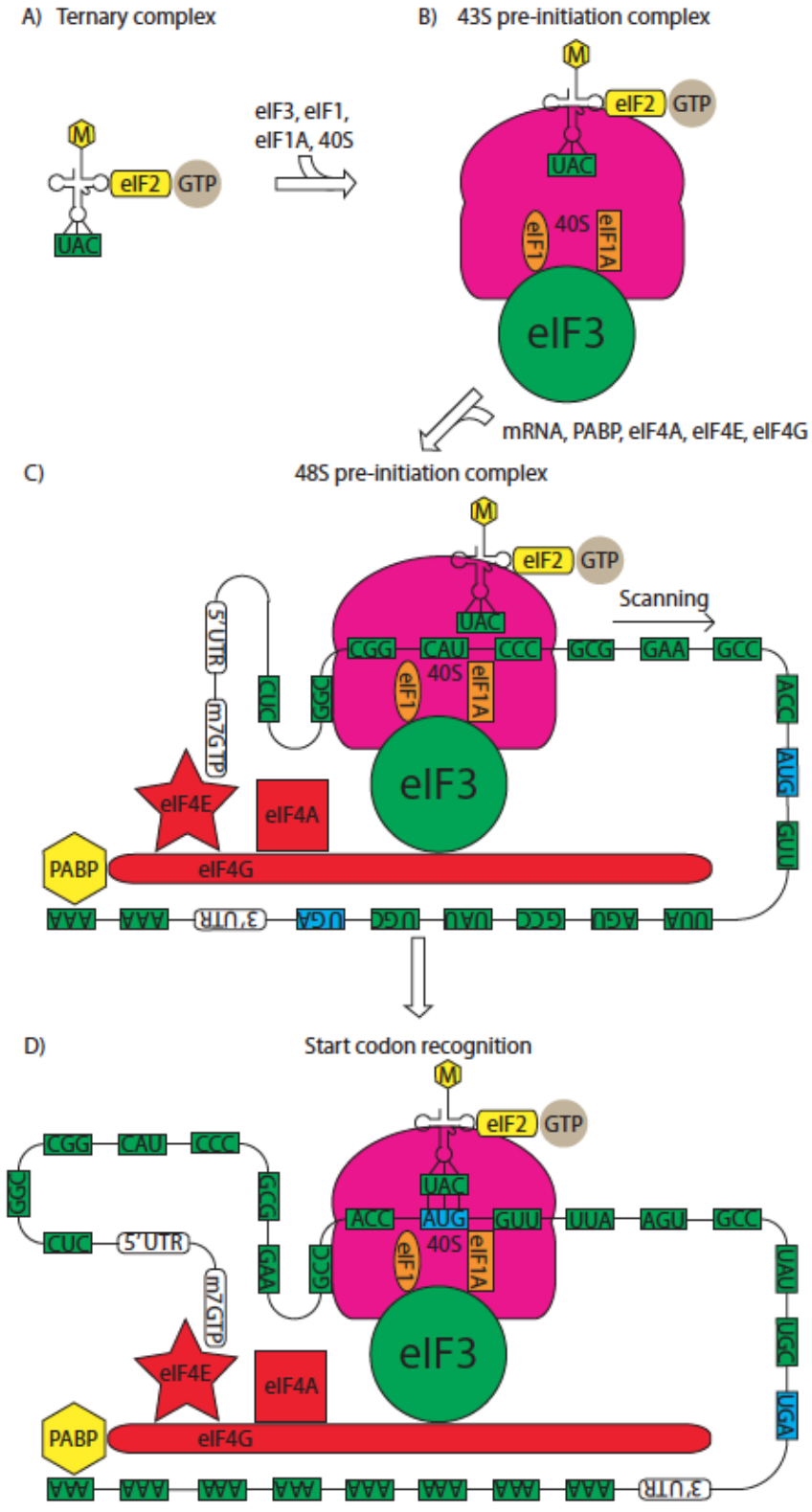

Figure 1: Schematic of start codon recognition during eukaryotic translation initiation. Poly adenosine binding protein (PABP) circularizes the mRNA strand by binding to the 3' poly A tail. PABP in concert with eIF4A, eIF4E and eIF4G constitute the cap dependent translation complex eIF4F (highlighted in red). [35]

Once the 40S ribosomal subunit has bound to the 5' end of mRNA, the AUG start codon is located via eIF1 and eIF1A-dependent scanning of the 40S ribosomal subunit in a 5' to 3' direction along the mRNA strand (**Figure 1:** C and D). Scanning of the 40S ribosomal subunit is assisted by eIF4F mediated melting of secondary structure in the mRNA 5' UTR. [29 36 37 38 39]

The primary and secondary structure of the 5' UTR prior to the AUG start codon also play a pivotal role in the regulation of translation. [40 41] For example, vital homeostatic proteins are required at all times and hence are encoded by efficiently translated (termed 'strong') mRNAs. Such mRNAs have short unstructured 5' UTRs, ensuring rapid scanning and selection of the start codon by the 40S ribosomal subunit, resulting in constitutive protein expression. [42 43] By contrast, a subset of transcription and translation factors, along with growth factors and angiogenic proteins are only required during cell proliferation. The expression of such genes is tightly regulated at the translational level via the Guanosine (G) and Cytosine (C) enriched highly structured 5' UTRs of their poorly translated (termed 'weak') mRNAs. [42 43] The presence of G and C base-pairing, stabilizes hairpin structures in the 5' UTR of weak mRNAs and inhibits the scanning mechanism of the 40S ribosomal subunit, which is used to locate the start codon. [44] Rapid expression of proliferative genes from weak mRNAs therefore requires melting of the stem loop structures of the 5' UTR. This is achieved via the recruitment of the cap-dependent translation initiation complex, eukaryotic translation initiation factor 4F (eIF4F, **Figure 1:** C). Effective translation of oncogenes encoded by weak mRNAs displays an absolute requirement for eIF4F mediated melting of 5' UTR hairpin structures. [45 46 47 48] eIF4F mediates melting of 5' UTR structure ahead of (3' to) the 40S ribosomal subunit and therefore facilitates scanning of the 40S ribosomal subunit in a 5' to 3' direction to locate the start codon. This eIF4F reliant 'cap-dependent' mechanism of translation is responsible for the regulation of oncogenic protein expression.

The primary mRNA structure proximal to the AUG start codon also plays a pivotal role in the stabilization of the interaction between the mRNA strand and the 40S ribosomal subunit. An examination of eukaryotic mRNAs revealed that there is a consensus sequence around the start codon corresponding to $G^{-6}C^{-5}C^{-4}R^{-3}C^{-2}C^{-1}A^{+1}U^{+2}G^{+3}G^{+4}$ (Adenosine (A), Uracil (U), Purine (R) is A or G). This mRNA sequence is known as the Kozak sequence (**Figure 1:** D) and is optimal for driving efficient start codon

recognition and subsequent 80S ribosome formation. [42] [49] Subsequent studies have revealed that the AUG start codon in addition to the purine at position -3 and the guanosine at position +4, are highly conserved and are required to efficiently recruit the 40S ribosomal subunit. [50] [51] [52] The cytosines (-5, -4, -2 and -1) of the Kozak sequence are not universally conserved, but do increase the stability of the start codon complex with the 40S ribosomal subunit. [51]

Start codon recognition is assisted via the presence of eIF1 and eIF1A, which hold the mRNA channel of the 40S ribosomal subunit in an open conformation until an AUG codon is encountered as part of a Kozak consensus sequence. [29] [53] [54] [55] [56] [57] [58] [59] [60] [61] [62] $^{Met}tRNA_i$ utilizes its 'UAC' anticodon to base-pair with the mRNA start codon, ensuring correct localization within the ribosome. [63] Start codon recognition prompts eIF1A to recruit eukaryotic translation initiation factor 5 (eIF5) to the 40S ribosomal subunit, which stimulates hydrolysis of GTP bound to eIF2 (**Figure 2:** E). [64] [65] [54] [66] [67] [68] [69] Guanosine diphosphate (GDP) bound eIF2, along with eIF1 and eIF5 dissociate from the 40S ribosomal subunit (**Figure 2:** F). [64] [53] The dissociation of eIF1 followed by release of eIF5 allows eukaryotic translation initiation factor 5B (eIF5B) to bind to the 40S subunit and recruit the 60S ribosome to the start codon, forming the 80S ribosome (**Figure 2:** G). [65] [29] [30] [70] [71] [70] [72] Subsequent release of eIF5B and eIF1A from the 80S ribosome is then triggered by GTP hydrolysis, yielding the competent 80S ribosome in preparation for elongation. [73] Polypeptide synthesis then proceeds in a cyclical manner from the N-terminal methionine, adding single amino acids depending on the identity of the mRNA codons.

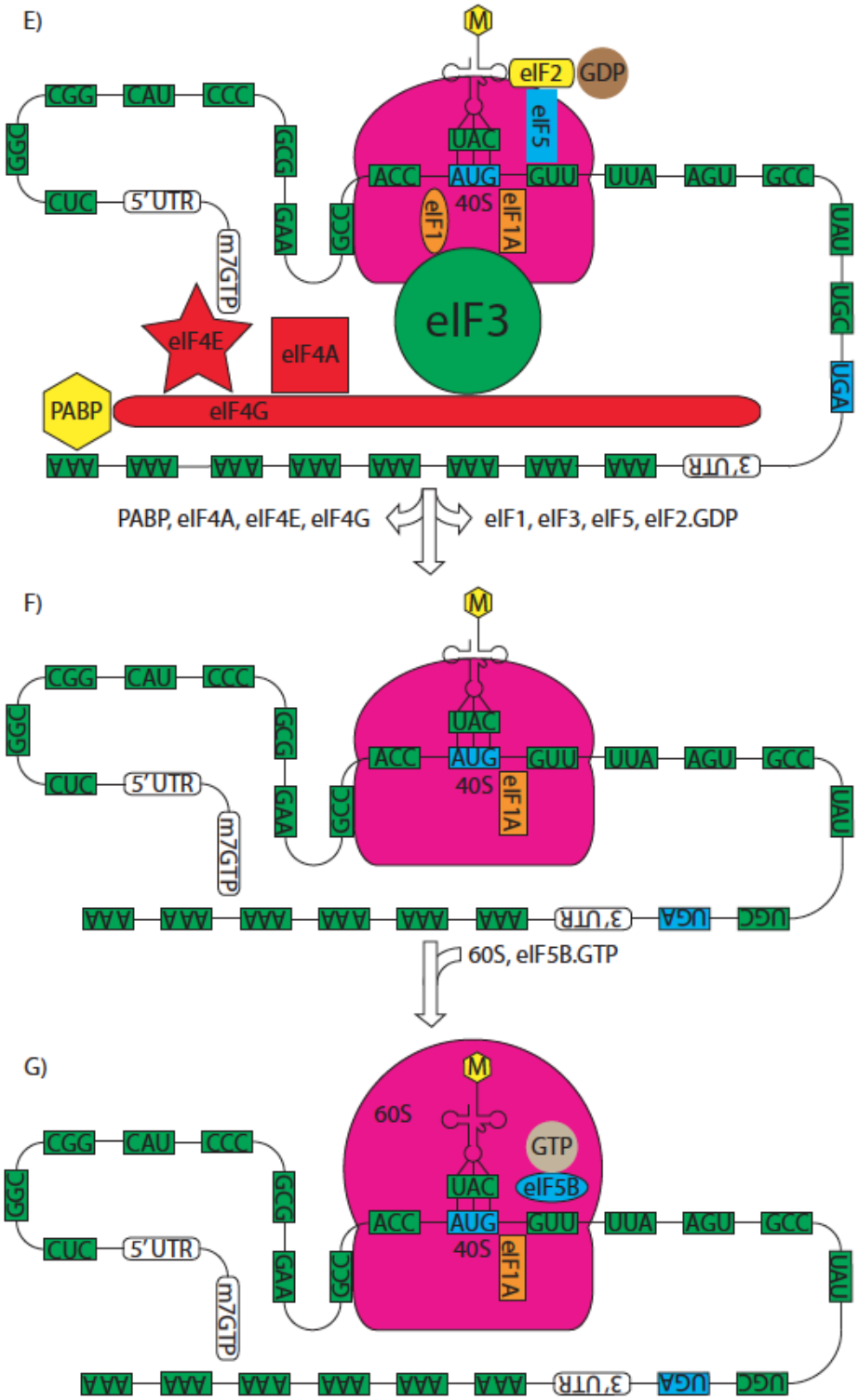

Figure 2: Schematic of eukaryotic translation initiation post start codon recognition. E) eIF1A recruits eIF5, which stimulates hydrolysis of eIF2 bound GTP. GDP bound eIF2 dissociates from the mRNA strand along with eIF1A, eIF3 and eIF5. F), G) and H) GTP bound eIF5B loads the 60S ribosomal subunit to the 40S ribosomal subunit. eIF5B hydrolyzes GTP and dissociates from the newly formed 80S ribosome with eIF1A.

9.2.2 Eukaryotic translation elongation

Eukaryotic translation elongation is the cyclical process by which specific amino acids are added to the growing polypeptide strand in an 'N' to 'C'-terminal direction, dictated by mRNA codons. Elongation is reliant on the formation of a competent 80S ribosome, which consists of three discrete transfer ribonucleic acid (tRNA) binding sites, of which only two can be occupied at any one time. The 'three site model' defines an acceptor ('A') site for interacting with incoming aminoacyl tRNAs, a peptidyl ('P') site to bind growing peptidyl tRNA chains and an exit ('E') site for the disposal of deacylated tRNAs (**Figure 3**). [74 75] All three sites utilize the specificity of the interaction of mRNA codons with tRNA anticodons to ensure correct loading of amino acids to the competent 80S ribosome. The elongation cycle is initiated by eukaryotic translation elongation factor 1 (eEF1), which loads aminoacyl-tRNAs into the 'A' site of the post-translocational (**Figure 3:** A) 80S ribosome. [76 77 78 79 80] Once the aminoacyl tRNA anticodon recognizes the cognate mRNA codon, eEF1 hydrolyzes GTP and dissociates from the 80S ribosome. [78 81] Optimal mRNA codon / tRNA anticodon interactions ensure correct loading of aminoacyl tRNAs into the 'A' site, whilst simultaneously ejecting empty tRNAs from the 'E' site (**Figure 3:** B). [78 82 83 84 85] This synergistic exclusion principle ensures that only two sites can be occupied at once and that only stabilization of the 'A' site by a fully complementary anticodon is sufficient to eject empty tRNA from the 'E' site. [86 87 88] This explains the high fidelity of polypeptide synthesis, which is due to the ability of the three sites of the 80S ribosome to differentiate between cognate and near-cognate codons. [74 75]

The amino group of aminoacyl tRNA (in the 'A' site) nucleophilically attacks the activated ester of the peptidyl-tRNA in the 'P' site, resulting in the formation of a new amide bond. This reaction yields the pre-translocational 80S ribosomal complex (**Figure 3:** C), with peptidyl-tRNA in the 'A' site, deacylated tRNA in the 'P' site and an empty 'E' site.

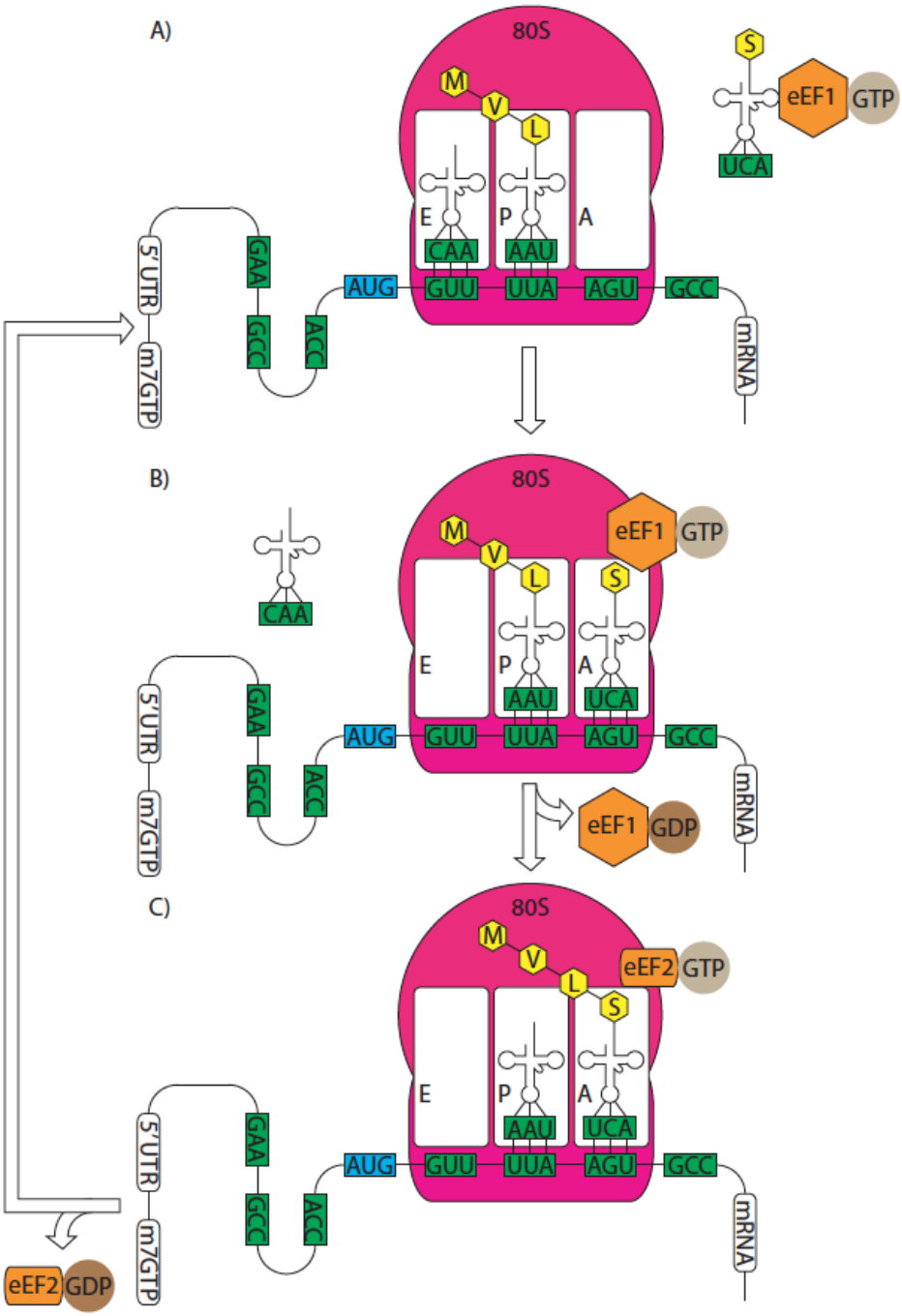

Figure 3: Schematic of the three-site model of eukaryotic translation elongation. [89] [90] [91] [92] **A) eEF1 loads aminoacyl-tRNAs to the 'A' site of the post-translocational 80S ribosome and simultaneously ejects the empty tRNA from the 'E' site. B) Once codon recognition occurs, eEF1 dissociates from the competent 80S ribosome and a new peptide bond forms between the aminoacyl tRNA in the 'A' site and the peptidyl tRNA in the 'P' site. C) eEF2 binds to the 'A' site of the pre-translocational ribosome and transfers peptidyl-tRNA from the 'A' site into the 'P' site and the empty tRNA from the 'P' site into the 'E' site.**

GTP-bound eukaryotic translation elongation factor 2 (eEF2) binds to the pre-translocational 80S ribosome (**Figure 3:** C) and catalyzes the translocation of peptidyl tRNA from the 'A' site to the 'P' site and simultaneously shifts deacylated tRNA from the 'P' site to the 'E' site. [77] [78] [93] [94] [95] [96] [97] eEF2 hydrolyzes GTP during this process and dissociates from the newly regenerated post-translocational 80S ribosome, (**Figure 3:** A) leaving a vacant binding site for eEF1. [78] [94] [98] [99] [100] [101] Codon / anticodon base-pairing of the empty tRNA in the 'E' site of the post-translocational 80S ribosome then serves to ensure high fidelity selection of the next aminoacyl-tRNA, via strict maintenance of a fully cognate codon / anticodon interaction. [97] [90] [102] [103] The elongation cycle then repeats via addition of aminoacyl-tRNAs with complementary anticodons to the mRNA codons until a stop codon is located within the 'A' site of the post-translocational ribosome.

9.2.3 Eukaryotic translation termination

Polypeptide elongation continues via scanning of the 80S ribosome along the mRNA strand until a stop codon (UAA, UAG or UGA) is located within the 'A' site of the ribosome (**Figure 4:** A). [104] [105] Eukaryotic release factor 1 (eRF1) mimics the cloverleaf structure of tRNA and utilizes this conformation to recognize all three mRNA stop codons within the 'A' site of the 80S ribosome (**Figure 4:** B). [106] [107] [108] [109] [110] The N-terminus of eRF1 utilizes two separate motifs to recognize the stop codons, with each mRNA base inserted into one of three eRF1 binding pockets. [111] [112] [113] [114] [115] Meanwhile, the C-terminus of eRF1 functions as a heterodimerization domain for the recruitment of the weak GTPase, eukaryotic release factor 3 (eRF3) (**Figure 4:** B). [105] [116] [117] [118] Binding of eRF3 allosterically modulates the conformation of eRF1 providing the correct orientation of the catalytic domain for hydrolysis of the peptidyl-tRNA ester linkage. [107] [108] [119] [120] The polypeptide chain is cleaved from the ribosome, which is followed by eIF3 and eIF1 mediated dissociation of the 80S ribosome. eRF1 stimulates GTP hydrolysis by eRF3, prompting dissociation of the two release factors from the mRNA strand (**Figure 4:** C). [117] [121] The 40S and 60S ribosomal subunits are then recycled to participate in the translation of additional polypeptide chains.

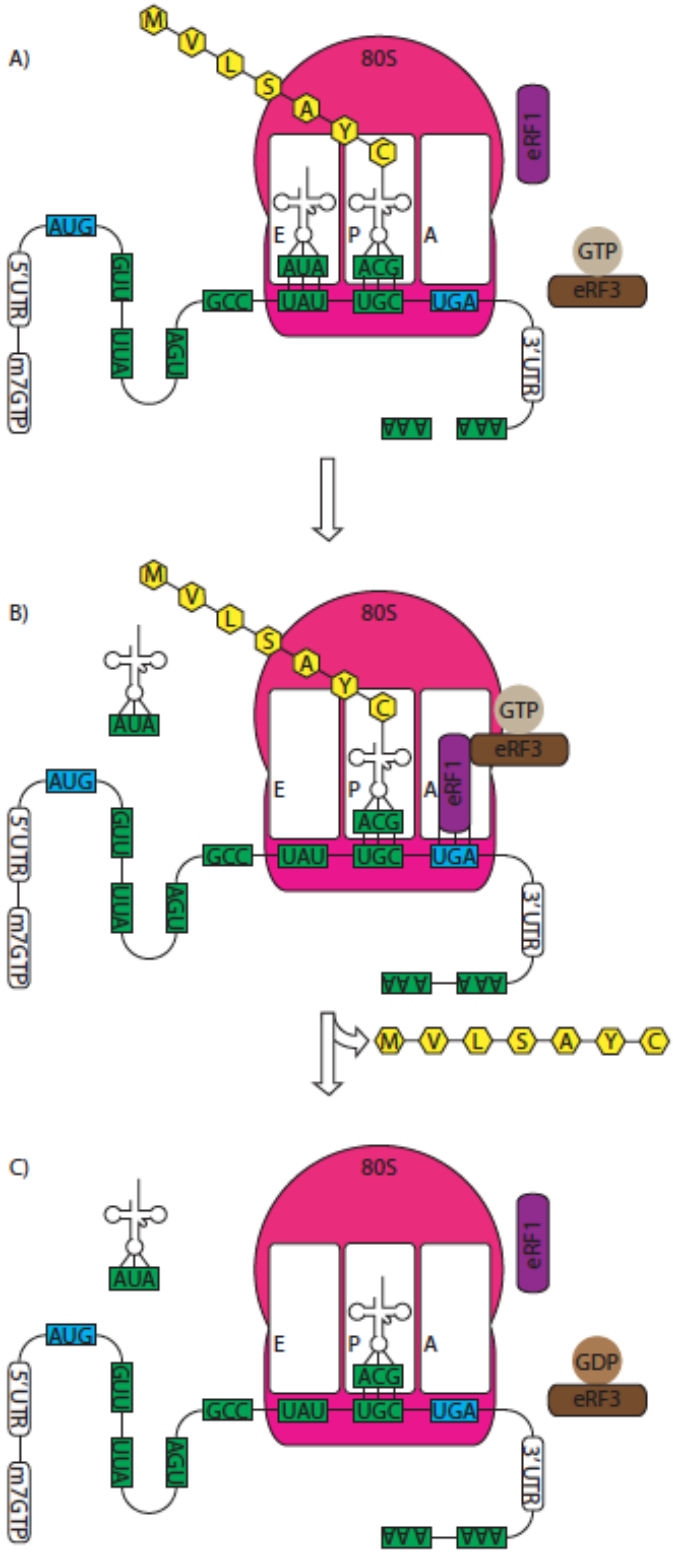

Figure 4: Schematic of eukaryotic translation termination. [92] **Eukaryotic release factor 1 (eRF1, purple) recruits eukaryotic release factor 3 (eRF3, dark brown) to the 'A' site of the 80S ribosome. eRF3 stimulates the eRF1-mediated hydrolysis of peptidyl-tRNA within the 'P' site, releasing the polypeptide chain (yellow hexagons) from the 80S ribosome.**

9.3 Cap-dependent translation initiation

The mechanism of translation of a particular mRNA is dictated by the presence or absence of secondary structure between the 5' cap and the AUG start codon. [37] [38] [39] Vital homeostatic proteins are required at all times and hence are encoded by strong mRNAs with short, unstructured 5' UTRs. This ensures rapid scanning and selection of the start codon by the 40S ribosome, resulting in constitutive protein expression. The unstructured 5' UTR of strong mRNAs allows the use of either cap-dependent or cap-independent translation to produce vital homeostatic proteins. [122] [123] By contrast, the expression of weak mRNAs encoding growth factors is tightly regulated by the presence of G and C base-pairing within the 5' UTR. The three hydrogen bonds formed by each G and C base-pair stabilize helical structure upstream of the AUG start codon that inhibits cap-independent translation. Many oncogenic proteins (oncogenes) such as basic fibroblast growth factor (FGF), vascular endothelial growth factor (VEGF) and ornithine decarboxylase (ODC) rely on cap-dependent translation due to the highly helical 5' UTRs of their weak mRNAs. [45] [46] [47] [48] [124] [125] These 5' helical regions of mRNA impair translation by inhibiting binding and scanning of the 40S ribosomal subunit, reducing the rate at which the small ribosomal subunit encounters the AUG start codon. [126] Such mRNA strands are weakly translated until the inhibitory helical structure of the 5' UTR is melted, whereupon translation of weak mRNAs is induced. Oncogenes therefore require an mRNA cap binding complex, termed eIF4F, which unwinds the 5' UTR to facilitate translation. [127] [122] The effective translation of 'weak' mRNAs thus displays an absolute requirement for eIF4F mediated cap-dependent translation initiation. [123]

Malignant transformation of cells is characterized by elevated levels of oncogenic mRNAs that facilitate rapid cell proliferation, accompanied by increased angiogenesis.[128] Maintenance of the cancerous phenotype requires the constitutive cap-dependent translation of oncogenic proteins encoded by weak mRNAs. It is therefore not surprising that overexpression of the limiting component of the eIF4F complex, eukaryotic translation initiation factor 4E (eIF4E), is correlated with malignant transformation of cells along with increasing resistance to apoptosis and chemotherapy. [129] [130] [131] [132] [133] As such, targeting of cap-dependent translation via the eIF4F complex is an attractive approach to selectively target weak mRNAs that encode oncogenic proteins. [134] In recent years there has been significant interest in the concept of inhibitors

of cap-dependent translation, due to their potency and specificity against malignancies in the presence of healthy tissue. Given the limiting intracellular availability of eIF4E and the necessity of cap-dependent translation for tumor progression, targeted inhibition of eIF4E function has become an attractive chemotherapeutic strategy.

9.3.1 Eukaryotic translation initiation factors

eIF4E and eukaryotic translation initiation factor 4G (eIF4G) are key components of the multimeric protein complex eIF4F (**Figure 5**), along with the ribonucleic acid (RNA) helicase eukaryotic translation initiation factor 4A (eIF4A). [135] [136] [137] [138] The eIF4G structural backbone of the eIF4F complex contains an N-terminal binding site for eIF4E, which is the protein responsible for binding to the m^7 GTP eukaryotic mRNA cap. [139] The adenosine triphosphate (ATP) dependent RNA helicase eIF4A, is associated with two separate binding sites in the central domain and C-terminus of eIF4G (**Figure 5**). [140] [141] [142] [143] [144] The N-terminus of eIF4G functions as a binding site for polyadenosine binding protein (PABP), which binds the 3'-polyadenylated tail of mRNA and helps to circularize the mRNA in preparation for polysome assembly and rapid protein translation. [145] The eIF4G C- terminus also contains an eIF3 binding site for recruitment of the 43S PIC in addition to a mitogen activated protein kinase interacting kinase (Mnk) binding site, which regulates the phosphorylation of eIF4E. [146] [147] [148]

Effective translation of weak mRNAs displays an absolute requirement for eIF4F mediated melting of 5' UTR hairpin structures and hence is reliant on cap-dependent translation (**Figure 5**: A). [122] [123] In turn, cap-dependent translation requires eIF4E-mediated binding to the m^7 GTP 5' cap of eukaryotic mRNAs, which facilitates localization of eIF4A to the 5' UTR via the interaction of the latter with eIF4G. [131] The RNA helicase, eIF4A then hydrolyzes ATP to unwind the helical 5' region of 'weak' mRNAs (**Figure 5**: B). [140] [142] [143] The 40S ribosomal subunit is then able to scan along the unwound 5' UTR until a start codon is located in a favorable Kozak consensus sequence. [37] [38] [39] The 60S ribosomal subunit is then recruited to the mRNA strand by eIF5B and translation proceeds in an N to C-terminal direction along the growing polypeptide strand, as previously described. The effective translation of oncogenic weak mRNAs with highly structured stem loops in their 5' UTRs is therefore totally reliant on eIF4F mediated cap-dependent translation.

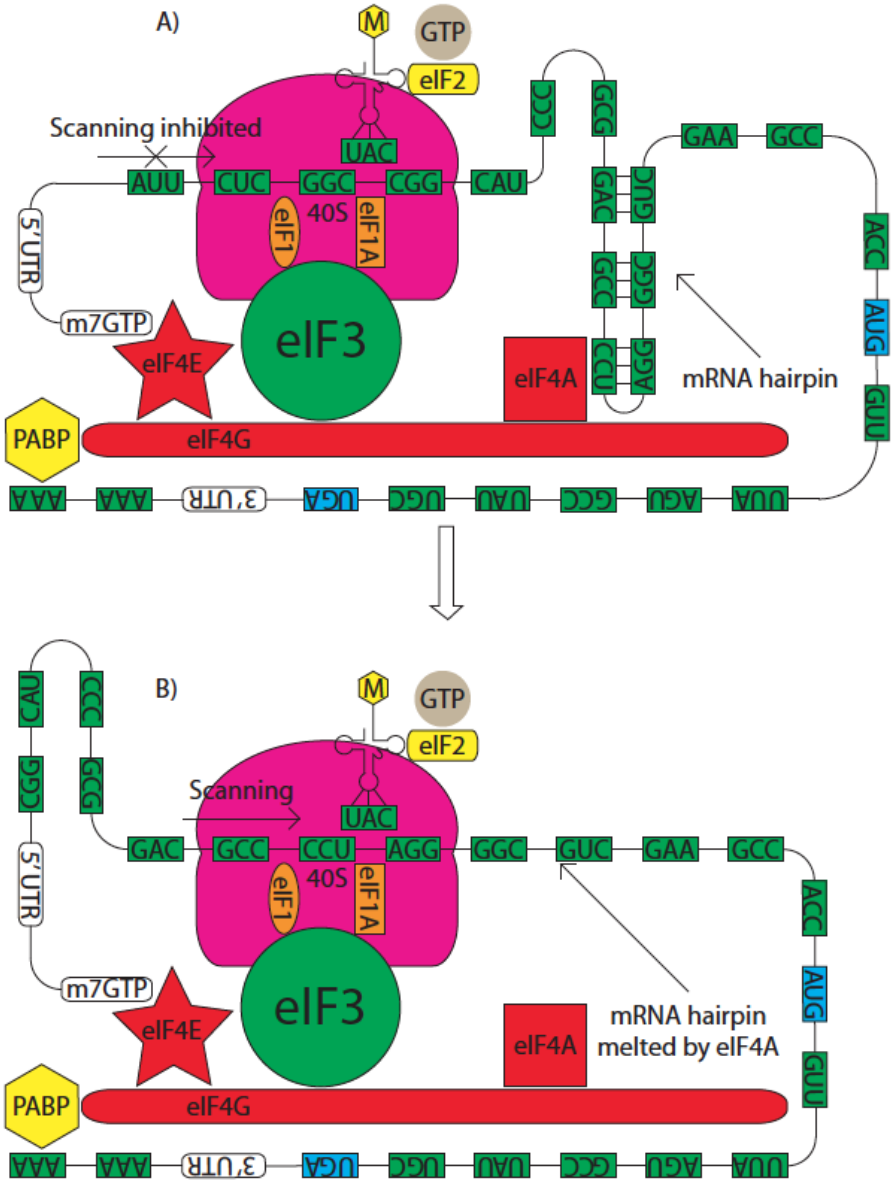

Figure 5: Schematic of the cap-dependent translation initiation machinery. eIF4F (highlighted in red) co-operates with polyadenosine-binding protein (PABP), eIF3, eIF2, eIF1 and eIF1A to facilitate delivery of initiator methionine transfer ribonucleic acid ($^{Met}tRNA_i$) to the start codon, AUG (highlighted in blue). [134] A) Guanosine (G) and cytosine (C) residues in the 5' UTR of weak mRNAs form stable hairpin or stem loop structures, which inhibit 5' to 3' scanning of the 40S ribosomal subunit along the mRNA strand. B) eIF4E binds to the m^7 GTP mRNA cap, localizing eIF4G and eIF4A to the 5' UTR. The RNA helicase eIF4A hydrolyzes ATP to unwind base-pair stabilized hairpin loops in the mRNA 5' UTR. [149] The 40S ribosomal subunit resumes scanning the mRNA strand until the start codon is located in a favorable Kozak consensus sequence.

9.3.2 Structure of the m^7 GTP binding site of eIF4E

The unique ability of eIF4E to bind m^7 GTP catalyzes the rapid translation of capped mRNAs, while the proximity of eIF4A yields selective induction of those mRNAs with highly structured 5' UTRs. [150] [151] [152] The binding affinity of eIF4E for the mRNA cap is enhanced by binding to eIF4G, yet is reduced via recruitment of Mnk to eIF4G, which phosphorylates Ser_{209} of eIF4E. [148] [153] [154] [155] [156] [157] This phosphorylation event is thought to cause electrostatic repulsion with the phosphate groups of the mRNA cap and provides one mechanism for the regulation of cap-dependent translation (discussed in section 9.2.4).

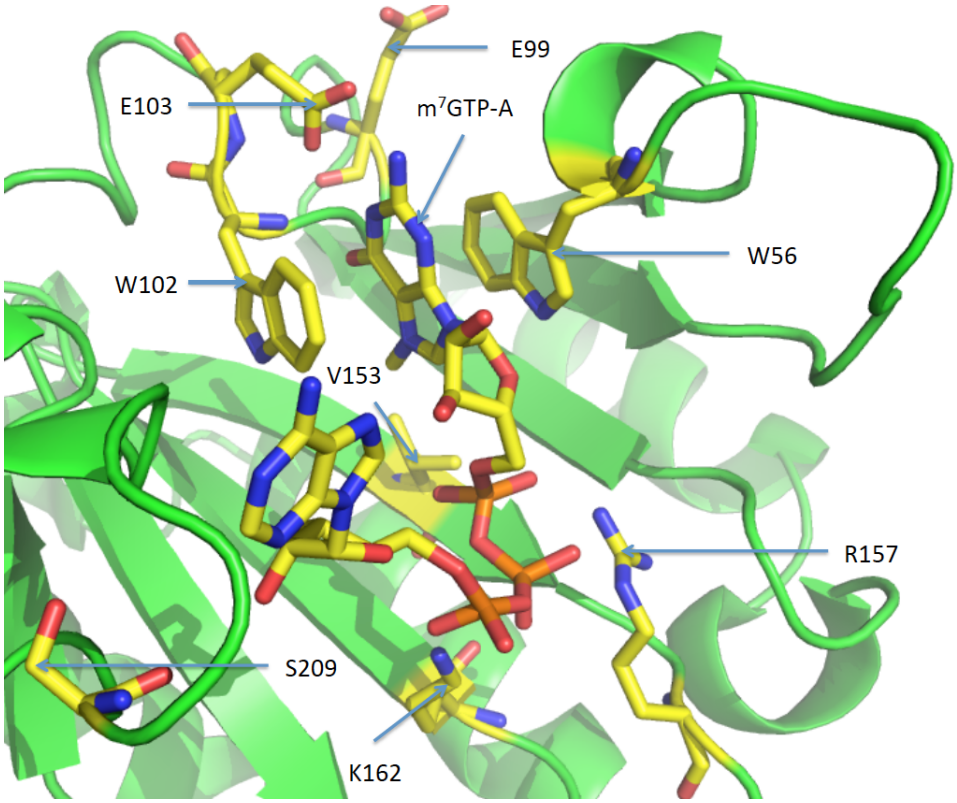

Figure 6: Binding of m^7 GTP mRNA cap to hydrophobic binding cleft of eIF4E (green), mediated via Trp_{102} and Trp_{56} π-stacking and electrostatic interactions with Glu_{99} and Glu_{103}. [158] Lys_{162}, Lys_{159} and Arg_{157} constitute the basic mRNA binding region. [159] Cap-binding is initiated and directed by the specific electrostatic binding of phosphate groups, which is then stabilized by the aromatic binding pocket and Van der Waals interactions with Val_{153} and hydrogen bond formation to Glu_{99} and Glu_{103}. (Adapted from Tomoo and Shen, Protein Data Bank (PDB) ID: 1IPB). [160]

eIF4E binds to the m^7GTP cap via a hydrophobic binding cleft lined with tryptophan (Trp) residues. [161] π-stacking interactions between the guanosine ring and binding pocket Trp residues combine with electrostatic interactions mediated by Glu_{99} and Glu_{103} of eIF4E to ensure specificity of binding (**Figure 6**). [162] Val_{153} ensures specificity for m^7 GTP binding over free GTP via Van der Waals interactions with the methyl group of the mRNA cap. The basic mRNA binding region around Arg_{157} forms salt bridges with phosphate groups of the m^7 GTP cap in addition to the phosphodiester backbone of the mRNA strand. [159] [160] [161]

9.3.3 Structure of the eIF4G binding site of eIF4E

eIF4G contains an N-terminal binding site for the mRNA cap-binding unit eIF4E, mediated by the helical heptamer peptide '$Y_0D_1R_2E_3F_4L_5L_6$' and stabilized via interactions with a 'SDVVL' motif (amino acids represented in single letter amino acid code). [139] [163] [164] [165] The helical peptide binding site (**Figure 7**) on the dorsal face of eIF4E binds several regulatory proteins in addition to eIF4G and hence functions as a key mechanism to regulate cap-dependent translation (discussed in section 9.2.4).

eIF4G shares a common eIF4E-binding domain consisting of the helical heptamer $Y_0D_1R_2X_3F_4L_5X_6$ amino acid motif (where 'X' is a variable amino acid) with the eIF4E binding proteins (4EBPs). [163] [166] Regulation of cap-dependent translation is achieved via the hyper- or hypo-phosphorylation of the 4EBPs in response to cellular energy stimuli and insulin, effectively blocking translation when intracellular adenosine monophosphate (AMP) levels are elevated (discussed in section 9.2.4). Hence competition between the eIF4G '$Y_0D_1R_2E_3F_4L_5L_6$' motif and the 4EBP '$Y_0D_1R_2K_3F_4L_5M_6$' helix regulates the assembly of the eIF4F complex and hence is a key mechanism to control cap-dependent translation. A similar '$Y_0T_1K_2E_3E_4L_5L_6$' motif has been found in the eIF4E nuclear transporter protein (4E-T), which also competes for the same eIF4E binding site. 4E-T has a role in the nuclear-cytoplasmic shuttling of eIF4E and mRNAs, which will be discussed in detail in section 9.2.4 [167]

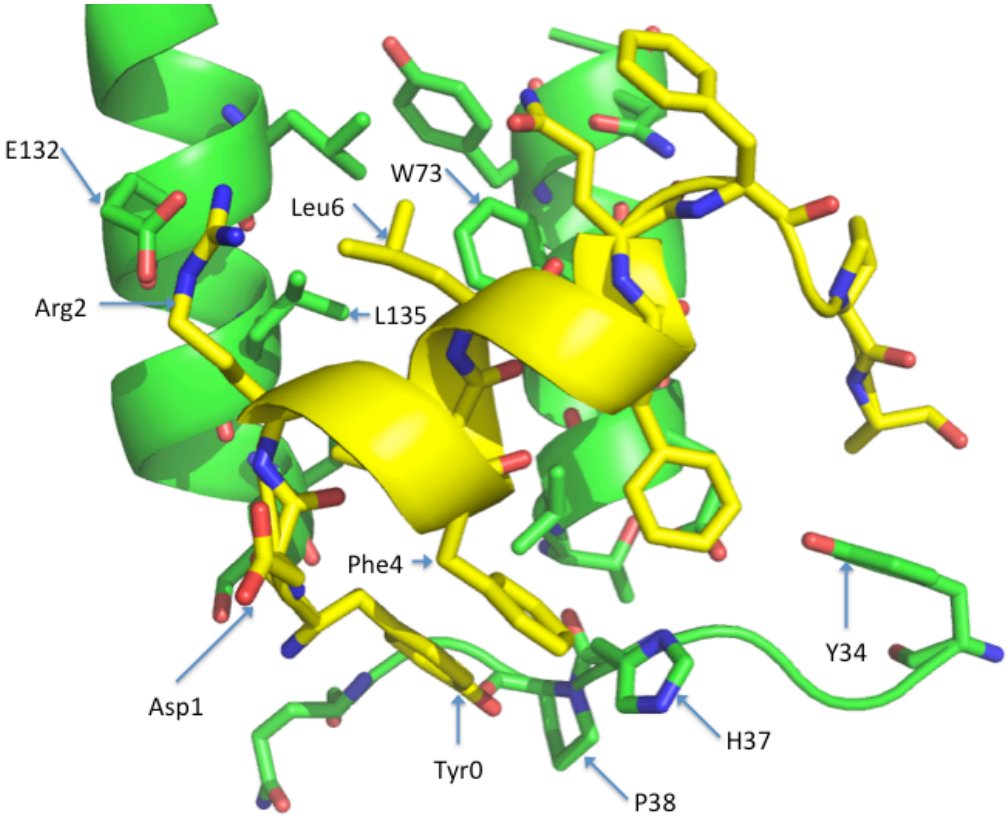

Figure 7: Interaction of eIF4E (green, residues labeled in single letter amino acid code) with the helical eIF4E binding peptide of eIF4G, $Y_0D_1R_2E_3F_4L_5L_6$ (yellow, residues labeled in triplet amino acid code). The common mammalian binding motif ($Y_0D_1R_2X_3F_4L_5X_6$) plays a vital role in regulating the assembly of the eIF4F complex. Key binding interactions can be observed between Arg_2 of eIF4G and E_{132} of eIF4E. Leu residues at positions 5 and 6 of the eIF4G peptide interact with W_{73}, L_{135}, V_{69} and I_{138} of eIF4E. (Adapted from Brown and Verma, PDB ID: 2W97). [168]

An important class of cap-dependent translation inhibitors have been developed that mimic the $Y_0D_1R_2X_3F_4L_5X_6$ motif of mammalian eIF4G / 4EBPs and thus bind eIF4E, preventing its sequestration into eIF4F. A wide variety of helical peptides have been developed, which were subsequently fused to cell penetrating peptide domains to improve membrane permeability. As expected, cell treatment with helical peptide inhibitors of cap-dependent translation induced apoptosis in a dose-dependent manner. [169] A key step in the development of eIF4G-mimics came with the identification of a cell permeable, water-soluble derivative isolated via phage display (**Table 1**, Phagesol). [170]

Peptide	Sequence	K_D / nM
4E-BPI peptide [164]	H_2N-RIIYDRKFLMECRNSPV-CO_2H	50
eIF4GI peptide [164]	H_2N-KKRYDREFLLGFQFIFA-CO_2H	27
eIF4GII peptide [164]	H_2N-KKQYDREFLLDFQFMPA-CO_2H	150
eIF4GI-OPT [170]	H_2N-KKRYSREFLLAF-CO_2H	52
Phagesol [170]	H_2N-KKRYSRDQLVAL-CO_2H	77
VL-Phagesol [170]	H_2N-KKRYSRDQLLAL-CO_2H	35
eIF4G1 D5S peptide [171]	H_2N-KKRYSREFLLGF-CO_2H	100
sTIP-03 [171]	H_2N-KKRYSREZLLZF-CO_2H	3.4
sTIP-04 [171]	H_2N-KKRYSRZQLLZL-CO_2H	5.0

Table 1: eIF4G / 4EBP derived mimics of eIF4E-binding peptides with the critical binding motif highlighted in red. 'Z' denotes incorporation of pentenyl alanine in the relevant position, which was subsequently stapled via Grubbs metathesis. [171]

The initial peptide eIF4G or 4EBP-mimics were found to have conformational flexibility, with a large percentage of the peptide existing as a disordered loop. [164] This finding prompted the development of stapled 'pre-organized' helical peptide mimics of eIF4G and the 4EBPs (**Table 1:** sTIP-03 and sTIP-04). Helical stapled peptides are forced to adopt a binding conformation in solution, overcoming the entropic cost upon association with eIF4E. [171] The helical stapled peptides of the sTIP family (**Table 1**) are currently undergoing further development and are a very recent and promising advance in the field of cap-dependent translation inhibitors. [172] [173] [174]

9.3.4 Significance and regulation of cap-dependent translation

Tight control of cap-dependent translation is vital to prevent the excessive expression of oncogenic proteins and the resulting malignant transformation of otherwise healthy cells. [175] Regulation of eIF4F mediated cap-dependent translation is achieved via two independent signaling pathways, which respond to distinct cellular criteria (**Figure 8**).

The adenosine mono phosphate activated protein kinase (AMPK) / mammalian target of rapamycin (mTOR) / 4EBP pathway responds to elevated cellular levels of AMP,

caused by consumption of ATP within rapidly proliferating cells. Control of cap-dependent translation is governed by negative regulators of the limiting component of the eIF4F complex, known as the 4EBPs. [176] Activation of AMPK by elevated AMP levels inhibits mTOR, which prevents mTOR-induced phosphorylation of 4EBPs. [177] [178] These hypophosphorylated 4EBPs then bind to eIF4E in an eIF4G-competitive manner and sequester eIF4E from the eIF4F complex. [163] [179] [176] [180] However in response to elevated intracellular ATP levels and the resulting inactivation of AMPK, the 4EBPs become hyperphosphorylated and lose their ability to bind to eIF4E. [181] The eIF4F complex assembles and facilitates rapid cap-dependent translation of weak mRNAs. Loss, down-regulation or hyper-phosphorylation of 4EBPs leads to accumulation of free eIF4E, which has been associated with rapid tumor growth. [129] [182] [183] Elevated free eIF4E levels are characteristic of transformed cells and predict poor prognosis, particularly when not restrained by the 4EBPs. [16] [132] [18] [184] [185]

The second cellular pathway that regulates cap-dependent translation responds to growth factors via the extracellular growth factor receptor (EGFR) pathway. [154] Binding of extracellular growth factors to transmembrane receptors alters the conformation of Rat sarcoma kinase (Ras), stabilizing its binding to GTP and the oncogenic serine / threonine kinase, Raf. [186] [187] This triggers a signaling phosphorylation cascade via activation of mitogen activated protein kinase kinase (MEK), through mitogen activated protein kinase (MAPK) and subsequently results in the phosphorylation and activation of MnK. [188] [189] [190] Mnk binds to eIF4G, which serves as a scaffold to deliver the kinase to phosphorylate eIF4E on Ser_{209}. [148] [155] [156] [157] At first, phosphorylated eIF4E was shown to bind to m^7 GTP with superior affinity when compared to non-phosphorylated protein; consistent with the theory that phosphorylated eIF4E was necessary for cellular transformation via an increase in the rate of cap-dependent translation. [191] This was also consistent with the observation that increased levels of phosphorylated eIF4E were correlated with rapidly proliferating tumors and hence were found to be inversely proportional to patient survival. [192] [193] [194] [195] The targeting of phospho-eIF4E either directly or via treatment with Mnk inhibitors such as Cercosporamide or CGP57380, has added further weight to the hypothesis that phospho-eIF4E is the causative agent responsible for rapidly proliferative, malignant tumors, but is not required for cellular homeostasis. [196] [197] [198] [199] [200]

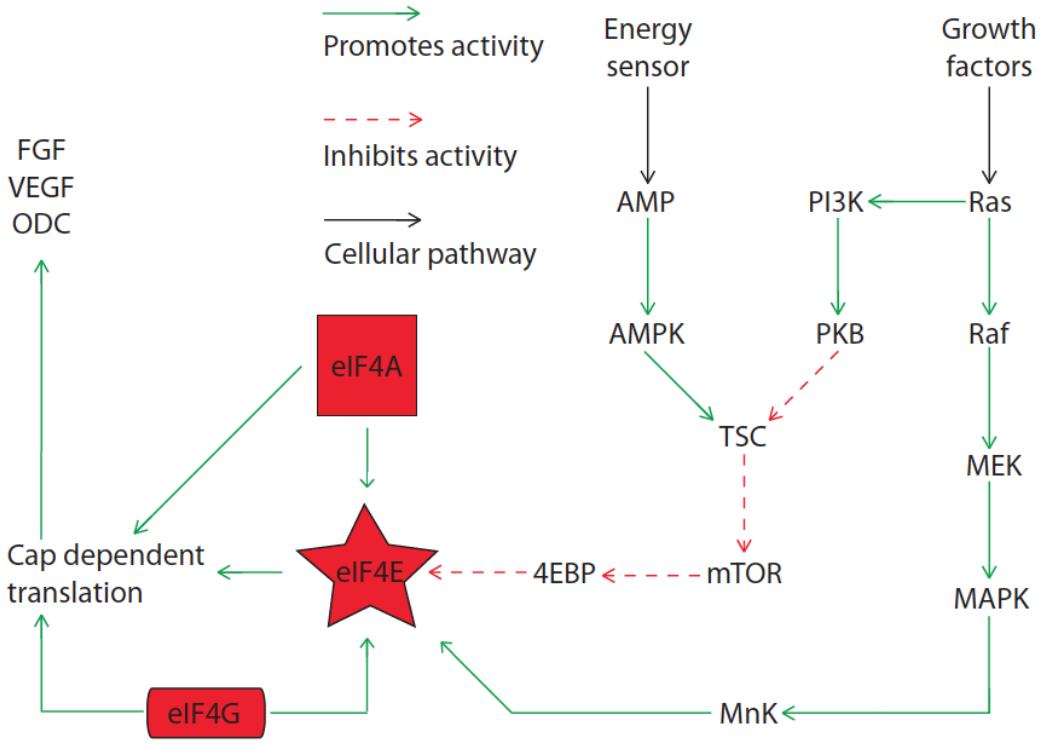

Figure 8: Schematic of the signaling pathways that regulate cap-dependent translation via the mRNA 5' cap-binding protein, eIF4E. Abbreviations used: adenosine mono phosphate (AMP), adenosine mono phosphate kinase (AMPK), phospho inositol 3 kinase (PI3K), protein kinase B (PKB), tuberous sclerosis complex (TSC), mammalian target of rapamycin (mTOR), eIF4E-binding proteins (4EBP), rat sarcoma kinase (Ras), proto-oncogene serine / threonine kinase (Raf), mitogen activated protein kinase kinase (MEK), mitogen activated protein kinase (MAPK), mitogen activated protein kinase interacting kinase (MnK), basic fibroblast growth factor (FGF), vascular endothelial growth factor (VEGF), ornithine decarboxylase (ODC). [201 202 203 204 181 176 205 186 206 207 188 189 45 46 47 48 124 125]

However the belief that the aggressively proliferative phenotype of phospho-eIF4E positive tumors is due to a superior affinity of the phosphorylated protein for the mRNA cap, has recently been called into question. [191] Enzyme-linked immunosorbent assay (ELISA) experiments observed no difference in the binding of eIF4E or phospho-eIF4E to immobilized His-4EBP and tryptophan fluorescence measurements indicated weaker binding of phospho-eIF4E to m^7 GTP compared to the dephosphorylated protein. [208] This finding was confirmed via kinetic experiments, which observed a reduction in the

rate of association of phospho-eIF4E with the m^7 GTP cap, whereas comparable dissociation rates were seemingly independent of phosphorylation status. This finding would seem consistent with the position of Ser_{209} in close proximity to a phosphate group of the m^7 GTP ligand, which may result in electrostatic repulsion. [209]

It had been previously established that eIF4E played a critical role in the nuclear export of Cyclin D1 mRNA, despite its lack of translational reliance on the cap-binding protein. [210] [211] Subsequent truncation-based mRNA binding experiments isolated a ~ 50 base 'eIF4E sensitivity element' (4E-SE) present in the 3' untranslated region (3' UTR) of Cyclin D1 mRNA that functions as a cap-binding protein-dependent nuclear export signal. [212] eIF4E thus not only regulates the cap-dependent translation of weak mRNAs with highly helical 5' UTRs, but also appears to play a pivotal role in the availability of mRNAs for translation in the cytoplasm. [213] eIF4E associates with an nuclear transporter protein (4E-T), which competes with eIF4G and the 4EBPs for binding to eIF4E and facilitates the nuclear import of the cap-binding protein. [167] Very recently a correlation between phospho-eIF4E and 4E-T localization within cellular processing bodies has been discovered, which is perhaps indicative of increased phospho-eIF4E affinity for 4E-T. [214] It is therefore possible that Mnk-induced phosphorylation of eIF4E promotes its nuclear import, which in turn results in the nuclear export of oncogenic mRNAs with 4E-SE present in their 3' UTRs. However the exact role of phosphorylated eIF4E and the physiological relevance of its co-localization with 4E-T, remains to be elucidated.

The eIF4E / eIF4G interaction constitutes a vital link between m^7 GTP cap recognition and eIF4A catalyzed melting of 5' UTR secondary structure in weak mRNAs. [123] As such, the disruption of this oncogenic protein-protein interaction (PPI) inhibits cap-dependent translation and represents a viable mechanism to selectively disrupt translation of weak mRNAs. Disruption of the eIF4F complex can therefore be used to suppress translation initiation of oncogenic mRNAs, without adversely inhibiting cap-independent translation. [122] Inhibiting the eIF4E / eIF4G interaction therefore permits the targeting of malignant proliferation in the presence of healthy tissue.

9.4 Two-hybrid systems

As discussed in section 8, the primary objective of the project was to develop cyclic peptide (CP) inhibitors of the eIF4E / eIF4G interaction. An *Escherichia coli (E. coli)* based reverse two-hybrid system (RTHS) was constructed to facilitate probing of the eIF4E / eIF4G interface *in vivo*. [215] [216] The construction of this model system was then combined with split intein circularization of peptides and proteins (SICLOPPS) technology to identify potential inhibitors of the PPI. [217] This combinatorial approach facilitated high throughput screening of compounds against the oncogenic eIF4E / eIF4G PPI and permitted the cost effective screening of large numbers of cyclic peptides.

9.4.1 Two-hybrid systems in *Escherichia coli*

Two-hybrid systems (THS) have become powerful tools to identify unknown PPIs, in addition to the identification of functional domains within established binding surfaces. [218] [219] [220] Initially THS were applied in *Saccharomyces cerevisiae* and exploited the separable N-terminal deoxyribonucleic acid (DNA) binding and C-terminal transcriptional activation domains present within the Gal 4 transcriptional activator protein. [221] [222] However when compared to *E. coli* the manipulation of DNA in yeast is limited by their slow growth rate and low transformation efficiency (~10^5 plasmid transformants in *Saccharomyces cerevisiae* compared to ~10^{10} in *E. coli*.). [223] [224] This prompted the development of THS within *E. coli,* which utilized the separable N-terminal DNA binding (NTD) and C-terminal dimerization (CTD) domains of the cI repressor protein of bacteriophage λ (**Figure 9**). [225] [226] [227] [228] [229]

The Bacteriophage λ cI repressor protein is a member of a family of DNA binding proteins with N-terminal helix-turn-helix motifs. [230] Within this motif, a single α helix (termed a recognition helix) is responsible for binding to DNA via insertion into the major groove of a DNA operator half site. [231] However, the binding of a single recognition helix to one operator half site is insufficient to secure binding of the repressor to the DNA double helix. [227] Bacteriophage λ cI repressor proteins utilize their C-terminal homodimerization domains to ensure the correct insertion of recognition helices from two cI monomers into the major grooves of two halves of a DNA operator site. [227] [232] [231]

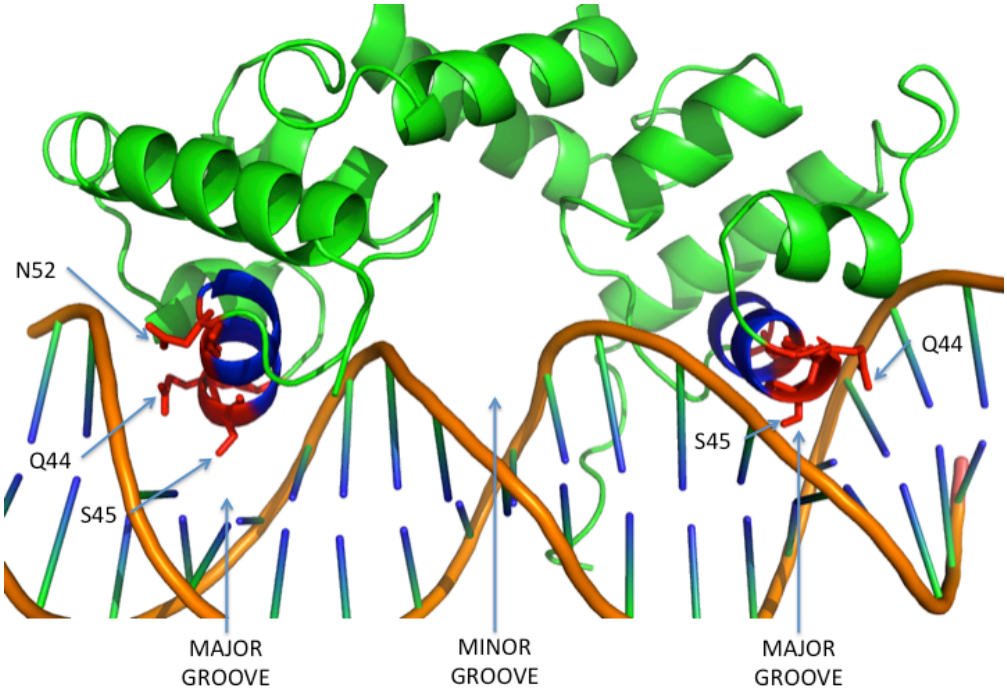

Figure 9: Crystal structure of the bacteriophage λ cI repressor protein dimer (green, residues 1-92 inc.) bound to a synthetic DNA operator (orange). [232] [231] **Critical binding residues (Q44, S45, N52, red) of the recognition helices (blue) that mediate specific interactions with each operator half site are highlighted. (Adapted from Beamer and Pabo, PDB ID: 1LMB).** [232]

The C-terminal domains (CTD) of the bacteriophage λ cI repressor proteins are also responsible for mediating co-operative interactions between DNA bound dimers at adjacent operator sites. [227] [233] [234] This property was exploited by Dove to generate a forward THS in *E. coli* (**Figure 10**). [229] The bacteriophage λ cI repressor (λcI NTD - λcI CTD) was utilized in tandem with a chimeric protein consisting of the C-terminal homodimerization domain of the cI repressor, fused to the N-terminal domain of the α subunit of RNA polymerase (λcI CTD - α NTD). Binding of the bacteriophage λ cI repressor dimer to the O_R2 operator recruited the chimeric λcI CTD - α NTD dimer to the promoter. The NTD of the α subunit of RNA polymerase was efficiently recruited to the β and σ subunits of RNA polymerase, which facilitate binding to core promoter elements including the Pribnow box (-10) and -35 consensus sequences. [219] [235] [236] [237] Transcription proceeded, enhancing expression of β-galactosidase from the *LacZ* gene of the reporter cassette. [229]

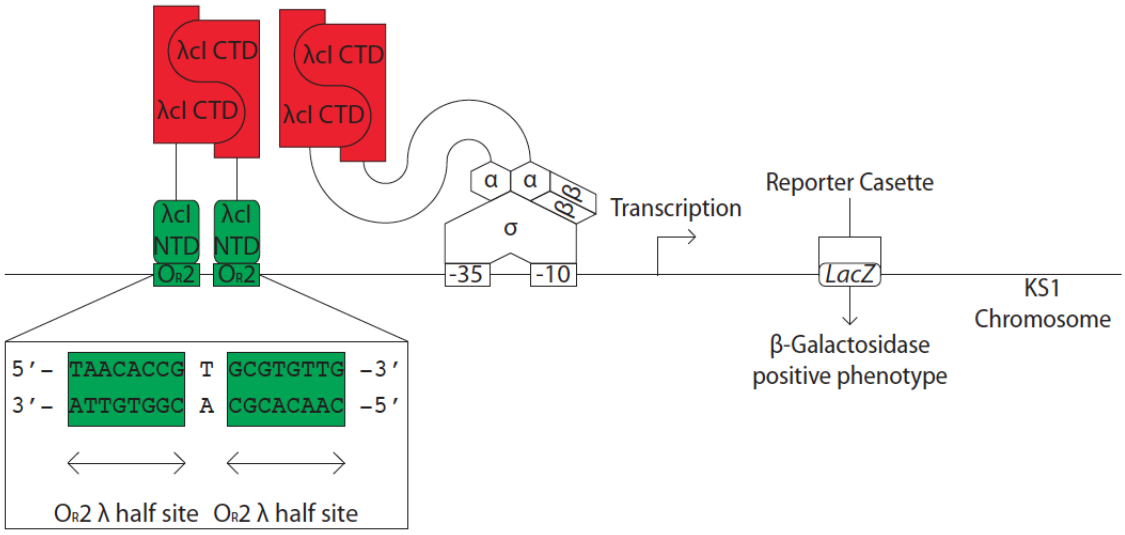

Figure 10: Schematic of the forward THS based on the Bacteriophage λ cI repressor protein developed by Dove in *E. coli*. [229] [238] Binding of a λ repressor (λcI NTD - λcI CTD) dimer to the O_R2 operator localizes a λcI CTD - α NTD dimer to the promoter. α, β and σ subunits of RNA polymerase assemble and transcribe β-galactosidase from the *LacZ* gene downstream of the promoter.

This concept was subsequently developed by Di Lallo, who generated a RTHS based on the bacteriophage λ cI repressor protein in *E. coli* (**Figure 11**). [239] [240] The key development employed by Di Lallo was the utilization of two bacteriophage λ DNA operator sites, overlapping the Pribnow (-10) box and -35 consensus sequences of the promoter. [219] [235] [236] [237] Binding of the bacteriophage λ cI repressor dimer to the high affinity O_R2 operator stabilized binding of a second repressor dimer to the lower affinity O_R1 operator. The occupation of the O_R2 and O_R1 operators by bacteriophage λ cI repressor dimers, blocked the recruitment of the σ subunit of RNA polymerase to the promoter. Transcription of downstream reporter genes was suppressed reducing expression of β-galactosidase from the *LacZ* gene. [239] [240]

THS in *E. coli* have been successfully used to analyze the dimerization of leucine zippers, in addition to screening for inhibitors of PPIs and DNA-protein interactions. [215] [216] [225] [241] [242] [243] As such, the construction of a RTHS in *E. coli* to investigate the interaction of eIF4E with eIF4G was deemed to be an appropriate method towards the development of inhibitors of cap-dependent translation.

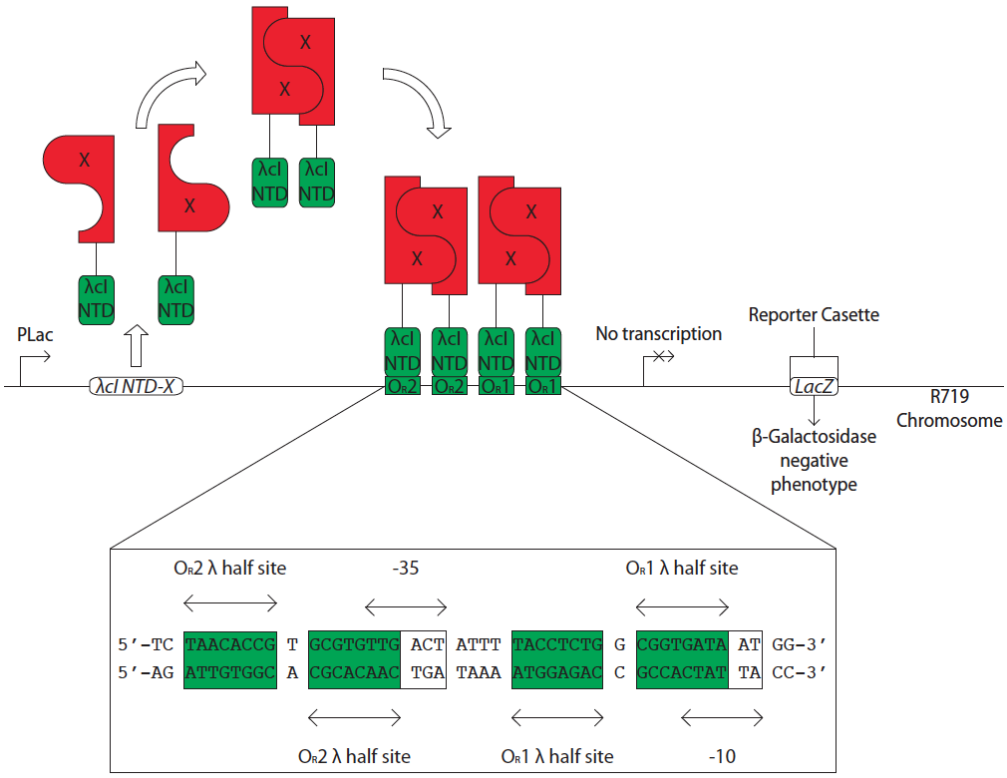

Figure 11: Schematic of the first reverse two-hybrid system (RTHS) based on the Bacteriophage λ cI repressor protein developed by Di Lallo in *E. coli*. [239] [240] Isopropyl β-D-thiogalactopyranoside (IPTG) induced expression of λcI NTD – protein X fusions from the promoter of the lactose operon (PLac), was followed by homodimerization, which reconstituted the DNA binding activity of the λ phage cI repressor.

9.4.2 Bacteriophage 434 repressor system

To construct a system to probe the interaction of eIF4E with eIF4G in *E. coli*, a RTHS based on the DNA binding domain of the Bacteriophage 434 repressor protein was chosen, in place of the previously described bacteriophage λ system. [244] [245] [246] [247] The 434 repressor consists of two distinct functional domains; an N-terminal helix-turn-helix motif responsible for binding the specific 434 DNA operator sequence and a C-terminal homo-dimerization domain. [248] The N terminus of each 434 repressor within the DNA binding homodimer, utilizes a recognition helix to ensure binding specificity. Each recognition helix is inserted into the major grove of one operator half site, facilitated by the C-terminal homodimerization domains, which ensure correct orientation of the alpha helices with respect to the DNA groove. [249]

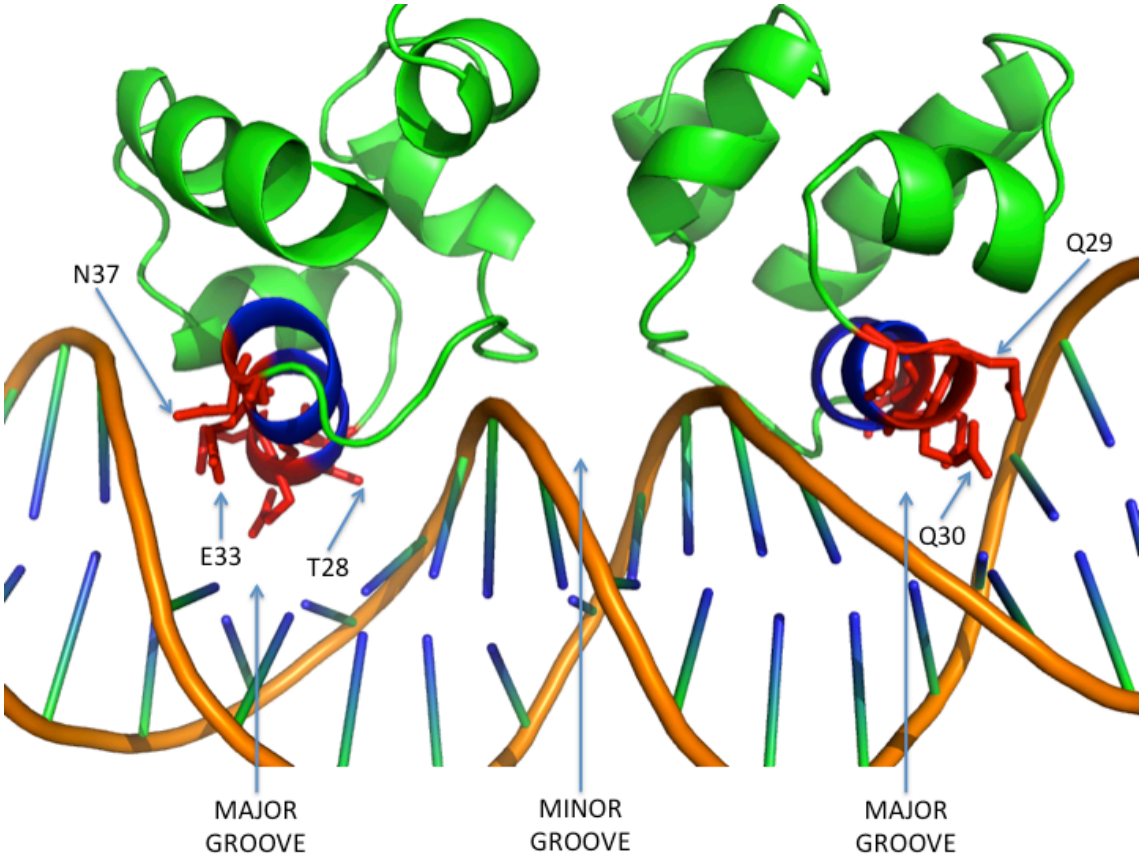

Figure 12: Crystal structure of the bacteriophage 434 repressor protein dimer (green, residues 1-63 inc.) bound to a synthetic DNA operator (orange). [249] [250] [251] [252] **Critical binding residues (T28, Q29, Q30, E33, N37, red)** [253] [254] **of the recognition helices (blue) that mediate specific interactions with each operator half site are highlighted. (Adapted from Aggarwal and Rodgers, PDB ID: 2OR1).** [251]

The 434 DNA binding repressor protein shares structural homology with several other repressor proteins, including those of the λ and P22 phages. [231] [230] [255] [256] The λ and P22 bacteriophage repressor proteins also consist of distinct C-terminal homodimerization domains teamed with N-terminal helix-turn-helix motifs that bind to DNA. [227] [234] [257] However, due to variations in the recognition helices of the λ and P22 phages, the DNA operator sequences bound by these repressors differs from the 434 repressor (**Figure 13**). [258]

	O_R1	
434	5′- ACAAGAA AGTTTGT -3′	434
434	3′- TGTTCTT TCAAACA -5′	434
P22	5′- ATTTAAGTG TTCTTTAAT -3′	P22
P22	3′- TAAATTCAC AAGAAATTA -5′	P22
λ	5′- TACCTCTG G CGGTGATA -3′	λ
λ	3′- ATGGAGAC C GCCACTAT -5′	λ
	O_R2	
434	5′- ACAAGAT ACATTGT -3′	434
434	3′- TGTTCTA TGTAACA -5′	434
P22	5′- ACTAAAGAT TCCTTTAGT -3′	P22
P22	3′- TGATTTCTA AGGAAATCA -5′	P22
λ	5′- TAACACCG T GCGTGTTG -3′	λ
λ	3′- ATTGTGGC A CGCACAAC -5′	λ
	O_R3	
434	5′- ACAAGAA AAACTGT -3′	434
434	3′- TGTTCTT TTTGACA -5′	434
P22	5′- AGTTAAGTC ATCTTAAAT -3′	P22
P22	3′- TCAATTCAG TAGAATTTA -5′	P22
λ	5′- TATCACCG C AAGGGATA -3′	λ
λ	3′- ATAGTGGC G TTCCCTAT -5′	λ

Figure 13: DNA operator binding site comparison of the 434 (NCBI Genbank accession number: X73093.1), P22 (NCBI Genbank accession number: M24302.1) and λ (NCBI Genbank accession number: M25081.1) bacteriophage repressor proteins. [259] [260] [261] **Each operator site consists of a pair of half sites, responsible for binding recognition helices. Bacteriophage P22 and 434 DNA operator half sites used for RTHS construction are highlighted.**

The substitution of five key residues (**Figure 14:** B, T28S, Q29N, Q30V, E33S, N37R) in the recognition helix of the 434 repressor with the corresponding amino acids of the P22 repressor, has been shown to be sufficient to abolish binding to the 434 DNA operator sequence. In addition, this chimeric 434 repressor (hereafter termed 'P22') displays enhanced binding to the P22 consensus DNA operator. [253] [254] [262] When both the wild type 434 and chimeric 'P22' repressor N-terminal sequences are fused to C-terminal heterodimerization domains, a dimer is generated that recognizes a chimeric 434 / P22 DNA operator sequence (**Figure 14:** A). [253] [263] Binding of the chimeric 434 / 'P22' repressor heterodimer to the indicated operator sites, inhibits interaction of RNA polymerase with critical promoter elements including the Pribnow box (-10) and -35 promoter consensus sequences. [219] [235] [236] [237] Therefore transcription of reporter genes downstream of the P_R promoter is suppressed, creating a causal link between heterodimerization of the 434 / 'P22' repressors and gene expression.

A)

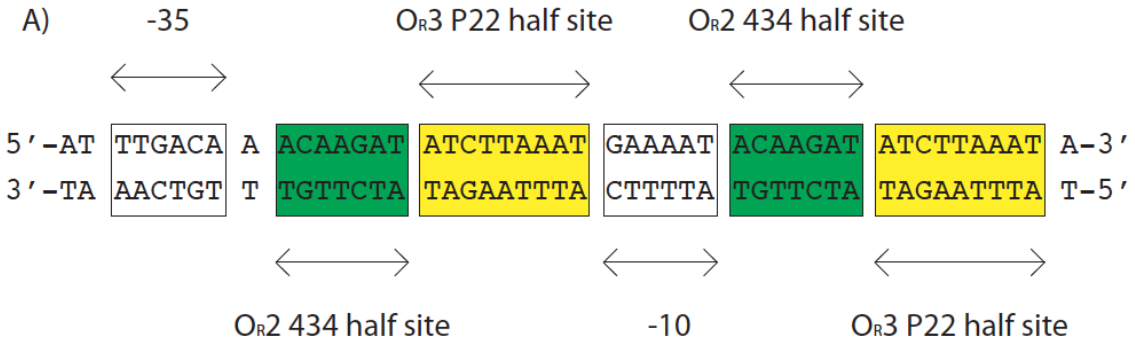

B)

434	28	TQQSIEQLEN	37	434
P22	31	SNVAISQWER	40	P22
λ	44	GQSGVGALFN	53	λ
'P22' Chimera	28	SNVSISQLER	37	'P22' Chimera

Figure 14: A) Sequence of the chimeric 434 / P22 DNA operator, with the composite 434 and 'P22' half sites indicated. [244] [247] [263] [262] **B) Sequence alignment of the recognition helices of the repressor proteins of the 434, (NCBI protein accession number: S32822) P22 (NCBI protein accession number: CAA24470) and λ (NCBI protein accession number: NP_040628.1) bacteriophages alongside the chimeric 'P22' repressor.** [253] [254] [264] [265]

9.4.3 The concept of the eIF4E / eIF4G RTHS

In order to analyze the association of eIF4E and eIF4G within *E. coli* a RTHS was constructed (**Figure 15**) that would allow the isolation of putative cyclic peptide inhibitors of the oncogenic eIF4E / eIF4G PPI. A pre-existing heterodimeric operator strain of *E. coli* (SNS126, developed by Horswill and Savinov) was previously gifted to the Tavassoli lab and was used as the basis for the eIF4E / eIF4G RTHS. [266]

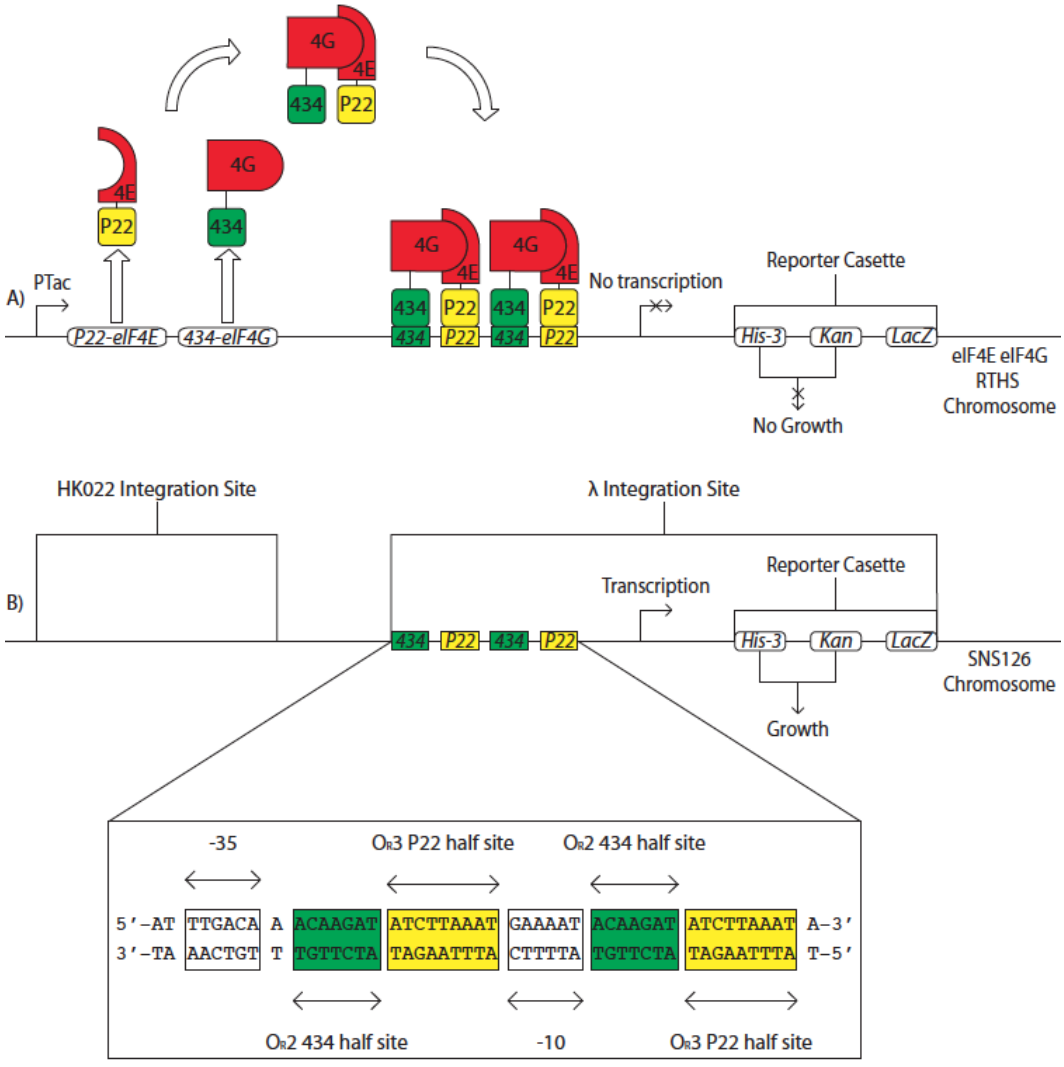

Figure 15: A) Schematic of the eIF4E / eIF4G RTHS. B) Schematic of the SNS126 strain. [266] Abbreviations used: 'P22' chimeric bacteriophage 434 repressor with *P22* operator binding specificity (P22), bacteriophage 434 repressor protein (434), imidazole glycerol phosphate dehydratase gene (*His-3*), neomycin phosphotransferase II gene (*Kan*), β-galactosidase gene (*LacZ*), mutant promoter of the lactose / tryptophan operon (PTac). [267] [268] [269]

Horswill and Savinov developed the SNS126 heterodimeric operator strain from the BW27786 strain of *E. coli*. The first step in the construction of the heterodimeric operator strain (SNS126) was the deletion of a key gene in the histidine biosynthesis pathway (imidazole glycerol phosphate dehydratase, *His-3*) from the chromosome of BW27786 *E. coli* to generate the BW27786 (*His-3* negative) strain. [266] [270] In tandem, an imidazole glycerol phosphate dehydratase (*His-3*), / neomycin phosphotransferase II (*Kan*), / β-galactosidase (*LacZ*), reporter cassette was genetically fused to the chimeric *434* / *P22* operator construct. [266] [267] [268] Horswill and Savinov integrated the chimeric *434* / *P22* / *His3* / *Kan* / *LacZ* construct into the λ site of the chromosome of the BW27786 (*His-3* negative) strain of *E. coli*, to generate the heterodimeric operator strain termed SNS126 (**Figure 15:** B). [266] [271] [272] Integration into the bacterial chromosome ensured only a single copy of the reporter cassette and the chimeric 434 / P22 operator would be present per SNS126 cell, eliminating potential copy number defects from vector encoded systems. Integration of genetically encoded 'P22'-eIF4E and 434-eIF4G protein fusions into the chromosomal HK022 site of the SNS126 strain would ensure that the repressor monomers were present as single copies within the heterodimeric operator strain, SNS126. The expression of the eIF4E / eIF4G RTHS *His3* / *Kan* / *LacZ* reporter cassette is therefore repressed by binding of two chimeric 434 / 'P22' repressor heterodimers to the two chimeric *434* / *P22* DNA operators present within the chimeric promoter.

The eIF4E / eIF4G RTHS utilizes the dimerization of the 434 repressor protein and the chimeric 'P22' repressor, to suppress transcription of a reporter cassette (**Figure 15:** A). 'P22'-eIF4E and 434-eIF4G protein fusions were genetically encoded downstream of a mutant 'PTac' promoter comprising the Pribnow (-10) box of the lactose operon, combined with the -35 consensus promoter sequence of the tryptophan operon. [269] The PTac promoter is efficiently repressed by the endogenous repressor protein of the lactose operon (LacI) within *E. coli*. Binding of a LacI tetramer to the PTac promoter sterically blocks the recruitment of RNA polymerase, inhibiting the transcription of genes encoding the chimeric protein repressor fusions. Disruption of the LacI tetramer by an allolactose mimic, such as isopropyl β-D-thiogalactopyranoside (IPTG), stimulates expression of 'P22'-eIF4E and 434-eIF4G protein fusions from the Tac promoter. [273] Heterodimerization of eIF4E and eIF4G then promotes formation of the chimeric 434 / 'P22' repressor, which binds to the chimeric operator. Binding of two

heterodimers to the chimeric operator disrupts recruitment of RNA polymerase to the -10 and -35 promoter elements, preventing transcription of the downstream reporter cassette (**Figure 15:** A). [219] [235] [236] [237] Subsequent introduction of a cyclic peptide inhibitor of the eIF4E / eIF4G interaction disrupts the heterodimer, preventing binding to the chimeric operator. The steric blockade of RNA polymerase is removed, facilitating expression of reporter cassette genes. The disruption of the eIF4E / eIF4G interaction within the SNS126 strain can therefore be linked to a kanamycin resistant, imidazole glycerol phosphate dehydratase positive and β-galactosidase positive phenotype, in the presence of IPTG.

9.5 Intein technology

Internal protein sequences (termed inteins) were first isolated from the vacuolar membrane proton ATPase of *Saccharomyces cerevisiae*. [274] [275] It was observed that a single unspliced mRNA of ~3500 bp encoded a protein, which exhibited amino acid sequence similarity to known homologues at the N (1-284) and C-termini (739-1071), but not within the central domain (285-738). It was therefore postulated that the intein central domain was post-translationally excised from the precursor protein with simultaneous ligation of the N and C-terminal protein segments (termed external proteins or exteins) to form the mature protein product (**Figure 16**). [274] [275] This phenomenon has since been observed in a range of proteins, including the DnaE intein of *Synechocystis sp. PCC6803* (termed the Ssp intein), which was utilized during this project. [276]

The pre and post-splicing crystal structures of the Ssp intein have been solved, revealing that the splicing mechanism consists of four distinct steps (**Figure 17**). [277] The first step is the rearrangement of the amide bond between Y_{-1} and C_1 at the N-terminal splice junction forming a thioester (**Figure 18:** A). [278] [279] [280] Interactions of the carbonyl group of this amide bond with intein residues R_{50} and D_{140} distort the trans conformation of the peptide bond, destabilizing the ground state (**Figure 18:** A). [277] [281] [282] T_{69} co-ordinates to the carbonyl group of C_1 of the N-intein to ensure optimal orientation of the thiol nucleophile, for attack on the amide bond at the N-terminal splice junction (**Figure 18:** A). [283] The second step of intein splicing is trans-thioesterification via attack of the thiol of C_{+1} of the C-extein on the thioester generated in step one (**Figure 18:** B). [278] [284] [279] [280]

[285] This results in the cleavage of the N-terminal splice junction and joining of the N-extein and C-extein via a thioester bond to generate a branched intermediate (**Figure 18:** C). [286] Resolution of the branched intermediate is the third step of intein splicing, which is promoted by H_{147}. H_{147} catalyzes nucleophillic attack of the γ amide of N_{159} on the amide bond of the C-terminal splice junction (**Figure 18:** C). [287] [277] [288] [279] [280] The oxyanion generated via this reaction is stabilized via interaction with R_{73}, prior to C-terminal cleavage of the scissile amide bond and formation of succinimide (**Figure 18:** D). [277] [278] Spontaneous re-arrangement of the thioester bond between the N and C-exteins to an amide yields the mature extein and constitutes the fourth and final step of intein splicing (**Figure 18:** E).

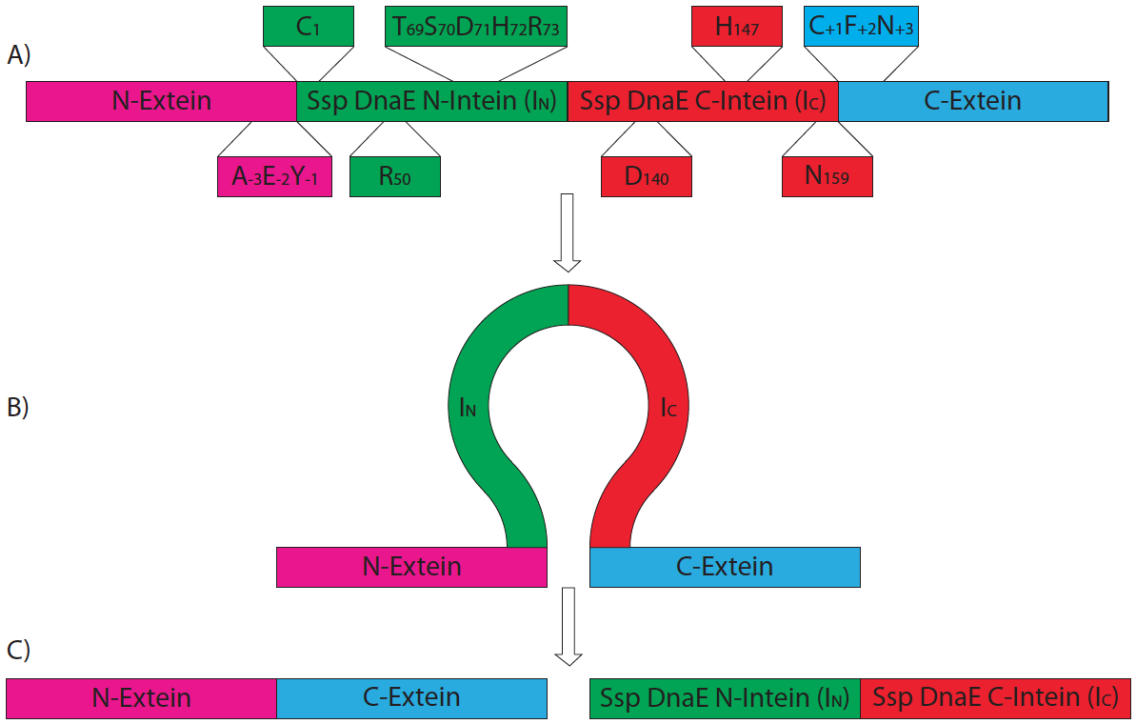

Figure 16: A) *Synechocystis sp. PCC6803* (Ssp) DnaE intein pre splicing construct, with catalytic N-intein (C_1, R_{50}, T_{69}, H_{72}, R_{73}) residues, catalytic C-intein (D_{140}, H_{147}, N_{159}) residues and optimal extein sequences (A_{-3}, E_{-2}, Y_{-1}, C_{+1}, F_{+2}, N_{+3}) highlighted. [276] [289] **B) Interaction of the Ssp N (I_N) and C-terminal (I_C) inteins forms the catalytic intein core. C) Intein splicing excises the mature intein (I_N-I_C) and simultaneously ligates the exteins to form the mature extein (N-extein-C-extein).** [276]

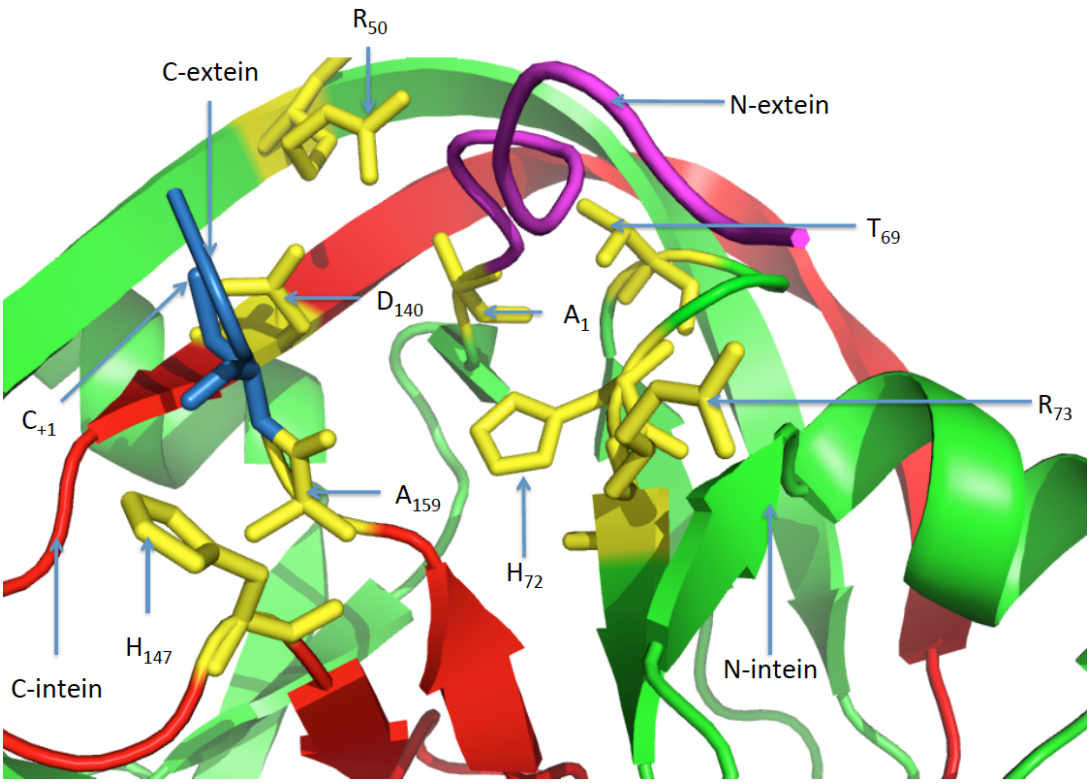

Figure 17: Crystal structure of *Synechocystis sp. PCC6803* (Ssp) DnaE intein pre-splicing construct, N-extein (magenta) / N-intein (green) / C-intein (red) / C-extein (blue) focused on the catalytic intein core. [277] Two point mutations (C1A and N159A) were introduced to block critical splicing residues to enable crystallization. [290] [288] Catalytic N-intein (A_1, R_{50}, T_{69}, H_{72}, R_{73}) and C-intein (D_{140}, H_{147}, A_{159}) residues are highlighted in yellow. (Adapted from Sun and Ye, PDB ID: 1ZDE). [277]

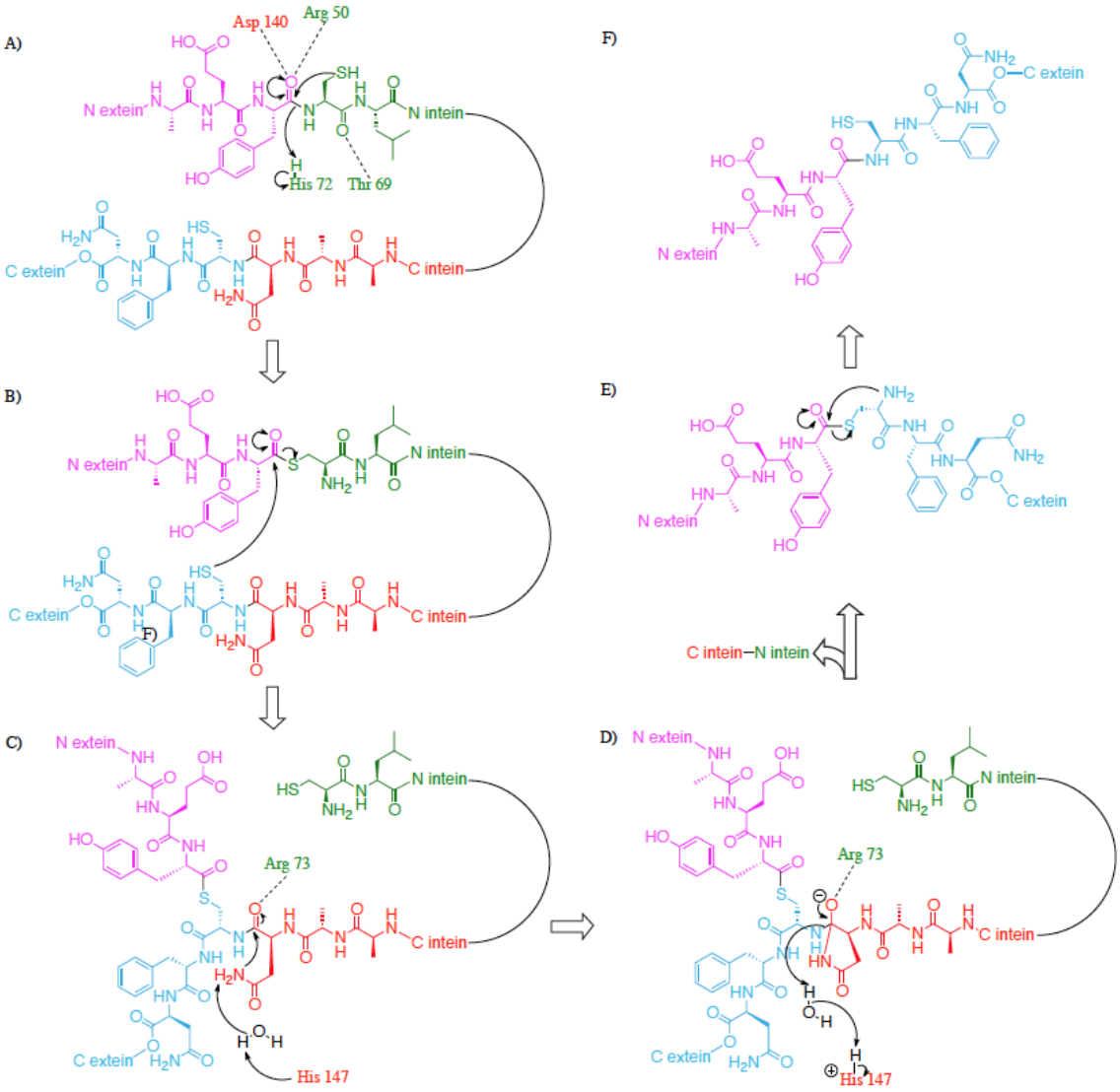

Figure 18: ***Synechocystis sp. PCC6803*** **(Ssp) DnaE intein splicing mechanism.** [277] **A) Thioester formation is catalyzed via co-ordination of key intein residues to N-terminal splice junction amide bonds.** [281] **B) Trans-thioesterification is mediated by the thiol of the C_{+1} residue of the C-extein. C) C-terminal cleavage is initiated by nucleophillic attack of the γ amide of N_{159} on the C-terminal splice junction, yielding a tetrahedral intermediate. D) Arg_{73} stabilizes the oxyanion hole of the tetrahedral intermediate in preparation for amide bond cleavage at the C-terminal splice junction. E) Succinimide formation at N_{159} drives release of the mature intein. F) Re-arrangement of the extein thioester bond to an amide is spontaneous, yielding the mature extein.**

9.6 SICLOPPS technology

Intein technology has subsequently been exploited for the *in vivo* generation of cyclic polypeptides from DNA encoded linear precursor proteins. Intein mediated peptide cyclization requires the use of artificially split inteins in an inverse cis configuration (**Figure 19**). [217 291] The C-terminal intein (I_C) is placed at the N-terminus of the peptide extein, which is C-terminally flanked by the N-terminal intein (I_N) within a single (cis) precursor protein (**Figure 19:** A). As such the inteins are at opposing ends of the pre-splicing construct (split) and in an inverse configuration (I_C at the extein N-terminus and I_N at the extein C-terminus). Resolution of this 'I_C-extein-I_N' pre-splicing construct proceeds via a thioester mediated mechanism (**Figure 20**) and yields split inteins and a cyclic peptide extein. Whilst the C_{+1} residue of the extein is a vital nucleophile for the transthioesterification step of intein splicing, the other extein residues do not participate in splicing. [217 291]

This prompted the development of SICLOPPS technology, which has been successfully employed to interrogate PPIs via screening against RTHSs in *E. coli*. [292] SICLOPPS employs a conserved C_{+1} (or S_{+1}) nucleophillic extein residue in tandem with a randomized extein region to generate a library of cyclic extein peptides.

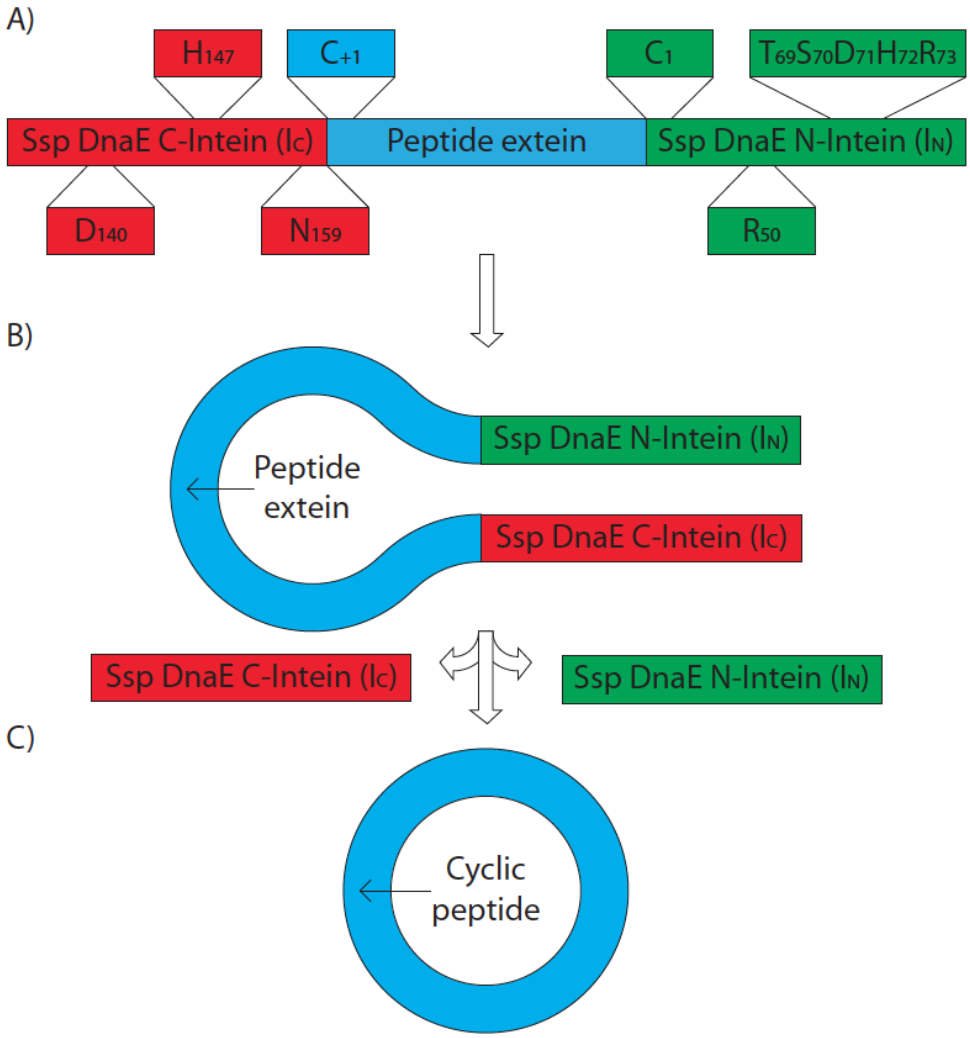

Figure 19: A) Split intein circularization of peptides and proteins (SICLOPPS) pre-splicing construct utilizing *Synechocystis sp. PCC6803* (Ssp) DnaE inteins in an inverse configuration. [217] [276] [291] [292] **B) Interaction of the Ssp N (I_N) and C-terminal (I_C) inteins forms the catalytic intein core. C) Intein splicing circularizes the peptide extein sequence between the inteins, to form the mature cyclic peptide.**

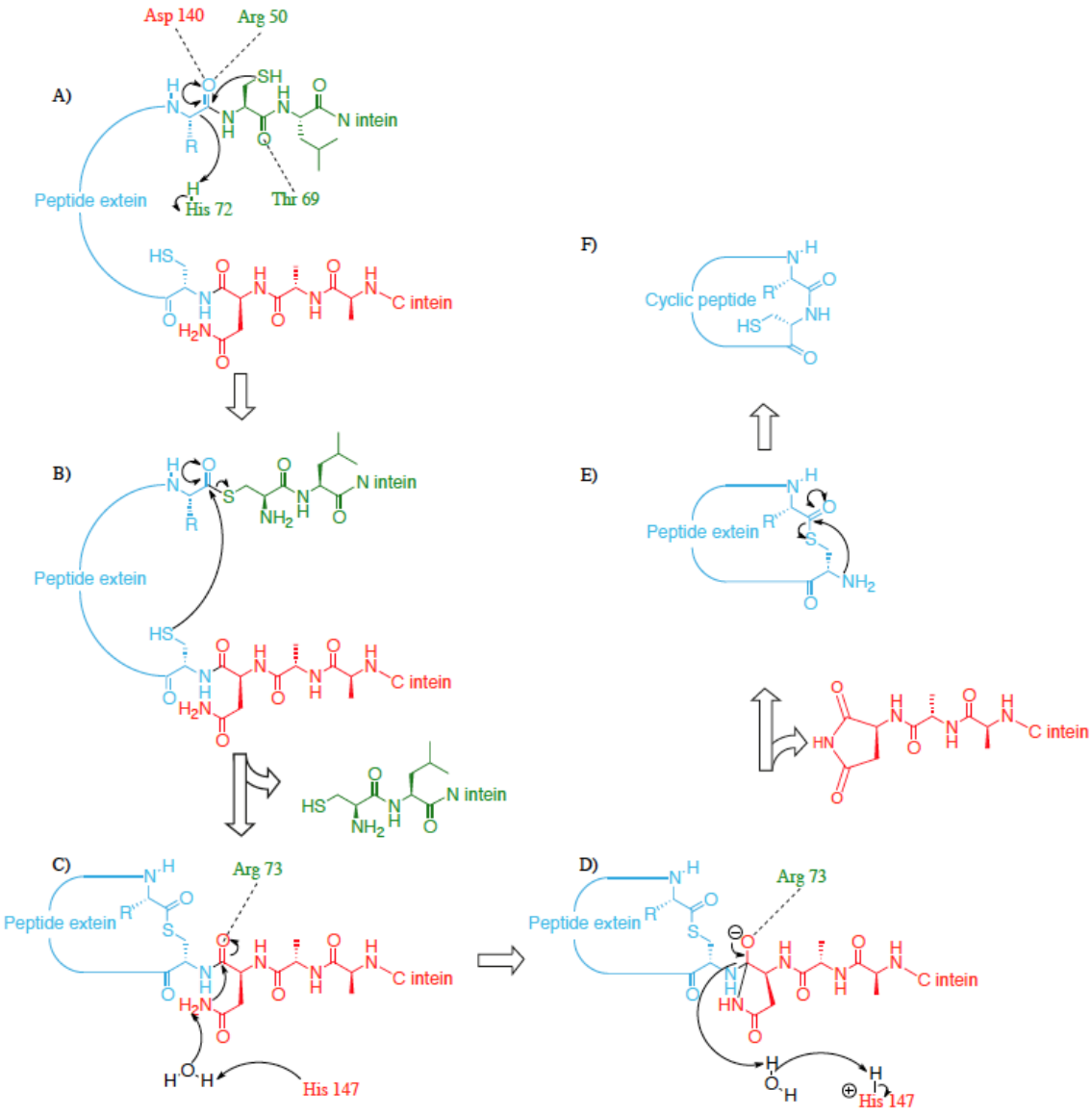

Figure 20: Split intein circularization of peptides and proteins (SICLOPPS) splicing mechanism. [217] [289] [293] **A) Thioester formation is catalyzed via co-ordination of key intein residues to C-terminal splice junction amide bonds. B) Trans-thioesterification is mediated by the thiol of the C_{+1} residue of the peptide extein. C) N-terminal cleavage is initiated by nucleophillic attack of the γ amide of N_{159} on the N-terminal splice junction, yielding a tetrahedral intermediate. D) Arg_{73} stabilizes the oxyanion hole of the tetrahedral intermediate in preparation for amide bond cleavage at the N-terminal splice junction. E) Succinimide formation at N_{159} drives release of the C-intein. F) Re-arrangement of the extein thioester bond to an amide is spontaneous, yielding the mature cyclic peptide extein.**

9.7 Solid phase peptide synthesis

The revolutionary concept of solid phase peptide synthesis (SPPS) was originally conceived by Merrifield in 1963 and has since been adapted to found the diverse field of solid phase organic synthesis. [294] SPPS utilizes an insoluble resin support, which is conjugated to a linker via a covalent bond. An α-amino protected (PG1) amino acid, with appropriate side-chain protecting groups (PG2) is then loaded via its C-terminus to the linker (**Figure 21:** A). The first step of SPPS is the selective deprotection of PG1 to liberate the free N-terminus of the immobilized peptide chain (**Figure 21:** B). The resin linker and PG2 must therefore be stable to the conditions used to remove PG1. SPPS therefore requires the use of two orthogonal sets of protecting groups that are labile to distinct reagents or conditions. The immobilization of the growing peptide chain to an insoluble resin support greatly simplifies the separation of PG1 deprotection reagents (via filtration) from the desired polypeptide. [295] The second step of SPPS is the coupling of an α-amino protected amino acid, with appropriate side-chain protecting groups to the free peptide N-terminus (**Figure 21:** C). Once again, both the resin linker and PG2, in addition to PG1 must be stable to coupling conditions. Amino acid coupling thus elongates the peptide chain by one residue in a C to N-terminal direction. Repeated cycles of PG1 deprotection, followed by amino acid coupling elongate the growing polypeptide chain (**Figure 21:** D). This process continues until the desired linear polypeptide sequence has been assembled on the insoluble resin, whereupon PG1 is deprotected to liberate the free peptide N-terminal amine (**Figure 21:** E). [294] The completed polypeptide is then cleaved from the linker with the simultaneous removal of all side-chain protecting groups (**Figure 21**: F).

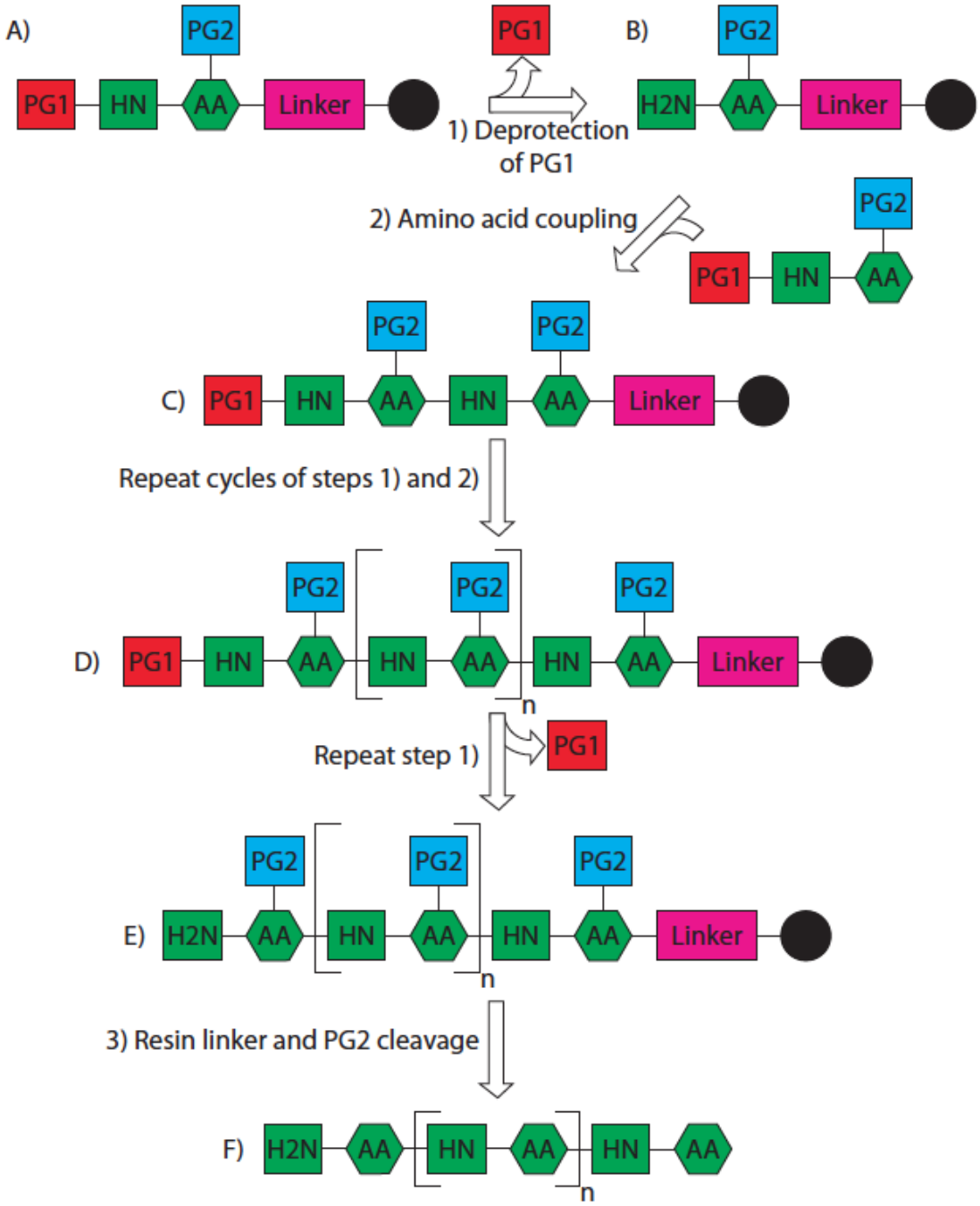

Figure 21: Schematic of solid phase peptide synthesis (SPPS). [294] [295] **A) An amino acid (AA) is loaded via its C-terminus to a resin (black circle) bound linker. B) The α-amino protecting group (PG1) is removed to liberate the free amine peptide N-terminus. C) and D) The polypeptide is elongated in a C to N-terminal direction via 'n' cycles of PG1 deprotection and amino acid coupling. E) The α-amino protecting group (PG1) is removed to liberate the free amine peptide N-terminus. F) The linear peptide is cleaved from the resin linker, with simultaneous cleavage of amino acid side-chain protecting groups (PG2).**

10 Results and discussion

10.1 Construction of the eIF4E / eIF4G RTHS

In order to construct a RTHS with a physiologically relevant eIF4E / eIF4G interaction, it was essential that fragments of both proteins were selected that accurately mimic the oncogenic PPI present within rapidly proliferating malignancies. The subsequent screening of cyclic peptide libraries against the eIF4E / eIF4G RTHS using SICLOPPS technology therefore facilitates the isolation of therapeutically relevant PPI inhibitors.

10.1.1 Selection of the eIF4E binding epitope of eIF4G

eIF4G functions as the primary scaffolding protein for both cap-dependent and cap-independent translation and as such interacts with a wide variety of binding partners. [136] [122] It is therefore not surprising that eIF4G is a large protein consisting of 1560 amino acids, with a combined molecular mass of 172 kilodaltons (kDa, **Figure 22**). [296] As a consequence, the length and complexity of the tertiary structure of the eIF4G (1-1560) protein hampers expression and folding in *E. coli*. [297] As a physiologically relevant interaction of eIF4E with eIF4G is reliant on the soluble expression of correctly folded proteins within *E. coli*; it became necessary to utilize a minimal eIF4E binding epitope of eIF4G for the construction of the RTHS. Translation has been shown to be suppressed within apoptotic cells, due to the Caspase 3 mediated formation of N-terminal (N-FAG), middle (M-FAG) and C-terminal (C-FAG) fragments of apoptotic cleavage of eIF4G (**Figure 23**). [297] M-FAG has been shown to retain interaction with eIF4E, eIF4A and eIF3, yet even this ~ 640 amino acid binding epitope still requires a Baculoviral host for effective protein expression. [297] Further experiments observed that the introduction of loss of function mutations into the eIF4A (672-970) and eIF3 (975-1078) binding sites of eIF4G had no effect on eIF4E association. [298] Based on these findings, a truncated M-FAG fragment, (**Figure 23:** RTHS fragment, 493-684) encompassing the two eIF4E binding epitopes was selected for RTHS construction. [163] [165] [299]

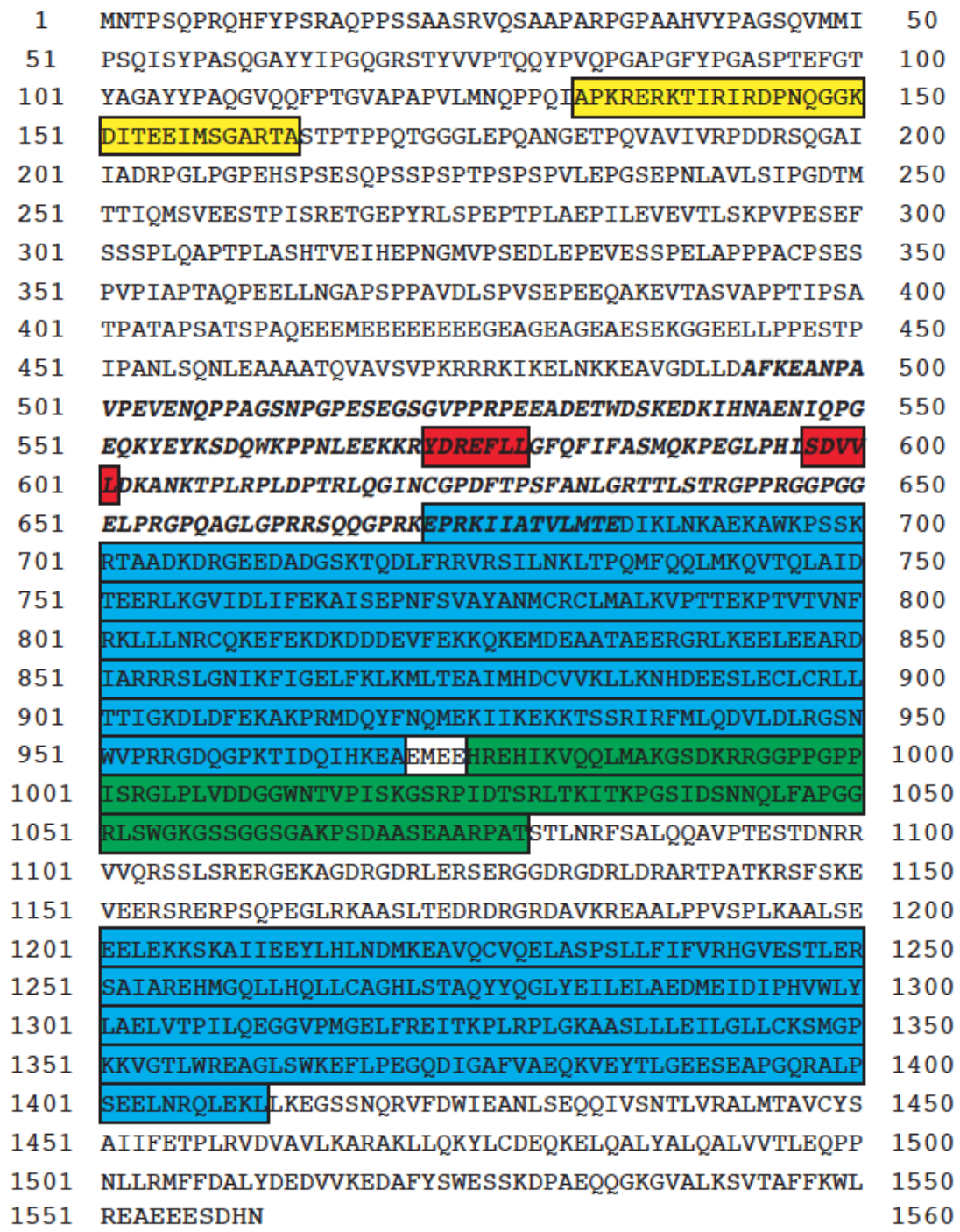

Figure 22: Primary amino acid sequence of eIF4GI 1-1560 (GenBank accession number: AF104913) based on the numbering system developed by Imataka and Sonenberg. [296] [300] [144] [145] **Minimal binding epitopes for PABP (yellow), eIF4E (red), eIF4A (blue) and eIF3 (green) are highlighted.** [163] [165] [299] [144] [145] [301] [164] [302] [146] [147] [139] **The C-terminal Mnk binding site of eIF4GI is poorly defined but is believed to reside between residues 884-1560.** [148] [303] **The eIF4G (493-684 inc.) fragment used for the construction of the RTHS is highlighted in bold italics.**

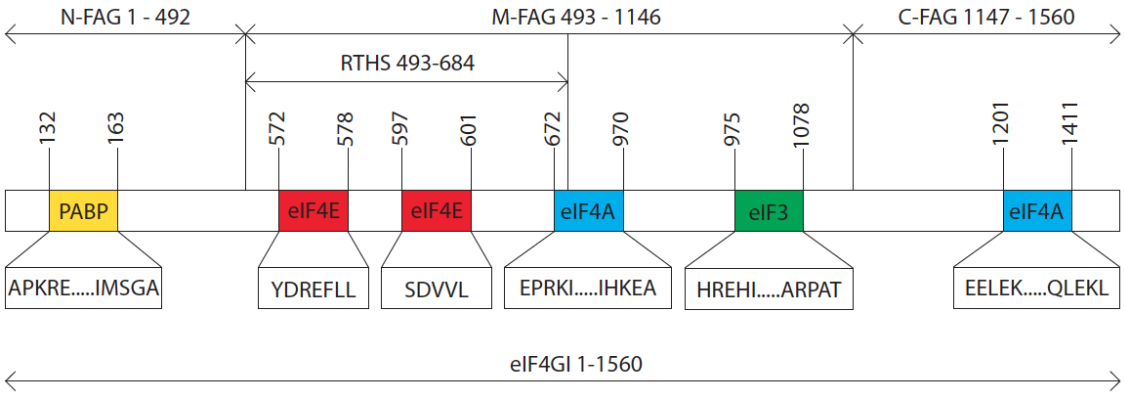

Figure 23: Schematic of the minimal protein binding domains of eIF4G. Numbering assignments for the amino acid sequence of eIF4GI 1-1560 (GenBank accession number: AF104913) are based on those developed by Imataka and Sonenberg. [296] [300] [144] [145] **The truncated Middle Fragment of Apoptotic cleavage of eIF4G1 (M-FAG) segment (containing both eIF4E binding epitopes, 493-684 inc.) that was used for the development of the eIF4E / eIF4G RTHS is indicated.** [297]

10.1.2 Selection of the eIF4G binding epitope of eIF4E

In contrast to eIF4G, eIF4E is a small protein consisting of 217 amino acids, with a molecular mass of 25 kDa and interacts with a very limited set of binding partners (eIF4G, 4EBPs and 4E-T). [139] [179] [167] As such, there is no published literature with regard to truncated variants of eIF4E that retain the capacity to bind eIF4G. However, there are several reports which claim that eIF4E can be expressed and purified directly via m7 GTP affinity chromatography from *E. coli*, [304] [305] suggesting correct folding of the cap binding protein in the bacterial environment. The entire human eIF4E sequence (1-217) was therefore selected for the construction of the RTHS (**Figure 24**).

The crystal structure of eIF4E has been solved with binding peptide epitopes of eIF4G and the 4EBPs, in addition to a range of helical peptide inhibitors of the eIF4E / eIF4G interaction. [164] [169] [170] [171] [172] [173] [174] A careful inspection of the interface (**Figure 25**) reveals interactions of the eIF4G helix with His_{37} and Pro_{38} within the N-terminus of eIF4E. The remainder of the N-terminus of eIF4E extends away from the interface and is largely disordered, providing the perfect flexible linker for fusion to the chimeric 'P22' repressor. [170]

```
  1   MATVEPETTPTPNPPTTEEEKTESNQEVANPEHYIKHPLQNRWALWFFKN  50
 51   DKSKTWQANLRLISKFDTVEDFWALYNHIQLSSNLMPGCDYSLFKDGIEP 100
101   MWEDEKNKRGGRWLITLNKQQRRSDLDRFWLETLLCLIGESFDDYSDDVC 150
151   GAVVNVRAKGDKIAIWTTECENREAVTHIGRVYKERLGLPPKIVIGYQSH 200
201   ADTATKSGSTTKNRFVV                                   217
```

Figure 24: Primary amino acid sequence of eIF4EI 1-217 (NCBI protein accession number: NP_001959.1) based on the numbering system developed by Rychlik and Domier. [158] [160] [306] Critical m7 GTP binding residues (Trp_{56}, Glu_{99}, Trp_{102}, Glu_{103}, Arg_{157}, Lys_{159} and Lys_{162}) are highlighted in yellow. Critical eIF4G / 4EBP / 4E-T binding residues (Tyr_{34}, His_{37}, Pro_{38}, Trp_{73}, Glu_{132} and Leu_{135}) are highlighted in red. Bold, italic sections represent the flexible loop ('YIKHPLQ') and the two helices of eIF4E responsible for binding to eIF4G / 4EBP / 4E-T. The entire eIF4E protein (1-217 inc.) was used for the construction of the RTHS.

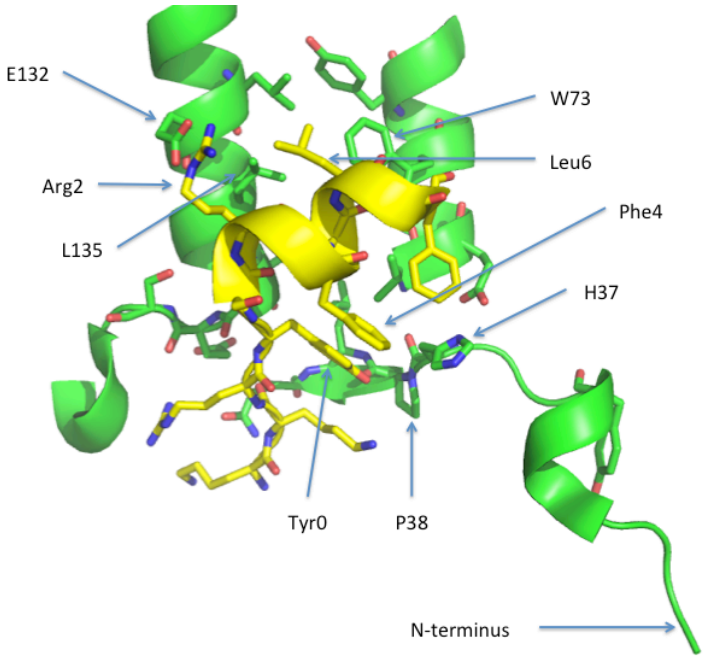

Figure 25: Interaction of eIF4E (green, residues labeled in single letter amino acid code) with binding fragment peptide derived from eIF4G (yellow, residues labeled in triplet amino acid code). The flexible N-terminus of eIF4E is clearly distant from the eIF4E / eIF4G interface. (Adapted from Zhou and Quah, PDB ID: 4AZA). [170]

10.1.3 Cloning of pTHCP14 eIF4E / eIF4G

The first requirement for the construction of the RTHS was the encoding of eIF4G (amino acids 493-684 inc.) and eIF4E (1-217 inc.) as fusion proteins, with the N-terminal DNA binding domains (amino acids 1-102 inc.) of 434 and the chimeric 'P22' repressor respectively. [244] [266] pTHCP14 (**Figure 26**) is a vector constructed by Horswill and Savinov that encodes the 434 and chimeric 'P22' repressors (1-102 inc.) at the N terminus of multiple cloning sites under the control of the mutant lactose / tryptophan operon promoter (PTac). [266] [269] The eIF4E (1-217) gene was amplified via the polymerase chain reaction (PCR), to introduce XhoI and KpnI restriction endonuclease (REN) sites and subsequently cloned into the pTHCP14 plasmid to generate a construct termed 'pTHCP14 eIF4E'. [307] [308] The eIF4G (493-684) gene was amplified via extension PCR to introduce SalI and SacI REN sites and subsequently cloned into 'pTHCP14 eIF4E' to generate a construct termed 'pTHCP14 eIF4E / eIF4G' (**Figure 27**).

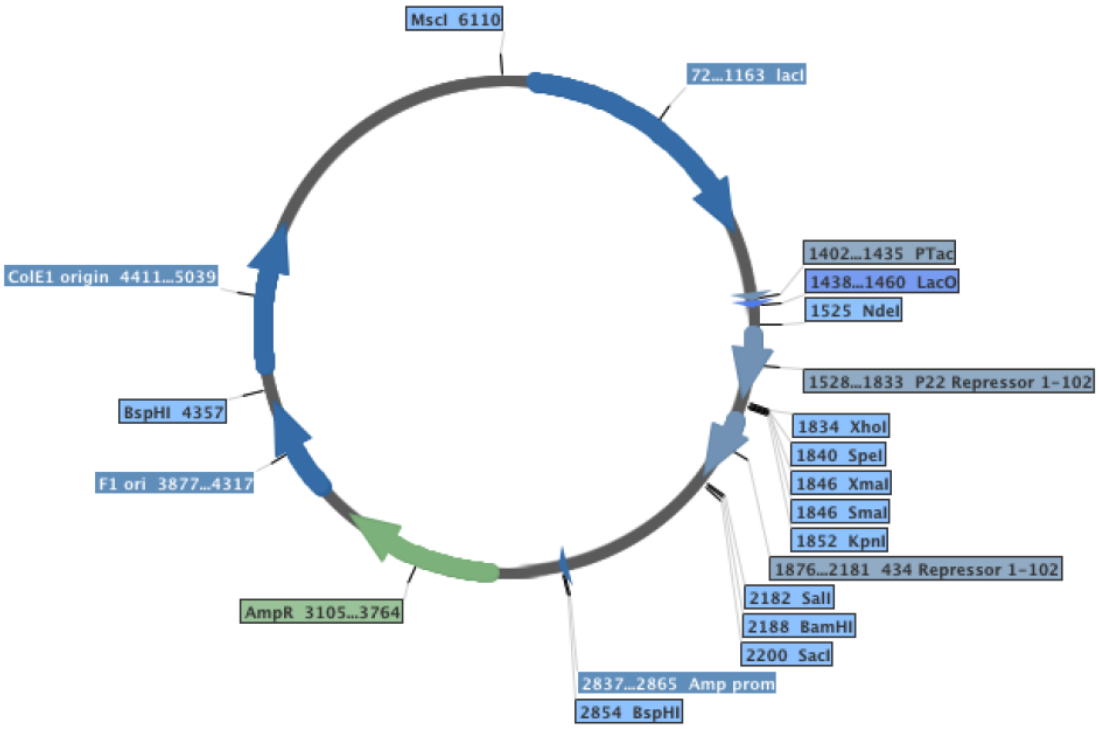

Figure 26: Schematic representation of pTHCP14. [266]

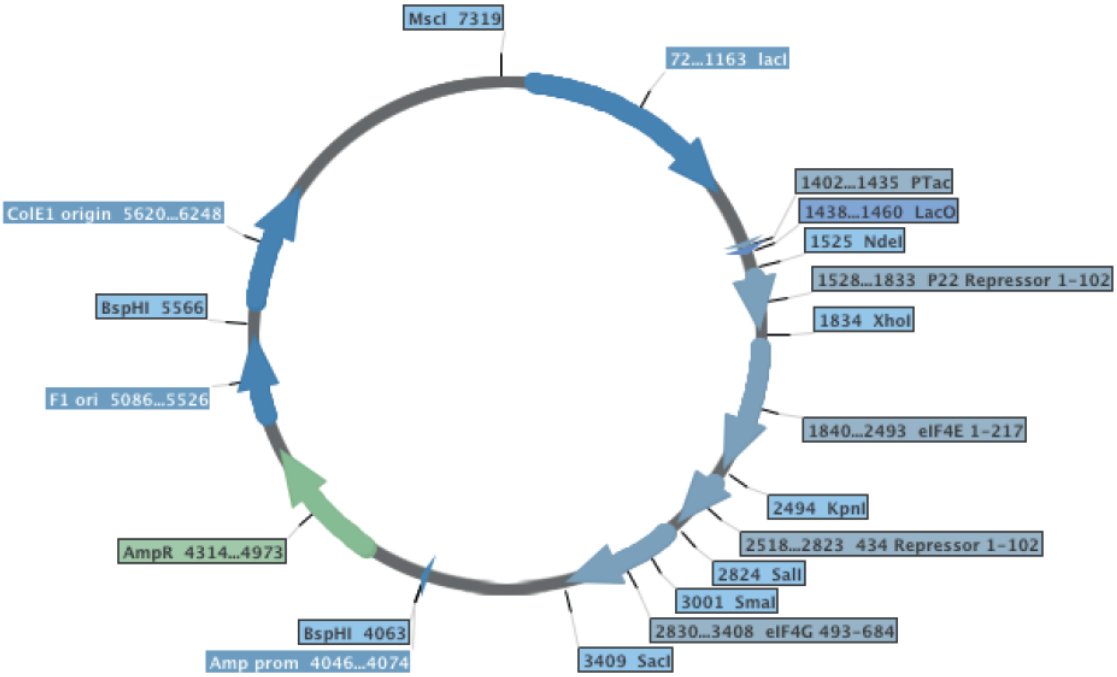

Figure 27: Schematic representation of pTHCP14 eIF4E / eIF4G. [266]

In order to perform qualitative screening of potential inhibitors of the eIF4E / eIF4G interaction, it is essential that the copy numbers of genes encoding the reporter cassette and the chimeric 434-eIF4G / 'P22'-eIF4E repressors are maintained at a constant level. Any variation in the ratio of reporter cassette to repressors between inhibitor candidate screens, could lead to bias. [309] To eliminate any plasmid copy number issues, it was necessary to integrate both the reporter cassette (present in the SNS126 strain) and the chimeric 'P22'-eIF4E / 434-eIF4G repressors into the bacterial chromosome to ensure a consistent ratio between screens. Integration of the chimeric 'P22'-eIF4E / 434-eIF4G repressor fusions into the HK022 site of the SNS126 chromosome was achieved via phage integrase mediated recombination. [310] This dictated the insertion of the PTac / 'P22'-eIF4E / 434-eIF4G construct into a conditional replication integration and modular (CRIM) pAH68 plasmid backbone, in preparation for integration to the HK022 bacterial attachment site (AttB) of SNS126. [272]

10.1.4 Cloning of pAH68 eIF4E / eIF4G

pAH68 (**Figure 28**) is an ampicillin resistant CRIM plasmid constructed by Haldimann and Wanner, which has a pir protein dependent origin of replication, oriVR6Kγ. [272] [311] [312] As such pAH68 is incapable of replication in a pir protein negative host strain such as SNS126, facilitating the selection of ampicillin resistant integrants. pAH68 contains a HK022 phage attachment site (AttP) that facilitates integration of the plasmid into the HK022 AttB in the SNS126 chromosome. [313] [314] pTHCP14 eIF4E / eIF4G was initially transformed into a DNA methylation negative strain of *E. coli* (GM2929). The plasmid was subsequently replicated in the GM2929 strain and extracted via mini-prep to provide non-methylated plasmid DNA that was compatible with MscI REN digestion. The PTac / 'P22'-eIF4E / 434-eIF4G construct was removed from pTHCP14 eIF4E / eIF4G via REN digestion with MscI / SacI / BspHI. The use of BspHI was necessary to cleave pTHCP14 in order to separate the PTac / 'P22'-eIF4E / 434-eIF4G insert from the pTHCP14 vector backbone. The PTac / 'P22'-eIF4E / 434-eIF4G insert was purified via agarose gel electrophoresis and subsequently cloned between the SmaI and SacI REN sites of pAH68 to generate 'pAH68 eIF4E / eIF4G' (**Figure 29**).

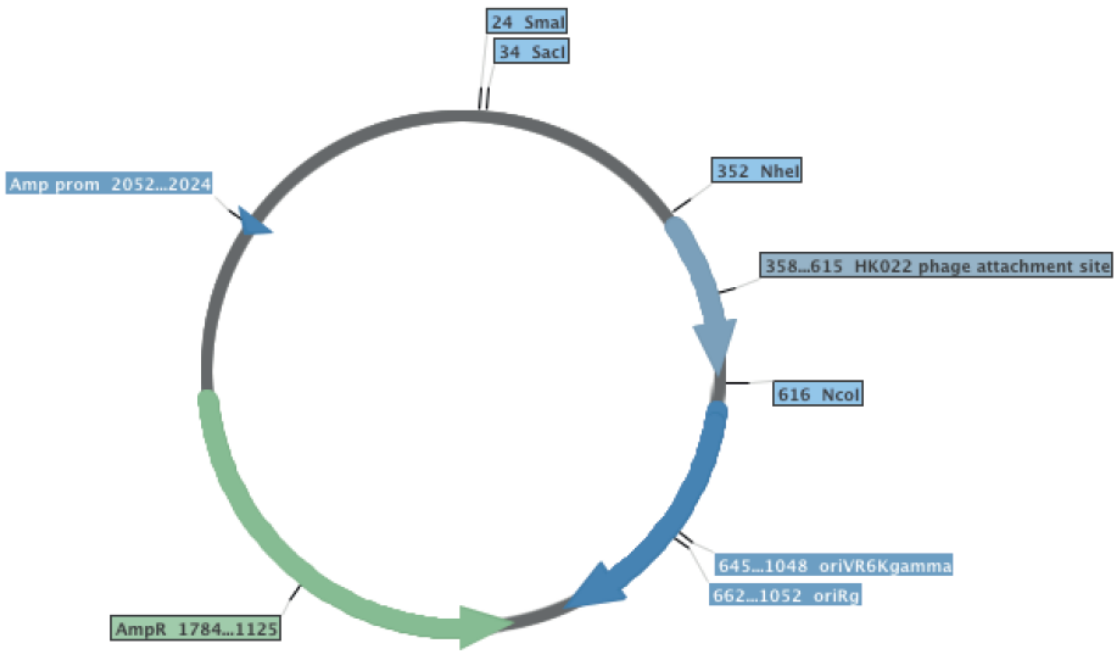

Figure 28: Schematic representation of pAH68. [272]

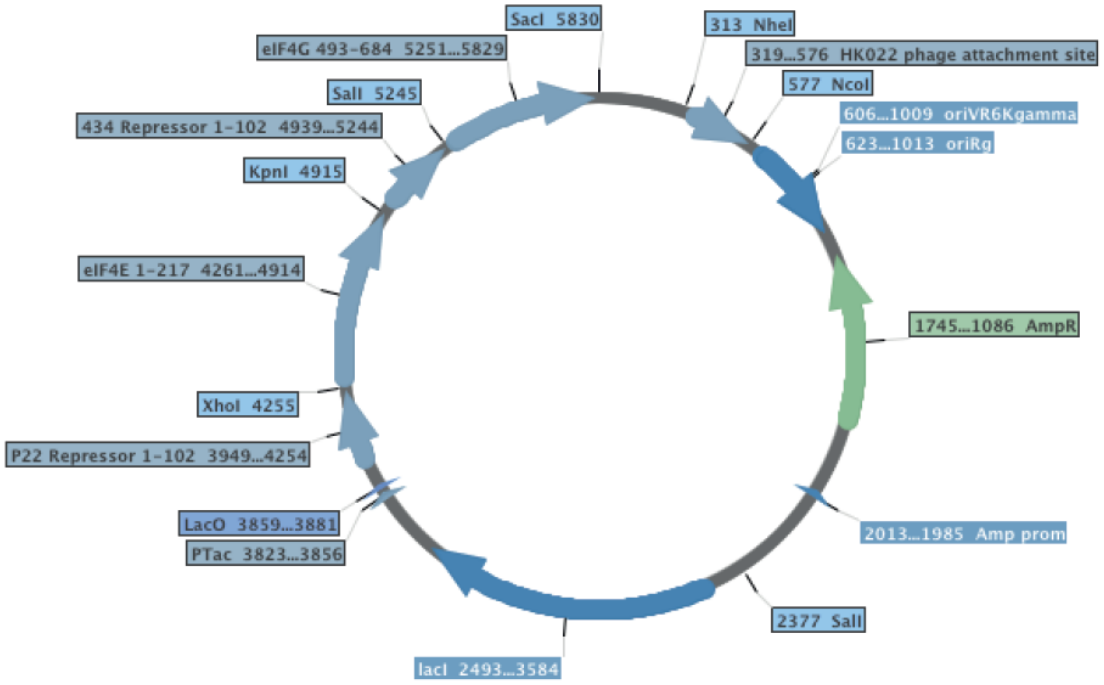

Figure 29: Schematic representation of pAH68 eIF4E / eIF4G. [272]

10.1.5 Integration of pAH68 eIF4E / eIF4G into the HK022 site of SNS126

Integration of CRIM plasmids into AttB requires the presence of phage integrase encoded on a so-called 'helper plasmid'. [272] Phage integrase introduces double stranded breaks in DNA, promotes Holliday junction formation and subsequently integration of the CRIM plasmid into the bacterial chromosome. [315]

In the case of pAH68, integration of the CRIM plasmid to the HK022 AttB requires HK022 phage integrase encoded by the helper plasmid pAH69 (**Figure 30**). [272] pAH69 expresses HK022 phage integrase from a P_R promoter under control of the temperature sensitive bacteriophage λ cI857 repressor. The repressor is active at 30 °C and suppresses transcription from the P_R promoter, but at 42 °C the cI857 repressor is thermally denatured and HK022 phage integrase expression is induced. [316] [317] The replication of pAH69 is also temperature dependent, via the use of the repA protein dependent origin of replication, oriR101. [318] [319] [320] RepA is stable at 30 °C, facilitating efficient replication of pAH69 when bacteria are cultured at low temperatures. Thermal denaturation of repA protein occurs at 42 °C, suppressing replication of pAH69 whilst simultaneously promoting expression of phage integrase from the P_R promoter. [316] The

oriR101 origin of replication of pAH69 therefore ensures that helper plasmids fail to replicate in cells expressing HK022 phage integrase. [320]

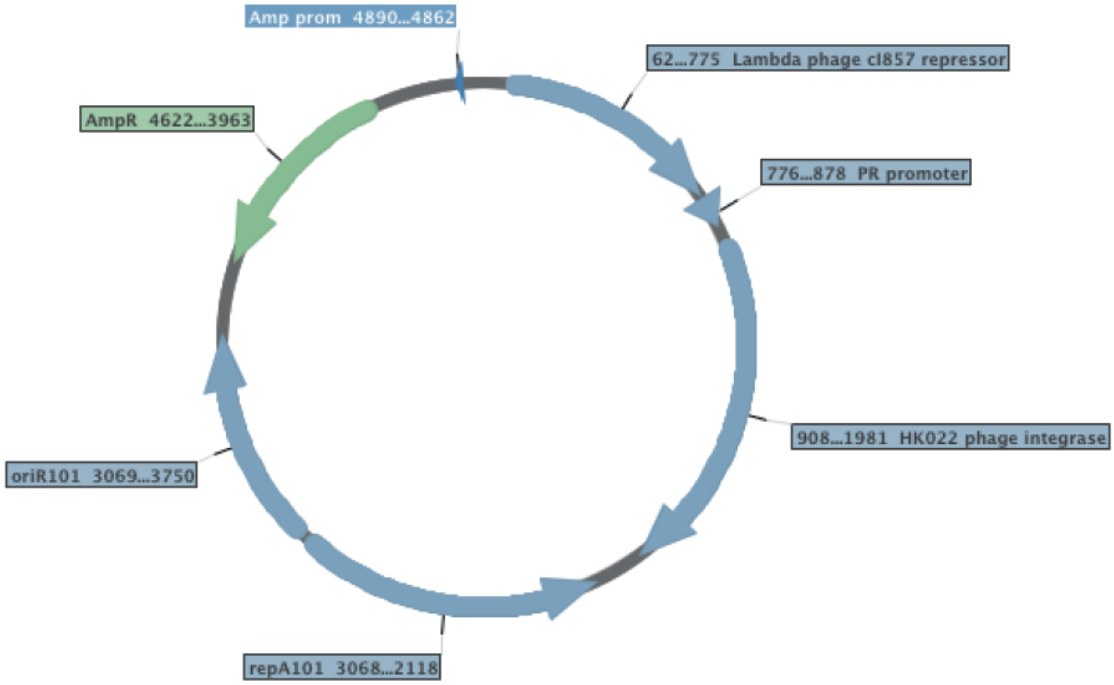

Figure 30: Schematic representation of the pAH69 helper plasmid expressing HK022 phage integrase. [272] [313]

In order to facilitate the integration of pAH68 eIF4E / eIF4G into the HK022 site of the SNS126 strain of *E. coli*, the pAH69 helper plasmid was transformed into SNS126 electro-competent cells. The transformation and plating of colonies was performed at 30 °C to maintain replication of pAH69 from the oriR101 origin of replication. pAH69 SNS126 electro-competent cells were prepared as outlined in experimental procedures to maximize integration frequency. pAH68 eIF4E / eIF4G was integrated into electro-competent SNS126 pAH69 cells via transformation as outlined in experimental procedures and then plated onto selective Luria Bertani (LB) agar plates with antibiotics at appropriate concentrations.

Phage integrase mediated recombination of pAH68 into the chromosome of SNS126 requires Holliday junction formation and therefore double-stranded cleavage of DNA. [315] As such, the frequency of single integration into the HK022 site was found to be limited and therefore required a high throughput method to identify desired single

integrants from multiple insertions of pAH68 eIF4E / eIF4G. The colony PCR methodology of Haldimann and Wanner with primers P1, P2, P3 and P4 (**Figure 31**, **Table 2**) was utilized to identify colonies with single integrations of pAH68 eIF4E / eIF4G into the HK022 site of SNS126. [272]

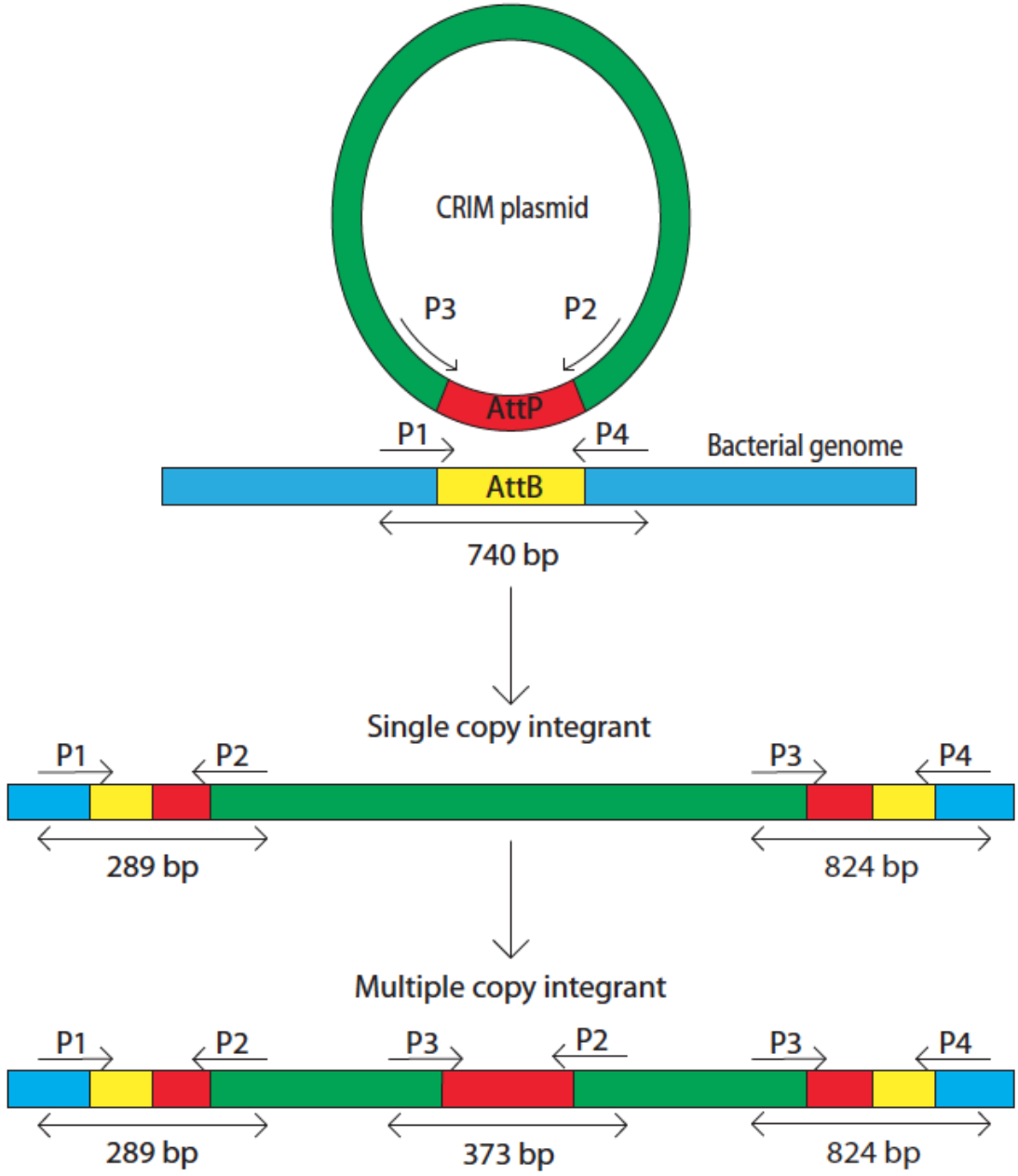

Figure 31: Schematic representation of the colony PCR strategy employed to select single copy CRIM plasmid integrants. [272] Abbreviations used: Phage attachment site (AttP), Bacterial attachment site (AttB). PCR amplicons P1-P2 (289 bp) and P3-P4 (824 bp) were indicative of single integration of pAH68 derivatives into the HK022 site of SNS126.

	Primer name	5' to 3' sequence
A)	eIF4E XhoI Fw	GTTGTTCTCGAGATGGCGACTGTCGAACCGGAAACC
B)	eIF4E KpnI Rev	GTTGTTGGTACCTTAAACAACAAACCTATTTTTAG
C)	eIF4G SalI Fw	GTTGTTGTCGACATGGCCTTCAAGGAGGCGAACC
D)	eIF4G SacI Rev	GTTGTTGAGCTCTCATTCGGTCATTAACACTGTG
1)	P1	GGAATCAATGCCTGAGTG
2)	P2	ACTTAACGGCTGACATGG
3)	P3	ACGAGTATCGAGATGGCA
4)	P4	GGCATCAACAGCACATTC

Table 2: Primers used for verification of single integration of pAH68 or pAH68 eIF4E / eIF4G into the HK022 site of SNS126. [272] **Restriction endonuclease (REN) sites (green), start and stop codons (blue) and regions complementary to genes of interest (red) are highlighted.**

E. coli colonies integrated with either pAH68 or pAH68 eIF4E / eIF4G were picked from selective LB agar plates and subjected to colony PCR alongside colonies of a positive control RTHS. PCR products were analyzed by agarose gel electrophoresis for DNA amplicons indicative of single integration into the HK022 site of SNS126. DNA amplicons of 289 base pairs (bp, P1-P2) and 824 bp (P3-P4) were indicative of single integration of a pAH68 derivative into the HK022 site of SNS126 (**Figure 31**). By contrast, PCR amplicons of 740 bp (P1-P4) were observed for SNS126 colonies that had failed to integrate a pAH68 derivative. If multiple integration of the pAH68 derivative into the HK022 site of SNS126 occurred, then the 373 bp (P2-P3) amplicon was observed in addition to the previously described P1-P2 and P3-P4 amplicons. [272]

Integration of the pAH68 parent vector into the HK022 site of SNS126 was performed in parallel with the integration of pAH68 eIF4E / eIF4G, to provide a comparison of integration efficiency (**Figure 32**). A previously constructed RTHS generated within the Tavassoli lab was plated in tandem to provide a positive control for colony PCR (**Figure 32:** lane 1). The integration efficiency of the parent pAH68 vector into the HK022 site of the SNS126 strain was found to be superior to that of pAH68 eIF4E / eIF4G. Despite the reduced integration efficiency of pAH68 eIF4E / eIF4G relative to

its parent vector; colonies were identified that yielded the P1-P2 and P3-P4 PCR amplicons, indicative of single integration into the HK022 site of SNS126 (**Figure 33**). Colonies that expressed the P1-P2 and P3-P4 PCR amplicons were subjected to a further round of colony PCR to confirm the presence of eIF4E (1-217) and eIF4G (493-684) genes. Primer pairs A / B (**Table 2**, to detect eIF4E) and C / D (**Table 2**, to detect eIF4G) were used for colony PCR of potential eIF4E / eIF4G RTHS colonies. All colonies that expressed P1-P2 and P3-P4 colony PCR amplicons also exhibited A-B (666 bp) and C-D (591 bp) colony PCR amplicons, consistent with single integration of pAH68 eIF4E / eIF4G into the HK022 site of SNS126 (**Figure 34**). Five colonies were selected that provided the correct P1-P2, P3-P4, A-B and C-D amplicons indicative of successful integration and were subsequently validated via drop spotting and β-galactosidase assay. [321] [322]

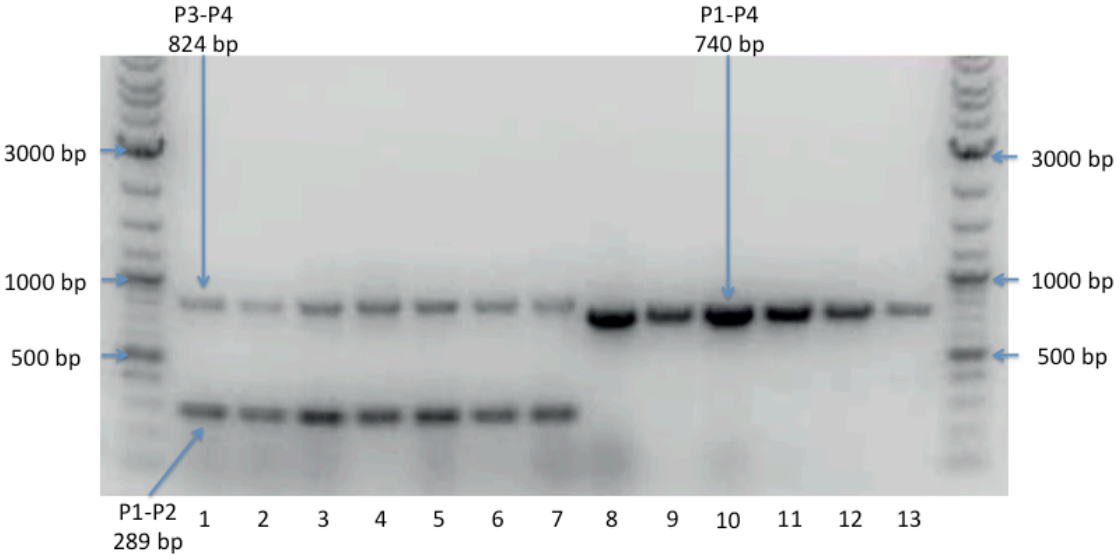

Figure 32: Agarose gel electrophoresis of colony PCR performed with primers P1, P2, P3 and P4 on potential pAH68 integrants into the HK022 site of the SNS126 strain. A previously constructed RTHS from the Tavassoli lab was used as a positive control for integration (lane 1) and analyzed alongside potential integrants. PCR products were separated on a 1 % (w:v) gel against a 2-Log DNA ladder, New England biolabs (NEB, N3200L). Single pAH68 integrants are visible (lanes 2-6 inc.), alongside failed integrations of pAH68 eIF4E / eIF4G (lanes 8-13 inc.) that display the characteristic 740 bp P1-P4 amplicon of SNS126.

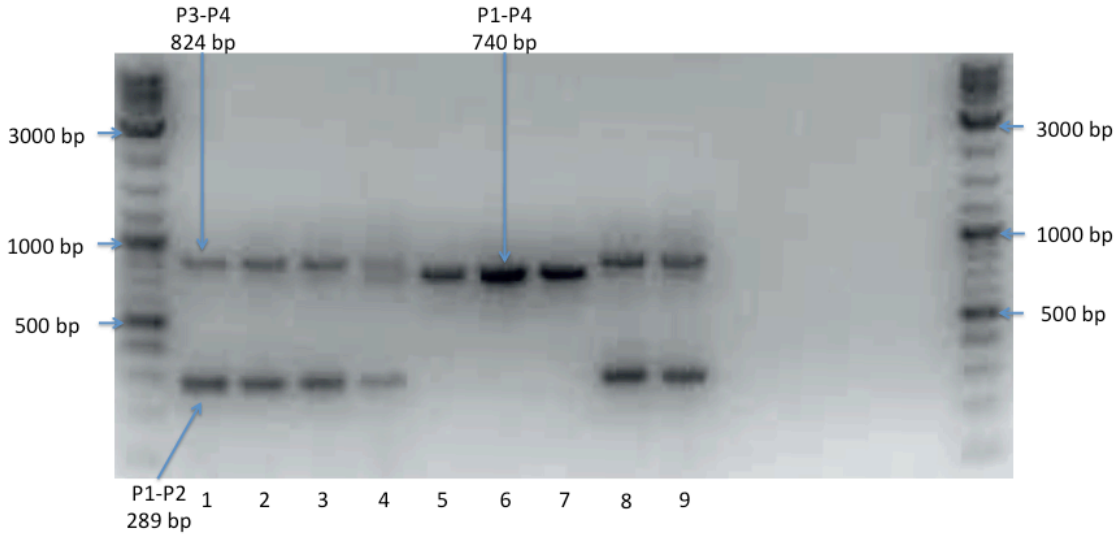

Figure 33: Agarose gel electrophoresis of colony PCR performed with primers P1, P2, P3 and P4 on potential pAH68 eIF4E / eIF4G integrants into the HK022 site of the SNS126 strain. A previously constructed RTHS from the Tavassoli lab was used as a positive control for integration (lane 1) and analyzed alongside potential integrants. PCR products were separated on a 1 % (w:v) gel against a 2-Log DNA ladder (NEB, N3200L). Single pAH68 eIF4E / eIF4G integrants are visible (lanes 2, 3, 8 and 9), a multiple pAH68 eIF4E / eIF4G integrant (lane 4), alongside failed integrations of pAH68 eIF4E / eIF4G (lanes 5-7 inc.) that display the characteristic ~740 bp P1-P4 amplicon of SNS126.

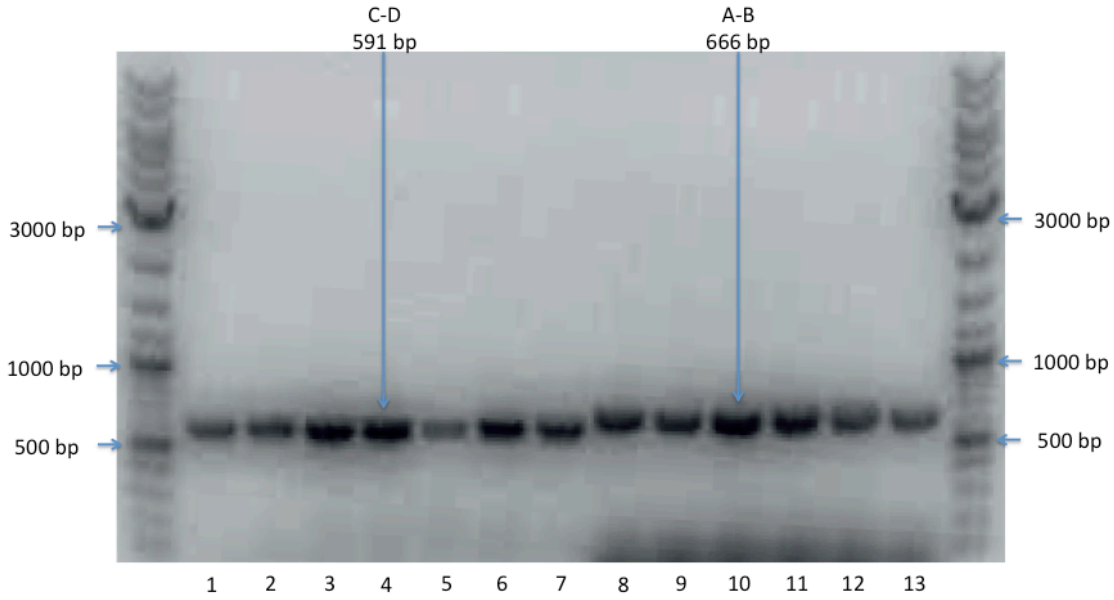

Figure 34: Agarose gel electrophoresis of colony PCR performed with primer pairs A / B (for eIF4E) and C / D (for eIF4G) on potential pAH68 eIF4E / eIF4G integrants into the HK022 site of the SNS126 strain. PCR products were separated on a 1 % (w:v) gel against a 2-Log DNA ladder (NEB, N3200L). All colonies tested produced A-B (666 bp, lanes 8-13 inc.) and C-D (591 bp, lanes 1-7 inc.) PCR amplicons indicative of the presence of eIF4E and eIF4G genes.

10.2 Validation of the eIF4E / eIF4G RTHS

Prior to screening potential inhibitors of the eIF4E / eIF4G interaction, it was first necessary to verify that a functional eIF4E / eIF4G interaction existed within the RTHS. A functional interaction of eIF4E with eIF4G and subsequent re-constitution of the DNA binding capability of the 434 / 'P22' heterodimeric repressor (**Figure 35:** A) was necessary to facilitate screening of potential heterodimerization inhibitors (**Figure 35:** B). This was achieved via two functional assays designed to determine the relative transcription of the reporter cassette in the presence of IPTG induced expression of 434-eIF4G and 'P22'-eIF4E from the PTac promoter. [269] [323]

It was hypothesized that as IPTG concentration was incrementally increased, expression of 434-eIF4G and 'P22'-eIF4E within the eIF4E / eIF4G RTHS would be stimulated. This would cause increased repressor binding to the chimeric operator, resulting in dose dependent shutdown of growth of the eIF4E / eIF4G RTHS. Binding of the

heterodimeric repressor to the operator would inhibit binding of RNA polymerase to the -10 and -35 promoter elements, yielding reduced expression from the *His-3*, *Kan* and *LacZ* genes of the reporter construct (**Figure 35:** A). Therefore it was hypothesized that increasing IPTG concentration would reduce histidine biosynthesis rates, kanamycin resistance and β-galactosidase expression of the eIF4E / eIF4G RTHS.

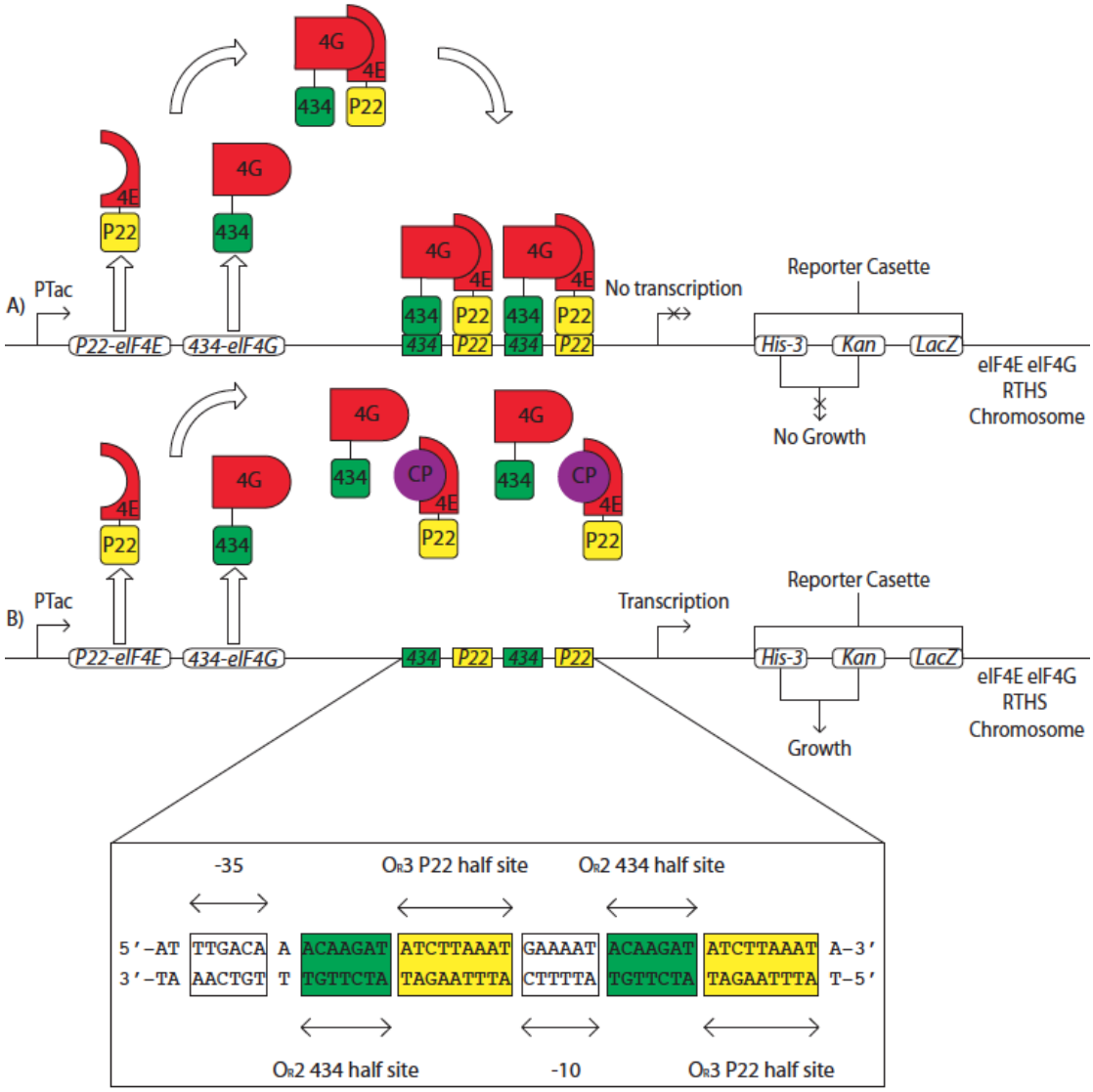

Figure 35: Schematic of the eIF4E / eIF4G RTHS. Abbreviations used: 'P22' chimeric bacteriophage 434 repressor with P22 operator binding specificity (P22), bacteriophage 434 repressor protein (434), cyclic peptide inhibitor of the eIF4E / eIF4G interaction (CP), imidazole glycerol phosphate dehydratase gene (*His-3*), neomycin phosphotransferase II gene (*Kan*), β-galactosidase gene (*LacZ*), mutant promoter of the lactose / tryptophan operon (PTac). [267] [268] [269]

10.2.1 Minimal media drop spotting of the eIF4E / eIF4G RTHS

This assay aimed to quantify the expression of imidazole glycerol phosphate dehydratase from the *His-3* gene and neomycin phosphotransferase II from the *Kan* gene of the reporter cassette. It was hypothesized that increasing IPTG concentration would stimulate increased binding of the heterodimeric repressor to the chimeric operator, with the concomitant reduction in histidine biosynthesis rates and kanamycin resistance. In order to test this hypothesis, the growth of the eIF4E / eIF4G RTHS on histidine deficient media was compared against a negative control (SNS126 pAH69) and the previously constructed positive control (C-terminal binding protein (CtBP) RTHS), in the presence of kanamycin. [321]

The eIF4E / eIF4G RTHS was cultured in parallel with positive and negative controls in Luria Bertani (LB) media with appropriate antibiotics for 16 hours (h). *E. coli* cultures were serially diluted via the addition of 180 μl of 10 % (v:v) sterile aqueous glycerol to 20 μl of culture. This process was repeated for each strain to give solutions corresponding to 10^{-1}, 10^{-2}, 10^{-3}, 10^{-4}, 10^{-5} and 10^{-6} dilutions of the *E. coli* cultures. 2.5 μl of each serial dilution was then drop-spotted onto minimal media agar plates with varying concentrations of carbenicillin, spectinomycin, kanamycin and IPTG. A competitive inhibitor of imidazole glycerol phosphate dehydratase, 3-amino triazole (3-AT), was also added in varying concentrations to the minimal media plates to improve the stringency of selection against the *His-3* gene of the reporter cassette. [324] Minimal media agar plates were incubated at 30 °C (to maintain pAH69 plasmid) for 66 h and the resulting drop spotting visualized. After several rounds of drop spotting incorporating 50 μg / ml carbenicillin and 25 μg / ml spectinomycin into the minimal media plates, no outgrowth of the eIF4E / eIF4G RTHS could be achieved, even in the absence of IPTG, kanamycin and 3-AT. Drop spotting of colonies onto minimal media with 50 μg / ml carbenicllin alone was performed the results compared to minimal media with 25 μg / ml spectinomycin alone. A comparison of the two plate sets (**Figure 36:** plate 6 vs **Figure 37:** plate 6) clearly revealed that the eIF4E / eIF4G RTHS was carbenicillin intolerant, which is unexpected due to the β-Lactamase gene encoded on the integrated pAH68 eIF4E / eIF4G vector.

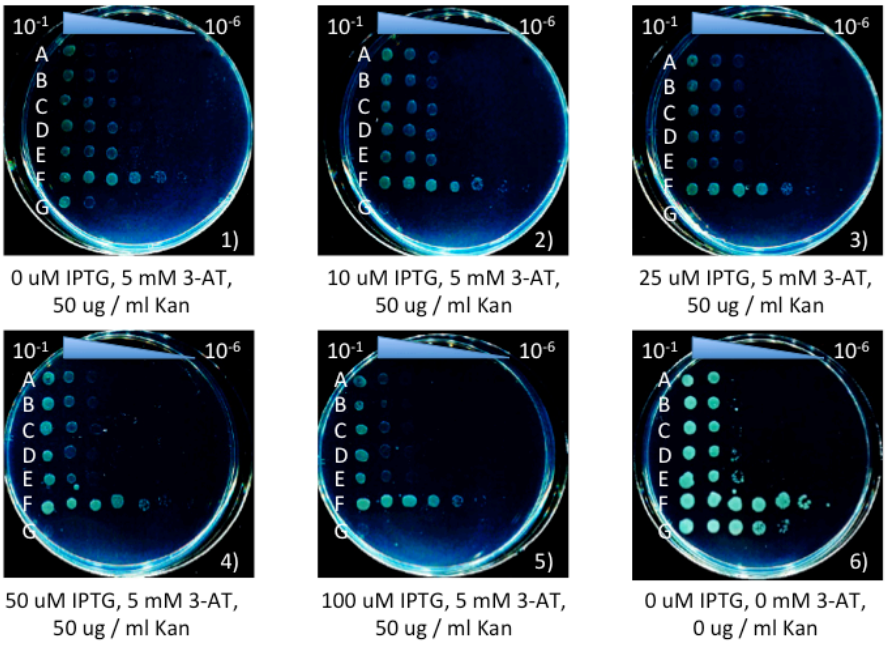

Figure 36: Drop spotting of serial dilutions of the eIF4E / eIF4G RTHS (A-E inc.) against the SNS126 pAH69 (F) negative and CtBP RTHS positive (G) controls on minimal media with 50 μg / ml carbenicillin and 0 μg / ml spectinomycin.

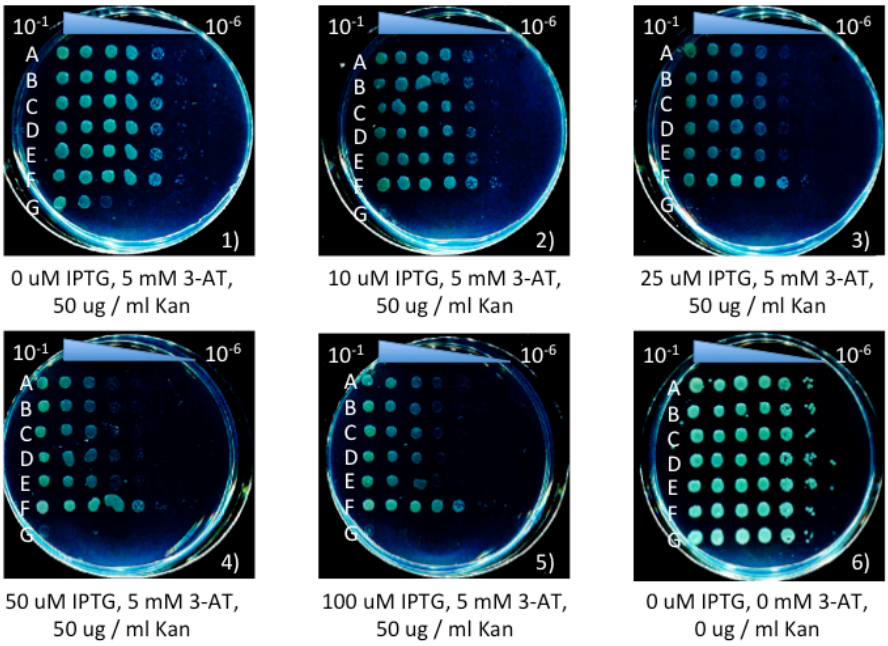

Figure 37: Drop spotting of serial dilutions of the eIF4E / eIF4G RTHS (A-E inc.) against the SNS126 pAH69 (F) negative and CtBP RTHS positive (G) controls on minimal media with 0 μg / ml carbenicillin and 25 μg /ml spectinomycin.

Carbenicillin was therefore removed from all future drop spotting, to facilitate visualization of the effect of IPTG on bacterial growth. Drop spotting of colonies on minimal media with 25 μg / ml spectinomycin (but without carbenicillin) revealed repression of growth of the eIF4E / eIF4G RTHS with increasing concentrations of IPTG (compare **Figure 37** plate 1 vs plate 4). This is consistent with the hypothesis that greater induction of 434-eIF4G and 'P22'-eIF4E repressor fusions inhibits expression of critical survival genes within the reporter cassette.

10.2.2 β-galactosidase assay of the eIF4E / eIF4G RTHS

This assay aimed to quantify the expression of β-galactosidase from the *LacZ* gene of the reporter cassette. [325] It was hypothesized that as IPTG concentration was incrementally increased, expression of 434-eIF4G and 'P22'-eIF4E would be stimulated, causing increased repressor binding to the chimeric operator. Binding of the heterodimeric repressor to the operator would inhibit binding of RNA polymerase to the -10 and -35 promoter elements, yielding reduced expression from the *LacZ* gene of the reporter construct. [266] In order to test this hypothesis, the β-galactosidase activity of the eIF4E / eIF4G RTHS was compared against a negative control (SNS126 pAH69) and the previously constructed positive control (CtBP RTHS). A synthetic substrate, Ortho-nitrophenyl-β-Galactoside (ONPG) was utilized, which is enzymatically hydrolyzed into galactose and the brightly coloured Ortho-nitrophenol chromophore by β-galactosidase (**Figure 38**). [322]

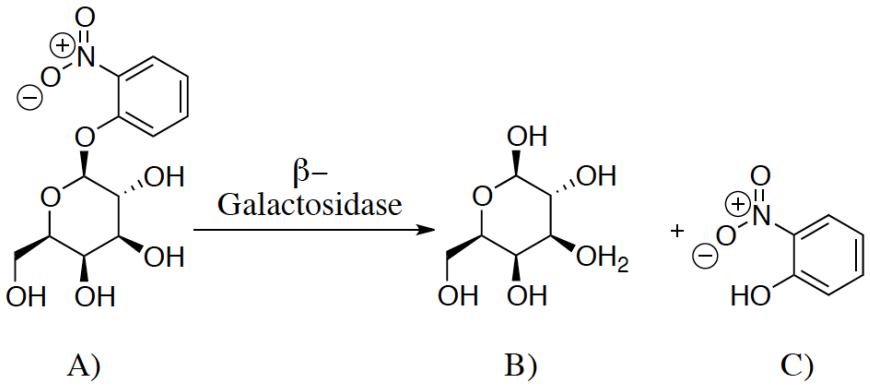

Figure 38: β-galactosidase assay utilizes the synthetic Ortho-nitrophenyl-β-Galactoside (ONPG) substrate (A), which is hydrolyzed to produce Galactose (B) and Ortho-nitrophenol (C).

The eIF4E / eIF4G RTHS was cultured in parallel with a positive control (CtBP RTHS) and a negative control (pAH69 SNS126) in LB media with appropriate antibiotics for 16 h. *E. coli* cultures were used to inoculate LB media containing appropriate antibiotics, which was then incubated at 30 °C until OD_{600} ~ 0.40 was reached. Triplicate cultures of all strains were then induced with IPTG (0, 10, 25, 50, 100 and 250 μM) to promote dose dependent expression of repressor protein fusions. All cultures were grown to OD_{600} ~ 0.70 and the expression of β-galactosidase was quantified via a timed ONPG assay. OD_{420} (λ_{max} of ortho-nitrophenol) and OD_{600} readings were recorded relative to an LB media alone blank and β-galactosidase activity was determined according to the Miller relationship below: [322]

$$\beta\text{-galactosidase activity} = \frac{1000 \times OD_{420}}{(\text{Reaction time} \times \text{Culture volume} \times OD_{600})}$$

The CtBP RTHS positive control exhibited significant dependence of β-galactosidase activity on IPTG concentration (**Figure 39**). This is consistent with incremental IPTG induced expression of repressor fusion proteins, dimerization and subsequent operator binding. The recruitment of RNA polymerase to the promoter is sterically hindered resulting in suppression of downstream reporter cassette gene expression. The incremental activation of repressor fusion protein expression is also consistent with the gradual decrease of the β-galactosidase activity of the CtBP RTHS with increasing IPTG concentration.

Similarly the pAH69 SNS126 negative control failed to exhibit significant dependence of β-galactosidase activity on IPTG concentration (**Figure 40**), as expected. This is consistent with the lack of heterodimeric 434 and 'P22' repressors within the HK022 site of the SNS126 strain, resulting in the efficient recruitment of RNA polymerase to the chimeric promoter and subsequent expression of downstream reporter cassette genes.

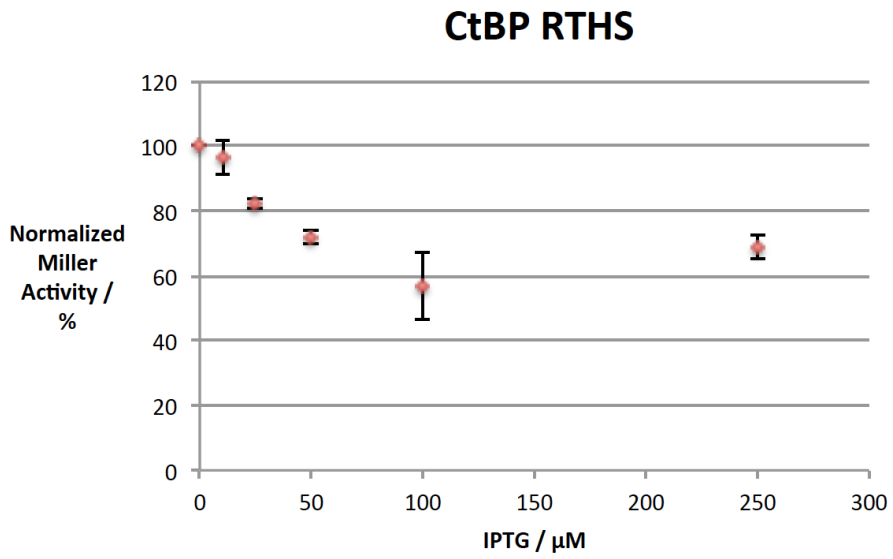

Figure 39: β-galactosidase assay performed as a positive control against the C-terminal binding protein (CtBP) RTHS. β-galactosidase activities are normalized relative to a CtBP RTHS culture that was not induced with IPTG. Error bars are representative +/- one standard deviation of the means of two independent experiments.

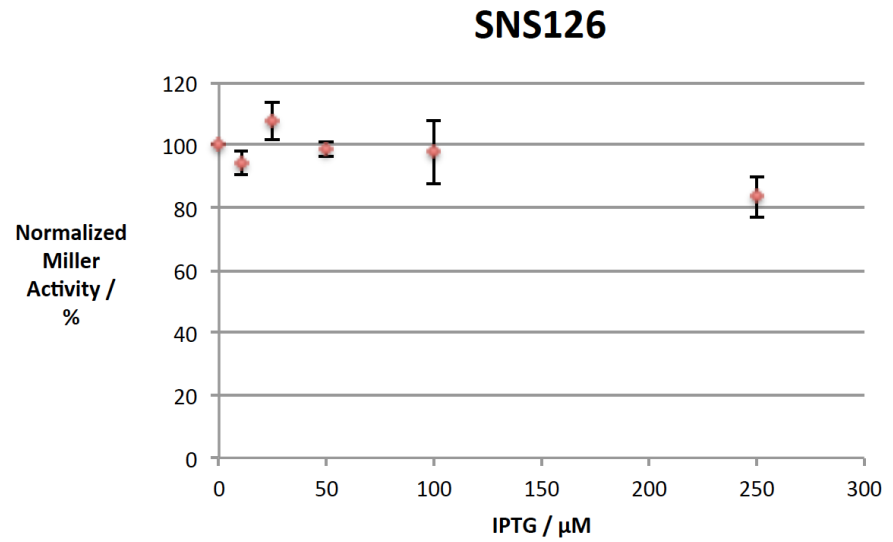

Figure 40: β-galactosidase assay performed as a negative control against the heterodimeric RTHS parent strain, SNS126. β-galactosidase activities are normalized relative to an SNS126 culture that was not induced with IPTG. Error bars are representative +/- one standard deviation of the means of two independent experiments.

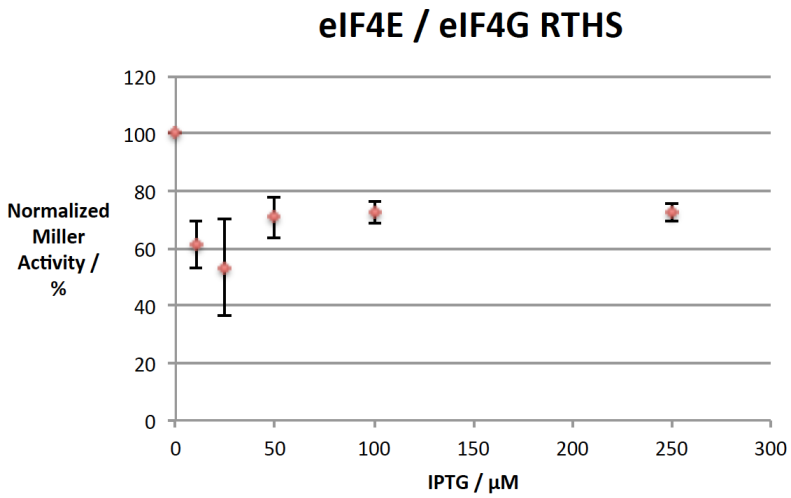

Figure 41: β-galactosidase assay performed against the eIF4E / eIF4G RTHS. β-galactosidase activities are normalized relative to an eIF4E / eIF4G RTHS culture that was not induced with IPTG. Error bars are representative +/- one standard deviation of the means of two independent experiments.

The expression of β-galactosidase within the eIF4E / eIF4G RTHS did not conform exactly to that of either the positive or negative controls (**Figure 41**). Between zero and 25 μM IPTG induction the expected trend of decreasing β-galactosidase expression was observed, consistent with increased expression and heterodimerization of 434-eIF4G and 'P22'-eIF4E repressors. This finding is also consistent with the apparent reduction of colony viability on minimal media in the presence of Kanamycin and 3-AT (**Figure 37**) with increasing IPTG concentration. The expression of β-galactosidase from the eIF4E / eIF4G RTHS unexpectedly plateaued above 25 μM IPTG, at around 70 % of the level of the non-induced system. This finding may be attributed to aggregation of eukaryotic proteins when overexpressed within the RTHS, which would lead to ineffective repressor construct binding to the chimeric operator. However, the suppression of β-galactosidase expression was comparable between the eIF4E / eIF4G RTHS and the CtBP RTHS when repressor protein fusions were induced with 50 μM IPTG. This finding is in agreement with the degree of suppression of colony viability on minimal media in the presence of 50 μM IPTG, when compared to the absence of IPTG (**Figure 37**). Drop spotting of the eIF4E / eIF4G RTHS onto minimal media containing 25 μg /ml spectinomycin, 50 μg / ml kanamycin, 5 mM 3-AT and 50 μM IPTG was therefore deemed an appropriate set of conditions for screening inhibitors against the eIF4E / eIF4G interaction.

10.3 The pARCBD SICLOPPS screening vector

As discussed in section 8, the primary objective of the project was to develop cyclic peptide inhibitors of the eIF4E / eIF4G interaction. The construction of the eIF4E / eIF4G RTHS, was subsequently coupled with SICLOPPS technology to facilitate the identification of potential inhibitors of this key oncogenic PPI. [217] This project employed the pARCBD intein-splicing vector (**Figure 42**) developed by Scott and Abel-Santos, which utilizes Ssp inteins in an inverse cis configuration to splice cyclic peptides within *E. coli*. [217] The Ssp I_C contained a single A158H point mutation (**Figure 49**) to mimic a catalytic histidine residue, which has been observed at the C-terminus of many C-terminal inteins and promotes succinimide formation.

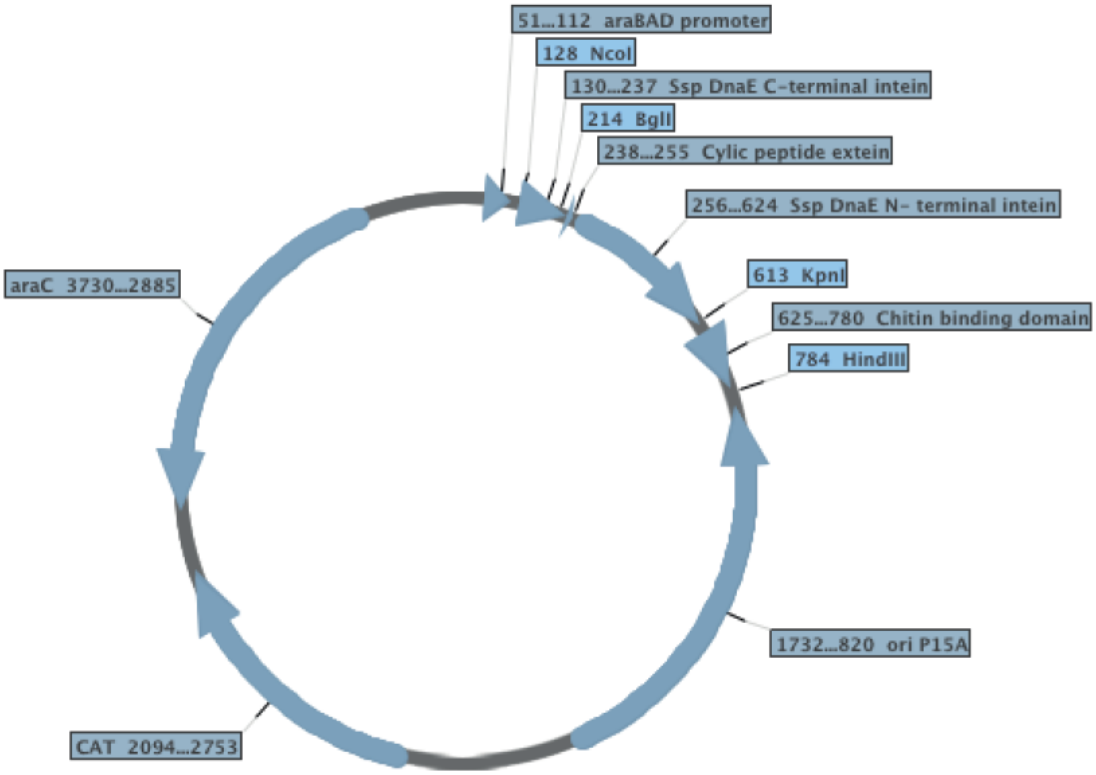

Figure 42: Schematic representation of pARCBD Ssp. [217] The P15A low copy number origin of replication prevents significant screening bias resulting from large variations in plasmid copy number between colonies. [326] [327] Chloramphenicol acetyl transferase (CAT) gene provides a selectable marker for retention of pARCBD. A chitin binding domain (CBD) is fused to the C-terminus of the N-intein to aid purification of the 'I_C-extein-I_N' pre-splicing construct. [293] [328]

pARCBD encodes the 'I_C-extein-I_N' pre-splicing construct under the control of the arabinose inducible araBAD promoter. [217] The regulatory gene of the arabinose operon (AraC), is encoded on the opposite strand of pARCBD to the pre-splicing construct. In the absence of arabinose, homodimerization of the AraC repressor promotes binding to the araBAD promoter, which inhibits transcription of the pre-splicing construct via DNA loop formation. The addition of arabinose disrupts the formation of the inhibitory DNA loop and re-orientates the AraC repressor dimer, which binds to the araBAD promoter in a manner similar to the helix-turn-helix repressor proteins of bacteriophages P22, 434 and λ. The AraC homodimer recruits RNA polymerase to the araBAD promoter and stimulates transcription of the downstream 'I_C-extein-I_N' pre-splicing construct. [329] [330] The araBAD promoter is therefore an ideal candidate for switching between stringent control (in the absence of arabinose) and significant induction of downstream genes (in the presence of arabinose). The use of the arabinose inducible araBAD promoter facilitates orthogonal induction of cyclic peptides and IPTG induced expression of the chimeric 'P22'-eIF4E and 434-eIF4G repressor fusions from the PTac promoter of the RTHS.

10.4 Selection of SICLOPPS screening motifs

Polypeptide synthesis occurs within the cytoplasm of mammalian cells and therefore translation inhibitors must be able to access the eIF4E / eIF4G interface. The phospholipid bilayer of the cell membrane represents a significant barrier that must be traversed by potential inhibitors of the eIF4E / eIF4G interaction. Several long chain linear polypeptides including penetratin, polyarginine and tat have been demonstrated to promote internalization of conjugated cargo molecules. [331] [332] [333] [334] [335] The conjugation of a cyclic peptide inhibitor of the eIF4E / eIF4G interaction to a cell permeable peptide represents an additional synthetic step and significantly increases the cost of the putative therapeutic. It is therefore desirable to incorporate cell permeability elements into the cyclic peptide inhibitor, ideally with a concomitant increase in water solubility. Therefore a strategy was devised to incorporate amino acids within the cyclic peptide that would promote cell permeability and water solubility of the drug, at the SICLOPPS screening stage. The introduction of multiple arginine residues within cyclic peptides has been previously demonstrated to promote cell permeability. [336] [337] It has been postulated that the protonated guanidine side-chains of arginine promote association of

the cyclic peptide with the phospholipid bilayer, whereupon the therapeutic is internalized via pinocytosis. [338] [339] [333] The introduction of multiple arginine residues that are charged at physiological pH increases the net positive charge of the cyclic peptide, promoting solubility in aqueous media.

An invariant 'CRRQ' motif was selected for incorporation into cyclic peptide libraries due to three major considerations. [337] Firstly, the 'RRQ' motif was selected to mimic a portion of the cell permeability domain of the cell permeable human immunodeficiency virus (HIV) tat peptide (49-57 inc., RKKRRQRRR). [331] [332] [340] Whilst it would have been desirable to incorporate a larger Tat peptide cell permeability motif, a compromise had to be made. The incorporation of a large cell permeability domain derived from the HIV tat peptide, plus a randomized domain for screening potential inhibitors of the eIF4E / eIF4G interaction would inevitably yield a large cyclic peptide ring. However, larger cyclic peptides display a greater degree of conformational flexibility and hence bind to target proteins with reduced affinity, when compared to smaller rings that are pre-organized into a binding conformation. [341] A maximum cyclic peptide ring size of nine amino acids was selected as a compromise between conformational constraint of smaller rings and incorporation of cell permeable motifs. It was hypothesized that a minimum of four to five amino acid residues would be required for screening potential inhibitors of the PPI. The invariant 'CRRQ' motif was therefore selected as the largest permissible domain to promote cell permeability.

Secondly, the invariant cysteine (C_{+1}) residue of the 'CRRQ' motif' is responsible for the transthioesterification step of the intein splicing mechanism and is therefore required for SICLOPPS screening. Cysteine was selected as a catalytic intein splicing residue due to its increased nucleophilicity compared to either serine or threonine. In addition the amino acid side-chain of cysteine provides a convenient mechanism for the selective attachment of functional groups to cyclic peptides via iodoacetamide or maleimide conjugation. Finally, the incorporation of a glutamine residue was necessary to facilitate on resin peptide cyclization for sequences that may not assemble in solution.

10.5 SICLOPPS library construction

Cyclic peptide libraries were prepared via the insertion of randomized extein sequences with a conserved C_{+1} nucleophile between the C and N-terminal inteins of pARCBD, according to the procedure of Tavassoli and Benkovic. [328] Briefly, the BglI – HindIII fragment was amplified from pARCBD Ssp via extension PCR with forward primer E, F or G and reverse primer H (**Table 18**) to introduce BglI and HindIII sites (**Figure 43:** A). Forward primers included a small region complementary to the C-terminal region of the I_C, followed by the conserved nucleophillic C_{+1} extein residue (encoded by TGC) and a randomized motif encoded by NNS (where N is any nucleotide and S is either guanosine or cytosine). The use of NNS codons (instead of NNN) was chosen to eliminate the Ochre (TAA) and Opal (TGA) stop codons, to minimize truncation of the pre-splicing construct. [289]

A total of three independent peptide motifs were chosen to develop three distinct pARCBD encoded cyclic peptide libraries, dictated by the choice of forward primer used to generate the first PCR product (**Figure 43**). CXXXXX (CX_5), CRRQXXXXX ($CRRQX_5$) and CRRQXXXX ($CRRQX_4$) peptide motifs were selected for screening potential inhibitors of the eIF4E / eIF4G interaction (amino acids in single letter code, X is a randomized amino acid). Introduction of degenerate oligonucleotides between the C and N-terminal inteins creates a library of extein sequences, each encoded within a unique PCR product. Due to the use of degenerate oligonucleotides within the forward primers, the first round of PCR does not create fully complementary double-stranded PCR products (**Figure 43:** B). As such, a second round of PCR (termed a 'zipper' PCR) was performed on round one PCR products to ensure completely cognate base-pairing, with primers I and H (**Table 18**). [292] [328] 'Zipper PCR' products were subsequently cloned into pARCBD and transformed by electroporation into the eIF4E / eIF4G RTHS, to generate a library of SICLOPPS vectors each encoding a unique cyclic peptide.

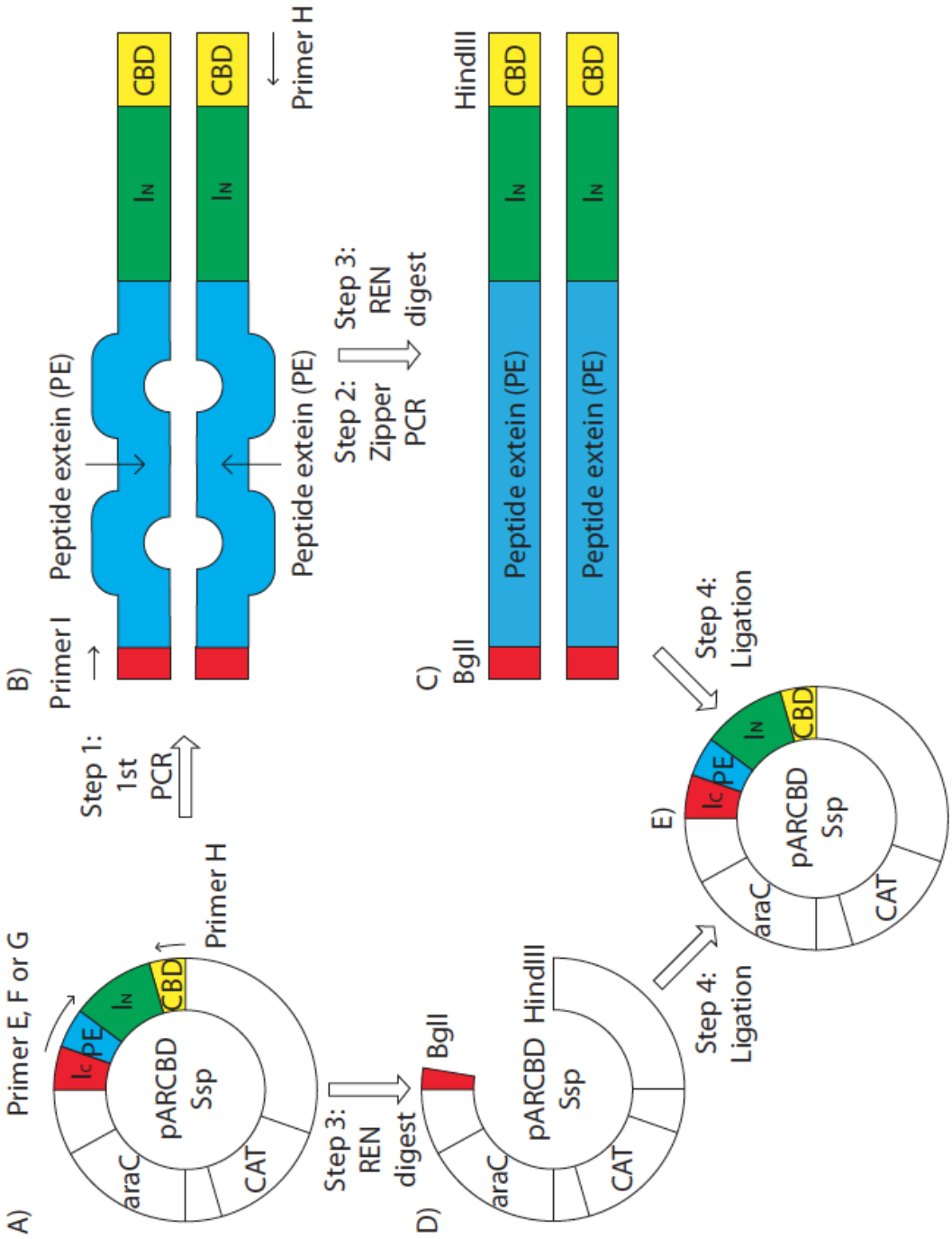

Figure 43: SICLOPPS library construction. [292] [328] **A) PCR using primer E, F or G is used to introduce randomized bases between the C (I_C) and N-terminal (I_N) inteins of pARCBD. B) The first PCR product contains mismatched DNA bases within the randomized extein region, necessitating zipper PCR. C) and D) The zipper PCR product and pARCBD are digested with BglI and HindIII RENs. E) The randomized library of digested zipper PCR products is ligated into pARCBD and transformed into the eIF4E / eIF4G RTHS.**

10.6 Primary SICLOPPS library screening

The library of pARCBD Ssp vectors within the eIF4E / eIF4G RTHS was plated onto minimal media agar plates supplemented with 5 mM 3-AT, 50 μg / ml kanamycin, 25 μg / ml spectinomycin, 35 μg / ml chloramphenicol, 50 μM IPTG and 6.5 μM arabinose, prior to being incubated at 37 °C for 90 h. In the eIF4E / eIF4G RTHS, IPTG induced expression of 'P22'-eIF4E and 434-eIF4G repressor protein fusions facilitates binding of the heterodimeric repressor to the chimeric operator. Transcription of genes within the reporter cassette encoding imidazole glycerol phosphate dehydratase, neomycin phosphotransferase II and β-galactosidase is repressed, reducing colony viability on minimal media with kanamycin and 3-AT (**Figure 44:** A).

Replication of the plasmid library within the eIF4E / eIF4G RTHS is ensured via the chloramphenicol acetyl transferase (CAT) gene of pARCBD Ssp, which promotes colony growth on minimal media with chloramphenicol. pARCBD Ssp derivatives which encode cyclic peptides that do not disrupt the eIF4E / eIF4G interaction, fail to reduce binding of the heterodimeric repressor to the chimeric operator. Hence transcription of reporter cassette genes downstream of the chimeric operator remains repressed in the presence of IPTG (**Figure 44:** A).

By contrast, pARCBD Ssp derivatives which encode cyclic peptides that disrupt the eIF4E / eIF4G interaction, abolish binding of the heterodimeric repressor to the chimeric operator. In the presence of arabinose, transcription of genes within the reporter cassette is stimulated, promoting colony viability on minimal media with kanamycin and 3-AT (**Figure 44:** B). Therefore pARCBD Ssp derivatives which encoded arabinose induced cyclic peptide inhibitors of the eIF4E / eIF4G interaction exhibited colony growth in the presence of IPTG and arabinose.

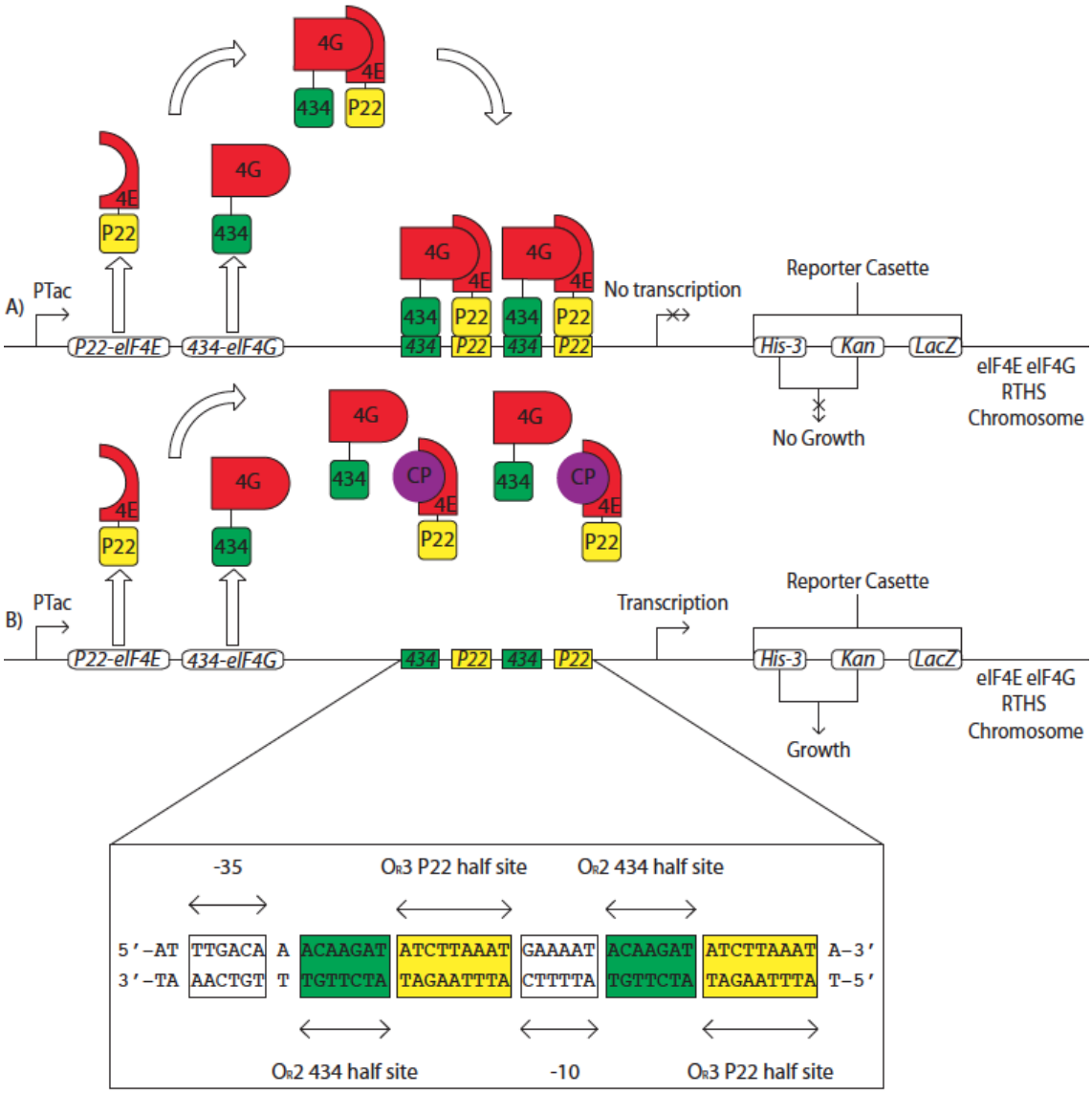

Figure 44: Schematic of the eIF4E / eIF4G RTHS. [239] [240] [244] [266] [321] [323] **Abbreviations used: 'P22' chimeric bacteriophage 434 repressor with P22 operator binding specificity (P22), bacteriophage 434 repressor protein (434), cyclic peptide inhibitor of the eIF4E / eIF4G interaction (CP), imidazole glycerol phosphate dehydratase gene (*His-3*), neomycin phosphotransferase II gene (*Kan*), β-galactosidase gene (*LacZ*), promoter of the lactose operon (PLac).**

Colonies that exhibited growth on SICLOPPS library construction plates were picked and cultured for 16 h and before being serially diluted and subjected to drop-spotting onto four minimal media SICLOPPS screening plates, numbered 1, 2, 3 and 4. All plates contained 5 mM 3-AT, 50 μg / ml kanamycin, 25 μg / ml spectinomycin, 35 μg / ml chloramphenicol and varying concentrations of IPTG and arabinose. Plate 1 lacked both IPTG and arabinose and functioned as a control plate in which expression of RTHS repressor fusion proteins and pARCBD Ssp encoded cyclic peptides was repressed. Plate 2 contained 50 μM IPTG but lacked arabinose and therefore functioned as a control plate in which expression of RTHS repressor fusion proteins was induced. Therefore a direct comparison between the growth of colonies on plate 2 and plate 1 was used to visualize the effect of binding of the heterodimeric repressor to the chimeric operator (**Figure 44:** A and **Figure 45**). Plate 3 contained 6.5 μM arabinose but no IPTG, therefore serving as a control plate in which expression of the pARCBD Ssp encoded cyclic peptides was induced. Therefore a direct comparison of the growth of colonies on plate 3 and plate 1 was used to visualize any toxicity resulting from the expression of cyclic peptides from pARCBD. Finally, plate 4 contained both 50 μM IPTG and 6.5 μM arabinose and functioned as a test plate to determine the dependence of the growth of the eIF4E / eIF4G RTHS on the presence of a functional cyclic peptide inhibitor of the PPI. Therefore a direct comparison of the growth of colonies on plate 4 and plate 2 was used to visualize the cyclic peptide-induced disruption of binding of the heterodimeric repressor to the chimeric operator (**Figure 44:** B and **Figure 45**). Serial dilutions (10^{-1}, 10^{-2}, 10^{-3}, 10^{-4}, 10^{-5} and 10^{-6}) of each *E. coli* culture were drop-spotted onto four minimal media agar plates containing a range of IPTG and arabinose concentrations and incubated at 37 °C for 90 h (**Figure 45**). [266]

Through comparing colony growth on plate 4 to viability on plate 2, colonies that exhibited arabinose-induced restoration of growth in the presence of IPTG were selected for further screening (**Figure 45**). These candidate colonies obtained from primary SICLOPPS screening were cultured for 16 h and pARCBD Ssp vectors encoding potential inhibitors of the eIF4E / eIF4G interaction were isolated via mini prep.

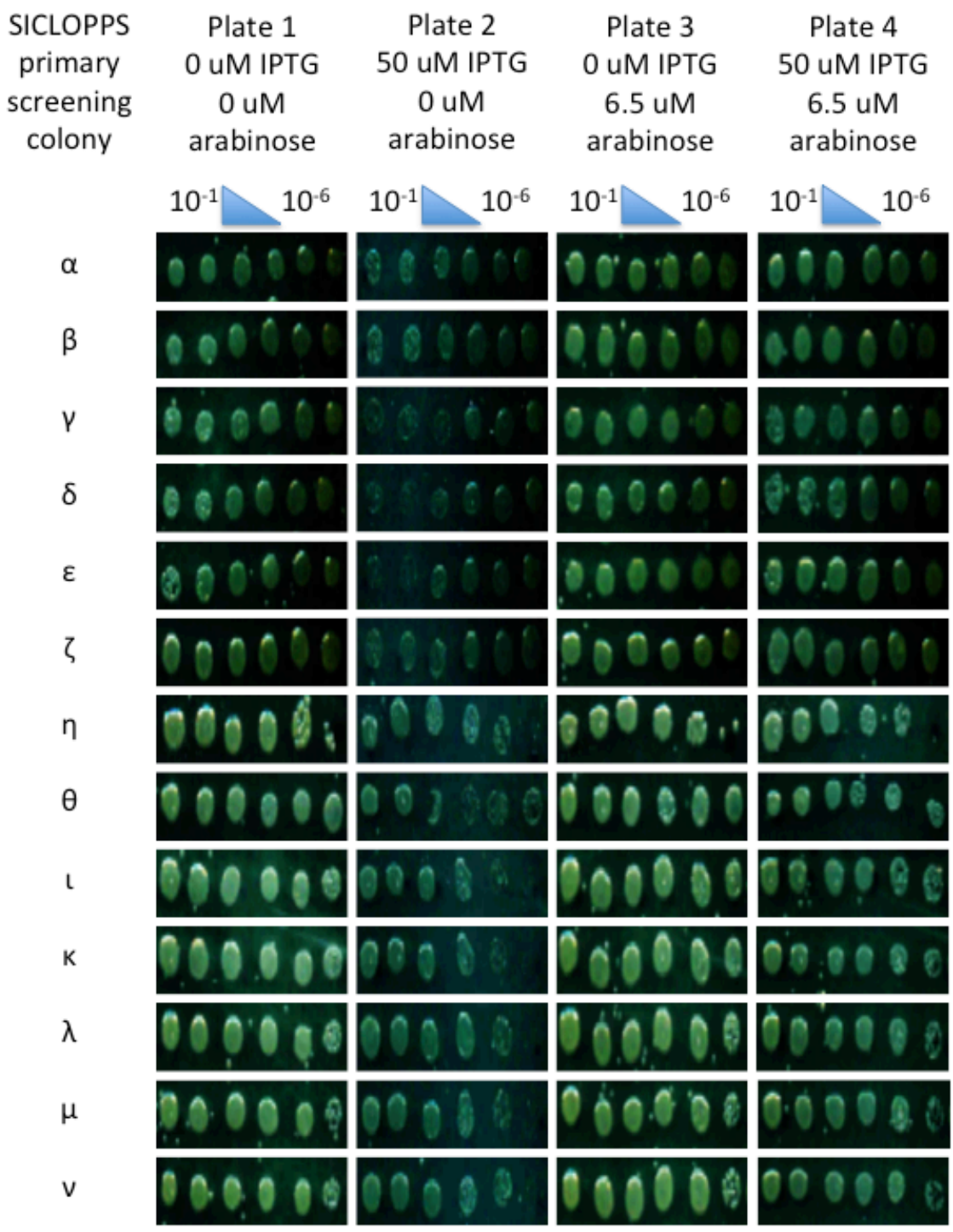

Figure 45: Primary SICLOPPS screening of the eIF4E / eIF4G RTHS transformed with pARCBD Ssp vectors encoding potential cyclic peptide inhibitors of the eIF4E / eIF4G interaction. [266] [321] [323] [324] **Serial dilutions of *E. coli* cultures were drop-spotted onto minimal media plates containing 5 mM 3-AT, 50 μg / ml kanamycin, 25 μg / ml spectinomycin, 35 μg /ml chloramphenicol and varying concentrations of IPTG and arabinose and incubated at 37 °C for 90 h.**

10.7 Secondary SICLOPPS screening

pARCBD Ssp vectors isolated from primary SICLOPPS screening may encode potential inhibitors of the eIF4E / eIF4G interaction. However it is also possible that cyclic peptide candidates disrupt the interaction between the heterodimeric repressor and the chimeric operator, instead of the oncogenic PPI. It is also conceivable that colony viability on selective media during primary SICLOPPS screening was subject to experimental error. It was therefore necessary to verify that pARCBD induced colony viability was plasmid dependent and specific to the eIF4E / eIF4E interaction. Plasmids were therefore re-transformed into the eIF4E / eIF4G RTHS to confirm phenotypic retention and into a previously constructed heterodimeric control RTHS. This critical step helped to eliminate pARCBD vectors that encoded cyclic peptide inhibitors of the interaction of 'P22' or 434 with the chimeric DNA operator. Drop spotting of pARCBD candidates isolated from primary SICLOPPS screening in the control and eIF4E / eIF4G RTHS was performed as previously described. Secondary screening candidates were defined as those colonies that exhibited arabinose induced restoration of colony growth in the presence of IPTG; specifically in the eIF4E / eIF4G RTHS (**Figure 46**), but not in the control system (**Figure 47**). The relative growth of eIF4E / eIF4G RTHS colonies on SICLOPPS screening plates was used to rank potential inhibitors of the eIF4E / eIF4G interaction in order of potency. pARCBD plasmids encoding secondary screening candidates were isolated by mini prep and the sequence of the randomized peptide motif between I_C and I_N was determined via DNA sequencing (**Table 3**).

Ultimately, a total of four cyclic peptide inhibitors were isolated following the screening procedures and these were ranked as the most potent putative inhibitors of the eIF4E / eIF4G interaction (**Table 3**). Of the four isolated candidates, B (CRRQVYVV), F (CRRQVYVH) and K (CRRQLFLF) exhibited a high degree of primary sequence homology, perhaps indicative of a common binding mechanism to the eIF4E / eIF4G interface.

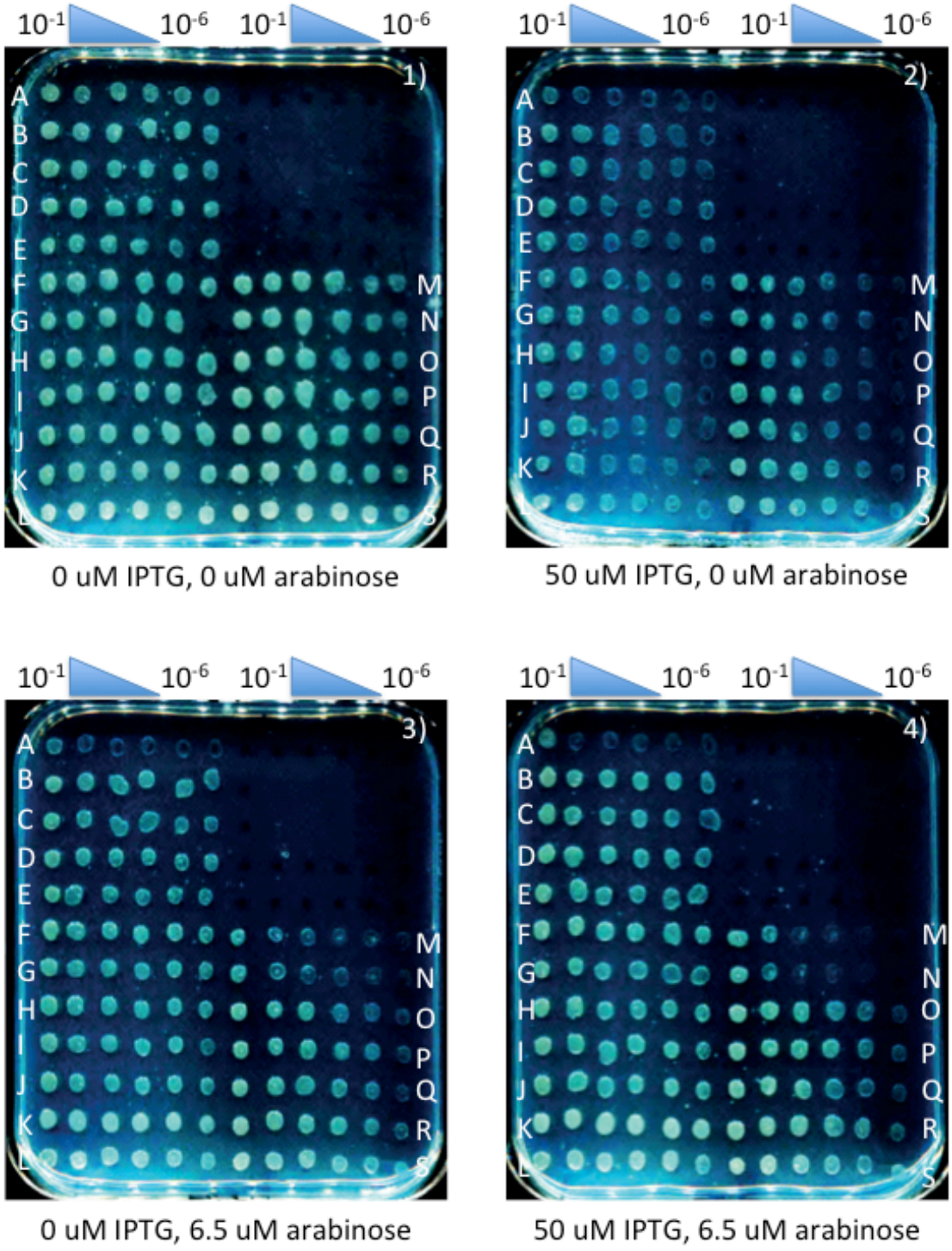

Figure 46: Drop spotting of the eIF4E / eIF4G RTHS re-transformed with pARCBD Ssp vectors encoding potential cyclic peptide inhibitors of the eIF4E / eIF4G interaction. [266] [321] [323] [324] **Serial dilutions of *E. coli* cultures were drop-spotted onto minimal media plates containing 5 mM 3-AT, 50 μg / ml kanamycin, 25 μg / ml spectinomycin, 35 μg /ml chloramphenicol and varying concentrations of IPTG and arabinose and incubated at 37 °C for 90 h.**

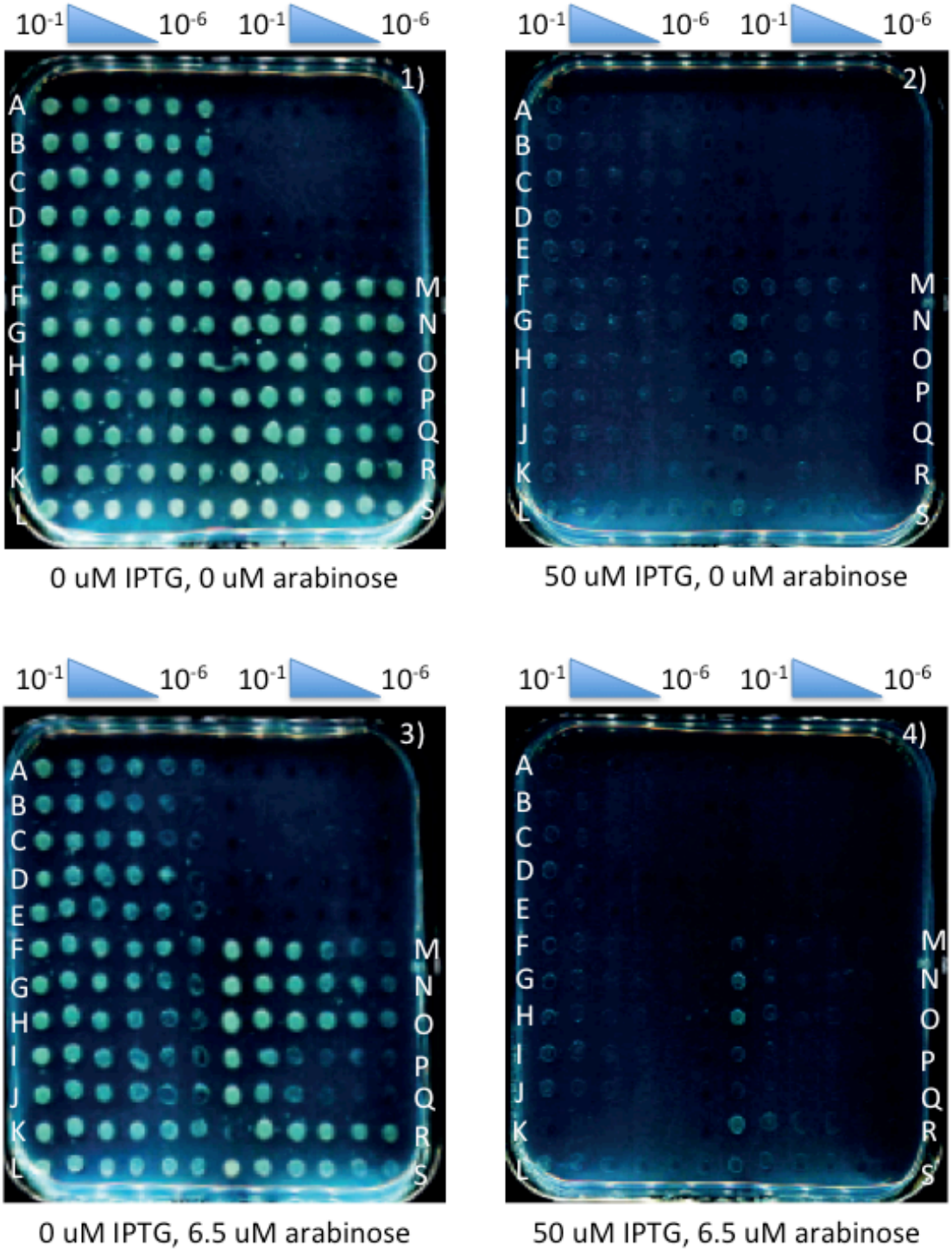

Figure 47: Drops spotting of the heterodimeric control RTHS transformed with pARCBD Ssp vectors encoding potential cyclic peptide inhibitors of the eIF4E / eIF4G interaction. [266] [321] [323] [324] **Serial dilutions of *E. coli* cultures were drop-spotted onto minimal media plates containing 5 mM 3-AT, 50 μg / ml kanamycin, 25 μg / ml spectinomycin, 35 μg /ml chloramphenicol and varying concentrations of IPTG and arabinose and incubated at 37 °C for 90 h.**

Colony identification	Potency ranking	Cyclic peptide sequence
B	1	CRRQVYVV
C	3	CRRQSRLWM
D	2	CRRQTYTY
E	3	CRRQLVYYQ
F	1	CRRQVYVH
G	3	CRRQLFLZA
H	2	CRRQZVKLA
I	2	CRRQZVKLA
J	2	CRRQLSVQL
K	1	CRRQLFLF
L	1	CRRQIHRY
O	2	CKIIIF
P	2	CVVYNY
Q	2	CIISVY
R	3	CSNARL
S	3	CWCLCS

Table 3: Sequences of pARCBD encoded potential cyclic peptide inhibitors of the eIF4E / eIF4G interaction in single letter amino acid code (Z denotes the presence of a 'TAG' amber stop codon by DNA sequencing, indicating truncation of the intein pre-splicing construct). Top ranked candidates B, F, K and L were selected for peptide synthesis and subsequent validation as inhibitors of the eIF4E / eIF4G interaction.

10.8 Intein splicing

Intein splicing within the eIF4E / eIF4G RTHS is a pre-requisite for the production of DNA-encoded cyclic peptide libraries and hence for the isolation of potential cyclic peptide inhibitors of the PPI. Therefore it became necessary to demonstrate splicing of the pARCBD Ssp encoded SICLOPPS screening candidates within the eIF4E / eIF4G RTHS. The incorporation of a chitin-binding domain (CBD) within pARCBD Ssp facilitates the use of affinity chromatography purification of the I_C-extein-I_N-CBD pre-splicing constructs of SICLOPPS candidates. [293] [328] Subsequent incubation of chitin affinity resin bound pre-splicing constructs promotes intein splicing and cyclic peptide production. Direct characterization of cyclic peptide production within the eIF4E / eIF4G RTHS is complicated by the low molecular weight of the cyclic peptide and the inseparable mixture of polypeptides obtained from *E. coli* cell lysates. However, intein splicing can be detected via the separation of the I_C and I_N-CBD byproducts via sodium dodecyl sulfate polyacrylamide gel electrophoresis (SDS-PAGE). This approach was therefore selected to visualize the splicing of pARCBD Ssp encoded SICLOPPS screening candidates. Controls for chitin affinity resin pull-down purification of pre-splicing constructs, were selected from previous work conducted in the Tavassoli laboratory. Cyclo CLLFVY is a selective heterodimerization inhibitor of the hypoxia inducible factor (HIF)-1α / HIF-1β interaction that was previously isolated via SICLOPPS screening. [16] As such, previously constructed pARCBD Ssp CLLFVY in the HIF-1α HIF-1β RTHS was selected as a positive control for intein splicing. [16]

pARCBD Ssp vectors encoding potential inhibitors of the eIF4E / eIF4G interaction or CLLFVY were transformed into the eIF4E / eIF4G RTHS and cultured in LB media with 25 μg / ml spectinomycin and 35 μg / ml chloramphenicol until an OD_{600} of 0.50 - 0.70 was achieved. Expression of the I_C-extein-I_N-CBD pre-splicing construct from the araBAD promoter was induced with arabinose, prior to incubation for 3 h. Cells were harvested, lysed in chitin buffer (**Table 17**) and the soluble fraction was incubated with chitin affinity resin for 2 h. Unbound material was removed by washing with chitin buffer and then intein splicing was allowed to proceed for 16 h. Resin bound proteins were eluted in SDS-PAGE loading buffer and analyzed on a 15 % SDS-PAGE gel.

Chitin affinity resin pull-down experiments (**Figure 48**) demonstrated that a minimal degree of Ssp intein splicing occurred for the positive control (lane 2, pARCBD Ssp

CLLFVY), due to the presence of a small percentage of Ssp I_N-CBD splicing byproduct. A similar degree of Ssp intein splicing was observed for two CX_5 inhibitors of the eIF4E / eIF4G interaction (lane 7, pARCBD Ssp CVVYNY and lane 8, pARCBD Ssp CKIIIF), again due to the evident Ssp I_N-CBD splicing byproduct. However there was little evidence of Ssp intein splicing in any of the $CRRQX_4$ inhibitors of the eIF4E / eIF4G interaction (lane 4, pARCBD Ssp CRRQVYVH; lane 5, pARCBD Ssp CRRQIHRY; lane 6, pARCBD Ssp CRRQVYVV), suggesting that the invariant CRRQ motif proved inhibitory to intein mediated peptide cyclization.

The failure of $CRRQX_4$ inhibitors of the eIF4E / eIF4G interaction to effectively splice with Ssp inteins prompted a review of the literature to identify promiscuous inteins that would tolerate the invariant CRRQ motif. The DnaE intein from *Nostoc punctiforme* (Npu) has been shown to splice more rapidly and provide higher yields of spliced mature extein product, when compared to the Ssp intein. [342] The Npu intein has subsequently been subjected to directed evolution to isolate mutant variants that splice at 37 °C and that tolerate a promiscuous range of extein residues at the C-terminal splice junction. Directed evolution introduced four point mutations within the primary amino acid sequence of the Npu intein, to generate the splicing efficient variant, termed Npu*. [343] Three point mutations (**Figure 49:** highlighted in green, E5D, L15I, L82M) were introduced into the N-terminal Npu intein and one mutation (**Figure 49:** highlighted in red, D125Y) into the C-terminal Npu intein to generate the Npu* intein. [343] The Npu* intein therefore represents an ideal candidate to examine the specific influence of the extein sequence on the rate and degree of intein splicing. pARCBD Npu* was previously constructed within the Tavassoli laboratory (Jaime Townend, unpublished work) and hence was used as the basis for construction of derivatives with specific extein inserts. Previously constructed pARCBD Npu* CLLFVY was used as a positive control for intein splicing alongside a newly constructed pARCBD Npu* CRRQVYVH vector, representing one of the class of potential eIF4E / eIF4G heterodimerization inhibitors. [16] Chitin affinity resin pull-down experiments were performed in tandem with pARCBD Ssp and pARCBD Npu* encoded inhibitors of the eIF4E / eIF4G interaction alongside positive control inhibitors of the HIF-1α / HIF-1β interaction (**Figure 48**).

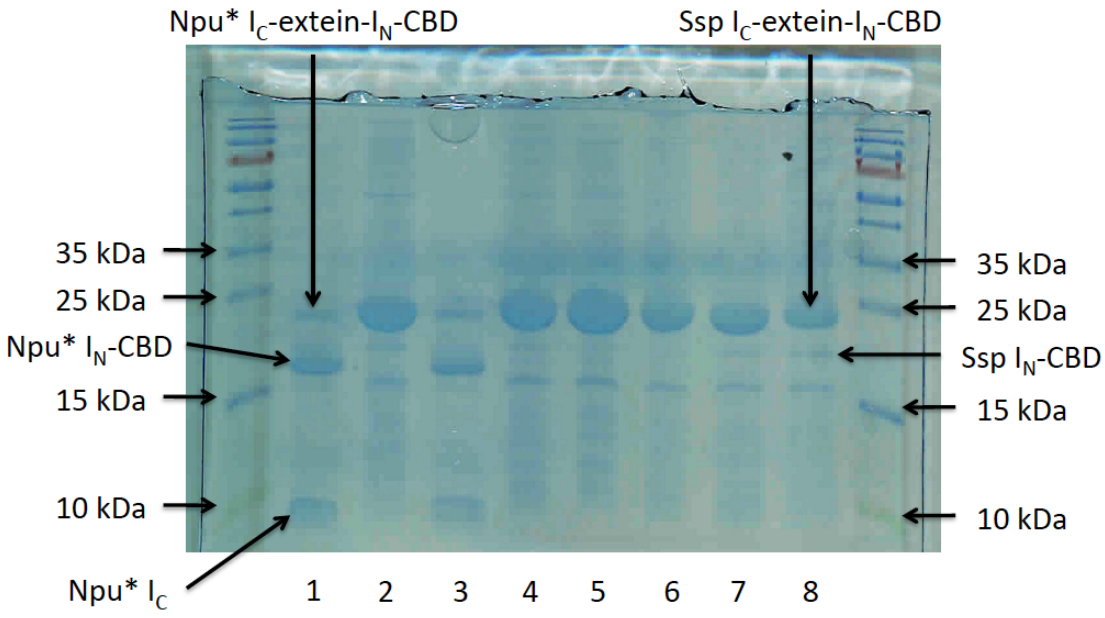

Figure 48: Sodium dodecyl sulfate polyacrylamide gel electrophoresis (SDS-PAGE) of chitin affinity resin pull-down products expressed from pARCBD vectors encoding potential eIF4E / eIF4G heterodimerization inhibitors. [293] **Previously constructed pARCBD Npu* (lane 1) and pARCBD Ssp (lane 2) constructs encoding the HIF inhibitor (cyclo CLLFVY) were used as positive controls for intein splicing. Chitin affinity resin pull-down products were separated on a 15 % gel against a Pageruler 10-170 kDa ladder (Thermo Scientific, 26616). pARCBD Npu* encoding cyclo CLLFVY (lane 1) or cyclo CRRQVYVH (lane 3) exhibited a superior degree of splicing compared to their pARCBD Ssp encoded counterparts (cyclo CLLFVY lane 2, cyclo CRRQVYVH lane 4). The only pARCBD Ssp derivatives to splice effectively encoded cyclo CVVYNY (lane 7) and cyclo CKIIIF (lane 8). pARCBD Ssp derivatives encoding cyclo CRRQIHRY (lane 5) or cyclo CRRQVYVV (lane 6) failed to splice effectively.**

Splicing of Npu* inteins (**Figure 48**) lane 1, pARCBD Npu* CLLFVY and lane 3, pARCBD Npu* CRRQVYVH) can be observed via the presence of the intein splicing byproducts; I_C and I_N-CBD. The quantity of Npu* intein byproducts greatly exceeds that of the Ssp intein byproducts, suggesting that the Npu* intein splices to a higher degree than Ssp. Given that both Npu* and Ssp inteins were allowed to splice in tandem for the same period of time, this further suggests that the Npu* intein splices at a faster rate than Ssp. These findings are supported by the relative depletion of the I_C-extein-I_N-CBD

pre-splicing constructs of the Npu* intein samples compared to their Ssp controls. Therefore pARCBD Npu* encoded cyclic peptides (**Figure 48:** lane 1, pARCBD Npu* CLLFVY and lane 3, pARCBD Npu* CRRQVYVH) spliced with much greater efficiency than the corresponding pARCBD Ssp encoded controls (**Figure 48:** lane 2, pARCBD Ssp CLLFVY and lane 4, pARCBD Ssp CRRQVYVH). The chitin affinity resin pull-down experiments supports previous work that demonstrated the Npu* intein splices faster and to a superior degree, when compared to Ssp inteins. [342] [343] [344]

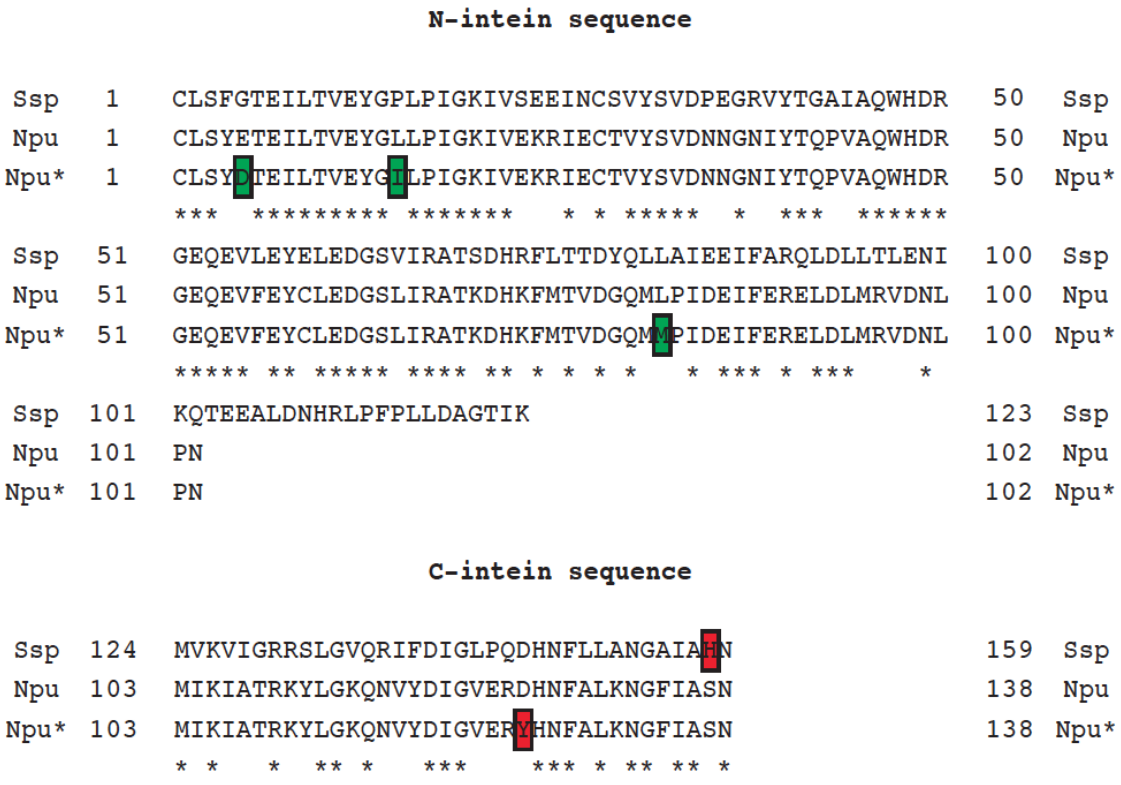

Figure 49: Sequence alignment of N and C-terminal Ssp and Npu inteins against the sequence of an evolved *Nostoc punctiforme* (Npu) intein that splices at higher temperatures and is tolerant of a greater range of extein sequences (Npu*). [276] [342] [343] **Point mutations within the Npu* N- intein (green, E5D, L15I, L82M) and the C-intein (red, D125Y) are highlighted, as is the single Ssp C-intein mutation (red, A158H).** [343]

Whilst the degree of splicing of the Ssp intein appeared to discriminate between CX_5 and $CRRQX_4$ inhibitors, no such disparity was observed for Npu* encoded inteins. Splicing of the pARCBD Npu* CLLFVY positive control (**Figure 48:** lane 1) appeared

to proceed to a similar degree to that of pARCBD Npu* CRRQVYVH (**Figure 48:** lane 3), suggesting that the Npu* intein is more tolerant of a range of extein sequences, when compared to the Ssp intein controls (**Figure 48:** lane 2, pARCBD Ssp CLLFVY and lane 4, pARCBD Ssp CRRQVYVH). [344] Evidence of the I_C and I_N-CBD Npu* intein byproducts (**Figure 48:** lane 3) suggests that pARCBD Npu* CRRQVYVH effectively splices a cyclic peptide from the I_C-extein-I_N-CBD pre-splicing construct. However this finding does not suggest that $CRRQX_4$ inhibitors of the eIF4E / eIF4G interaction were spliced during SICLOPPS screening with Ssp inteins. It is therefore likely that a library of peptide extein loops was screened, constrained by the conformational interactions of the I_N and I_C. As such, the primary amino acid sequence of each SICLOPPS hit may still represent a potential source of cyclic peptide inhibitors of the PPI.

Due to the failure of $CRRQX_4$ inhibitors to be spliced by Ssp inteins, it was necessary to validate that cyclic peptides spliced by the Npu* intein stimulated colony viability of the eIF4E / eIF4G RTHS in the presence of arabinose and IPTG. pARCBD Ssp and pARCBD Npu* plasmids encoding potential inhibitors of the eIF4E / eIF4G interaction were re-transformed into the eIF4E / eIF4G RTHS. pARCBD Ssp CLLFVY and pARCBD Npu* CLLFVY plasmids were re-transformed into the HIF-1α HIF-1β RTHS as positive controls. pARCBD derivatives in their appropriate RTHS were cultured for 16 h and then serially diluted prior to drop-spotting onto four minimal media plates, as previously described.

All colonies exhibited binding of the heterodimeric repressor to the chimeric operator, (**Figure 50:** compare plate 2 and plate 1) yielding reduced colony viability in the presence of IPTG, as expected. The subsequent addition of arabinose abolished the IPTG-induced reduction of colony viability, (**Figure 50:** compare plates 3, 4 and 5 against plate 2) consistent with cyclic peptide induced disruption of the heterodimeric repressor. Comparison of the growth of pARCBD Npu* CLLFVY (**Figure 50:** row G) against the growth of pARCBD Ssp CLLFVY (**Figure 50: row** F) revealed that the Npu* inteins did not restore colony growth to the same extent, when compared to Ssp. Reduction of the arabinose concentration serendipitously improved colony viability of the HIF-1α HIF-1β RTHS transformed with pARCBD Npu* CLLFVY (**Figure 50:** compare plates 3, 4 and 5). This unexpected result is consistent with the large degree of Npu* intein splicing, possibly yielding increased toxicity within *E. coli* due to the

abundance of the I_C and I_N-CBD splicing byproducts. A similar phenomenon is also observed via a comparison of the growth of pARCBD Npu* CRRQVYVH (**Figure 50:** row E) against the growth of pARCBD Ssp CRRQVYVH (**Figure 50:** row D), albeit to a lesser degree.

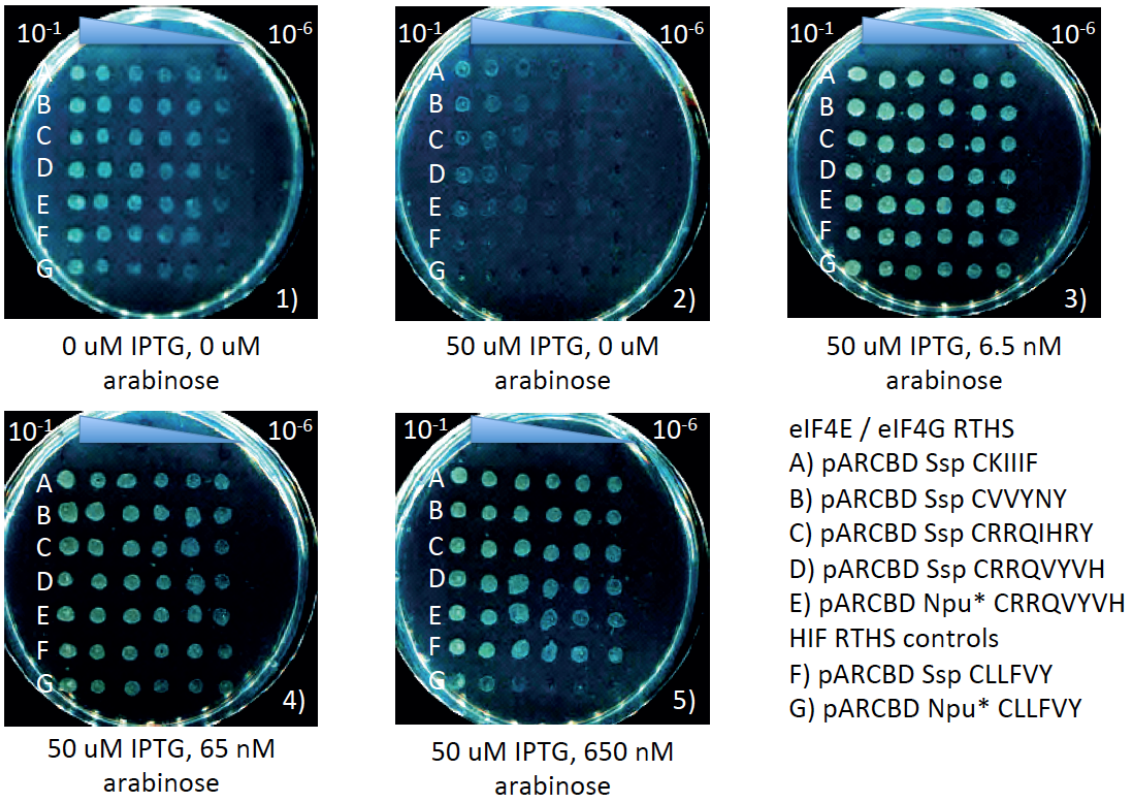

Figure 50: Drops spotting of the eIF4E / eIF4G RTHS transformed with pARCBD vectors encoding potential cyclic peptide inhibitors of the eIF4E / eIF4G interaction. [266] [321] [323] [324] **Serial dilutions of *E. coli* cultures were drop-spotted onto minimal media plates containing 5 mM 3-AT, 50 *μ*g / ml kanamycin, 25 *μ*g / ml spectinomycin, 35 *μ*g /ml chloramphenicol and varying concentrations of IPTG and arabinose and incubated at 37 °C for 90 h. A) pARCBD Ssp CKIIIF, B) pARCBD Ssp CVVYNY, C) pARCBD Ssp CRRQIHRY, D) pARCBD Ssp CRRQVYVH, E) pARCBD Npu* CRRQVYVH, F) HIF inhibitor control, pARCBD Ssp CLLFVY, G) HIF inhibitor control, pARCBD Npu* CLLFVY.**

Despite toxicity of the Npu* I_C and I_N-CBD byproducts, arabinose induced Npu* intein splicing still promotes colony viability in the presence of IPTG (**Figure 50:** compare plate 3 and plate 2). These findings are consistent with the hypothesis that arabinose induced Npu* intein splicing synthesizes a cyclic peptide that disrupts the eIF4E / eIF4G interaction. Disruption of the PPI abolishes binding of the heterodimeric repressor to the chimeric operator, facilitating transcription of reporter cassette genes and promoting colony viability. Increased colony viability was observed for pARCBD Ssp CRRQVYVH and for pARCBD Npu* CRRQVYVH, which is consistent with the hypothesis that intein splicing is not absolutely required to disrupt the eIF4E / eIF4G interaction. This suggests that either the presence of the cyclic peptide (spliced by the Npu* inteins) or the peptide extein loop (formed by the Ssp inteins) is sufficient to abolish the eIF4E / eIF4G interaction. As such, cyclic peptide sequences isolated via SICLOPPS screening with Ssp inteins were deemed appropriate candidates for potential inhibitors of the eIF4E / eIF4G interaction.

SICLOPPS screening led to the isolation of four cyclic peptides that displayed considerable inhibition of the eIF4E / eIF4G PPI as shown by drop spotting assays within the RTHS (**Table 3**). These four cyclic peptides, CRRQIHRY, CRRQLFLF, CRRQVYVV and CRRQVYVH were selected as potential inhibitors of the eIF4E / eIF4G interaction. In order to validate that the aforementioned cyclic peptides disrupt the eIF4E / eIF4G interaction it was necessary to synthesize milligram quantities of each. SPPS was therefore selected to synthesize potential cyclic peptide inhibitors of the eIF4E / eIF4G interaction.

10.9 Solid phase peptide synthesis

The α-amino protecting group selected for this project was 9-Fluorenylmethoxycarbonyl (Fmoc), which was utilized in tandem with a *tert*-butyl (tBu) amino acid side-chain protection strategy. [345] [346] [347] [348] Linear peptides were assembled on pre-loaded Fmoc – Gln (Trt) - Wang resin, which was swollen prior to synthesis in *N,N*-dimethylformamide (DMF). [349] [350] Fmoc deprotection was achieved with a 20 % (v:v) solution of piperidine / DMF, (**Figure 51:** A and B) yielding dibenzofulvene as a byproduct. Fmoc deprotection was entropically promoted via liberation of CO_2 and driven to completion via exposure to two separate aliquots of 20 % piperidine / DMF. [345] [346] Excess piperidine and deprotection byproducts were removed by washing with DMF, prior to coupling of α-amino Fmoc protected amino acids with appropriate side-chain protecting groups. Amino acid coupling was achieved using an *N,N'*-diisopropylcarbodiimide (DIC) mediated strategy with Hydroxybenzotraizole (HOBt) as a racemization suppressing additive (**Figure 51:** E and F). [351] [352] [353] Reaction of the free amine peptide N-terminus with benzotriazole activated esters of α-amino Fmoc protected amino acids resulted in the formation of a new amide bond and the extension of the polypeptide chain (**Figure 51:** C and D). Colourimetric free amine tests were used to ensure coupling completion and hence correct polypeptide assembly. [354] [355] [356] Sequential cycles of Fmoc deprotection and DIC / HOBt mediated amino acid coupling were used to synthesize linear peptides on the solid phase. Cysteine residues were incorporated with the Tert-butylthio (StBu) side chain protecting group (**Figure 53:** A) instead of the more commonly used Cys (Trt) (**Figure 52:** B) derivative to ensure that cysteine residues remained protected during cleavage of the polypeptide from the resin. [357] [358] All other amino acid residues were incorporated with acid labile side-chain protecting groups commonly used in Fmoc SPPS, including His (Trt), Gln (Trt), Arg (Pbf), and Tyr (tBu) (**Figure 52:** C, D, E and F). [350] [359] [360] Once the entire linear peptide had been assembled on resin, the N-terminal Fmoc group was removed with piperidine. The resin bound peptide was dried using dichloromethane (DCM) and diethyl ether (Et_2O) washes in preparation for cleavage of the polypeptide from the Wang resin linker. [349]

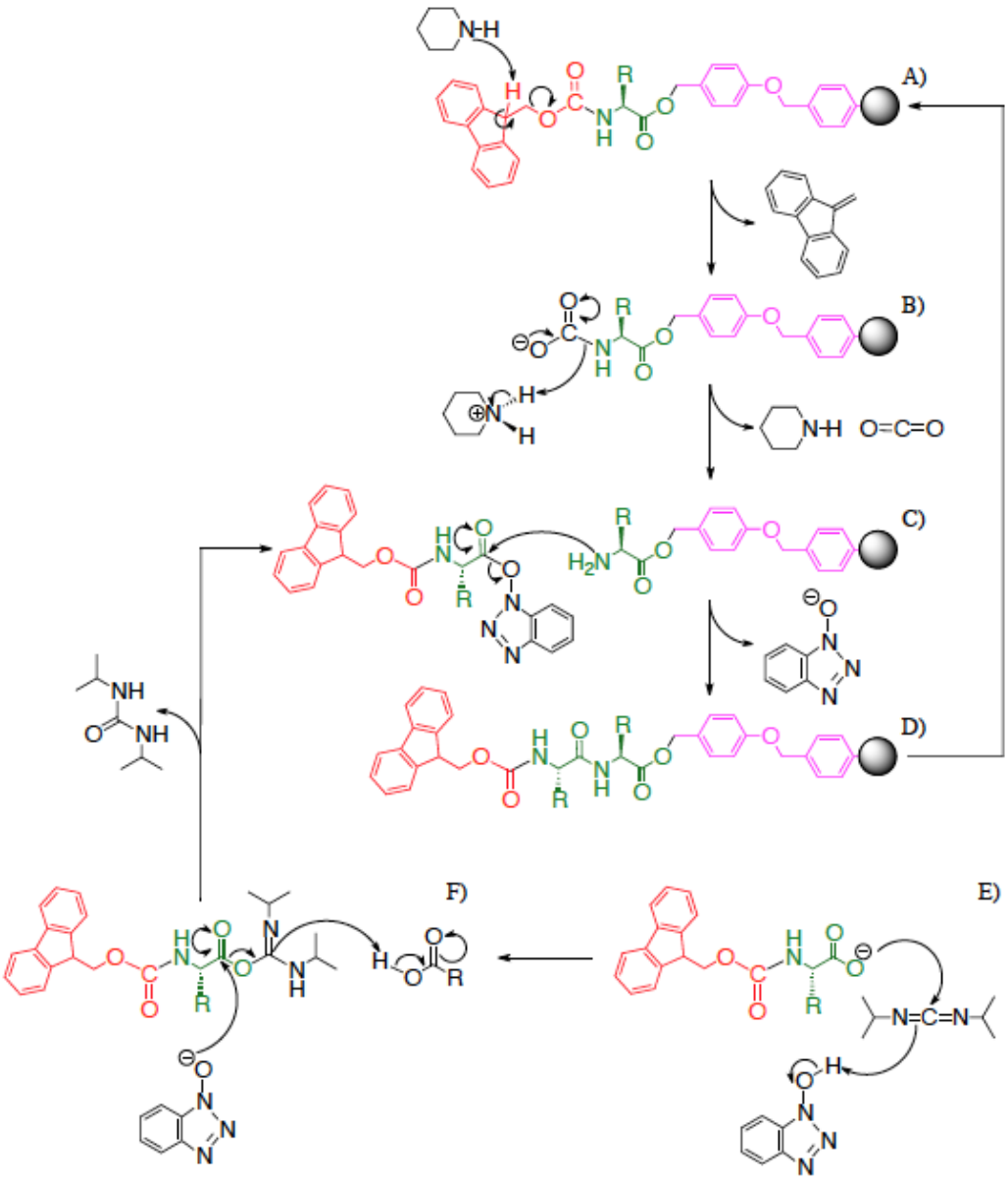

Figure 51: Mechanism of 9-Fluorenylmethoxycarbonyl (Fmoc, highlighted in red) solid phase peptide synthesis (SPPS), immobilized onto a solid support via a Wang resin linker (highlighted in magenta). [345 346 349 350 351 352 353 359 360] **A) and B) Piperidine catalyzed Fmoc deprotection liberates the free amine N-terminus of the growing peptide chain. C) The free amine N-terminus of the peptide chain nucleophilically attacks the benzotriazole activated ester to form an amide bond. D) The Fmoc α-amino protected polypeptide chain is then subjected to cycles of steps A) to F) inc., until all desired amino acids have been added. E) The C-terminus of an Fmoc α-amino and side-chain protected amino acid is activated as an O-acylisourea. F) The O-acylisourea is converted to an activated benzotriazole ester, forming the stable diisopropylurea byproduct.**

10.9.1 Peptide resin cleavage

Linear peptides were released from Wang resin linkers via treatment with trifluoroacetic acid (TFA) cleavage cocktail, with concomitant deprotection of amino acid side-chain protecting groups (**Figure 52**). [349] [350] [359] [360] Cleavage of the Wang resin linker and amino acid side-chain protecting groups liberated cationic species (**Figure 52**) that were scavenged by the addition of water and triisopropylsilane (TIS) to the resin cleavage cocktail. [361] [362] [363] Cleavage cocktails were subsequently concentrated by rotary evaporation and peptides were precipitated with Et_2O. Linear peptides were purified via reverse phase high performance liquid chromatography (RP-HPLC) and lyophilized to give white powders.

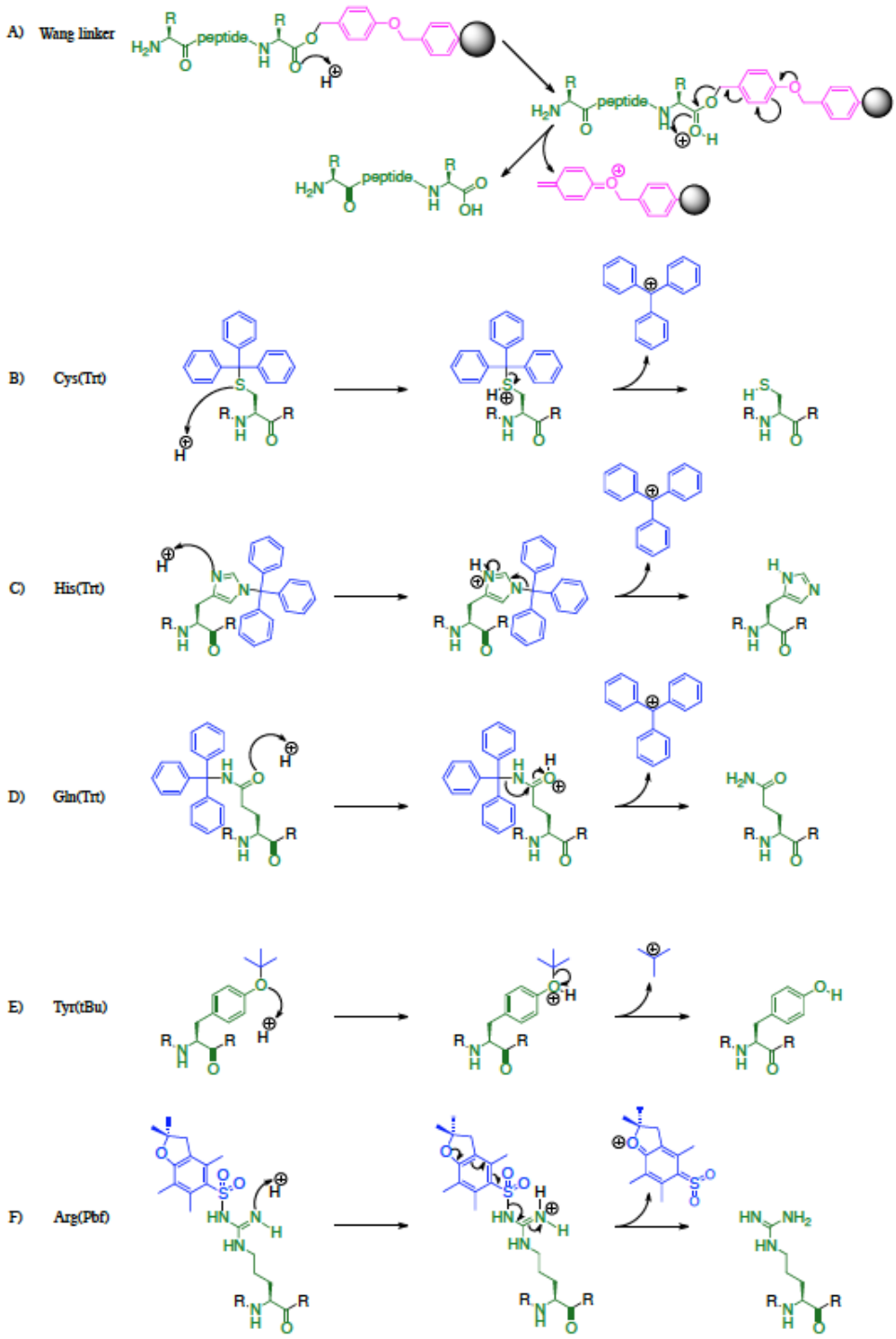

Figure 52: Mechanism of acid catalyzed cleavage of polypeptides assembled on resin. [361] [364] **A) Mechanism of Wang linker cleavage.** [349] **B) Mechanism of cleavage of the Trityl (Trt) protecting group of Cysteine.** [362] [365] **C) Mechanism of cleavage of the Trt protecting group of Histidine.** [359] **D) Mechanism of cleavage of the Trt protecting group of Glutamine.** [350] **E) Mechanism of cleavage of the Tert-butyl (tBu) protecting group of Tyrosine.** [366] **F) Mechanism of cleavage of the 2, 2, 4, 6, 7-Pentamethyldihydrobenzofuran-5-sulfonyl (Pbf) protecting group of Arginine.** [360]

10.9.2 Peptide cyclization in solution

Cys(StBu) protected linear peptides were dissolved in DMF and diluted until a final concentration of less than 1 mM was achieved. Peptides were cyclized in high dilution to promote intramolecular cyclization, whilst minimizing intermolecular polymerization (**Figure 53**). Cysteine residues were protected with the StBu group to prevent nucleophillic attack or oxidation of the thiol side-chain from interfering with cyclization. [357] [358]

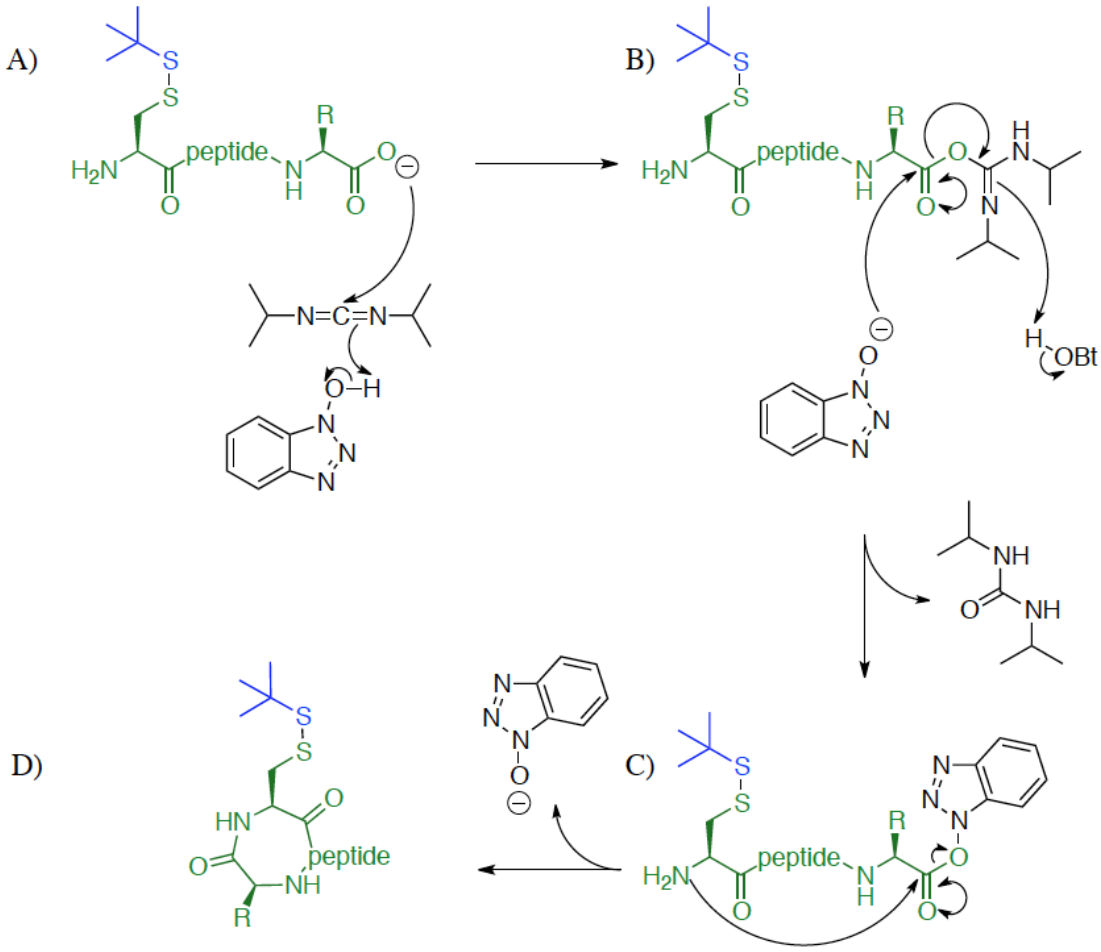

Figure 53: Mechanism of the cyclization of Cys(StBu) protected linear peptides when dissolved in DMF under high dilution conditions. A) The C-terminus of the peptide is activated as an O-acylisourea. B) The O-acylisourea is converted to an activated benzotriazole ester, forming the diisopropylurea byproduct. C) and D) The free amine N-terminus of the polypeptide chain nucleophilically attacks the benzotriazole activated ester to form the cyclic peptide.

Cyclization was achieved by using a 10 fold excess of DIC / HOBt to compensate for the large reaction volume and hence low coupling reagent concentration. Reactions were stirred under argon for 64 h to maximize the probability that the free amine N-terminus would encounter the C-terminal activated benzotriazole ester. Reactions were concentrated by rotary evaporation and crude Cys(StBu) protected cyclic peptides were isolated via Et_2O precipitation.

10.9.3 Deprotection of Cys(StBu)

Crude Cys(StBu) protected cyclic peptides were dried under argon and deprotected without further purification. Cys(StBu) protected cyclic peptides were dissolved in a minimal volume of DMF and then diluted with 0.1 M aqueous ammonium carbonate until the limit of solubility was achieved. The peptide solution was degassed with argon, prior to the addition of excess dithiothreitol (DTT) to reduce the disulfide bond of the Cys(StBu) protecting group. The solution was stirred under argon for 2 h to promote nucleophillic displacement of the StBu protecting group from the cyclic peptide cysteine residue (**Figure 54**). The solution was adjusted to pH ~ 3 with TFA, prior to concentration via rotary evaporation. [357] [358] Cyclic peptides were purified via RP-HPLC and lyophilized to give white powders. The cyclization of H_2N-LFLFC(StBu)RRQ-CO_2H and H_2N-VYVVC(StBu)RRQ-CO_2H in high dilution in DMF proceeded smoothly and the corresponding peptides were isolated.

However the cyclizations of H_2N-IHRYC(StBu)RRQ-CO_2H and H_2N-VYVHC(StBu)RRQ-CO_2H in high dilution failed to give a homogeneous cyclic peptide product. One possible rationale for the failure of these cyclizations could be due to the presence of a histidine residue within each peptide. It is conceivable that histidine could act as an anchiomeric base, promoting deprotonation of the arginine residues of the invariant 'CRRQ' motif. This in turn may have yielded increasingly nucleophillic arginines, which could have competed with the peptide N-terminus resulting in the formation of multiple cyclization products.

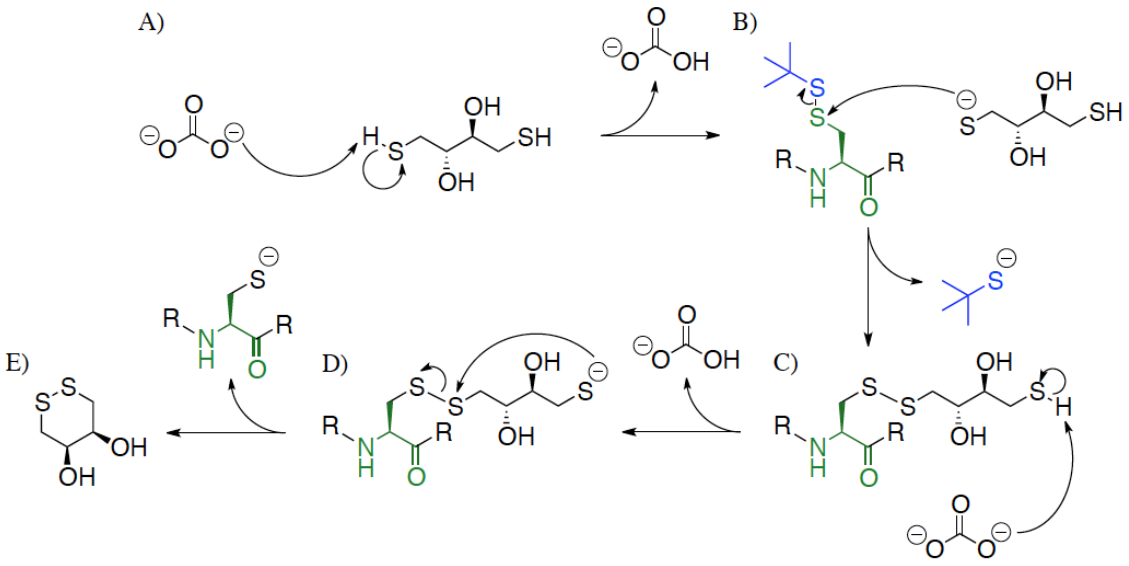

Figure 54: Mechanism of dithiothreitol (DTT) induced deprotection of Cys(StBu) residues within cyclic peptides. [357] [358] **A) Deprotonation of a thiol group of DTT generates the active thiolate nucleophile. B) The thiolate nucleophile attacks the disulfide bond of Cys(StBu), liberating the free cysteine containing cyclic peptide. C) and D) Intramolecular nucleophillic attack of the DTT thiolate on the disulfide bond forms a stable hexameric ring, liberating the StBu protecting group.**

10.9.4 On resin peptide cyclization

To overcome this synthetic limitation, an on resin cyclization methodology was devised (**Figure 55**). It was envisaged that immobilization of the peptide through an amino acid side-chain (specifically that of glutamine) would allow assembly of the linear peptide and subsequent cyclization on resin. [367] This concept required the use of an orthogonal protecting group for the peptide C-terminus that was stable to both piperidine and amino acid coupling conditions (**Figure 55:** B). The peptide could then be synthesized from the C-terminal glutamine via standard Fmoc SPPS until the entire linear peptide was assembled (**Figure 55:** C). Subsequent removal of the orthogonal glutamine C-terminal protecting group would yield the carboxyl group of the peptide chain, whilst maintaining the integrity of all other amino acid side-chain protecting groups (**Figure 55:** E). Subsequent on resin cyclization could therefore only occur between the N-terminal amine and the carboxyl group of the immobilized polypeptide. Cleavage of the polypeptide from the resin would then yield the N to C-terminal cyclic peptide (**Figure 55:** F). The orthogonal 4-(*N*-(1-(4,4-dimethyl-2,6-dioxocyclohexylidene)-3-methyl butyl) amino) benzyl ester (Dmab) protecting group was selected for blocking of the glutamate C-terminus (highlighted in blue, **Figure 55:** A). The Dmab group has been previously shown to be stable to both piperidine and amino acid coupling reagents and has been successfully employed for the on resin synthesis of cyclic peptides. [368] [369] [370]

An α-amino Fmoc protected glutamic acid residue, with a C-terminal Dmab protecting group was immobilized via a rink amide linker to a Chemmatrix polyethyleneglycol resin (**Figure 55:** A and B) via HOBt / DIC mediated amide bond formation. [371] Peptides were assembled on resin via SPPS in a C to N-terminal direction via sequential cycles of Fmoc deprotection and amino acid coupling until the final free amine sequence was achieved (**Figure 55:** C). It was necessary to use a polyethyleneglycol matrix to ensure adequate swelling of the resin (and thus access of reagents to peptide strands) in a range of solvents including DMF, methanol (MeOH) and water. [372] Coupling of a glutamic acid side-chain to a rink amide linker provided a convenient method to load Fmoc-Glu-ODmab to the resin and reconstituted the desired glutamine side-chain upon cleavage of the polypeptide from the resin (**Figure 55:** F and G).

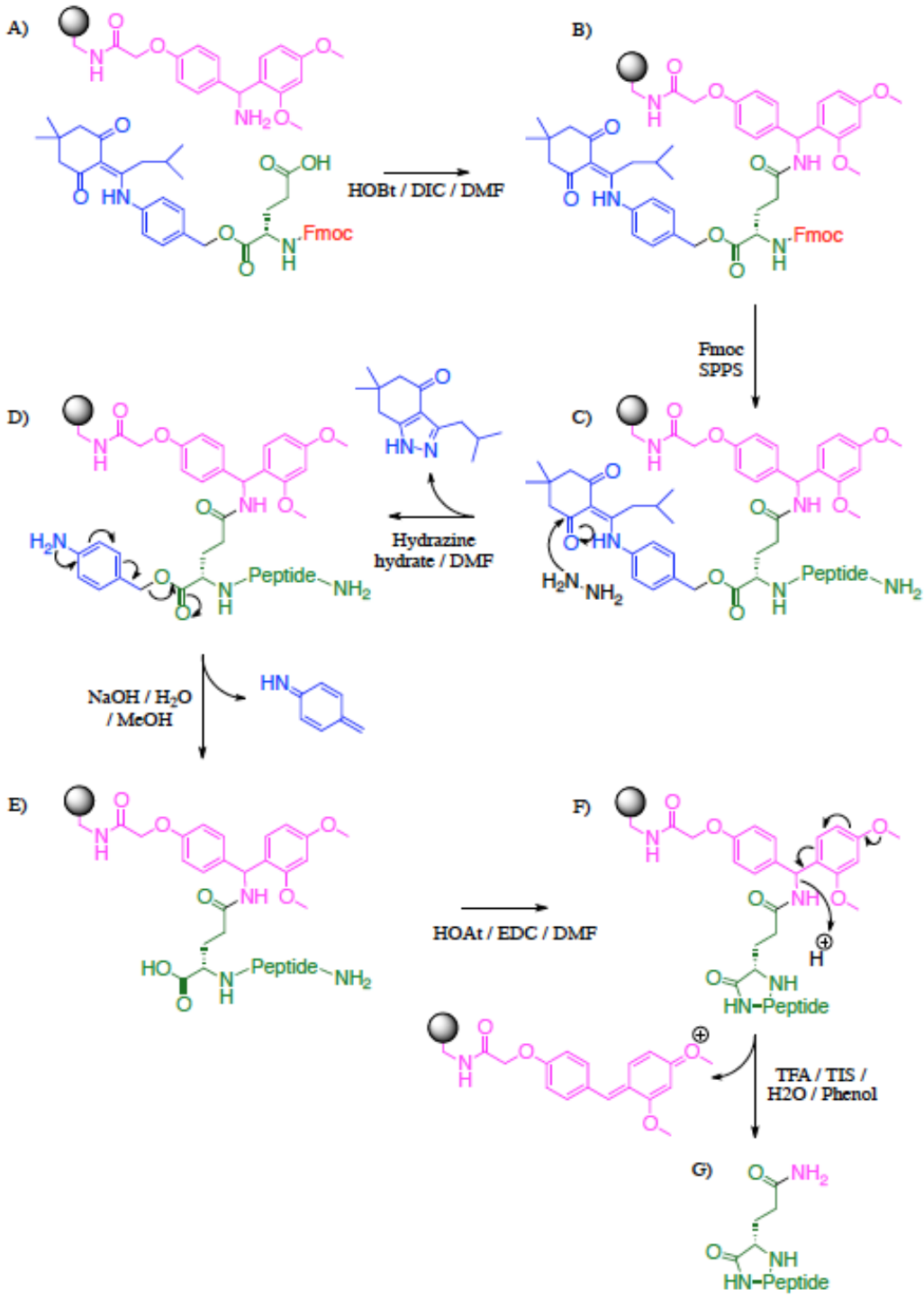

Figure 55: On resin peptide cyclization mechanism. [368] [369] [370] [371] **C) and D) Exposure to hydrazine cleaves the Dmab protecting group, liberating the carboxylic acid at the peptide C-terminus.** [368] [369] [370] **E) and F) On resin peptide cyclization was achieved using 1-Hydroxy-7-azabenzotraizole (HOAt) and *N*-(3-Dimethylaminopropyl)-*N*'-ethylcarbodiimide (EDC).** [353] [373] [374] [375] **G) The rink amide linker and amino acid side-chain protecting groups were cleaved with Trifluoroacetic acid (TFA) / Triisopropylsilane (TIS) / water / phenol deprotection cocktail.**

Cleavage of the C-terminal Dmab protecting group was achieved with 2 % hydrazine monohydrate in DMF yielding the 4-aminobenzylester intermediate (**Figure 55:** D). Spontaneous collapse of the intermediate was promoted with 5 mM NaOH in water / MeOH to yield the free carboxyl group at the C-terminus of the peptide strand (**Figure 55:** E). [368] [369] [370] On resin peptide cyclization was subsequently achieved via *N*-(3-Dimethylaminopropyl)-*N'*-ethylcarbodiimide (EDC) mediated coupling with 1-Hydroxy-7-azabenzotraizole (HOAt) as a racemization suppressing additive (**Figure 55:** F). [353] [373] [374] [375] Whilst the amino acid side-chain protecting groups promote the formation of a homogeneous N to C-terminal cyclic peptide, they also represent a significant steric barrier to peptide cyclization. As such long reaction times were necessary and produced reduced yields when compared to cyclization in highly diluted DMF solutions. The cyclic peptide was subsequently cleaved from the rink amide resin linker via TFA cleavage cocktail, yielding the desired glutamine amino acid side chain (**Figure 55:** G). Cleavage cocktails were concentrated by rotary evaporation and crude cyclic peptides were precipitated with Et_2O. Cyclic peptides were purified via RP-HPLC and lyophilized to give white powders in acceptable yields (**Table 4**).

Synthesis code	Peptide sequence	Yield / mg	Yield / %
AEG001	H_2N-VYVVC(StBu)RRQ-CO_2H	343	62
AEG002	H_2N-VYVHC(StBu)RRQ-CO_2H	149	26
AEG003	H_2N-IHRYC(StBu)RRQ-CO_2H	334	55
AEG004	H_2N-LFLFC(StBu)RRQ-CO_2H	396	68
AEG005	H_2N-VYVVC(SH)RRQ-CO_2H	27	54
AEG006	H_2N-VYVHC(SH)RRQ-CO_2H	38	77
AEG007	H_2N-IHRYC(SH)RRQ-CO_2H	27	58
AEG008	H_2N-LFLFC(SH)RRQ-CO_2H	16	16
AEG009	Cyclo VYVVC(SH)RRQ	40	22
AEG010	Cyclo VYVHC(SH)RRQ	20	8
AEG011	Cyclo IHRYC(SH)RRQ	30	11
AEG012	Cyclo LFLFC(SH)RRQ	41	24

Table 4: Sequences and yields of synthetic peptides.

All peptides were characterized (see section 14.2) by positive mode electrospray ionization mass spectrometry (ESI+ MS), analytical RP-HPLC, infrared spectroscopy (IR) and UV-vis spectroscopy (UV-vis). A variety of nuclear magnetic resonance (NMR) techniques including one-dimensional proton (^{1}H 1D), two-dimensional proton correlation spectroscopy (^{1}H COSY) and two-dimensional proton total correlation spectroscopy (^{1}H TOCSY), were used for additional peptide characterization. Cys(SH) linear peptides were obtained from Cys(StBu) protected precursors, purified by RP-HPLC and subsequently characterized (see section 14.2) to validate the DTT induced removal of the StBu protecting group. Cyclization of peptides reduces the conformational degrees of freedom when compared to their linear precursors. This pre-organization of cyclic peptides into a limited number of conformations minimizes the entropic cost of binding to the target protein. Peptide cyclization therefore increases the binding affinity of therapeutics and enhances their target binding affinity. [341] Therefore cyclic peptides were selected for validation as potential inhibitors of the eIF4E / eIF4G interaction.

10.10 Validation of cap-dependent translation inhibitors

SICLOPPS screening isolated four cyclic peptides with an invariant 'CRRQ' motif that disrupted the eIF4E / eIF4G interaction within the RTHS (**Table 4**). The two arginine residues within the invariant 'CRRQ' motif used during SICLOPPS screening were incorporated to improve the water solubility and cell permeability of the cyclic peptides.[337] The disruption of this PPI within *E. coli* marks a significant step towards the development of cap-dependent translation inhibitors. However, it is still necessary to validate that these SICLOPPS derived cyclic peptides disrupt the eIF4E / eIF4G interaction *in cellulo*. A series of assays performed in immortalized cancerous cell lines were therefore devised to interrogate the disruption of the eIF4E / eIF4G interaction by the novel cyclic peptides within the malignant environment.

10.10.1 Thiazolyl blue tetrazolium bromide assay

The thiazolyl blue tetrazolium bromide assay (commonly referred to as the MTT assay) has become a popular high throughput method for testing how compounds effect the viability of mammalian cells *in vitro*.[376] The MTT assay indicates changes in cell viability by differentiating between the capability of live cells to reduce the yellow MTT dye to the water insoluble purple formazan, a reaction which does not occur in non-viable cells (**Figure 56**). Cell viability is then measured by dissolving the formazan produced by live cells in an organic solvent, followed by quantification via visible spectroscopy at 570 nm.

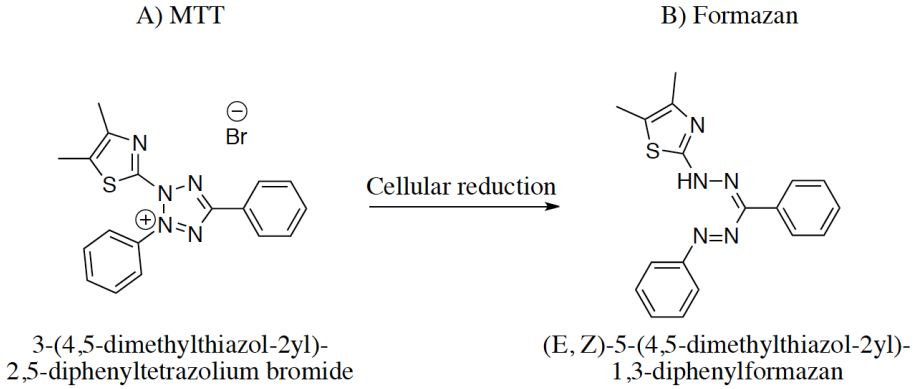

Figure 56: Thiazolyl blue tetrazolium bromide (MTT) assay.[376] The cell permeable yellow MTT dye (A) is reduced by live cells to the water insoluble purple formazan (B).

In order to test inhibitors of the eIF4E / eIF4G interaction, it was essential to choose an immortalized cancer cell line with a high degree of cap-dependent translation. The human breast adenocarcinoma cell line MCF-7 produces elevated levels of the mRNA that encodes eIF4E, when compared to a non-cancerous tissue control. [377] In addition, elevated intracellular eIF4E levels have been linked to increased rates of cap-dependent translation. [131] [152] [180] The MCF-7 cell line was therefore selected for testing potential inhibitors of the eIF4E / eIF4G interaction. It was hypothesized that treatment of MCF-7 cells with potential cyclic peptide inhibitors of the eIF4E / eIF4G interaction would inhibit cap-dependent translation. In turn this should reduce the viability of MCF-7 cells, by depriving the malignant tissue of oncogenic proteins that are encoded by weak mRNAs. [17] [175] Screening of cyclic peptides against the MCF-7 cell line via MTT assay provided a rapid method to quantify cell viability and allowed for ranking of potential inhibitors of the eIF4E / eIF4G interaction.

5000 MCF-7 cells per well were sub cultured onto 96 well microplates and incubated for 24 h to allow cells to adhere to the plate. Following incubation, the cells were treated with cyclic peptide or vehicle alone control (0.5 % dimethyl sulfoxide, negative control) for 24 h. At the conclusion of the treatment cells were washed with phosphate buffered saline (PBS) and exposed to MTT solution for 4 h, while submerged in cell culture media that did not contain phenol red pH indicator. [378] The spent media and remaining MTT dye was aspirated and the formazan contained within live cells was then solubilized with dimethyl sulfoxide (DMSO). Live cell metabolism of MTT dye to formazan was then quantified at 570 nm, relative to a reference wavelength of 650 nm. [379] [380] The reference wavelength was used to correct for any non specific background absorbance and was subtracted from all measurements. Cell viability was subsequently normalized to the vehicle alone (0.5 % DMSO) treated control cells.

Treatment of MCF-7 cells with cyclo LFLFCRRQ revealed a clear dose-dependent reduction of cell viability, with a median lethal dose (LD_{50}) of ~ 14 μM (**Figure 57**). This is consistent with the hypothesis that the cyclic peptide is disrupting the eIF4E / eIF4G interaction, thereby inhibiting cap-dependent translation. Cyclo LFLFCRRQ was therefore selected as a promising candidate for further validation as a potential inhibitor of the eIF4E / eIF4G interaction.

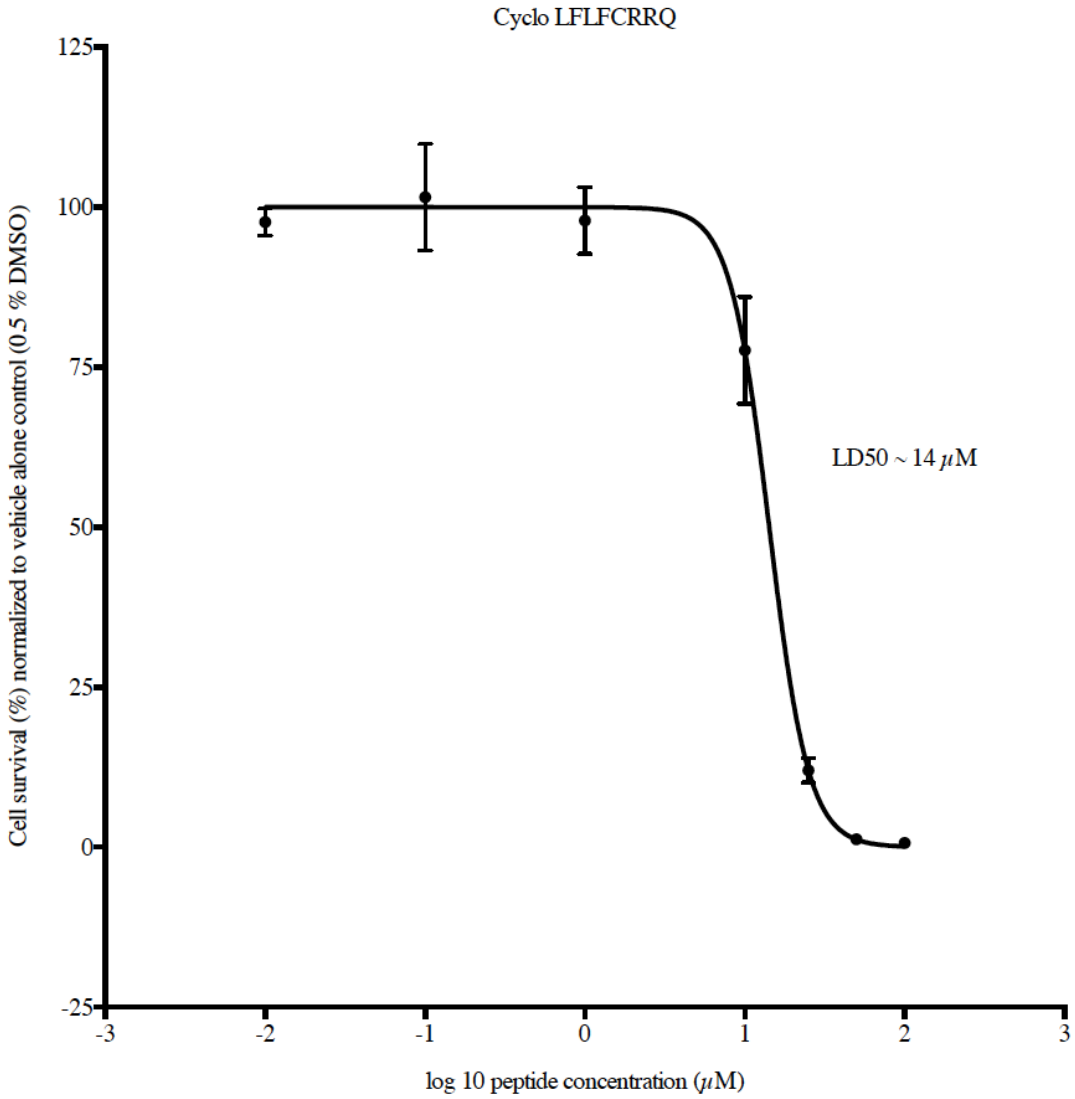

Figure 57: Dose-response curve of the effect of cyclo LFLFCRRQ on MCF-7 cell viability over a 24 h period as determined by MTT assay. Error bars are representative +/- one standard deviation of the means of three independent experiments.

Treatment of MCF-7 cells with cyclo VYVVCRRQ revealed a reduction of cell viability, but only at the highest concentrations of cyclic peptide. Attempts were made to observe the effects of higher concentrations of cyclo VYVVCRRQ on cell viability, however the relatively poor solubility of the cyclic peptide in the 100 X stock solutions limited further experiments. It was therefore impossible to obtain an accurate LD_{50} determination, however at concentrations greater than 100 μM it is unlikely that cyclo VYVVCRRQ is a therapeutically relevant inhibitor of the eIF4E / eIF4G interaction.

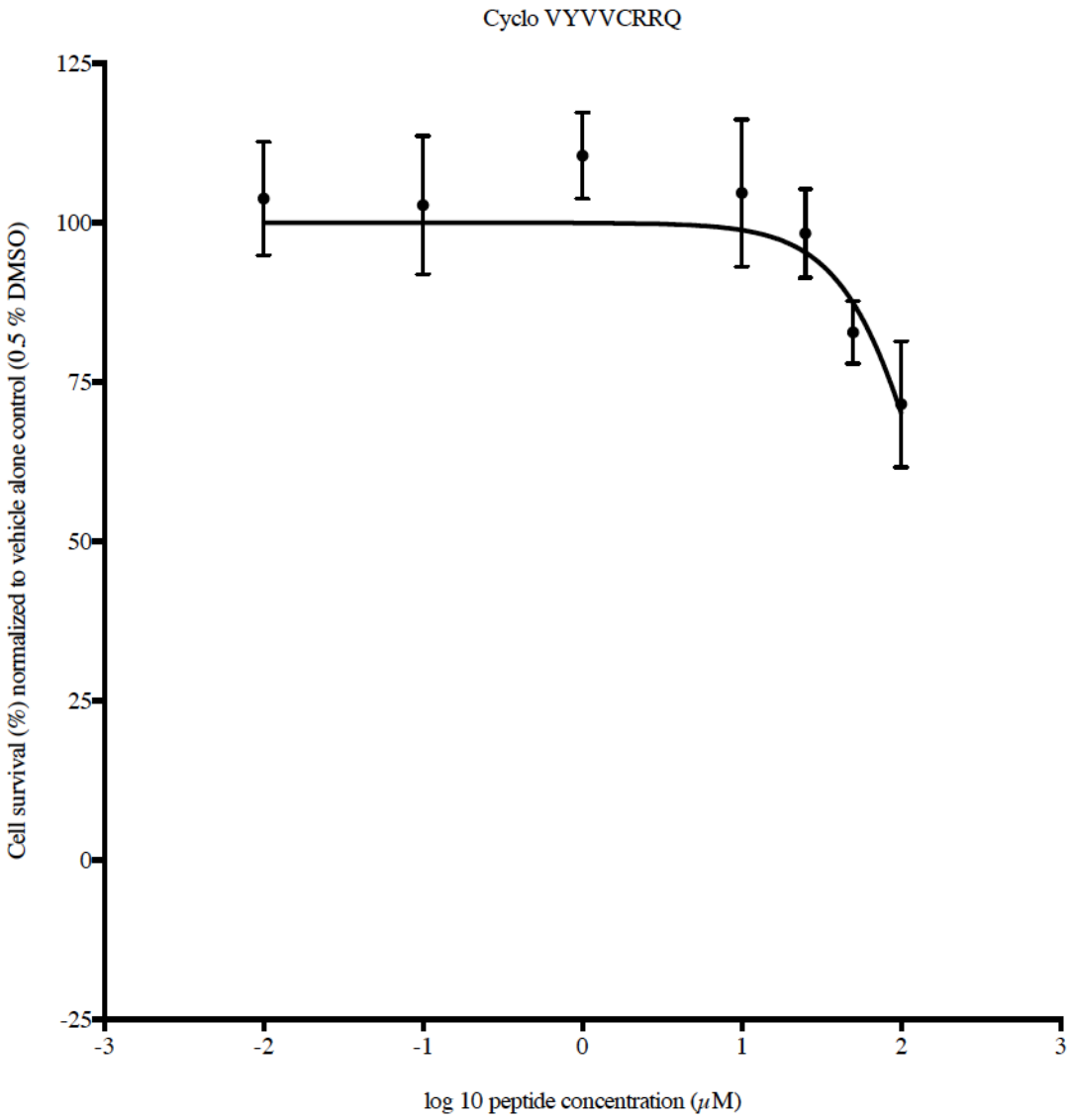

Figure 58: Dose-response curve of the effect of cyclo VYVVCRRQ on MCF-7 cell viability over a 24 h period as determined by MTT assay. Error bars are representative +/- one standard deviation of the means of three independent experiments.

Treatment of MCF-7 cells with cyclo VYVHCRRQ (**Figure 59**) or cyclo IHRYCRRQ (**Figure 60**) revealed that cell viability did not exhibit any dependence on cyclic peptide concentration. This is consistent with failure to disrupt the eIF4E / eIF4G interaction, thereby permitting cap-dependent translation. It is interesting to note that the ability of cyclic peptides to reduce the cell viability of MCF-7 cells exhibits a trend, depending on the hydrophobicity of the four amino acid variable motif. MTT assay showed clearly that SICLOPPS derived cyclic peptides with invariant 'CRRQ' motifs decreased cell

viability in the order 'LFLF' > 'VYVV' >>> 'VYVH' ~ IHRY. It is therefore interesting to speculate that cyclic peptides may inhibit the eIF4E / eIF4G interaction via the disruption of hydrophobic van der Waals or π-stacking interactions.

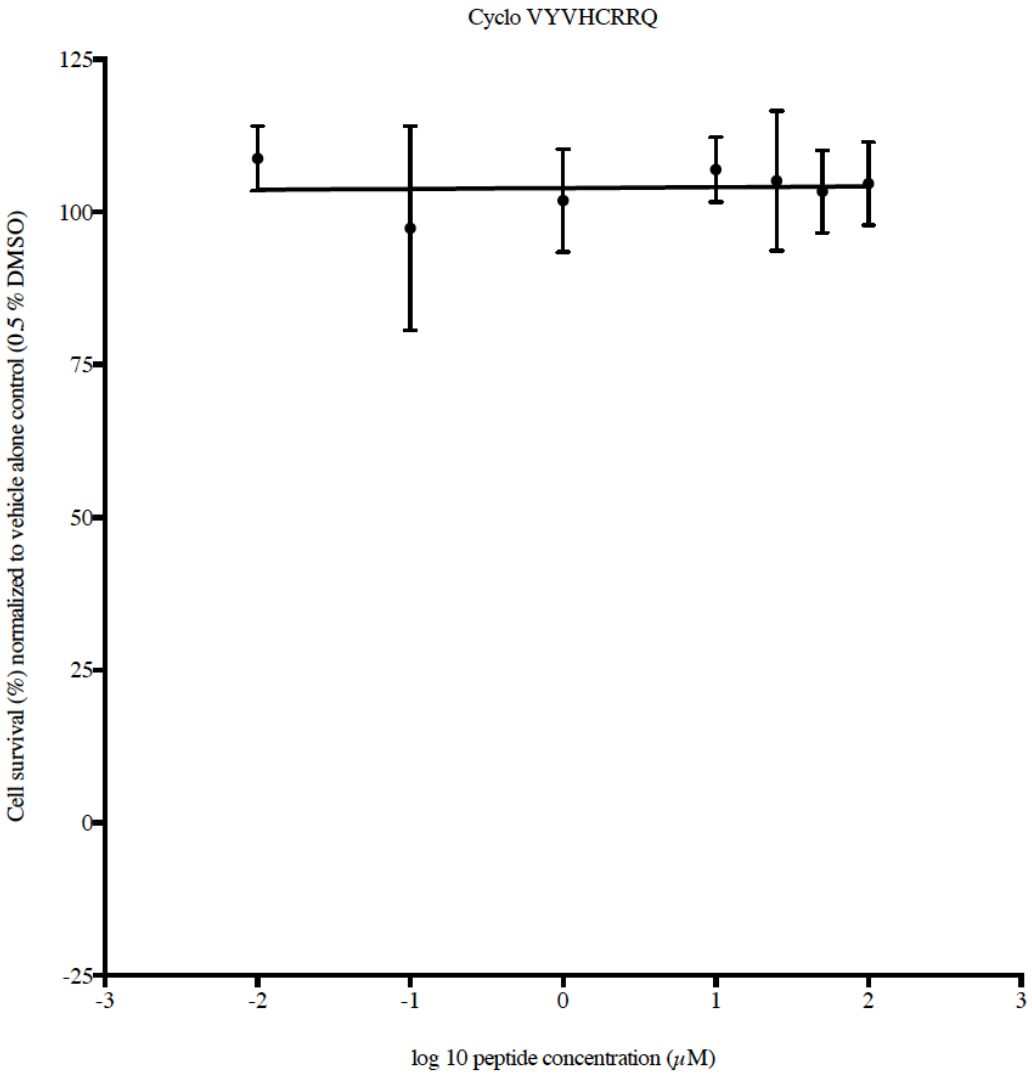

Figure 59: Dose-response curve of the effect of cyclo VYVHCRRQ on MCF-7 cell viability over a 24 h period as determined by MTT assay. Error bars are representative +/- one standard deviation of the means of three independent experiments.

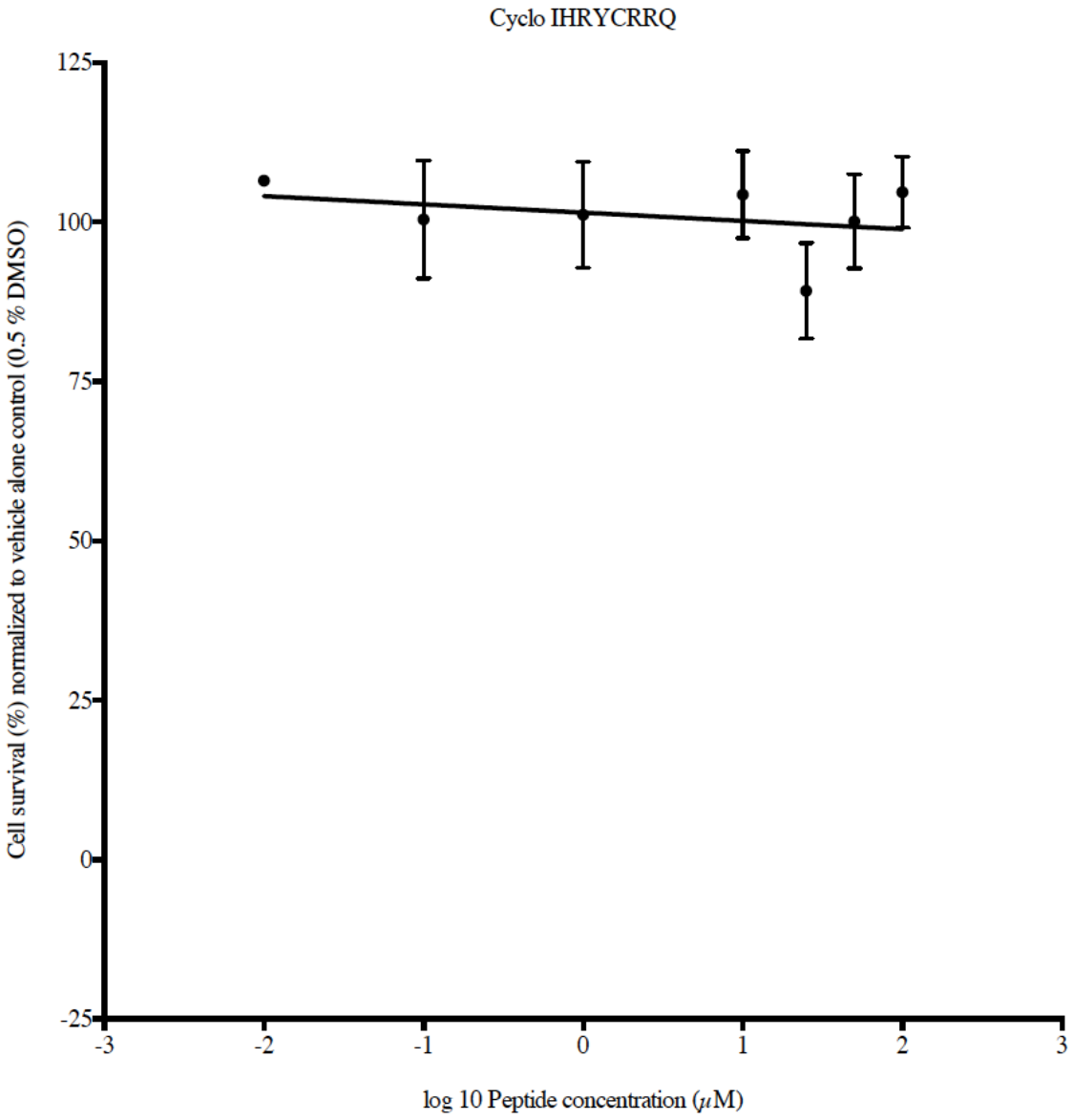

Figure 60: Dose-response curve of the effect of cyclo IHRYCRRQ on MCF-7 cell viability over a 24 h period as determined by MTT assay. Error bars are representative +/- one standard deviation of the means of three independent experiments.

10.10.2 Luciferase translation assay

Whilst the MTT assay provided a rapid method of ranking potential cyclic peptide inhibitors by their LD_{50} in MCF-7 cells, the assay does not provide direct evidence of the disruption of the eIF4E / eIF4G interaction within the malignant environment. The eIF4E / eIF4G interaction represents the vital link between eIF4E mediated recognition of the 5' m^7 GTP mRNA cap and the recruitment of eIF4A to unwind stem loop structures within the 5' UTR. [150] [152] [123] As such the formation of the eIF4F complex and the resulting effective translation of oncogenic weak mRNAs displays an absolute requirement for the eIF4E / eIF4G interaction. [136] [139] By contrast the effective cap-independent translation of strong mRNAs with short and unstructured 5' UTRs, does not display an absolute requirement for the eIF4F complex. [381] It was therefore hypothesized that cyclic peptide inhibitors of the eIF4E / eIF4G interaction would inhibit eIF4F assembly and therefore selectively inhibit cap-dependent translation, with little or no effect on cap-independent translation. The luciferase assay is a commonly used technique to assess the effect of compound treatment on cellular translation and was therefore selected to test inhibitors of the eIF4E / eIF4G interaction.

10.10.2.1 Firefly luciferase

Luciferase enzymes were first isolated from a species of firefly, *Phontinus pyralis* and as such this enzyme is commonly named 'firefly luciferase'. [382] Firefly luciferase (Fluc) catalyzes the oxidation of luciferin to oxyluciferin via luciferyl adenylate and a dioxetanone intermediate (**Figure 61**). The first step of the mechanism requires ATP and Mg^{2+} to form the activated ester, luciferyl adenylate (**Figure 61:** B). The enolate of luciferyl adenylate then nucleophilically attacks oxygen, resulting in the generation of the dioxetanone (**Figure 61:** D E F). The dioxetanone intermediate consists of a highly strained four membered ring containing a weak peroxide bond and is therefore unstable (**Figure 61:** F). The four membered ring collapses via a chemically induced electron exchange luminescence (CIEEL) mechanism, involving the transfer of a single electron from the electron rich aryl system of luciferin to the peroxide bond. [383] This transient intermediate (**Figure 61:** G) collapses via liberation of carbon dioxide, which entropically drives the reaction to completion. [384] [385] The hydrolysis of ATP, combined with the generation of the entropically and enthalpically favorable CO_2 electronically excites electrons within the oxyluciferin product (**Figure 61:** H I). [386] The

chemiluminescent reaction generates an electronically excited singlet spin state, which decays to the triplet ground state, yielding photons of visible light.

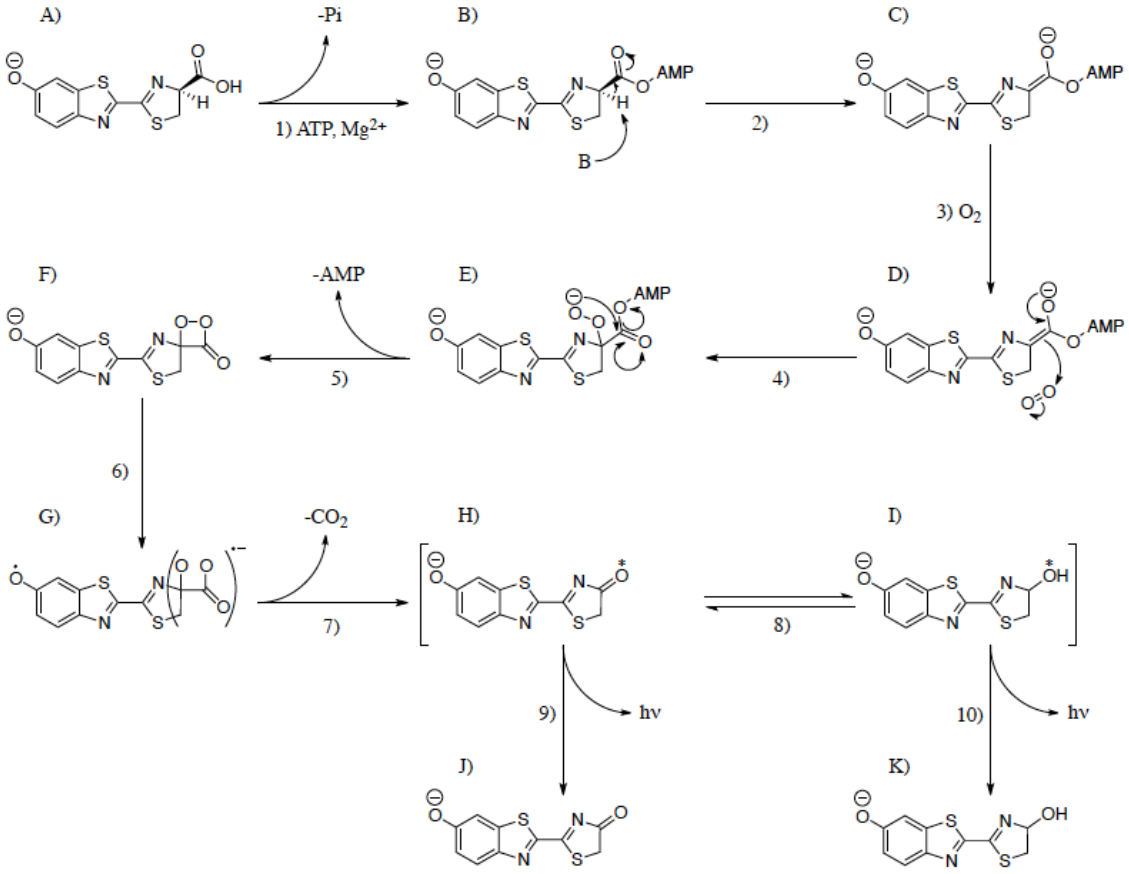

Figure 61: Mechanism of the oxidation of luciferin by the firefly luciferase (Fluc) of *Phontinus pyralis*. A) and B) Luciferin reacts with adenosine triphosphate (ATP) to produce luciferyl adenylate yielding inorganic phosphate (P_i). C), D), E) and F) Fluc abstracts a proton to form an enolate, which then reacts with oxygen to form the highly strained dioxetanone intermediate F). [387] **G), H) and I) The unstable dioxetanone intermediate collapses to yield oxyluciferin in an electronically excited state.** [384] **J) and K) Excited (*) oxyluciferin decays to its electronic ground state via the emission of a photon of light.**

10.10.2.2 Renilla luciferase

Renilla luciferase (Rluc) is an enzyme isolated from *Renilla reniformis* (sea pansy) that catalyzes the oxidation of coelenerazine to coelenteramide (**Figure 62**). [388] [389] [390] [391] Coelenterazine nucleophilically attacks oxygen to form the strained dioxetanone intermediate (**Figure 62:** C). The four membered ring collapses via a CIEEL mechanism, involving the transfer of a single electron from one of the electron rich aryl system of the substrate to the peroxide bond of the dioxetanone intermediate. [392] Lysis of the four membered dioxetane ring, combined with the generation of the entropically and enthalpically favorable CO_2 electronically excites electrons within the coelenteramide product (**Figure 62:** E). The chemiluminescent reaction generates photons of visible light upon relaxation of the excited coelenteramide product to its electronic ground state (**Figure 62:** F).

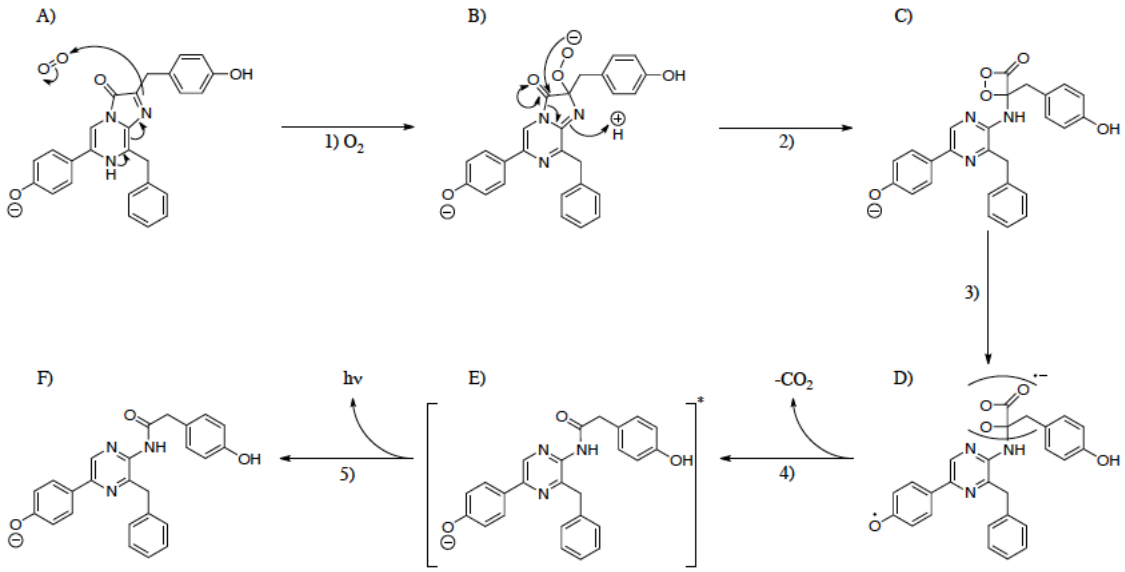

Figure 62: Mechanism of the oxidation of coelenterazine by the renilla luciferase (Rluc) of *Renilla reniformis*. A) and B) Coelenterazine reacts with oxygen to form the highly strained dioxetanone intermediate C). D), E) The unstable dioxetanone intermediate collapses to yield coelenteramide in an electronically excited state. E) and F) Excited (*) coelenteramide decays to its electronic ground state via the emission of a photon of light.

The chemiluminescent reactions catalyzed by Fluc and Rluc have been extensively studied and are known to display high quantum yields. [393] Under conditions where the enzyme substrate is in large excess over the enzyme, the level of expression of luciferase is proportional to the observed chemiluminescence. This relationship has been exploited by employing luciferase as a genetic reporter for translation assays. Luciferase genes have commonly been cloned downstream (3') of highly structured 5' UTRs to determine the inhibitory effect of tertiary mRNA structure on translation. This approach has subsequently been adapted to the identification and delineation of the boundaries of IRESs within the 5' UTRs of certain mRNAs. [33] [34] Fluc and Rluc were therefore chosen as suitable reporter gene candidates for the construction of a translation assay.

10.10.2.3 Construction of luciferase reporter vectors

In order to test the ability of cyclic peptides to disrupt the eIF4E / eIF4G interaction, a series of luciferase vectors were constructed based on a previously constructed luciferase reporter plasmid (**Figure 63**). [391] The 'PIC test' vector was previously described by Stewart and Cowan and was used as the basis for construction of a luciferase assay (**Figure 63:** A). [394] PIC test contains two distinct and separate systems (termed cistrons), where translation of the upstream (first) Fluc cistron can be directly compared to that of the downstream (second) Rluc cistron. The Fluc gene of the PIC test vector was fused at its 3' terminus to a sequence rich in proline (P), glutamic acid (E), serine (S) and threonine (T) called a 'PEST' domain, which has been shown to significantly reduce intracellular protein half-life. [395] Transcription of the upstream Fluc test cistron in mammalian cells was driven by the incorporation of the Simian virus 40 (SV40) promoter sequence. [396] PIC test incorporated a polyadenylation signal at the 3' end of the PEST domain for recruitment of poly A polymerase and synthesis of the 3' polyadenylated mRNA tail.

The PIC test vector also incorporates a second Rluc reference cistron to allow accurate quantification of transfection efficiency. [394] Transcription of the second cistron is driven by the Herpes simplex virus thymidine kinase (HSV TK) promoter to ensure efficient transcription of the Rluc gene. [397] [398] [399] [400] [401] An optimal Kozak consensus sequence is incorporated around the start codon of the Rluc gene to ensure efficient AUG recognition by the 40S ribosomal subunit. [43] [402] The Rluc gene was incorporated without

being fused to a PEST protein degradation domain so that the intracellular half-life of Rluc exceeds that of Fluc. This configuration therefore maintains a constant level of Rluc expression, which can be used to normalize data to account for variations in plasmid transfection efficiency between separate transfections. Translation of Fluc from the first cistron of PIC test can therefore be used as a reporter assay to quantify the effect of inhibitors on cap-dependent translation. The PIC test vector was therefore selected as a suitable candidate for testing inhibitors of the eIF4E / eIF4G interaction, via the concurrent suppression of cap-dependent translation.

Disruption of the eIF4E / eIF4G interaction selectively inhibits cap-dependent translation, with little effect on the cap-independent mechanism. [136] [139] [152] [164] It is conceivable however that inhibitors could suppress both cap-dependent and cap-independent translation, perhaps by inhibiting elements of the translation elongation machinery. It was therefore vital to establish that SICLOPPS derived cyclic peptides selectively disrupted the eIF4E / eIF4G interaction without adversely affecting cap-independent translation. In order to assess the effect of inhibitors on cap-independent translation, a series of PIC test derivatives were constructed where the translation of Fluc from the first cistron is under control of an IRES (**Figure 63:** B C D E). [33] [34] IRES within the 5' UTR of mRNAs consist of a series of defined stem loops which function to directly recruit the 40S ribosomal subunit. The 40S ribosomal subunit is therefore recruited downstream (3') of the m^7GTP 5' mRNA cap and is therefore recruited in a cap-independent fashion. IRES elements are also guanosine and cytosine rich and hence form highly stable hairpin structures within the 5' UTR. These structures impede the 5' to 3' scanning of any 40S ribosomal subunits that have been recruited upstream (5') of the IRES. [37] [38] [39] [40] [41] Therefore as cap-dependent translation recruits the 40S ribosomal subunits close to the m^7GTP 5' mRNA cap, the presence of an IRES within the 5' UTR inhibits scanning of 40S ribosomal subunits that have been recruited in a cap-dependent fashion. The insertion of an IRES upstream (5') to the Fluc gene of the first cistron therefore impedes cap-dependent translation and directs cap-independent translation of Fluc. [403] [404] A variety of previously validated IRES sequences were selected for insertion into PIC test, upstream (5') of the Fluc gene of cistron one (**Figure 63:** B, C, D and E).

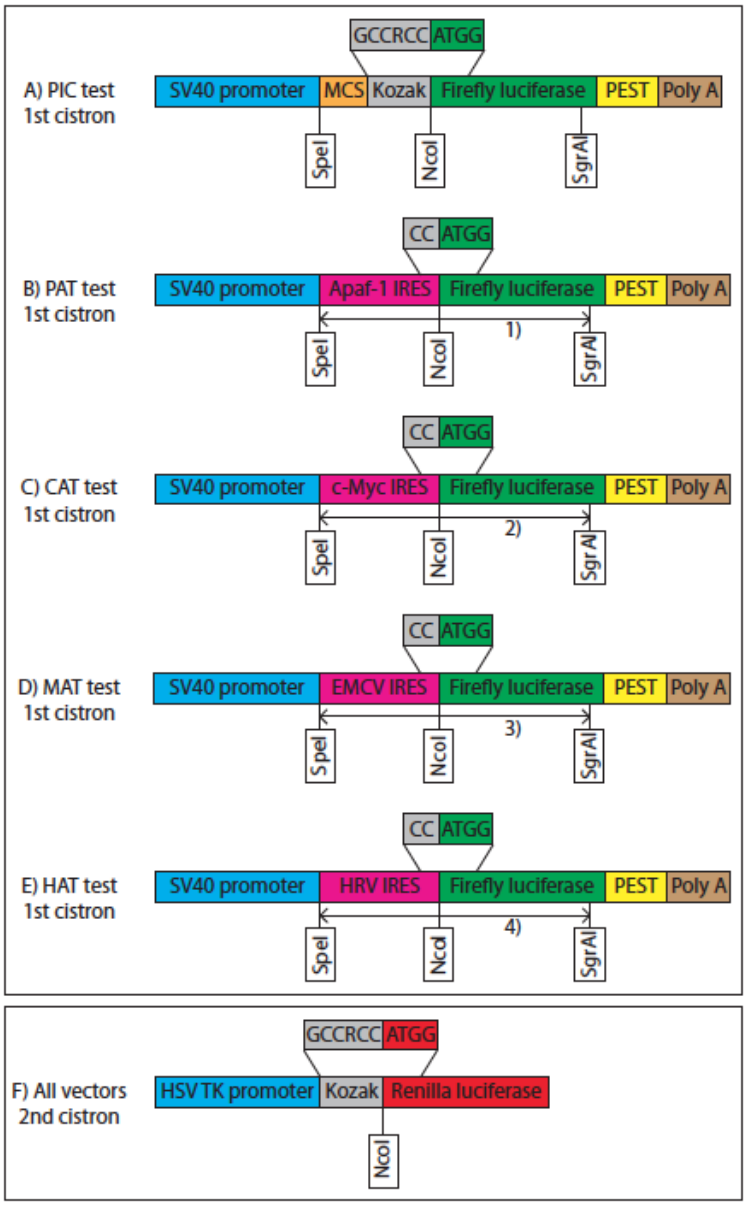

Figure 63: Schematic representation of two cistron PIC test vector derivatives. A) PIC test vector used to determine the effect of inhibitors on the cap-dependent translation of Fluc from cistron 1. [394] B) PAT test vector uses the apoptotic protease activating factor 1 (Apaf-1) IRES to direct cap-independent translation of Fluc from cistron 1. [403] [405] [406] C) CAT test vector uses the myelocytomatosis oncogenic transcription factor (c-Myc) IRES to direct cap-independent translation of Fluc from cistron 1. [404] [407] [408] D) MAT test vector uses the encephalomyocarditis virus (EMCV) IRES to direct cap-independent translation of Fluc from cistron 1. [409] [410] [411] [412] E) HAT test vector uses the human rhinovirus (HRV) IRES to direct cap-independent translation of Fluc from cistron 1. [413] [414] F) Rluc reference second cistron present in all PIC test vector derivatives.

Cap-dependent translation is suppressed within apoptotic cells via the caspase 3 mediated cleavage of eIF4G. [297] [415] As such, proteins that are required during apoptosis often utilize cap-independent translation. The 5' UTR of apoptotic protease activating factor 1 (Apaf-1) has been previously demonstrated to contain an IRES, which is capable of recruiting the 40S ribosomal subunit to the mRNA strand. [403] [405] [406] The Apaf-1 IRES was therefore selected to be inserted upstream of the Fluc reporter gene to direct cap-independent translation of Fluc (**Figure 63:** B). The second IRES selected for insertion upstream of the Fluc gene was derived from the 5' UTR of the mRNA that encodes the myelocytomatosis oncogenic transcription factor (c-Myc). [404] [407] [408] Although c-Myc translation can be effectively induced by cap-dependent translation, an IRES has been isolated from the mRNA 5' UTR that effectively directs cap-independent translation. [404] [407] [408] The boundaries of the c-Myc IRES have been delineated by a series of mRNA truncation experiments and hence the selected fragment corresponds to the minimal IRES epitope (**Figure 63:** C). [404] [407] [408] The Apaf-1 and c-Myc IRES were selected as representative examples of 5' UTR motifs derived from the human genome that efficiently recruit the 40S ribosomal subunit. The concept of an IRES however, was initially discovered by studying the translation of pathogenic viral RNA within host cells. [33] [34] Therefore the IRES derived from the 5' UTR of the RNA genomes of the encephalomyocarditis virus (EMCV, **Figure 63:** D) and the human rhinovirus (HRV, **Figure 63:** E) were selected as representative candidates of this important class. [409] [410] [411] [412] [413] [414]

The cloning of IRES elements directly upstream of the Fluc gene of PIC test was hampered by the presence of two NcoI REN sites (CCATGG) within the vector, one at the start codon of both luciferase genes (**Figure 63:** A and F). Therefore the cloning of IRES elements upstream (5') of the Fluc gene could not be achieved by inserting DNA between the NcoI and SpeI REN sites of PIC test (**Figure 63:** A). As such an alternative cloning strategy was devised based on a series of previously constructed luciferase vectors where the desired IRESs had already been fused to the 5' terminus of the Fluc gene. [408] [403] [404] The pRF vector is a di-cistronic luciferase reporter vector that was constructed by Stoneley and Paulin. [408] A variety of IRES elements have previously been inserted upstream (5') of the Fluc gene of pRF between the SpeI and NcoI REN sites to generate a series of vectors where the translation of Fluc is cap-independent. The pRF derivatives termed pRAF (Apaf-1 IRES), pRMF (c-Myc IRES), pRemcvF

(EMCV IRES) and pRhrvF (HRV IRES) were used as sources of the desired IRES fused upstream (5') of the Fluc gene. [408] [403] [404] pRF derivatives contained the desired IRESs cloned between the SpeI and NcoI REN sites, in addition to a unique SgrAI REN site towards the 3' end of the Fluc gene. In this study, SpeI / IRES / Fluc / SgrAI fragments (**Figure 63:** 1, 2, 3 and 4) were isolated from the relevant pRF derivative via REN digestion and ligated between the SpeI and SgrAI sites of PIC test (**Figure 63: A**). This generated a series of reporter vectors where the desired IRES was fused to the 5' terminus of the Fluc gene of the first cistron (**Figure 63:** B, C, D and E). PAT test (Apaf-1 IRES / Fluc), CAT test (c-Myc IRES / Fluc), MAT test (EMCV IRES / Fluc) and HAT test (HRV IRES / Fluc) were therefore selected as suitable control vectors to analyze the effect of inhibitors on cap-independent translation.

10.10.2.4 Validation of luciferase reporter vectors

An examination of the literature on the Apaf-1, c-Myc, EMCV and HRV IRESs revealed that the ability of an IRES to recruit the 40S ribosome is dependent on the presence of intracellular protein co-factors. [416] [406] [405] [414] [417] [409] The Apaf-1 IRES has been shown to direct cap-independent translation of Fluc from the pRAF vector approximately five fold more efficiently in the HeLa cervical cancer cell line than in MCF-7 cells. [406] [403] Similarly the c-Myc IRES has been shown to direct the cap-independent translation of Fluc from pRMF approximately ten fold more efficiently in HeLa cells than in MCF-7 cells. [404] [408] [416] The pRF derivatives containing the EMCV (pRemcvF) and HRV (pRhrvF) IRES sequences have also been used to direct cap-independent translation of Fluc within HeLa cells, albeit with reduced efficiency compared to the c-Myc IRES. [404] The luciferase assay was therefore conducted by transient transfection of the PIC test vector (and its derivatives PAT, CAT, MAT and HAT test) into HeLa cells.

It was necessary to verify the luciferase vectors as valid assay tools to determine the effect of cyclic peptides on cap-dependent and cap-independent translation. This was achieved via the testing of a range of specific cap-dependent translation inhibitors against the luciferase vectors. Rapamycin is an indirect selective inhibitor of the function of the mTORC1 complex (one of the subunits of mTOR) that is responsible for phosphorylation of the 4EBPs. Rapamycin treatment inactivates mTORC1, which results in hypophosphorylation of the 4EBPs, accompanied by increased association with eIF4E. Hypophosphorylated 4EBPs compete effectively with eIF4G for binding to eIF4E and therefore sequester the cap-binding protein. This inhibits eIF4F assembly and has been shown to result in decreased rates of cap-dependent translation. [418] [419] [420] By contrast, the more recently developed therapeutic PP242 is a more effective inhibitor of mTORC1 and also inhibits the mTORC2 complex (the second subunit of mTOR). PP242 has been shown to be a more effective inhibitor of the mTORC1 subunit and suppresses cap-dependent translation to a greater degree than Rapamycin. [421] [422] However both rapamycin and PP242 selectively inhibit cap-dependent translation in an indirect manner, via promoting the association of hypohphosphorylated 4EBPs with eIF4E.

The small molecule therapeutic 4EGi was included as a positive control because it has been shown to disrupt the interaction of eIF4E with the helical eIF4G peptide 'YDREFLL' and thus functions as a direct inhibitor of cap-dependent translation via disruption of the eIF4E / eIF4G interaction. [423]

Two positive control compounds were included that inhibit elements of the translation initiation or elongation machinery and exhibit no differentiation between cap-dependent and cap-independent translation. Cycloheximide is a direct inhibitor of the translocation step of translation elongation. [424] [425] Recent mechanistic studies have shown that cycloheximide treatment results in the accumulation of dipeptides, implying that one cycle of elongation is allowed to proceed prior to termination of translation. Cycloheximide stabilizes the binding of deacylated tRNAs to the 'E' site of the 80S ribosome, preventing efficient recruitment of aminoacyl tRNAs to the 'A' site. This traps the 80S ribosome in the post-translocational state and inhibits peptide chain elongation. [426] By contrast, thapsigargin is an indirect inhibitor of the loading of $^{Met}tRNA_i$ to the TC. Thapsigargin treatment triggers intracellular release of Ca^{2+} stored within the endoplasmic reticulum, which triggers a signaling cascade that results in the phosphorylation of eIF2. Phosphorylated eIF2 becomes trapped in a GDP bound state, which cannot form the TC and therefore cannot initiate translation. [427] [428] [429]

It was hypothesized that treatment of HeLa cells with positive control compounds would selectively inhibit cap-dependent translation (PP242, rapamycin, 4EGi) or inhibit global translation (cycloheximide, thapsigargin). HeLa cells were plated onto 96 well plates and incubated for 24 h prior to transient transfection with luciferase assay vectors for 48 h. Spent transfection media was removed and cells were washed with PBS prior to treatment with positive control compounds or vehicle alone control for 4 h. At the conclusion of the treatment, spent media was removed and cells were washed with PBS, prior to cell lysis. Quantification of Fluc and Rluc reporters was achieved using a duel luciferase reporter assay system kit with a Glomax multi detection system (Promega).

Transient transfection of MAT test and HAT test into HeLa cells failed to yield quantities of luciferase that were significantly above background and hence compound validation against these vectors could not be performed. Minimal luciferase expression suggests that cloning of either EMCV or HRV IRES at the 5' end of the Fluc gene

failed to stimulate translation of significant quantities of Fluc. This is contrary to the published literature, as Stoneley and Subkhankulova observed efficient translation of Fluc from both pRemcvF and pRhrvF, upon transient transfection into HeLa cells. [404] One possible explanation for the inefficient translation of Fluc from the MAT test vector could be related to the direct fusion of the EMCV IRES against the NcoI REN site at the start of the Fluc gene. An examination of the nucleotide sequence around the AUG start codon of the Fluc gene of MAT test revealed that it contained a non-optimal Kozak consensus sequence. MAT test exhibited an '$A^{-6}T^{-5}G^{-4}G^{-3}$CC**ATG**G' motif around the start codon, which differs significantly from the optimal '$G^{-6}C^{-5}C^{-4}R^{-3}$CC**ATG**G' Kozak consensus sequence (NcoI REN site underlined; start codon highlighted in bold; purine (R) is A or G). [402] [43] Whilst the NcoI REN site and the purine in position -3 have been maintained within the MAT test motif, the nucleotides at positions -4, -5 and -6 are sub-optimal for start codon recognition. It is therefore possible that decreased translation of Fluc from MAT test is a consequence of scanning of the 40S ribosomal subunit past the Fluc start codon, with initiation occurring at a downstream AUG codon. However, this explanation does not explain the poor HRV IRES directed translation of Fluc from HAT test, which has a near optimal '$G^{-6}G^{-5}C^{-4}A^{-3}$CC**ATG**G' motif for start codon recognition. It is interesting to note that both viral IRES sequences failed to promote efficient translation when placed at the 5' terminus of the downstream Fluc gene. IRES domains are typically located downstream (3') of highly structured 5' UTRs and not typically as close to the 5' terminus of the mRNA. It is therefore possible that the atypical placement of the viral IRESs has compromised their ability to efficiently recruit the 40S ribosome.

The PIC test vector was validated against a range of known translation inhibitors. Treatment of HeLa cells with PP242, cycloheximide and thapsigargin depressed translation significantly, consistent with their accepted inhibitory mechanisms (**Figure 64**). However treatment of cells with Rapamycin and 4EGi failed to elicit the expected inhibition of cap-dependent translation, as observed via the Fluc / Rluc ratio. Rapamycin has been shown to inhibit mTORC1, which results in the hypophosphorylation of the 4EBPs. Early studies suggested that rapamycin inhibited cap-dependent translation, as demonstrated by luciferase assay and ^{35}S methionine incorporation. [418] [419] [420]

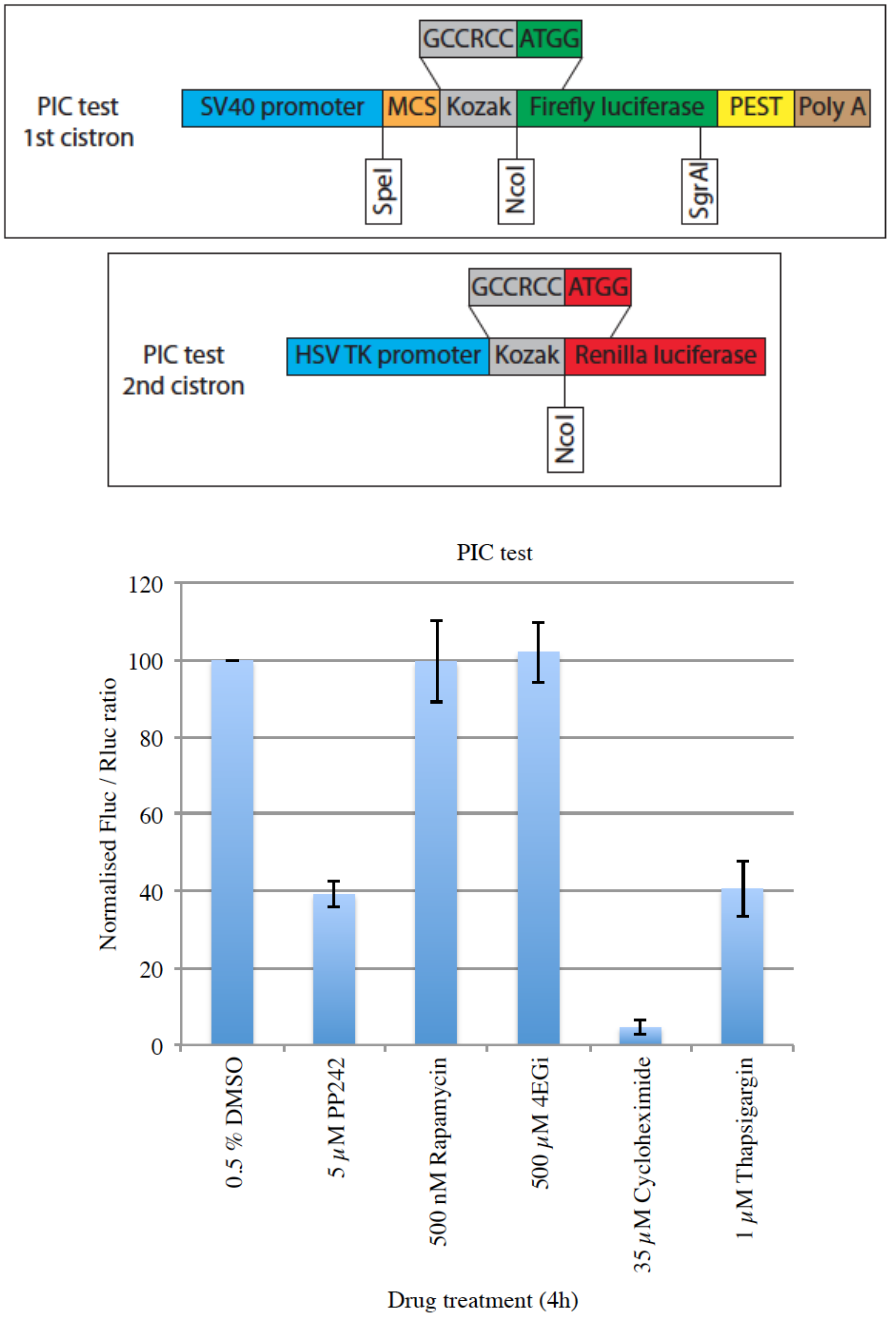

Figure 64: Validation of the two cistron reporter vector PIC test against a range of specific cap-dependent translation (PP242, Rapamycin and 4EGi) and non-specific translation (Cycloheximide, Thapsigargin) inhibitors. Error bars are representative of +/- one standard deviation of the means of three independent experiments. All results were normalized to negative control cells treated for 4h with drug delivery vehicle (0.5 % DMSO), which were analyzed in parallel with samples treated with positive control compounds. Fluc / Rluc ratio was determined in cells treated with drug delivery vehicle alone, then set as 100 % and subsequently used to normalize Fluc / Rluc ratio for all samples.

However subsequent studies have indicated that inhibition of mTORC1 by rapamycin, results in the activation of Mnk2, which phosphorylates eIF4E. Phosphorylated eIF4E stimulates translation to compensate for the hypophosphorylation of the 4EBPs. [430] [431] The phosphorylation of eIF4E constitutes a plausible explanation for the failure of rapamycin to suppress cap-dependent translation of Fluc from the PIC test vector. At first, the apparent failure of 4EGi to suppress cap-dependent translation of Fluc from PIC test seemed completely contrary to the published literature. [423] This prompted a comparison of the raw luminescence readings obtained for Fluc and Rluc from 4EGi treated cells against cells treated with other positive controls. 4EGi did suppress the cap-dependent translation of Fluc from cistron 1 of PIC test (**Figure 65**), but also suppressed expression of the Rluc transfection control from the second cistron (**Figure 66**). The suppression of Rluc expression upon 4EGi treatment surpassed that induced by treatment with cycloheximide, which is known to induce apoptosis. This may indicate that 4EGi treatment interferes with Rluc directly, or may induce cellular apoptosis. In addition, the large fluctuations observed in the Rluc data are suggestive of variable transfection efficiency between experiments, re-enforcing the need to incorporate a reference gene within the test vector (**Figure 66**).

HeLa cells were transfected with PAT test and then treated with cycloheximide and thapsigargin, which both suppressed translation to a similar degree as that previously observed for HeLa cells transfected with PIC test (**Figure 67**). This is consistent with thapsigargin mediated inhibition of TC formation and cycloheximide induced suppression of the elongation phase of translation. The similar degree of translational suppression observed in the presence (PAT test) and absence (PIC test) of the Apaf-1 IRES supports the hypothesis that cycloheximide and thapsigargin suppress both cap-dependent and cap-independent translation to a similar degree. The introduction of the Apaf-1 IRES in PAT test stimulated translation of the downstream Fluc gene by ~ 20% relative to PIC test when treated with PP242. This supports the hypothesis that the Apaf-1 IRES upstream of the Fluc gene is directing cap-independent translation. However, the introduction of the Apaf-1 IRES does not appear to completely compensate for the inhibition of cap-dependent translation by PP242, as demonstrated by the level of Fluc translation at ~ 60 % of that of the vehicle alone control. This may be an indication that the placement of a highly structured IRES without a lengthy 5' UTR allows some cap-dependent translation to occur.

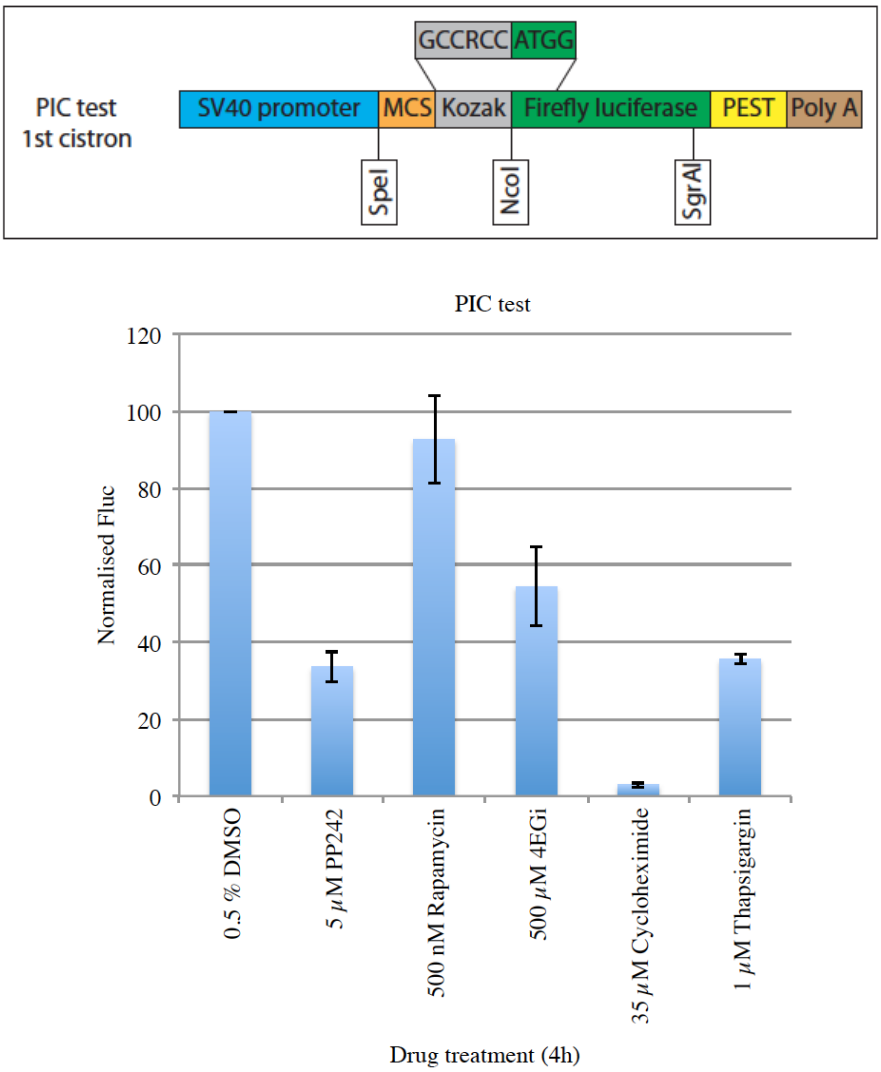

Figure 65: Effect of positive control compounds on the cap-dependent translation of Fluc from PIC test. Error bars are representative of +/- one standard deviation of the means of three independent experiments. All results were normalized to negative control cells treated for 4h with drug delivery vehicle (0.5 % DMSO), which were analyzed in parallel with samples treated with positive control compounds. Fluc expression was determined in cells treated with drug delivery vehicle alone, then set as 100 % and subsequently used to normalize Fluc expression for all samples.

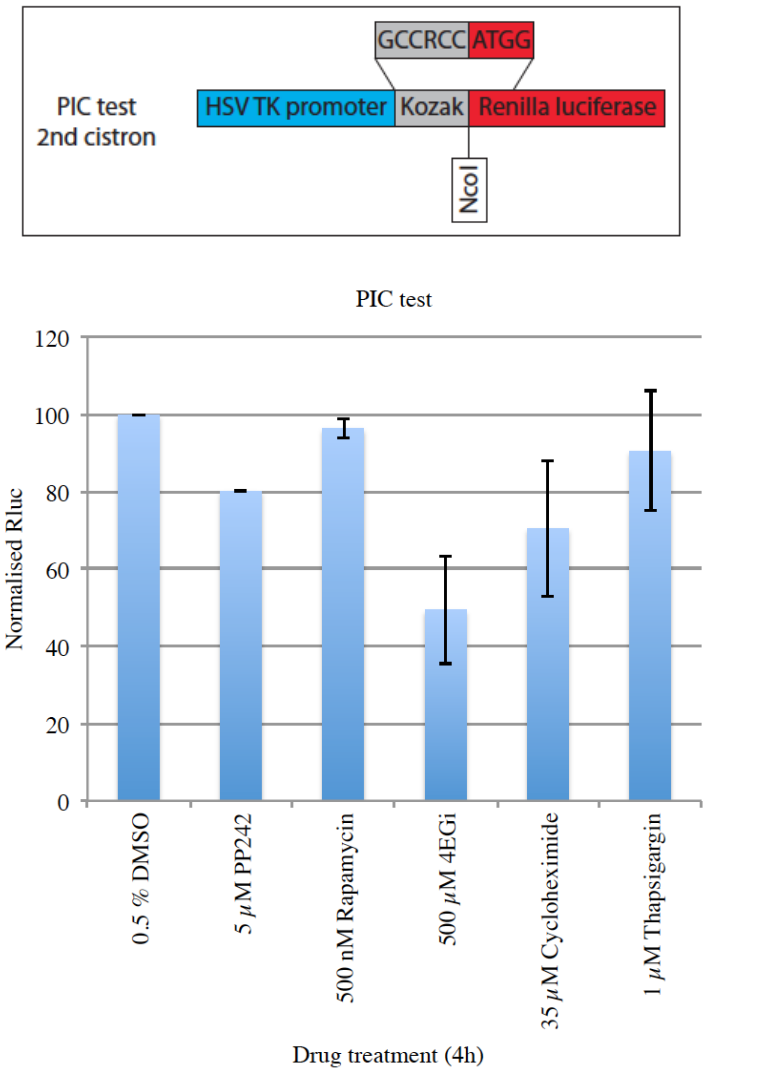

Figure 66: Effect of positive control compounds on the translation of the Rluc transfection control gene of PIC test. Error bars are representative of +/- one standard deviation of the means of three independent experiments. All results were normalized to negative control cells treated for 4h with drug delivery vehicle (0.5 % DMSO), which were analyzed in parallel with samples treated with positive control compounds. Rluc expression was determined in cells treated with drug delivery vehicle alone, then set as 100 % and subsequently used to normalize Rluc expression for all samples.

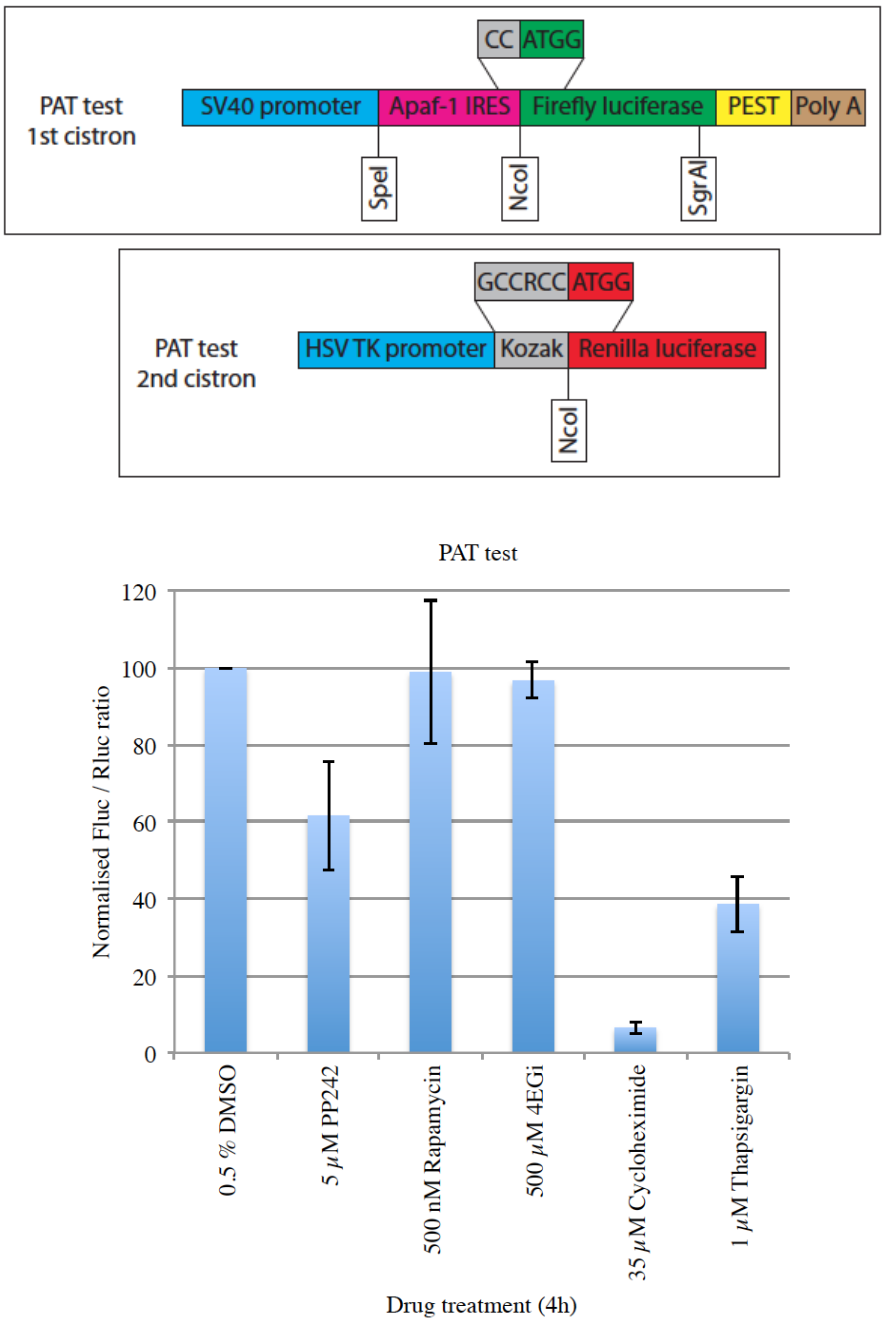

Figure 67: Validation of the two cistron reporter vector PAT test against a range of specific cap-dependent translation (PP242, Rapamycin and 4EGi) and non-specific translation (Cycloheximide, Thapsigargin) inhibitors. Error bars are representative of +/- one standard deviation of the means of three independent experiments. All results were normalized to negative control cells treated for 4h with drug delivery vehicle (0.5 % DMSO), which were analyzed in parallel with samples treated with positive control compounds. Fluc / Rluc ratio was determined in cells treated with drug delivery vehicle alone, then set as 100 % and subsequently used to normalize Fluc / Rluc ratio for all samples.

Rapamycin treatment of HeLa cells transfected with PAT test failed to inhibit translation to any degree, as previously observed for PIC test. It has previously been observed that treatment of cells with specific inhibitors of the cap-dependent translation machinery such as 4EGi, 4E1RCat and 4E2RCat, can yield increased rates of cap-independent translation. [423] [14] [15] This effect has been attributed to the liberation of 40S ribosomal subunits (among other components of the translation machinery) from cap-dependent translation and their subsequent utilization via a cap-independent mechanism. It is interesting to note that rapamycin treatment did not increase the cap-independent translation of Fluc under the direction of the Apaf-1 IRES, although the reasons for this are currently unclear. As expected 4EGi treatment of HeLa cells transfected with PAT test failed to elicit a reduction in the cap-independent translation of Fluc from the Apaf-1 IRES. Given the anomalous effect of 4EGi on the translation of the Rluc transfection control of PIC test, raw luminescence readings obtained for Fluc and Rluc were examined. 4EGi again exhibited apparent suppression of Rluc expression, possibly due to cytotoxicity, hence 4EGi was not deemed an appropriate control for the luciferase assay.

HeLa cells were transfected with CAT test and then treated with cycloheximide and thapsigargin, which both suppressed translation to a similar degree as that previously observed for HeLa cells transfected with PIC test and PAT test (**Figure 68**). This is consistent with thapsigargin induced inhibition of TC formation and cycloheximide mediated suppression of the elongation phase of translation. The similar degree of translational suppression observed in the presence (CAT test) and absence (PIC test) of the c-Myc IRES supports the hypothesis that cycloheximide and thapsigargin suppress cap-dependent and cap-independent translation to a similar degree. The introduction of the c-Myc IRES in CAT test stimulated translation of the downstream Fluc gene by ~ 35% relative to PIC test when treated with PP242. This supports the hypothesis that the c-Myc IRES upstream of the Fluc gene is directing cap-independent translation. However, the introduction of the c-Myc IRES does not appear to completely compensate for the inhibition of cap-dependent translation by PP242, as demonstrated by the level of Fluc translation at ~ 75 % of that of the vehicle alone control. This may again be an indication that the placement of a highly structured IRES without a lengthy 5' UTR allows a certain degree of cap-dependent translation to occur.

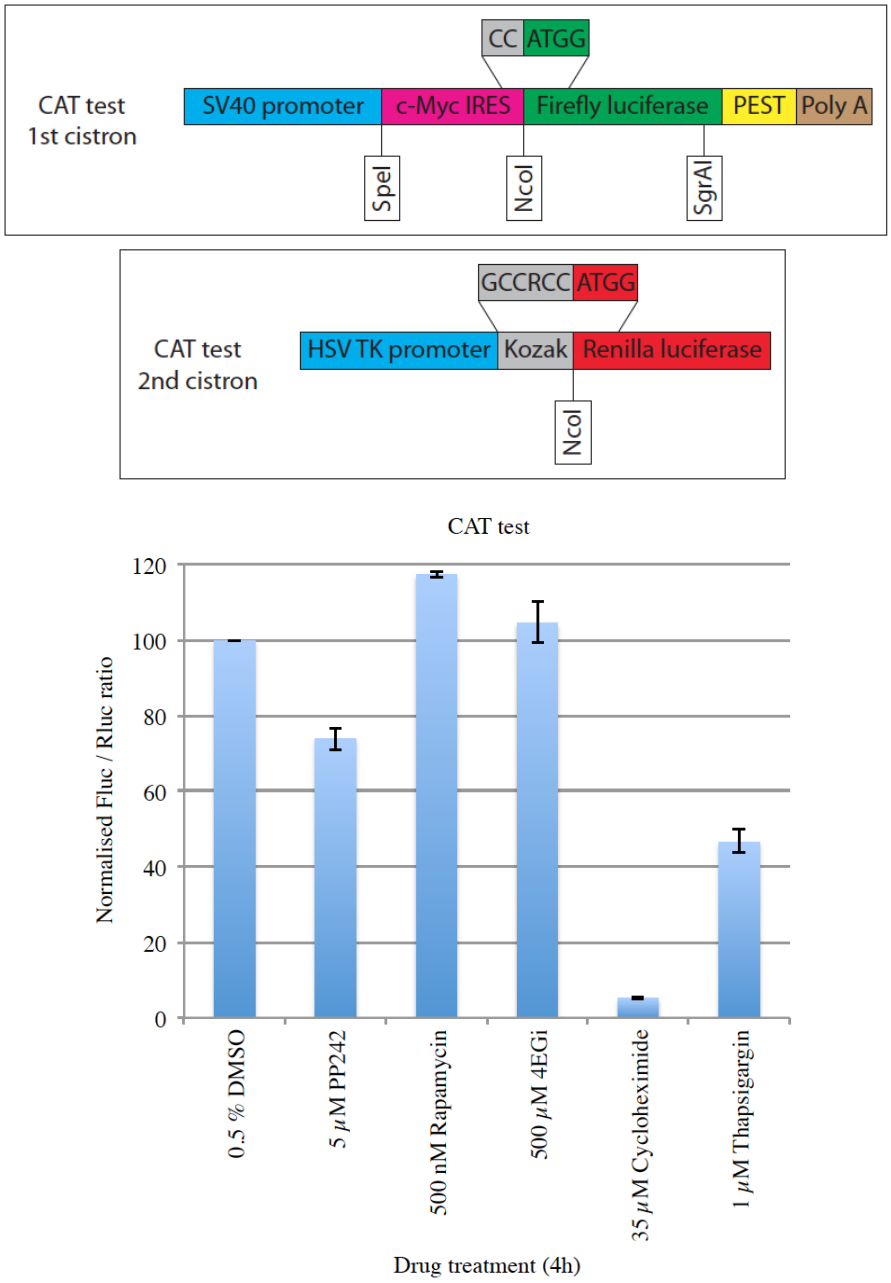

Figure 68: Validation of the two cistron reporter vector CAT test against a range of specific cap-dependent translation (PP242, Rapamycin and 4EGi) and non-specific translation (Cycloheximide, Thapsigargin) inhibitors. Error bars are representative of +/- one standard deviation of the means of three independent experiments. All results were normalized to negative control cells treated for 4h with drug delivery vehicle (0.5 % DMSO), which were analyzed in parallel with samples treated with positive control compounds. Fluc / Rluc ratio was determined in cells treated with drug delivery vehicle alone, then set as 100 % and subsequently used to normalize Fluc / Rluc ratio for all samples.

Rapamycin treatment of HeLa cells transfected with CAT test yielded a slight increase in the c-Myc IRES directed cap-independent translation of Fluc. This effect is consistent with rapamycin induced liberation of translation factors from cap-dependent translation complexes, which are subsequently used via cap-independent mechanism. 4EGi treatment of HeLa cells transfected with CAT test, failed to elicit a reduction in the cap-independent translation of Fluc from the c-Myc IRES as expected. Given the anomalous effect of 4EGi on the translation of the Rluc transfection control of PIC test, raw luminescence readings obtained for Fluc and Rluc were examined. 4EGi again exhibited apparent suppression of Rluc expression, possibly due to cytotoxicity, hence 4EGi was not deemed an appropriate control for the luciferase assay. PIC test, PAT test and CAT test were therefore deemed to be appropriate luciferase reporter vectors to analyze the effects of potential cyclic peptide inhibitors of the eIF4E / eIF4G interaction on cap-dependent translation.

10.10.2.5 Cyclic peptide screening against luciferase reporter vectors

It was hypothesized that treatment of HeLa cells with cyclic peptide inhibitors of the eIF4E / eIF4G interaction would selectively inhibit cap-dependent translation with little impact on cap-independent translation. HeLa cells were transiently transfected with luciferase assay vectors prior to treatment with cyclic peptides or vehicle alone control for 4 h, as described previously. Fluc and Rluc reporter gene expression was quantified using a duel luciferase reporter assay system kit with a Glomax multi detection system (Promega).

Cyclic peptide treatment of HeLa cells transfected with PIC test reduced cap-dependent translation of Fluc to ~ 80 % of that observed in the negative control (**Figure 69**). This is consistent with the hypothesis that cyclic peptides are disrupting the eIF4E / eIF4G interaction, with the concomitant reduction in the rate of cap-dependent translation. Cyclic peptide treatments were repeated in HeLa cells transfected with either PAT test or CAT test, to determine if the translational suppression elicited by cyclic peptides was specific to a cap-dependent mechanism. Cyclic peptide treatment of HeLa cells transfected with the former reduced Apaf-1 IRES directed translation of Fluc by up to 10 % relative to the vehicle alone control (**Figure 70**). It is therefore likely that the cyclic peptides are exhibiting cytotoxicity, thereby reducing the observed level of cap-dependent and cap-independent translation. However, it was previously observed that

the translation of Fluc from PAT test was not entirely immune to inhibition by PP242, which is a selective inhibitor of cap-dependent translation. Therefore it is also possible that the observed ~10 % reduction in the translation of Fluc upon cyclic peptide treatment is due to inhibition of the cap-dependent component of the translation of Fluc when under control of the Apaf-1 IRES.

Cyclic peptides were therefore tested against the IRES containing PIC test derivative that exhibited the greatest PP242 independent translation of Fluc, which was the CAT test vector. Cyclo VYVVCRRQ treatment of HeLa cells transfected with CAT test reduced c-Myc IRES directed translation of Fluc by up to 20 % relative to the vehicle alone control, perhaps indicating that this peptide has cytotoxic effects. The other three cyclic peptides exerted little influence on the c-Myc IRES directed cap-independent translation of Fluc from cistron 1 of CAT test. This is consistent with the hypothesis that the disruption of Fluc translation from PIC test is selective for a cap-dependent mechanism and has little effect on cap-independent translation. In turn, this finding is consistent with the cyclic peptide mediated selective disruption of the eIF4E / eIF4G interaction.

Whilst the luciferase assay provides an indication of the selectivity of cyclic peptide treatment on cap-dependent over cap-independent translation, it is difficult to confirm that IRES driven Fluc expression proceeds entirely via a cap-independent mechanism. It was therefore necessary to determine the effect of cyclic peptide treatment on global translation via monitoring of ^{35}S radioactively tagged amino acid incorporation.

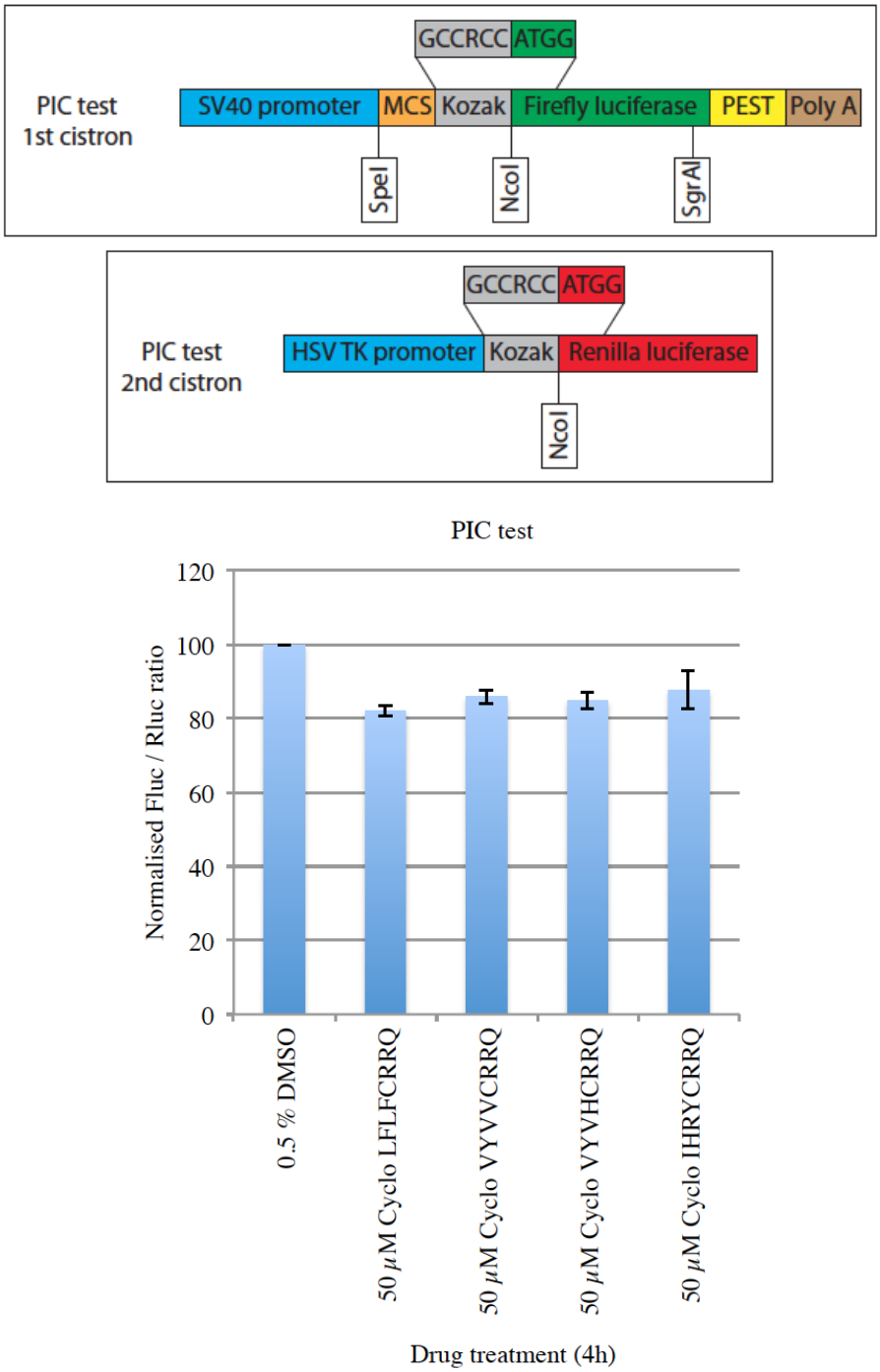

Figure 69: The effect of treatment of HeLa cells with potential cyclic peptide inhibitors of the eIF4E / eIF4G interaction on the cap-dependent translation of Fluc from PIC test. Error bars are representative of +/- one standard deviation of the means of three independent experiments. All results were normalized to negative control cells treated for 4h with drug delivery vehicle (0.5 % DMSO), which were analyzed in parallel with samples treated with cyclic peptides. Fluc / Rluc ratio was determined in cells treated with drug delivery vehicle alone, then set as 100 % and subsequently used to normalize Fluc / Rluc ratio for all samples.

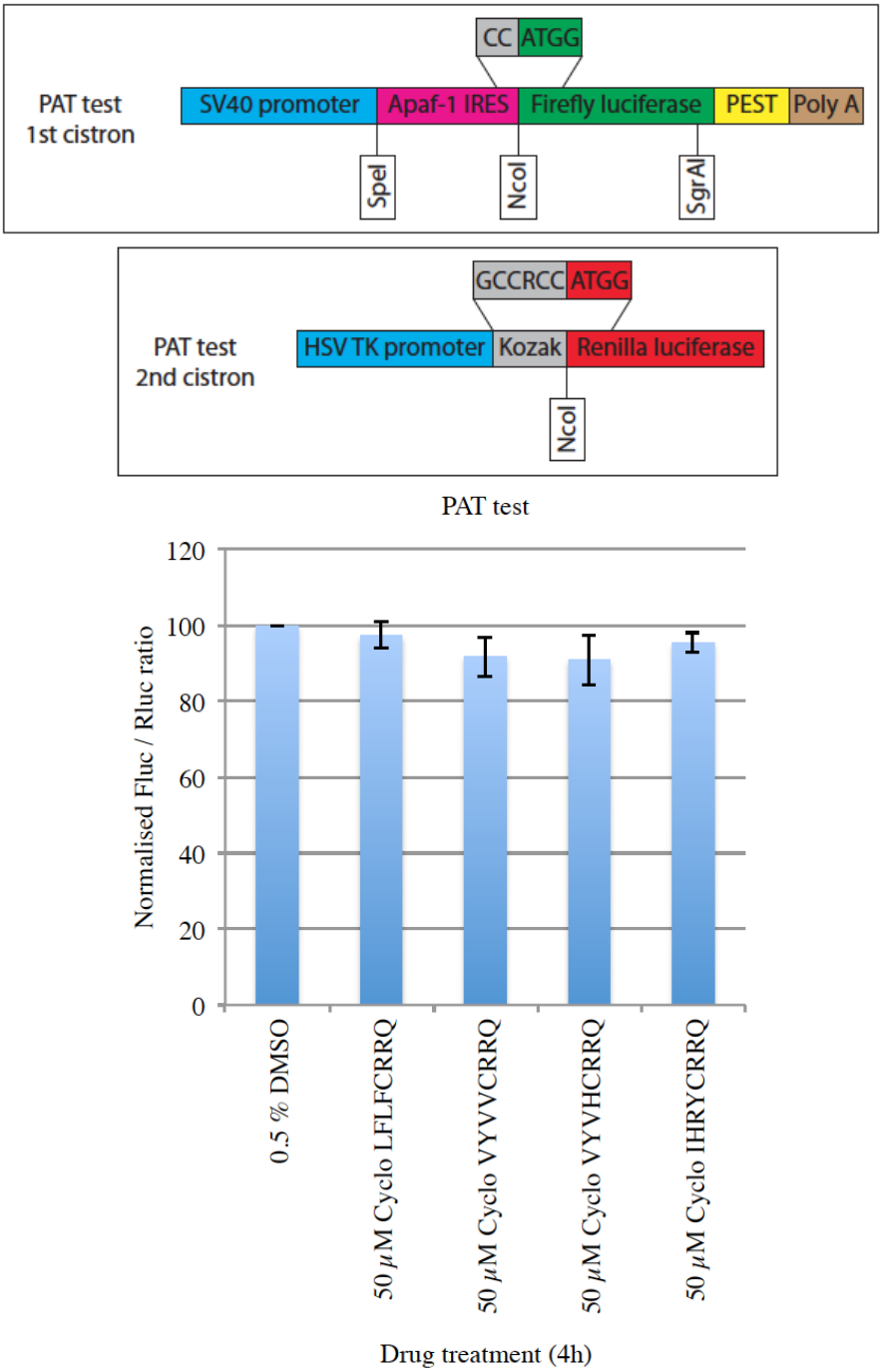

Figure 70: The effect of treatment of HeLa cells with potential cyclic peptide inhibitors of the eIF4E / eIF4G interaction on the cap-independent translation of Fluc from PAT test. Error bars are representative of +/- one standard deviation of the means of three independent experiments. All results were normalized to negative control cells treated for 4h with drug delivery vehicle (0.5 % DMSO), which were analyzed in parallel with samples treated with cyclic peptides. Fluc / Rluc ratio was determined in cells treated with drug delivery vehicle alone, then set as 100 % and subsequently used to normalize Fluc / Rluc ratio for all samples.

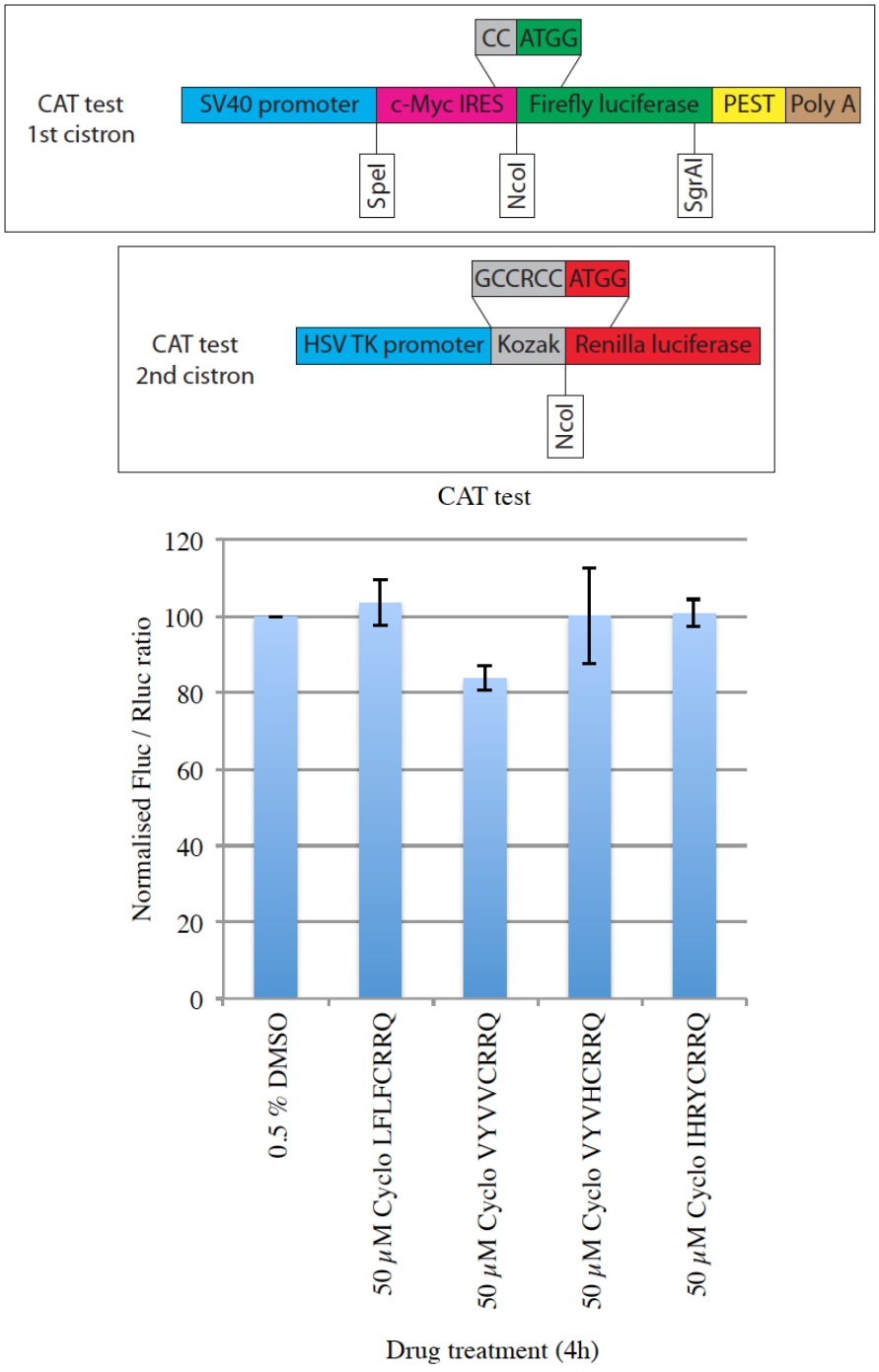

Figure 71: The effect of treatment of HeLa cells with potential cyclic peptide inhibitors of the eIF4E / eIF4G interaction on the cap-independent translation of Fluc from CAT test. Error bars are representative of +/- one standard deviation of the means of three independent experiments. All results were normalized to negative control cells treated for 4h with drug delivery vehicle (0.5 % DMSO), which were analyzed in parallel with samples treated with cyclic peptides. Fluc / Rluc ratio was determined in cells treated with drug delivery vehicle alone, then set as 100 % and subsequently used to normalize Fluc / Rluc ratio for all samples.

10.10.3 ^{35}S radioactive methionine incorporation assay

Radioactive methionine incorporation into proteins has become a standard technique to monitor effects on global translation. [432] [15] [14] [418] [419] [422] The ^{35}S isotope is a β particle emitter with a half-life of 87 days and therefore its presence can be readily detected by scintillation counting. [433] The selection of the ^{35}S isotope is compatible with the labeling of the two sulfur containing amino acids, methionine and cysteine. This represents a particularly appropriate choice, as translation of every protein is initiated by AUG codon recognition and the subsequent recruitment of aminoacyl initiator methionine tRNA. Therefore ^{35}S labeling of methionine ensures that every translated polypeptide is radioactively labeled at its N-terminus (**Figure 72**). [434] [63] The additional incorporation of ^{35}S labeled cysteine allows for the selective radioactive labeling of cysteine containing peptides during the elongation phase of translation (**Figure 72**). Whilst the assay does not differentiate between cap-dependent and cap-independent translation, significant inhibition of one or both mechanisms should be detectable. It was hypothesized that cyclic peptide inhibitors of the eIF4E / eIF4G interaction would inhibit eIF4F assembly and therefore inhibit cap-dependent translation. In turn this should result in reduced incorporation of ^{35}S tagged methionine and cysteine into polypeptides.

10.10.3.1 Validation of the ^{35}S methionine incorporation assay

It was first necessary to validate that treatment of HeLa cells with the positive control compounds (PP242, rapamycin, 4EGi, cycloheximide and thapsigargin) would inhibit translation and hence reduce incorporation of ^{35}S tagged methionine and cysteine into proteins. [422] [419] [423] [426] [427] HeLa cells were sub cultured into 6 cm dishes and incubated for 24 h to allow cells to adhere to the plate. Spent media was removed and cells were treated with positive control compounds or vehicle alone control for 4 h. After 3 h 30 min of treatment, cells were pulse labeled with ^{35}S labeled methionine / cysteine for exactly 30 min. Cell pellets were isolated via centrifugation, lysed with mammalian protein extraction reagent (MPER) and spotted in triplicate onto filter paper discs. Protein was precipitated onto filter discs and radioactivity of triplicate samples was quantified by scintillation counting. Cell lysate concentration was determined via Bradford assay and used to correct observed radioactive counts per μg of protein. Triplicate readings were averaged and then normalized to cells treated with delivery vehicle alone (0.5 % DMSO), which was set as 100 %.

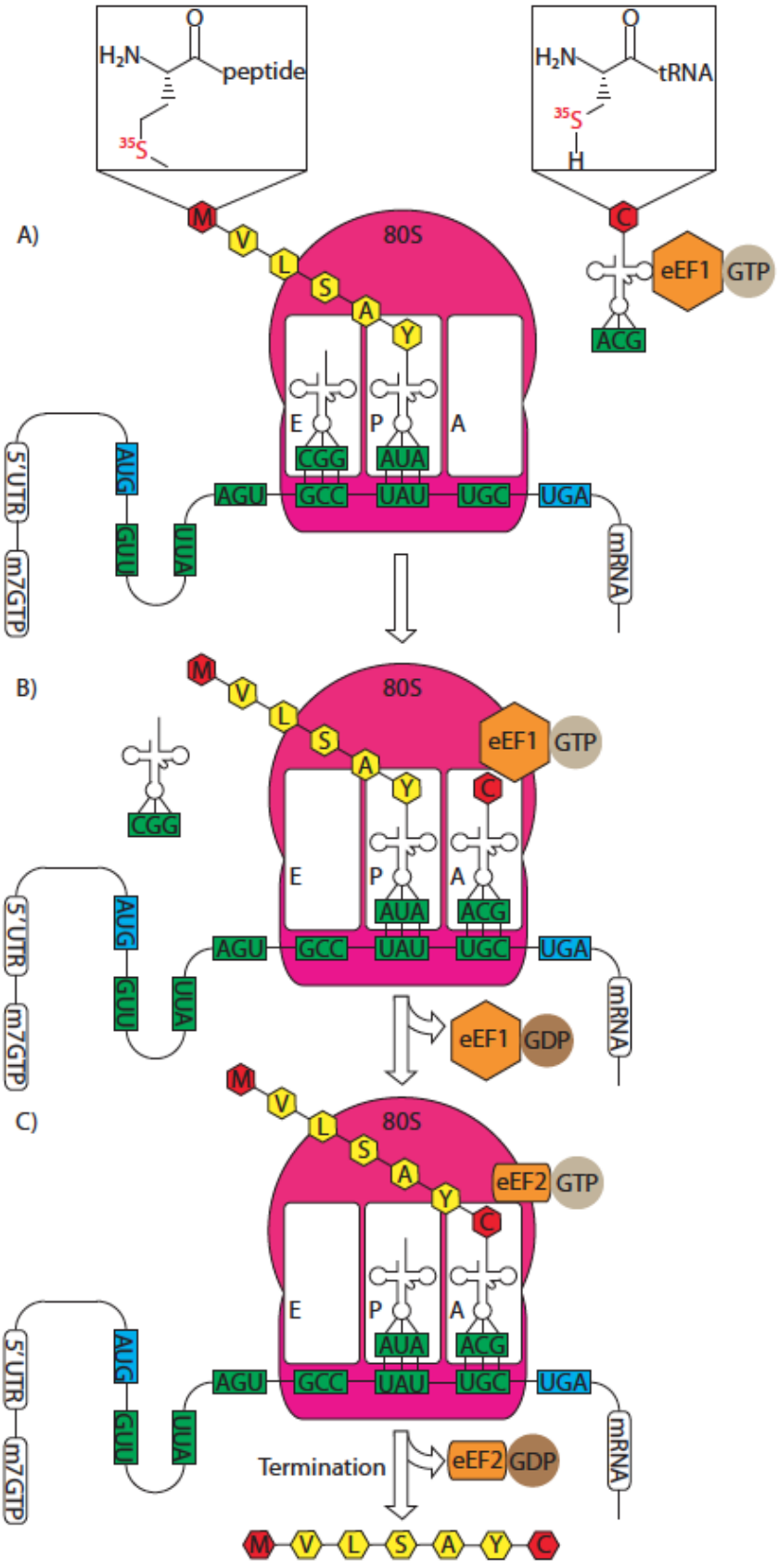

Figure 72: Schematic representation of the incorporation of ^{35}S labeled methionine and cysteine residues into polypeptides during translation elongation. [89] [90] [91] [92]

Treatment of HeLa cells with PP242 suppressed the incorporation of ^{35}S tagged methionine and cysteine by ~ 50 % (**Figure 73**). This is consistent with inhibition of the mTORC1 subunit yielding hypophosphorylated 4EBPs that bind to eIF4E, with a concomitant reduction in the rate of cap-dependent translation. [422] The effect of PP242 treatment on global translation rates by ^{35}S incorporation (~ 50 % of vehicle alone control) is less potent than the inhibitory effect exerted on cap-dependent Fluc translation from PIC test (~ 40 % of vehicle alone control). This disparity may be due to the PP242 induced liberation of 40S ribosomal subunits (among other components of the translation machinery) from cap-dependent translation and their subsequent utilization via a cap-independent mechanism. [423] [14] [15] It is interesting to note that the mTORC1 selective inhibitor rapamycin, failed to reduce the incorporation of ^{35}S labeled amino acids into proteins (**Figure 73**). This result is entirely consistent with the failure of rapamycin to suppress cap-dependent translation of Fluc from PIC test and supports the hypothesis that Mnk2 induced eIF4E phosphorylation compensates for decreased 4EBP phosphorylation. [430] [431]

Cell treatment with the eIF4E / eIF4G interaction inhibitor 4EGi reduced incorporation of ^{35}S amino acids into proteins to ~ 15 % of the level of incorporation exhibited by the vehicle alone treated control (**Figure 73**). This finding is indicative of disruption of eIF4F formation with concomitant suppression of cap-dependent translation. However the degree to which 4EGi inhibits translation is similar to that induced by cycloheximide, which may suggest that a degree of apoptosis has been induced by 4EGi treatment. The degree of suppression of ^{35}S incorporation in response to 4EGi treatment supports the hypothesis that 4EGi inhibited expression of the Rluc gene from PIC test (and its derivatives) via the induction of apoptosis.

Cycloheximide suppressed ^{35}S incorporation into HeLa cell protein (10 % of vehicle alone control, **Figure 73**) to a similar degree to the suppression of Fluc translation from PIC test (5 % of vehicle alone control) PAT test (7 % of vehicle alone control) and CAT test (5 % of vehicle alone control). This data is consistent with the published literature that cycloheximide inhibits the translocation step of elongation, thereby reducing incorporation of ^{35}S labeled methionine and cysteine into HeLa cell protein. [426]

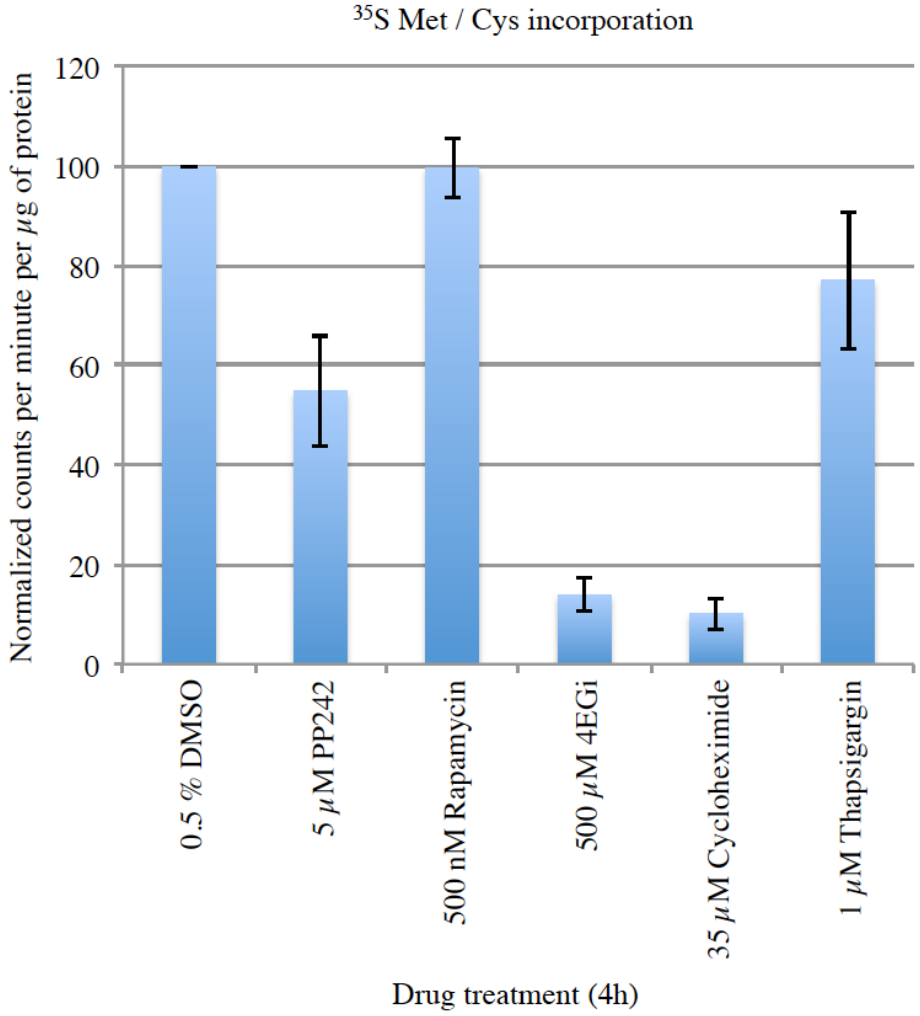

Figure 73: The effect of positive control compound treatment on translation as inferred from incorporation of ^{35}S labeled methionine and cysteine into HeLa cell protein. Error bars are representative of +/- one standard deviation of the means of three independent experiments. All results were normalized to negative control cells treated for 4h with drug delivery vehicle (0.5 % DMSO), which were analyzed in parallel with samples treated with positive control compounds. Incorporation of ^{35}S labeled methionine and cysteine into cells treated with drug delivery vehicle alone was set as 100 % and subsequently used to normalize scintillation counts per minute per µg of protein for all samples.

Treatment of HeLa cells with thapsigargin suppressed the incorporation of ^{35}S tagged methionine and cysteine into proteins to ~ 75 % of the level of incorporation exhibited by the vehicle alone treated control (**Figure 73**). However the degree of translational suppression observed by ^{35}S incorporation (~ 75 % of vehicle alone control) exceeds the degree of the suppression of translation of Fluc from PIC test (No IRES, ~ 40 % of vehicle alone control) PAT test (Apaf-1 IRES, ~ 38 % of vehicle alone control) and CAT test (c-Myc IRES, ~ 47 % of vehicle alone control). The reasons for this discrepancy however remain unclear. The incorporation of ^{35}S labeled methionine and cysteine into HeLa cell protein was therefore deemed to be a suitable assay to determine the effect of cyclic peptide treatment on global translation rates.

10.10.3.2 Cyclic peptide screening by ^{35}S methionine incorporation

HeLa cells were sub cultured into 6 cm dishes and incubated for 24 h to allow cells to adhere to the plate. Spent media was removed and the cells were subsequently treated with cyclic peptides or vehicle alone control for 4 h. After 3 h 30 min of treatment, cells were pulse labeled with ^{35}S labeled methionine / cysteine for exactly 30 min. Cell pellets were harvested and soluble protein was extracted and quantified as previously described. Cyclic peptide treatment failed to significantly suppress incorporation of ^{35}S labeled amino acids into HeLa cell protein (**Figure 74**).

This is therefore entirely inconsistent with the hypothesis that the cyclic peptides are disrupting the eIF4E / eIF4G interaction, with the concomitant suppression of cap-dependent translation. It should be noted however that the ^{35}S incorporation assay quantifies global translation rates and does not distinguish between cap-dependent and cap-independent mechanisms. It is therefore conceivable that cyclic peptide treatment weakly suppresses cap-dependent translation, but that the concomitant increase in the rate of cap-independent translation masks its detection by ^{35}S incorporation assay. It is however more likely that the peptides do not disrupt the eIF4E / eIF4G within the malignant environment. In order to test the integrity of the eIF4E / eIF4G PPI within the malignant intracellular environment in the presence of cyclic peptides, an m^7 GTP affinity resin pull-down assay was developed.

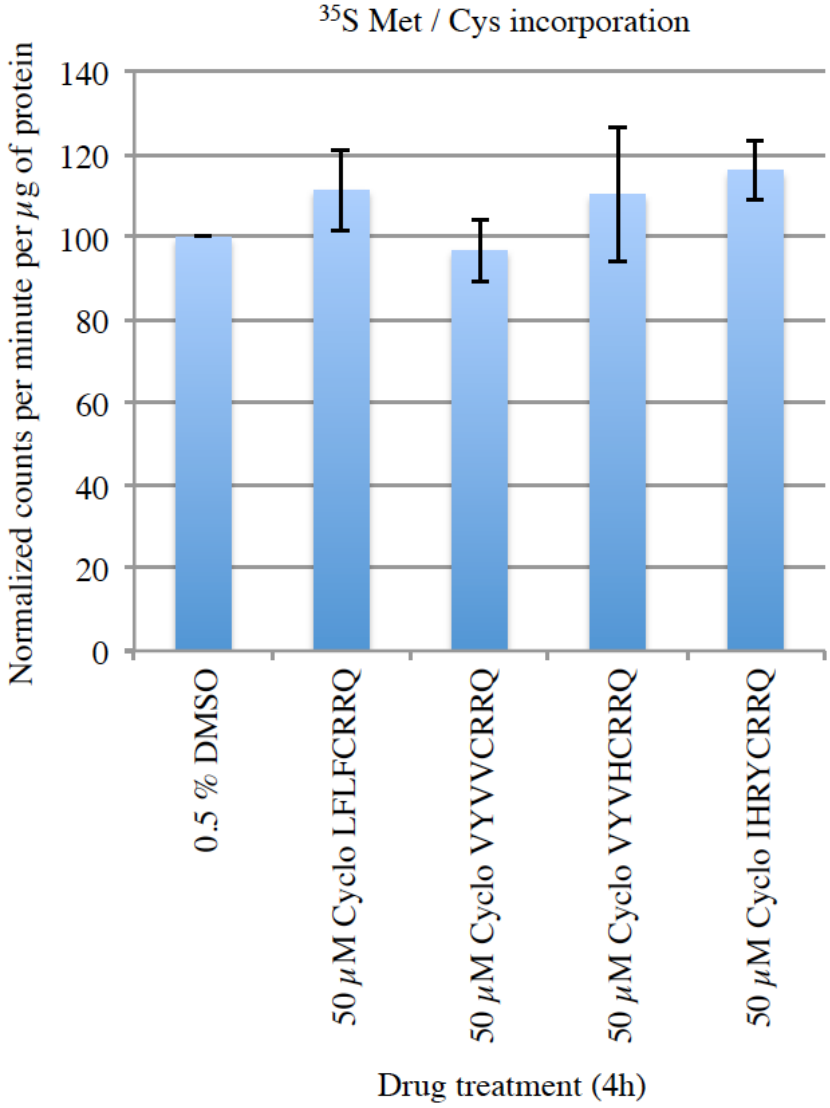

Figure 74: The effect of cyclic peptide treatment on translation as inferred from incorporation of ^{35}S labeled methionine and cysteine into HeLa cell protein. Error bars are representative of +/- one standard deviation of the means of three independent experiments. All results were normalized to negative control cells treated for 4h with drug delivery vehicle (0.5 % DMSO), which were analyzed in parallel with samples treated with cyclic peptides. Incorporation of ^{35}S labeled methionine and cysteine into cells treated with drug delivery vehicle alone was set as 100 % and subsequently used to normalize scintillation counts per minute per μg of protein for all samples.

10.10.4 m^7 GTP pull-down assay

The previously described cellular assays aimed to determine the effect of cyclic peptide treatment on the integrity of the eIF4E / eIF4G interaction by examining concomitant changes in translation rates. These assay are therefore an indirect method of examining the disruption of the eIF4E / eIF4G interaction. It was therefore decided to directly visualize the effect of cyclic peptide treatment on the eIF4E / eIF4G interaction within HeLa cells. The m^7 GTP pull-down assay is a commonly used method to examine the effect of compound treatment on the assembly of the eIF4F complex. [435] [423] [14] [15] This assay uses an m^7 GTP affinity resin to mimic the 5' mRNA cap, which then binds to eIF4E. [436] [304] [437] [438] The interaction of eIF4E with the 'YDREFLL' motif of eIF4G recruits the scaffolding protein to the affinity resin. [163] [164] The eIF4E mediated localization of eIF4G to the affinity resin subsequently facilitates recruitment of PABP, eIF4A and eIF3 to the m^7 GTP affinity resin, via their interaction with the scaffolding protein (**Figure 75:** B). [145] [144] [139] [147] It was therefore hypothesized that cyclic peptide inhibitors of the eIF4E / eIF4G interaction would inhibit the assembly of the eIF4F complex on the m^7 GTP affinity resin. Therefore hypothetically treatment of HeLa cells with cyclic peptide inhibitors of the eIF4E / eIF4G interaction should significantly reduce the association of eIF4G, PABP, eIF4A and eIF3 with the m^7 GTP affinity resin (**Figure 75:** C), which should be detectable by western blotting.

HeLa cells were plated into 10 cm dishes and incubated for 48 h to allow cells to adhere to the plate. Compound treatments were then performed against either intact cells, or against freshly prepared cell lysate to elucidate the influence of cell permeability on the efficacy of cyclic peptides. Intact cell treatments were performed by incubating cells with media containing vehicle alone control (0.5 % DMSO), cyclic peptides (50 μM) or rapamycin (500 nM) for 4 h. Cells were lysed in MPER and soluble cell lysate was isolated via centrifugation. Protein concentration in soluble cell lysate was determined via Bradford assay. [439] Cell lysate treatments were performed by incubating cell lysate in MPER with vehicle alone control (0.5 % DMSO) or cyclic peptides (50 μM) for 4 h. Meanwhile m^7 GTP resin (either m^7 GTP agarose resin, Jena Bioscience, AC-155 or m^7 GTP sepharose, GE Healthcare, discontinued) was equilibrated with two PBS washes.

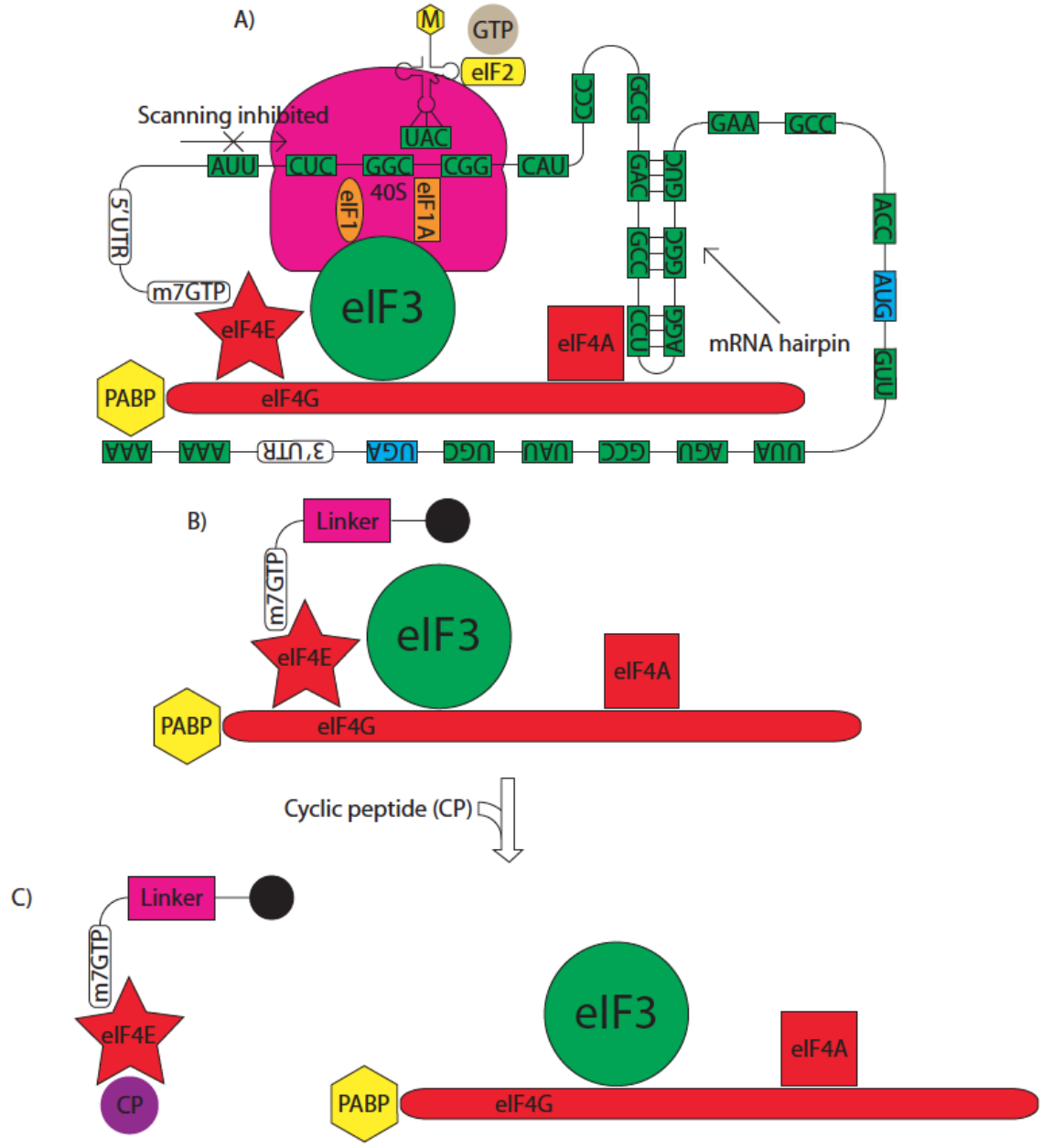

Figure 75: A) Schematic of the cap-dependent translation initiation machinery. eIF4F (highlighted in red) co-operates with polyadenosine-binding protein (PABP), eIF3, eIF2, eIF1 and eIF1A to facilitate delivery of initiator methionine transfer ribonucleic acid ($^{Met}tRNA^{i}$) to the start codon, AUG (highlighted in blue). [134] Guanosine (G) and cytosine (C) residues in the 5' UTR of weak mRNAs form stable hairpin or stem loop structures, which inhibit 5' to 3' scanning of the 40S ribosomal subunit along the mRNA strand. B) m^7 GTP affinity resin (black circle) mimics the 5' cap of mRNA and sequesters the eIF4F complex. C) Cylic peptide (CP) disrupts the eIF4E / eIF4G interaction, resulting in the dissociation of eIF4G, PABP, eIF4A and eIF3 from the m^7 GTP affinity resin.

Vehicle alone or compound treated cell lysate was loaded to m^7 GTP resin and resin was isolated via centrifugation. m^7 GTP resin bound protein was washed with PBS, with the first wash retained for subsequent analysis by western blotting. Protein bound m^7 GTP resin was isolated via centrifugation and reserved for analysis by western blotting.

Proteins were separated on a 10 % or 12 % SDS-PAGE gel, then transferred to nitrocellulose membranes via western blotting, which were then cut with a scalpel into segments for primary antibody probing. Membranes were exposed to primary antibodies for 16 h, washed with TBST and exposed to fluorescently tagged secondary antibodies for 1 h. Membrane segments were then washed with TBST and then PBS, prior to imaging on an Odyssey scanner (Li-cor).

10.10.4.1 Validation of the m^7 GTP pull-down assay

It was first necessary to verify that treatment of HeLa cells with a known inhibitor of cap-dependent translation would yield a reduction in the association of eIF4G, PABP and eIF4A with an m^7 GTP affinity resin. The mTORC1 inhibitor rapamycin has been shown to cause hypophosphorylation of the 4EBPs, which compete effectively with eIF4G for binding to eIF4E. [419] Previous m7 GTP pull-down experiments with rapamycin treated cells have shown a reduction in the quantity of resin associated eIF4G that accompanies 4EBP hypophosphorylation. [420] The mutually exclusive binding of the 4EBPs or eIF4G to eIF4E is unsurprising due to the highly homologous binding helices (4EBP 'YDRKFLM' vs eIF4G 'YDREFLL') that are used to bind to an identical site on the dorsal face of eIF4E. [163] [166] [164] Both the hypophosphorylation of the 4EBPs and the rapamycin induced suppression of eIF4G association with m^7 GTP resins can be readily detected by western blotting. As such, despite the lack of translational inhibition by rapamycin observed by both luciferase and ^{35}S Met / Cys incorporation assays; rapamycin was deemed an appropriate control for the m^7 GTP pull-down assay.

A commercially available m^7 GTP agarose resin (Jena Bioscience, AC-155) was used to analyze the phosphorylation status of the 4EBPs in the absence or presence of rapamycin. HeLa cells were treated with vehicle alone control (0.5 % DMSO) or rapamycin (500 nM) for 4 h and cells were harvested as previously described. Rapamycin treated or vehicle alone treated cell lysates were subjected in parallel to m^7 GTP pull-down assay and the results analyzed by western blotting (**Figure 76**). 4EBP

was readily detected by western blotting as a closely migrating group of four bands, consistent with the hierarchical phosphorylation mechanism that governs the ability of 4EBP to suppress translation. [177 183] 4EBP hypophosphorylation can readily be observed by the increased intensity of the faster migrating two bands, presumably due to decreased negative charge of the 4EBP protein (**Figure 76**). Rapamycin treated samples of cell lysate (lane 2), m^7 GTP resin unbound protein (lane 4), m^7 GTP resin bound protein (lane 6) and resin washings (lane 8) all exhibited increased 4EBP hypophosphorylation when compared to their corresponding vehicle alone treated controls (lanes 1, 3, 5 and 7). This is consistent with the published literature, which suggests that 4EBP hypophosphorylation occurs concomitantly with inhibition of mTORC1. [17 420 177 183 430]

The same rapamycin or vehicle alone treated samples were analyzed by western blotting with primary antibodies against eIF4G, PABP, eIF4A and eIF4E to determine the influence of rapamycin on the eIF4E / eIF4G interaction (**Figure 77**). There was little significant difference observed between the quantity of m^7 GTP resin bound PABP, eIF4A or eIF4E in the absence (lane 5) or presence (lane 6) of rapamycin. In addition the quantities of all proteins within cell lysate (lanes 1 and 2) and m^7 GTP resin unbound samples (lanes 3 and 4) appeared comparable. It was however frustrating to observe that eIF4G quantification was impeded by a large smeared signal at the top of the resin bound protein lanes (lanes 5 and 6). It was noted that the smeared signal stopped abruptly at the point the nitrocellulose membrane had been cut to allow exposure to the eIF4G primary antibody. Further attempts to quantify eIF4G association with m^7 GTP agarose (Jena Bioscience, AC-155) proved unsuccessful due to this resin and eIF4G antibody specific smearing issue.

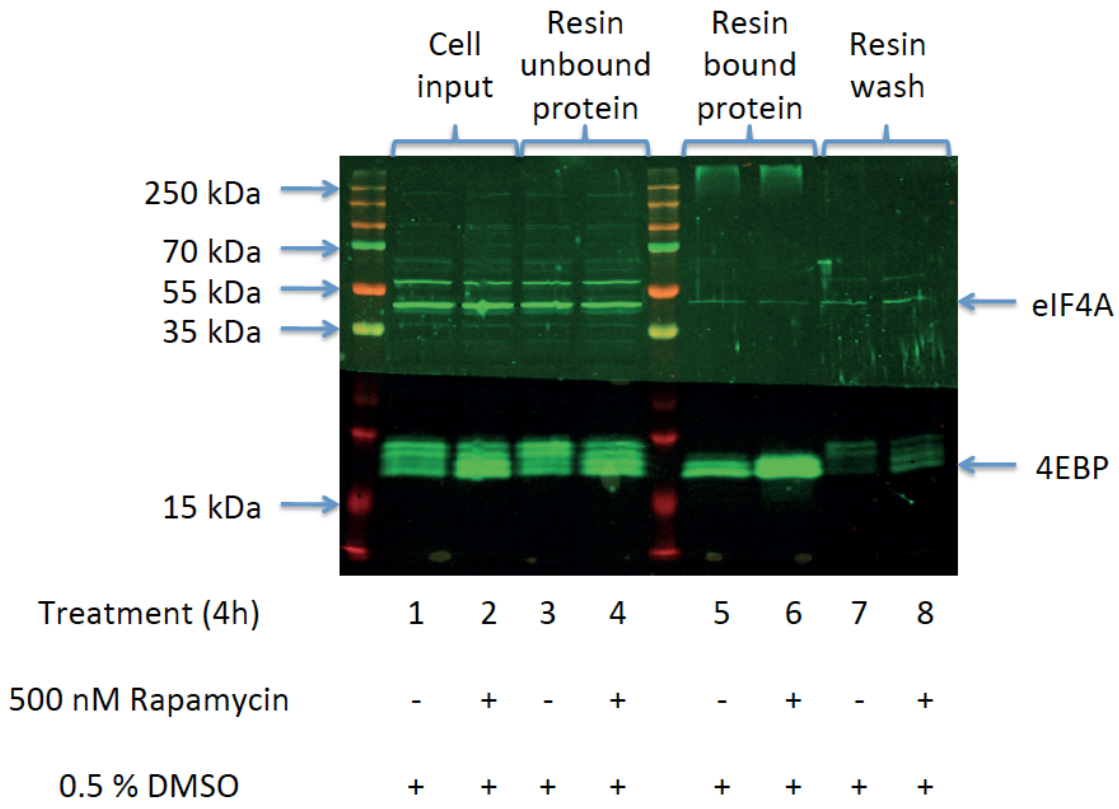

Figure 76: Representative western blot for eIF4A and 4EBP to analyze the effect of the treatment of HeLa cells with 500 nM rapamycin on the assembly of the eIF4F complex. m^7 GTP agarose (Jena Bioscience, AC-155) pull-down products were separated on a 12 % SDS-PAGE gel against a Pageruler 10-250 kDa ladder. Equal quantities of vehicle alone treated (lane 1) and rapamycin treated (lane 2) cell lysate were loaded to provide an indication of protein levels in cell lysate. Equal quantities of m^7 GTP agarose unbound protein for vehicle alone treated (lane 3) and rapamycin treated (lane 4) samples were loaded to visualize protein depletion via resin exposure. m^7 GTP agarose bound protein for vehicle alone treated (lane 5) and rapamycin treated (lane 6) samples were loaded to visualize the effect of compound treatment on eIF4A and 4EBP resin association. Resin washings from vehicle alone treated (lane 7) and rapamycin treated (lane 8) samples were loaded to visualize protein dissociation during wash steps.

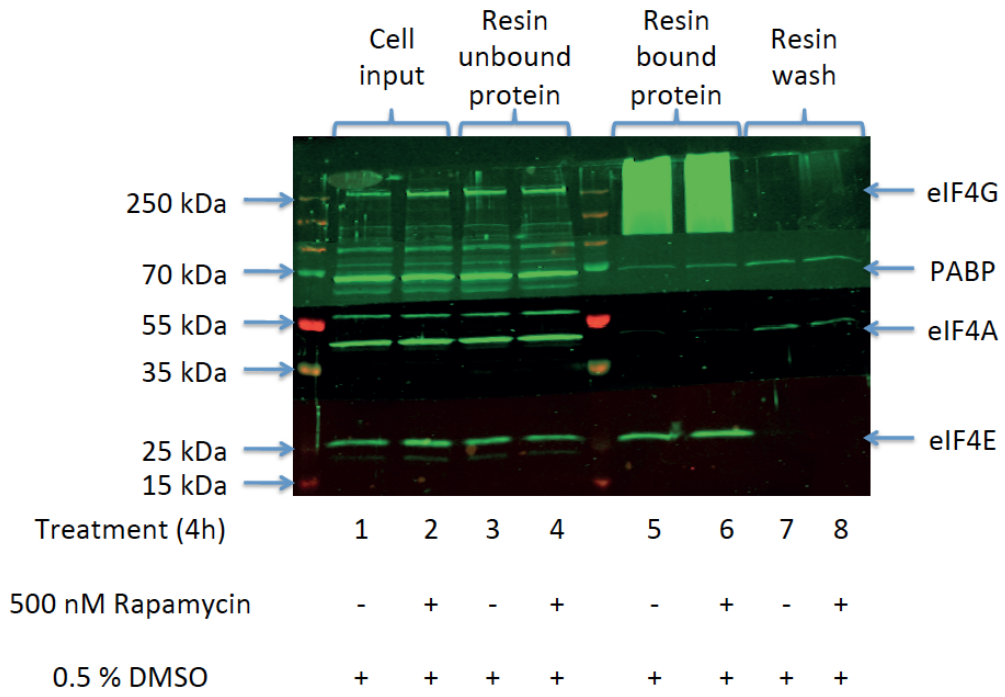

Figure 77: Representative western blot for eIF4G, PABP, eIF4A and eIF4E to analyze the effect of the treatment of HeLa cells with 500 nM rapamycin on the assembly of the eIF4F complex. m^7 GTP agarose (Jena Bioscience, AC-155) pull-down products were separated on a 10 % SDS-PAGE gel against a Pageruler 10-250 kDa ladder. Equal quantities of vehicle alone treated (lane 1) and rapamycin treated (lane 2) cell lysate were loaded to provide an indication of protein levels in cell lysate. Equal quantities of m^7 GTP agarose unbound protein for vehicle alone treated (lane 3) and rapamycin treated (lane 4) samples were loaded to visualize protein depletion via resin exposure. m^7 GTP agarose bound protein for vehicle alone treated (lane 5) and rapamycin treated (lane 6) samples were loaded to visualize the effect of compound treatment on eIF4G, PABP, eIF4A and eIF4E resin association. Resin washings from vehicle alone treated (lane 7) and rapamycin treated (lane 8) samples were loaded to visualize protein dissociation during wash steps.

In an attempt to resolve this issue, a limited quantity of an alternative m^7 GTP affinity resin (m^7 GTP sepharose, GE Healthcare, discontinued) was obtained. Pull-down experiments were then repeated with vehicle alone or rapamycin treated cells to determine the relative performance of the two m^7 GTP affinity resins. 4EBP hypophosphorylation was again observed in response to rapamycin treatment (**Figure 78:** compare rapamycin treated lanes 2, 4, 6 and 8 against their vehicle alone controls lanes 1, 3, 5 and 7), which is entirely consistent with the published literature. [17 420 177 183 430] m^7 GTP sepharose (GE Healthcare, discontinued) exhibited increased resin association of eIF4A (lanes 1 and 2) when compared to that of m^7 GTP agarose (Jena Bioscience, AC-155, lanes 3 and 4). It was encouraging to note that small smeared signal appeared at the top of lanes containing m^7 GTP agarose bound protein (Jena Bioscience, AC-155, lanes 3 and 4), but not at the top of the corresponding m^7 GTP sepharose bound protein lanes (GE Healthcare, discontinued, lanes 1 and 2).

The same rapamycin or vehicle alone treated samples were probed with primary antibodies against eIF4G, PABP, eIF4A and eIF4E to determine the influence of affinity resin on the resulting western blot (**Figure 79**). Once again, m^7 GTP sepharose (GE Healthcare, discontinued) exhibited increased resin association of eIF4A (lanes 1 and 2) when compared to that of m^7 GTP agarose (Jena Bioscience, AC-155, lanes 3 and 4). This phenomenon is probably the result of the increased eIF4E binding capacity of m^7 GTP sepharose (GE Healthcare, discontinued, lanes 1 and 2) when compared to that of m^7 GTP agarose (Jena Bioscience, AC-155, lanes 3 and 4). This finding is totally inconsistent with the published m^7 GTP loading of the GE sepharose (0.2 μmol ml^{-1}) compared to that of the Jena Bioscience agarose (5 μmol ml^{-1}).

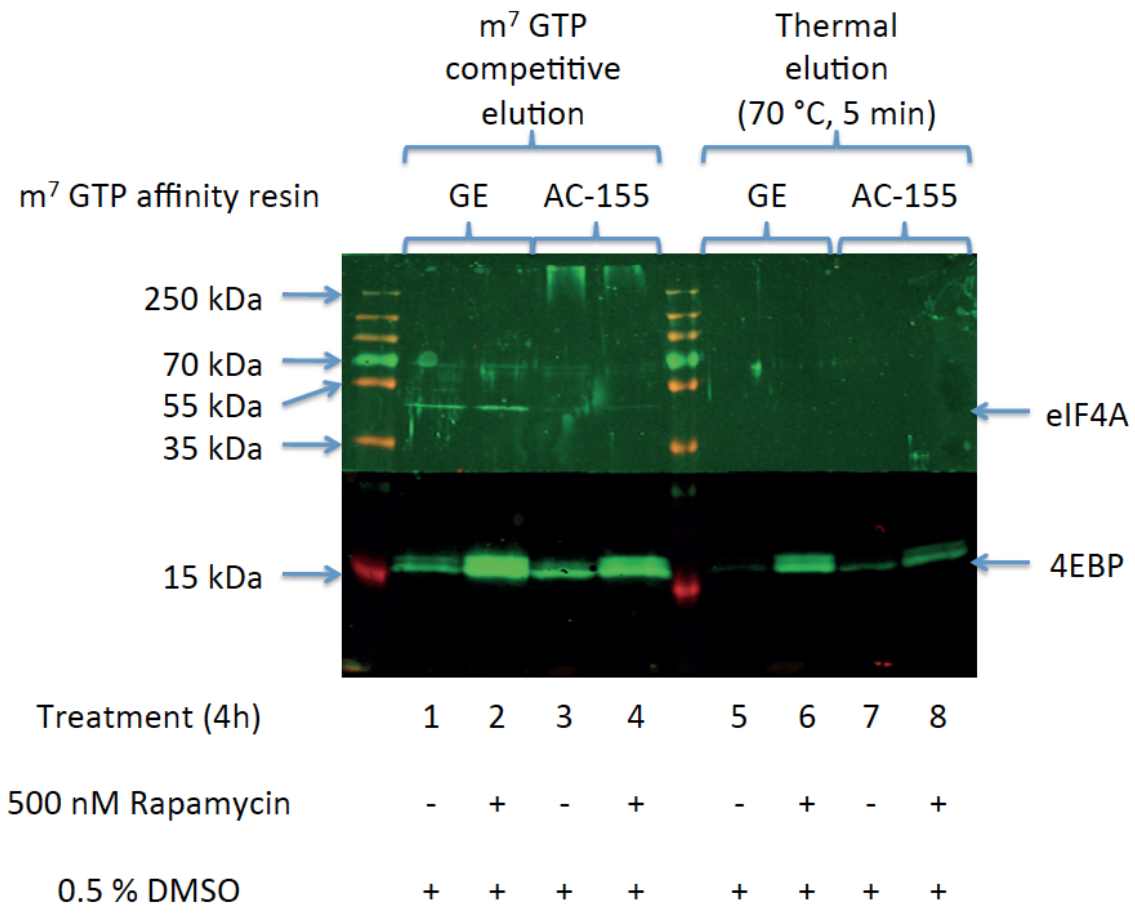

Figure 78: Comparison of the eIF4F binding capacity of m^7 GTP sepharose (GE Healthcare, discontinued) vs that of m^7 GTP agarose (Jena Bioscience, AC-155) via western blotting for eIF4A and 4EBP. m^7 GTP resin pull-down products were separated on a 12 % SDS-PAGE gel against a Pageruler 10-250 kDa ladder. m^7 GTP resin bound protein was eluted by competitive elution with m^7 GTP (lanes 1 - 4 inc.) or via thermal denaturation (lanes 5 – 8 inc.). m^7 GTP sepharose (GE Healthcare, discontinued) was loaded with vehicle alone treated (lane 1, lane 5) or rapamycin treated (lane 2, lane 6) HeLa cell lysate. m^7 GTP agarose (Jena Bioscience, AC-155) was loaded with vehicle alone treated (lane 3, lane 7) or rapamycin treated (lane 4, lane 8) HeLa cell lysate.

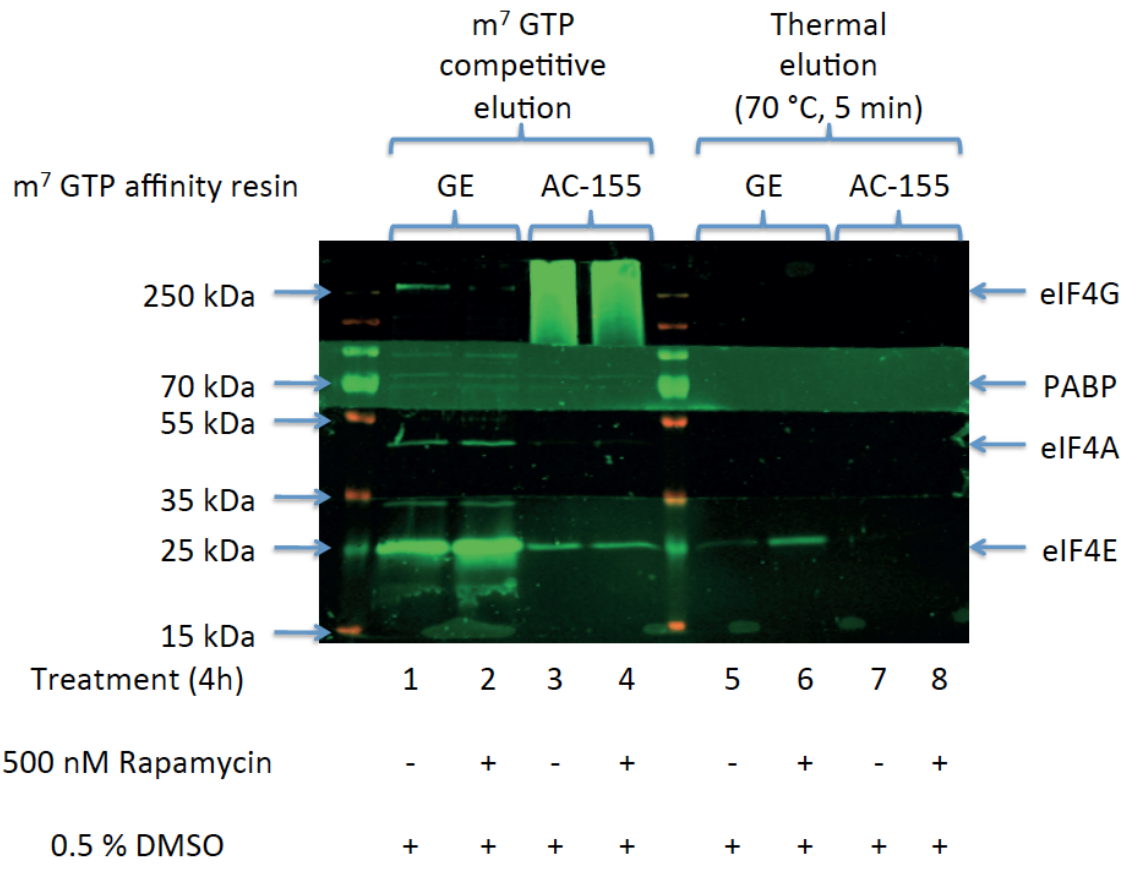

Figure 79: Comparison of the eIF4F binding capacity of m^7 GTP sepharose (GE Healthcare, discontinued) vs that of m^7 GTP agarose (Jena Bioscience, AC-155) via western blotting for eIF4G, PABP, eIF4A and eIF4E. m^7 GTP resin pull-down products were separated on a 10 % SDS-PAGE gel against a Pageruler 10-250 kDa ladder. m^7 GTP resin bound protein was eluted by competitive elution with m^7 GTP (lanes 1 - 4 inc.) or via thermal denaturation (lanes 5 – 8 inc.). m^7 GTP sepharose (GE Healthcare, discontinued) was loaded with vehicle alone treated (lane 1, lane 5) or rapamycin treated (lane 2, lane 6) HeLa cell lysate. m^7 GTP agarose (Jena Bioscience, AC-155) was loaded with vehicle alone treated (lane 3, lane 7) or rapamycin treated (lane 4, lane 8) HeLa cell lysate.

Rapamycin treatment yielded a slight increase in the quantity of eIF4E (compare lane 2 and lane 6 against lanes 1 and 5 respectively) that was associated with m^7 GTP sepharose (GE Healthcare, discontinued). The exact reasons for this phenomenon remain to be elucidated, but it is conceivable that rapamycin induces eIF4E phosphorylation by Mnk2, which may help to explain the disparity. [430] [431] It is however interesting to note that rapamycin treatment decreased the quantity of eIF4G associated with m^7 GTP sepharose (GE Healthcare, discontinued), when compared to the vehicle alone treated control (compare lane 2 against lane 1). This is consistent with the hypothesis that rapamycin causes hypophosphorylation of the 4EBPs, which in turn effectively compete with eIF4G for binding to eIF4E. [420] The attempts to validate m^7 GTP agarose (Jena Bioscience, AC-155) with rapamycin clearly demonstrated that the affinity resin was not suitable for visualizing the effect of cyclic peptide treatment on the eIF4E / eIF4G interaction in HeLa cells. m^7 GTP sepharose (GE Healthcare, discontinued) was therefore deemed to be an appropriate affinity resin for the testing of potential cyclic peptide inhibitors of the eIF4E / eIF4G interaction.

The discontinuation of m^7 GTP sepharose by GE Healthcare however presented an issue for the testing of potential cyclic peptide inhibitors of the eIF4E / eIF4G interaction. The limited available quantity of m^7 GTP sepharose dictated careful selection of just two cyclic peptides for testing as potential inhibitors of the eIF4E / eIF4G interaction in HeLa cells. None of the four SICLOPPS isolated cyclic peptides exerted significant influence on global translation rates via ^{35}S Met / Cys incorporation. However treatment with both cyclo LFLFCRRQ and cyclo VYVVCRRQ elicited a dose-dependent reduction in the cell viability of MCF-7 cells via MTT assay. Treatment with either of these cyclic peptides inhibited the cap-dependent translation of Fluc from the PIC test vector, whilst exhibiting minimal suppression of cap-independent Fluc translation from PAT test. Therefore cyclo LFLFCRRQ and cyclo VYVVCRRQ were selected for validation as potential inhibitors of the eIF4E / eIF4G interaction via m^7 GTP pull-down assay.

10.10.4.2 Cyclic peptide screening by m^7 GTP pull-down assay

It was hypothesized that cyclic peptide inhibitors of the eIF4E / eIF4G interaction would inhibit the assembly of the eIF4F complex on m^7 GTP sepharose resin. Intact cell treatments were performed by incubating cells with media containing vehicle alone control (0.5 % DMSO) or cyclic peptides (50 μM) for 4 h and then HeLa cells were harvested as previously described. Cyclic peptide or vehicle alone treated cell lysates were subjected in parallel to m^7 GTP pull-down assay and the results analyzed by western blotting (**Figure 80**).

Treatment of HeLa cells with 50 μM cyclo LFLFCRRQ did not effect the phosphorylation state of the 4EBPs and hypophosphorylated 4EBPs were found to preferentially associate with eIF4E bound to m^7 GTP sepharose (compare lanes 5 and 6 against lanes 3 and 4), as expected. [430] Resin washings contained hyperphosphorylated 4EBPs, which dissociated from eIF4E bound to m^7 GTP sepharose (lanes 7 and 8), as anticipated. The quantities of all proteins within cell lysate (lanes 1 and 2) and m^7 GTP resin unbound samples (lanes 3 and 4) appeared comparable. There was little significant difference observed between the quantity of m^7 GTP resin bound eIF4G, PABP, eIF4A or 4EBP in the absence (lane 5) or presence (lane 6) of cyclo LFLFCRRQ. This is entirely inconsistent with the hypothesis that cyclo LFLFCRRQ inhibits the eIF4E / eIF4G interaction or the concomitant formation of the eIF4F complex on m^7 GTP affinity resin.

The same cyclo LFLFCRRQ or vehicle alone treated samples were analyzed by western blotting with primary antibodies against eIF4G, PABP, eIF4A and eIF4E to determine the influence of the cyclic peptide on the eIF4E / eIF4G interaction (**Figure 81**). The quantities of all proteins within cell lysate (lanes 1 and 2) and m^7 GTP resin unbound samples (lanes 3 and 4) appeared comparable. It is interesting to note that despite the high affinity of the m^7 GTP sepharose resin for eIF4E (lanes 5 and 6), there is little evident depletion of eIF4E within resin unbound protein samples (lanes 3 and 4). m^7 GTP sepharose bound proteins from vehicle alone treated control cells (lane 5) were compared against resin bound proteins from cells treated with cyclo LFLFCRRQ (lane 6). The comparison revealed that cyclic peptide treatment slightly enhanced association of eIF4G, PABP, eIF4A and eIF4E with the affinity resin. This phenomenon is again inconsistent with the hypothesis that cyclo LFLFCRRQ inhibits the eIF4E / eIF4G

interaction or the concomitant formation of the eIF4F complex on m^7 GTP affinity resin. It is therefore highly probable that treatment of HeLa cells with cyclo LFLFCRRQ fails to inhibit the eIF4E / eIF4G interaction within the malignant environment.

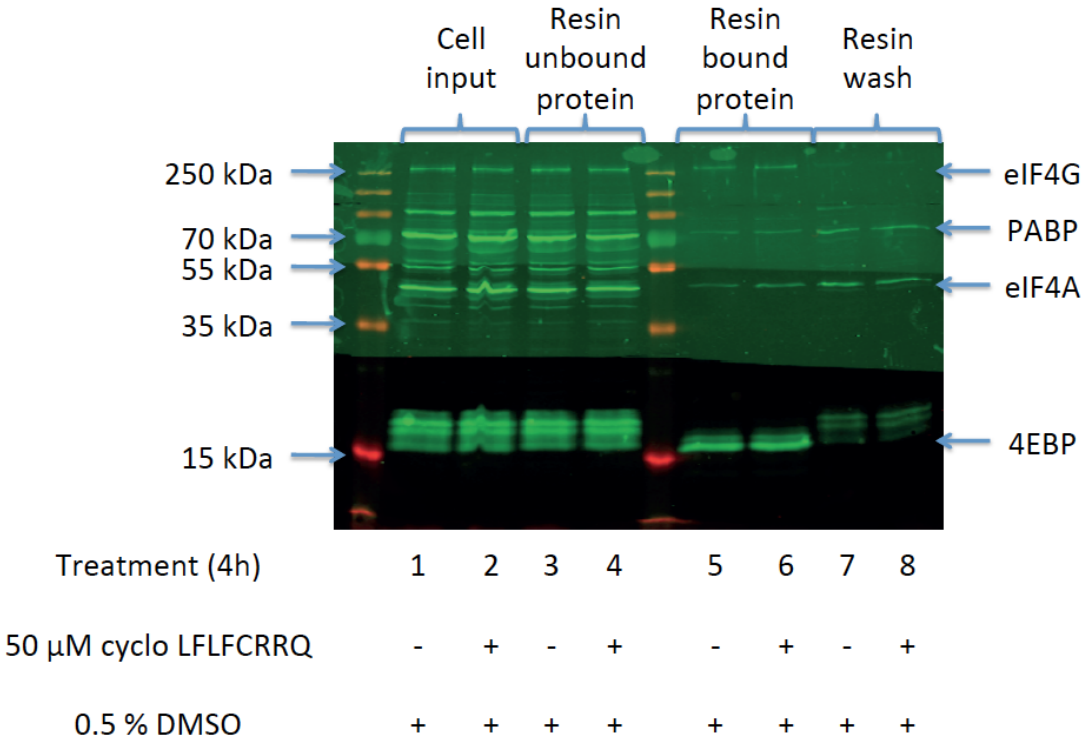

Figure 80: Representative western blot for eIF4G, PABP, eIF4A and 4EBP to analyze the effect of the treatment of HeLa cells with 50 μM cyclo LFLFCRRQ on the assembly of the eIF4F complex. m^7 GTP sepharose pull-down products were separated on a 12 % SDS-PAGE gel against a Pageruler 10-250 kDa ladder. Equal quantities of vehicle alone treated (lane 1) and cyclic peptide treated (lane 2) cell lysate were loaded to provide an indication of protein levels in cell lysate. Equal quantities of m^7 GTP sepharose unbound protein for vehicle alone treated (lane 3) and cyclic peptide treated (lane 4) samples were loaded to visualize protein depletion via resin exposure. m^7 GTP sepharose bound protein for vehicle alone treated (lane 5) and cyclic peptide treated (lane 6) samples were loaded to visualize the effect of compound treatment on eIF4G, PABP, eIF4A and 4EBP resin association. Resin washings from vehicle alone treated (lane 7) and cyclic peptide treated (lane 8) samples were loaded to visualize protein dissociation during wash steps.

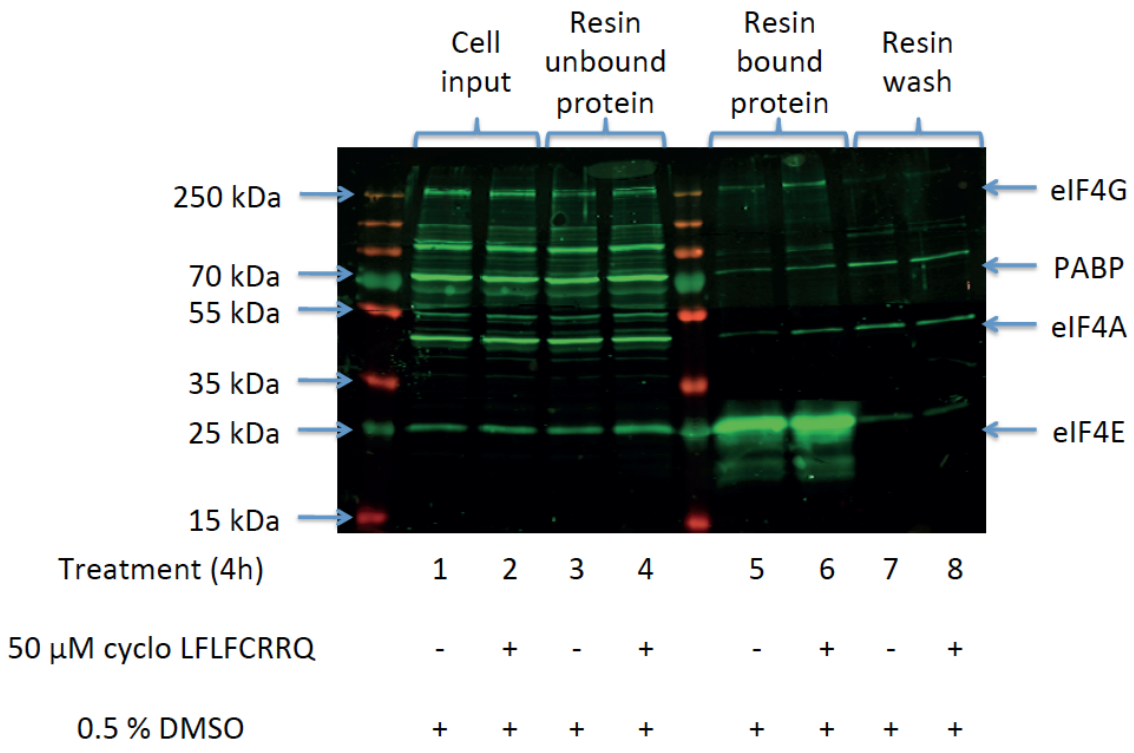

Figure 81: Representative western blot for eIF4G, PABP, eIF4A and eIF4E to analyze the effect of the treatment of HeLa cells with 50 μM cyclo LFLFCRRQ on the assembly of the eIF4F complex. m^7 GTP sepharose pull-down products were separated on a 10 % SDS-PAGE gel against a Pageruler 10-250 kDa ladder. Equal quantities of vehicle alone treated (lane 1) and cyclic peptide treated (lane 2) cell lysate were loaded to provide an indication of protein levels in cell lysate. Equal quantities of m^7 GTP sepharose unbound protein for vehicle alone treated (lane 3) and cyclic peptide treated (lane 4) samples were loaded to visualize protein depletion via resin exposure. m^7 GTP sepharose bound protein for vehicle alone treated (lane 5) and cyclic peptide treated (lane 6) samples were loaded to visualize the effect of compound treatment on eIF4G, PABP, eIF4A and eIF4E resin association. Resin washings from vehicle alone treated (lane 7) and cyclic peptide treated (lane 8) samples were loaded to visualize protein dissociation during wash steps.

Intact HeLa cells were treated with vehicle alone control or 50 μM cyclo VYVVCRRQ, harvested and then subjected to m^7 GTP pull-down assay and western blotting. Treatment of HeLa cells with 50 μM cyclo VYVVCRRQ (**Figure 82**) did not effect the phosphorylation state of the 4EBPs and hypophosphorylated 4EBPs were found to preferentially associate with eIF4E bound to m^7 GTP sepharose (compare lanes 5 and 6 against lanes 3 and 4). [430] Resin washings contained hyperphosphorylated 4EBPs, which dissociated from eIF4E bound to m^7 GTP sepharose (lanes 7 and 8). The quantities of all proteins within cell lysate (lanes 1 and 2) and m^7 GTP resin unbound samples (lanes 3 and 4) appeared comparable. Once again, there was little significant difference observed between the quantity of m^7 GTP resin bound eIF4G, PABP, eIF4A or 4EBP in the absence (lane 5) or presence (lane 6) of cyclo VYVVCRRQ. This is entirely inconsistent with the hypothesis that cyclo VYVVCRRQ inhibits the eIF4E / eIF4G interaction or the concomitant formation of the eIF4F complex on m^7 GTP affinity resin.

The same cyclo VYVVCRRQ or vehicle alone treated samples were analyzed by western blotting with primary antibodies against eIF4G, PABP, eIF4A and eIF4E to determine the influence of the cyclic peptide on the eIF4E / eIF4G interaction (**Figure 83**). The quantities of all proteins within cell lysate (lanes 1 and 2) and m^7 GTP resin unbound samples (lanes 3 and 4) appeared comparable. It is again interesting that despite the high affinity of the m^7 GTP sepharose resin for eIF4E (lanes 5 and 6), there is little depletion of eIF4E within resin unbound protein samples (lanes 3 and 4). m^7 GTP sepharose bound proteins from vehicle alone treated control cells (lane 5) were compared against resin bound proteins from cells treated with cyclo VYVVCRRQ (lane 6). The comparison revealed that cyclic peptide treatment did not significantly effect association of eIF4G, PABP, eIF4A and eIF4E with the affinity resin. This phenomenon is again inconsistent with the hypothesis that cyclo VYVVCRRQ inhibits the eIF4E / eIF4G interaction or the concomitant formation of the eIF4F complex on m^7 GTP affinity resin. It is therefore highly probable that treatment of HeLa cells with cyclo VYVVCRRQ fails to inhibit the eIF4E / eIF4G interaction within the malignant environment. The failure of both cyclic peptides to inhibit the eIF4E / eIF4G interaction by m^7 GTP pull-down assay is consistent with the lack of translational suppression observed via the ^{35}S Met / Cys incorporation assay (**Figure 74**).

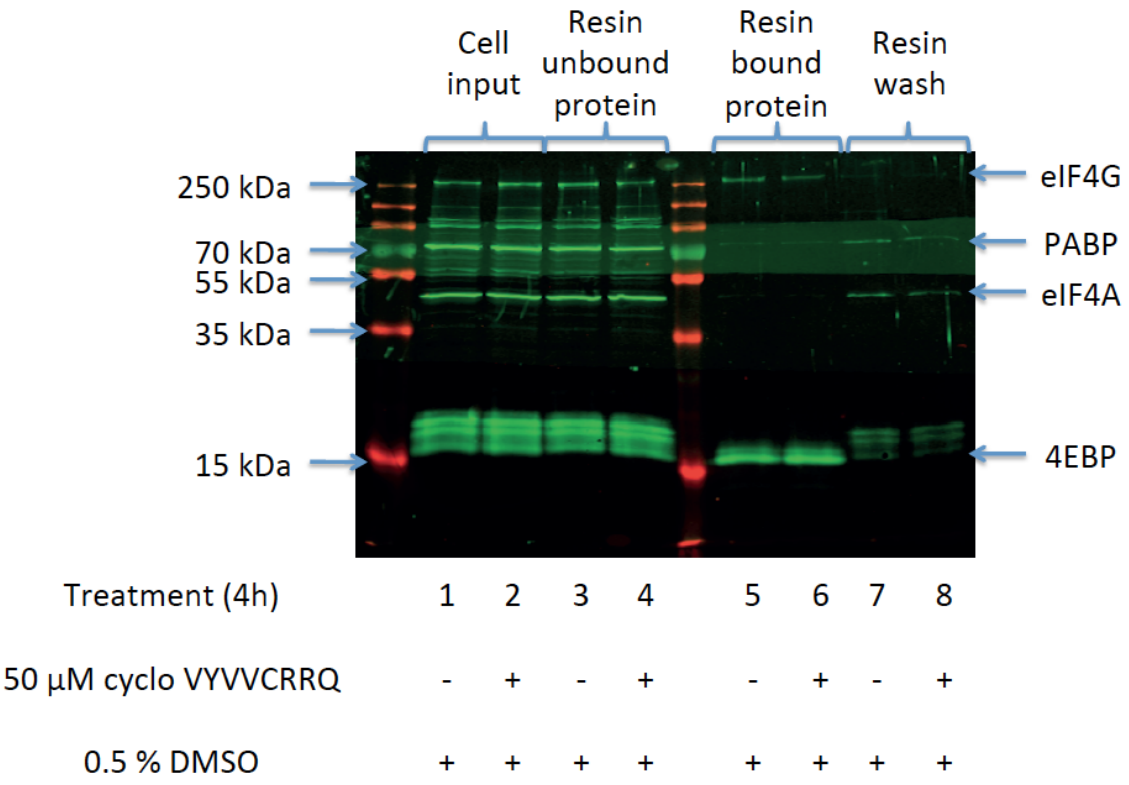

Figure 82: Representative western blot for eIF4G, PABP, eIF4A and 4EBP to analyze the effect of the treatment of HeLa cells with 50 μM cyclo VYVVCRRQ on the assembly of the eIF4F complex. m^7 GTP sepharose pull-down products were separated on a 12 % SDS-PAGE gel against a Pageruler 10-250 kDa ladder. Equal quantities of vehicle alone treated (lane 1) and cyclic peptide treated (lane 2) cell lysate were loaded to provide an indication of protein levels in cell lysate. Equal quantities of m^7 GTP sepharose unbound protein for vehicle alone treated (lane 3) and cyclic peptide treated (lane 4) samples were loaded to visualize protein depletion via resin exposure. m^7 GTP sepharose bound protein for vehicle alone treated (lane 5) and cyclic peptide treated (lane 6) samples were loaded to visualize the effect of compound treatment on eIF4G, PABP, eIF4A and 4EBP resin association. Resin washings from vehicle alone treated (lane 7) and cyclic peptide treated (lane 8) samples were loaded to visualize protein dissociation during wash steps.

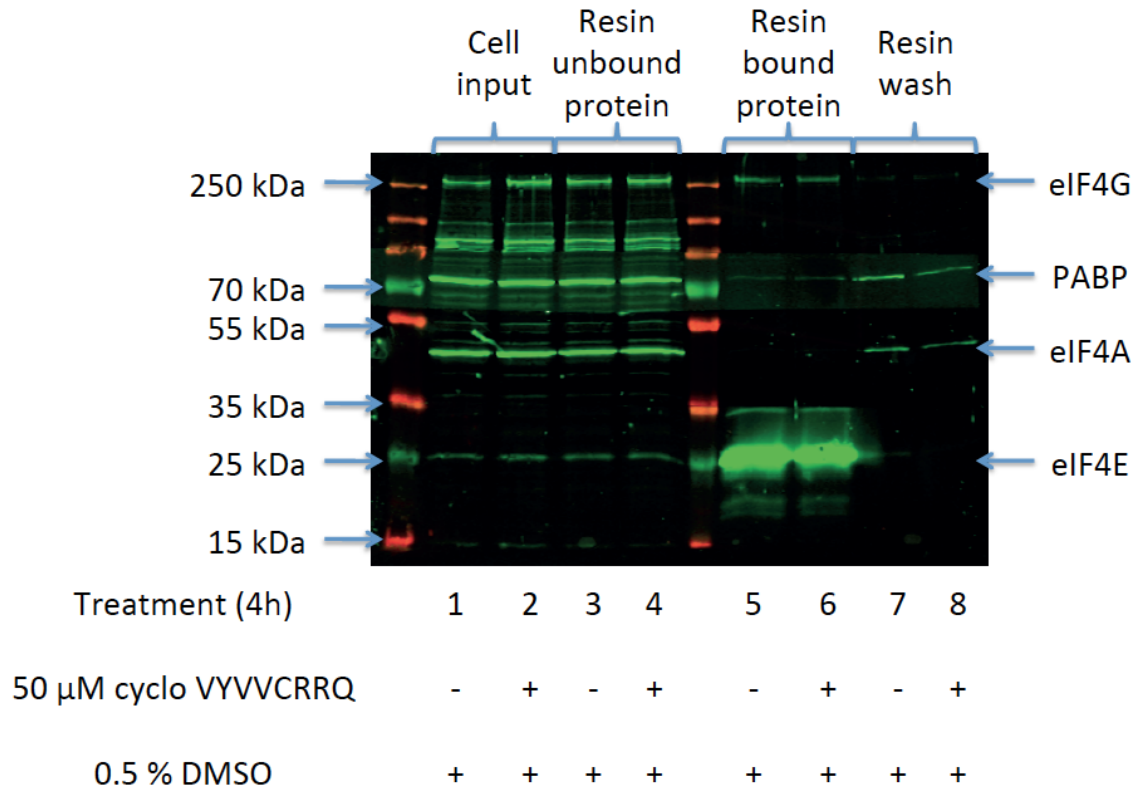

Figure 83: Representative western blot for eIF4G, PABP, eIF4A and eIF4E to analyze the effect of the treatment of HeLa cells with 50 μM cyclo VYVVCRRQ on the assembly of the eIF4F complex. m^7 GTP sepharose pull-down products were separated on a 10 % SDS-PAGE gel against a Pageruler 10-250 kDa ladder. Equal quantities of vehicle alone treated (lane 1) and cyclic peptide treated (lane 2) cell lysate were loaded to provide an indication of protein levels in cell lysate. Equal quantities of m^7 GTP sepharose unbound protein for vehicle alone treated (lane 3) and cyclic peptide treated (lane 4) samples were loaded to visualize protein depletion via resin exposure. m^7 GTP sepharose bound protein for vehicle alone treated (lane 5) and cyclic peptide treated (lane 6) samples were loaded to visualize the effect of compound treatment on eIF4G, PABP, eIF4A and eIF4E resin association. Resin washings from vehicle alone treated (lane 7) and cyclic peptide treated (lane 8) samples were loaded to visualize protein dissociation during wash steps.

It was subsequently proposed that the inability of cyclo LFLFCRRQ and cyclo VYVVCRRQ to disrupt the cytoplasmic eIF4E / eIF4G interaction could be caused by poor cell membrane permeability. Therefore the cyclic peptides would be unable to

access the translation machinery and hence would be ineffective at disrupting the eIF4E / eIF4G interaction. In order to test this hypothesis, the m^7 GTP pull-down assay was repeated where compound treatments were performed on HeLa cell lysate instead of live cells with intact phospholipid bilayers. HeLa cells were cultured and harvested as previously described and then cell lysate treatments were performed by incubating lysate in MPER with vehicle alone control (0.5 % DMSO) or cyclic peptides (50 μM) for 4 h. Treated cell lysates were loaded to m^7 GTP sepharose (GE Healthcare, discontinued) as previously described and subsequently analyzed by western blotting.

Treatment of HeLa cell lysate with 50 μM cyclo LFLFCRRQ (**Figure 84**) did not effect the phosphorylation state of the 4EBPs and hypophosphorylated 4EBPs were found to preferentially associate with eIF4E bound to m^7 GTP sepharose (compare lanes 5 and 6 against lanes 3 and 4). [430] The quantities of all proteins within cell lysate (lanes 1 and 2) and m^7 GTP resin unbound samples (lanes 3 and 4) appeared comparable. There was little significant difference observed between the quantity of m^7 GTP resin bound eIF4G, PABP, eIF4A or 4EBP in the absence (lane 5) or presence (lane 6) of cyclo LFLFCRRQ. This is entirely inconsistent with the hypothesis that cyclo LFLFCRRQ inhibits the eIF4E / eIF4G interaction or the concomitant formation of the eIF4F complex on m^7 GTP affinity resin.

The same cyclo LFLFCRRQ or vehicle alone treated cell lysate samples were analyzed by western blotting with primary antibodies against eIF4G, PABP, eIF4A and eIF4E to determine the influence of the cyclic peptide on the eIF4E / eIF4G interaction (**Figure 85**). The quantities of all proteins within cell lysate (lanes 1 and 2) and m^7 GTP resin unbound samples (lanes 3 and 4) appeared comparable. m^7 GTP sepharose bound proteins from vehicle alone treated control cell lysate (lane 5) were compared against resin bound proteins from cell lysate treated with cyclo LFLFCRRQ (lane 6). The comparison revealed that cyclic peptide treatment did not significantly effect association of eIF4G, PABP, eIF4A and eIF4E with the affinity resin. This phenomenon is again inconsistent with the hypothesis that cyclo LFLFCRRQ inhibits the eIF4E / eIF4G interaction or the concomitant formation of the eIF4F complex on m^7 GTP affinity resin. It is therefore highly probable that treatment of HeLa cell lysate with cyclo LFLFCRRQ fails to inhibit the eIF4E / eIF4G interaction. The identical result of cyclo LFLFCRRQ treatment on the eIF4E / eIF4G interaction within intact cells

(**Figure 80**, **Figure 81**) or within HeLa cell lysate (**Figure 84**, **Figure 85**) suggests that poor cell permeability was not a limiting factor.

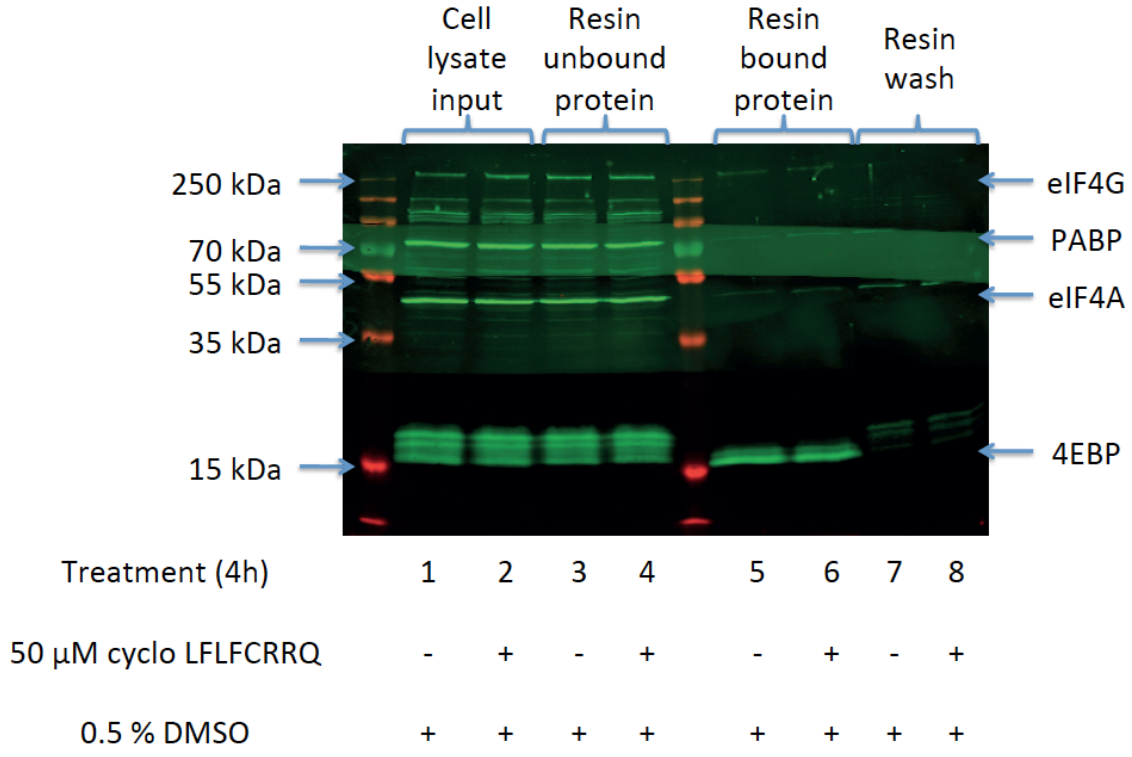

Figure 84: Representative western blot for eIF4G, PABP, eIF4A and 4EBP to analyze the effect of the treatment of HeLa cell lysate with 50 *µ*M cyclo LFLFCRRQ on the assembly of the eIF4F complex. m^7 GTP sepharose pull-down products were separated on a 12 % SDS-PAGE gel against a Pageruler 10-250 kDa ladder. Equal quantities of vehicle alone treated (lane 1) and cyclic peptide treated (lane 2) cell lysate were loaded to provide an indication of protein levels in cell lysate. Equal quantities of m^7 GTP sepharose unbound protein for vehicle alone treated (lane 3) and cyclic peptide treated (lane 4) samples were loaded to visualize protein depletion via resin exposure. m^7 GTP sepharose bound protein for vehicle alone treated (lane 5) and cyclic peptide treated (lane 6) samples were loaded to visualize the effect of compound treatment on eIF4G, PABP, eIF4A and 4EBP resin association. Resin washings from vehicle alone treated (lane 7) and cyclic peptide treated (lane 8) samples were loaded to visualize protein dissociation during wash steps.

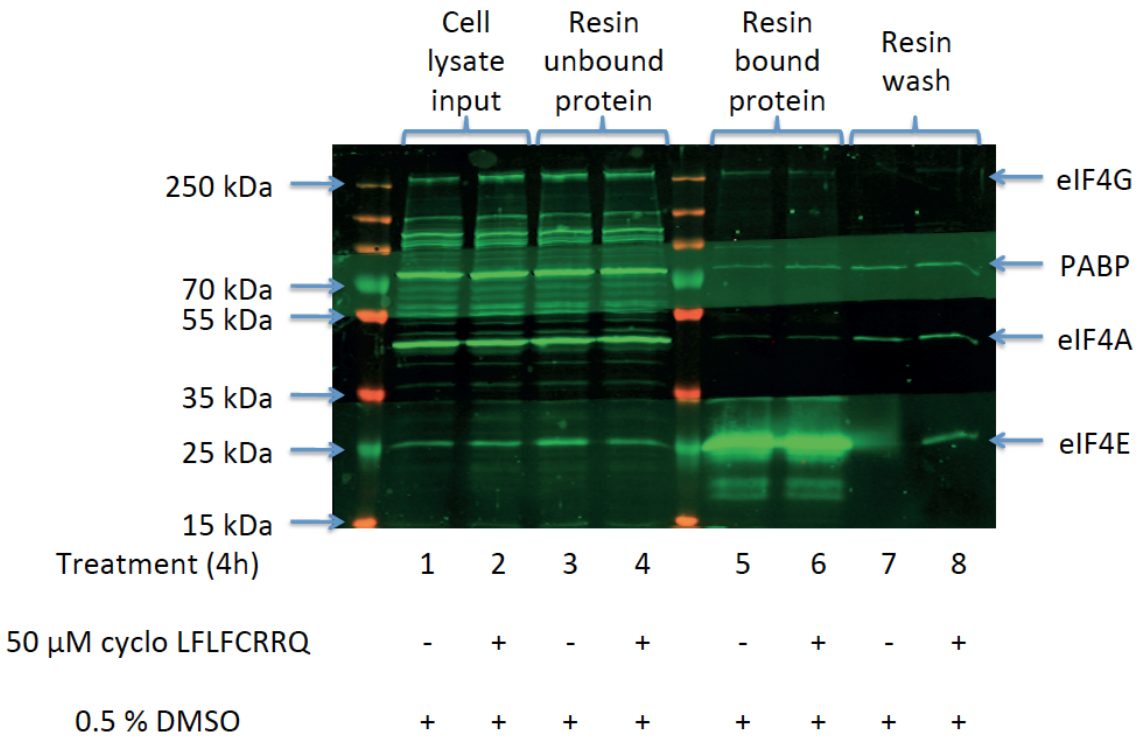

Figure 85: Representative western blot for eIF4G, PABP, eIF4A and eIF4E to analyze the effect of the treatment of HeLa cell lysate with 50 μM cyclo LFLFCRRQ on the assembly of the eIF4F complex. m^7 GTP sepharose pull-down products were separated on a 10 % SDS-PAGE gel against a Pageruler 10-250 kDa ladder. Equal quantities of vehicle alone treated (lane 1) and cyclic peptide treated (lane 2) cell lysate were loaded to provide an indication of protein levels in cell lysate. Equal quantities of m^7 GTP sepharose unbound protein for vehicle alone treated (lane 3) and cyclic peptide treated (lane 4) samples were loaded to visualize protein depletion via resin exposure. m^7 GTP sepharose bound protein for vehicle alone treated (lane 5) and cyclic peptide treated (lane 6) samples were loaded to visualize the effect of compound treatment on eIF4G, PABP, eIF4A and eIF4E resin association. Resin washings from vehicle alone treated (lane 7) and cyclic peptide treated (lane 8) samples were loaded to visualize protein dissociation during wash steps.

HeLa cell lysate was treated with vehicle alone control or 50 μM cyclo VYVVCRRQ, harvested and then subjected to m^7 GTP pull-down assay and western blotting. Treatment of HeLa cell lysate with 50 μM cyclo VYVVCRRQ (**Figure 86**) did not effect the phosphorylation state of the 4EBPs and hypophosphorylated 4EBPs were found to preferentially associate with eIF4E bound to m^7 GTP sepharose (compare lanes 5 and 6 against lanes 3 and 4). [430] The quantities of all proteins within cell lysate (lanes 1 and 2) and m^7 GTP resin unbound samples (lanes 3 and 4) appeared comparable. There was little significant difference observed between the quantity of m^7 GTP resin bound eIF4G, PABP, eIF4A or 4EBP in the absence (lane 5) or presence (lane 6) of cyclo VYVVCRRQ. This is entirely inconsistent with the hypothesis that cyclo VYVVCRRQ inhibits the eIF4E / eIF4G interaction or the concomitant formation of the eIF4F complex on m^7 GTP affinity resin.

The same cyclo VYVVCRRQ or vehicle alone treated cell lysate samples were analyzed by western blotting with primary antibodies against eIF4G, PABP, eIF4A and eIF4E to determine the influence of the cyclic peptide on the eIF4E / eIF4G interaction (**Figure 87**). The quantities of all proteins within cell lysate (lanes 1 and 2) and m^7 GTP resin unbound samples (lanes 3 and 4) appeared comparable. It is once again interesting to note that despite the high affinity of the m^7 GTP sepharose resin for eIF4E (lanes 5 and 6), there is little evident depletion of eIF4E within resin unbound protein samples (lanes 3 and 4). m^7 GTP sepharose bound proteins from vehicle alone treated control cell lysate (lane 5) were compared against resin bound proteins from cell lysate treated with cyclo VYVVCRRQ (lane 6). The comparison revealed that cyclic peptide treatment did not significantly effect association of eIF4G, PABP, eIF4A and eIF4E with the affinity resin. This phenomenon is again inconsistent with the hypothesis that cyclo VYVVCRRQ inhibits the eIF4E / eIF4G interaction or the concomitant formation of the eIF4F complex on m^7 GTP affinity resin. It is therefore highly probable that treatment of HeLa cell lysate with cyclo VYVVCRRQ fails to inhibit the eIF4E / eIF4G interaction. The identical result of cyclo VYVVCRRQ treatment on the eIF4E / eIF4G interaction within intact cells (**Figure 82**, **Figure 83**) or within HeLa cell lysate (**Figure 86**, **Figure 87**) suggests that poor cell permeability was not a limiting factor.

m7 GTP pull-down assays revealed little influence of cyclo LFLFCRRQ or cyclo VYVVCRRQ treatment on the eIF4E / eIF4G interaction and therefore no significant

disruption of eIF4F formation was observed. This result appeared to reproducible regardless of whether cyclic peptide treatment was performed on intact HeLa cells or on cell lysate. It is therefore probable that the cyclic peptides isolated by SICLOPPS screening do not disrupt the oncogenic PPI.

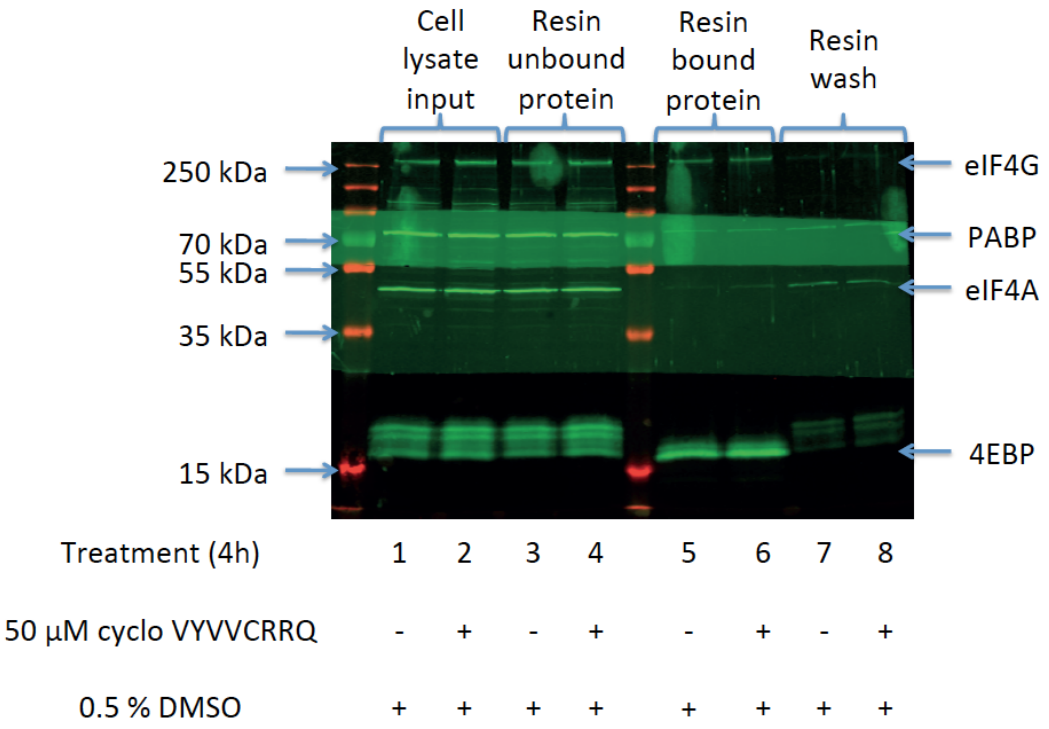

Figure 86: Representative western blot for eIF4G, PABP, eIF4A and 4EBP to analyze the effect of the treatment of HeLa cell lysate with 50 μM cyclo VYVVCRRQ on the assembly of the eIF4F complex. m^7 GTP sepharose pull-down products were separated on a 12 % SDS-PAGE gel against a Pageruler 10-250 kDa ladder. Equal quantities of vehicle alone treated (lane 1) and cyclic peptide treated (lane 2) cell lysate were loaded to provide an indication of protein levels in cell lysate. Equal quantities of m^7 GTP sepharose unbound protein for vehicle alone treated (lane 3) and cyclic peptide treated (lane 4) samples were loaded to visualize protein depletion via resin exposure. m^7 GTP sepharose bound protein for vehicle alone treated (lane 5) and cyclic peptide treated (lane 6) samples were loaded to visualize the effect of compound treatment on eIF4G, PABP, eIF4A and 4EBP resin association. Resin washings from vehicle alone treated (lane 7) and cyclic peptide treated (lane 8) samples were loaded to visualize protein dissociation during wash steps.

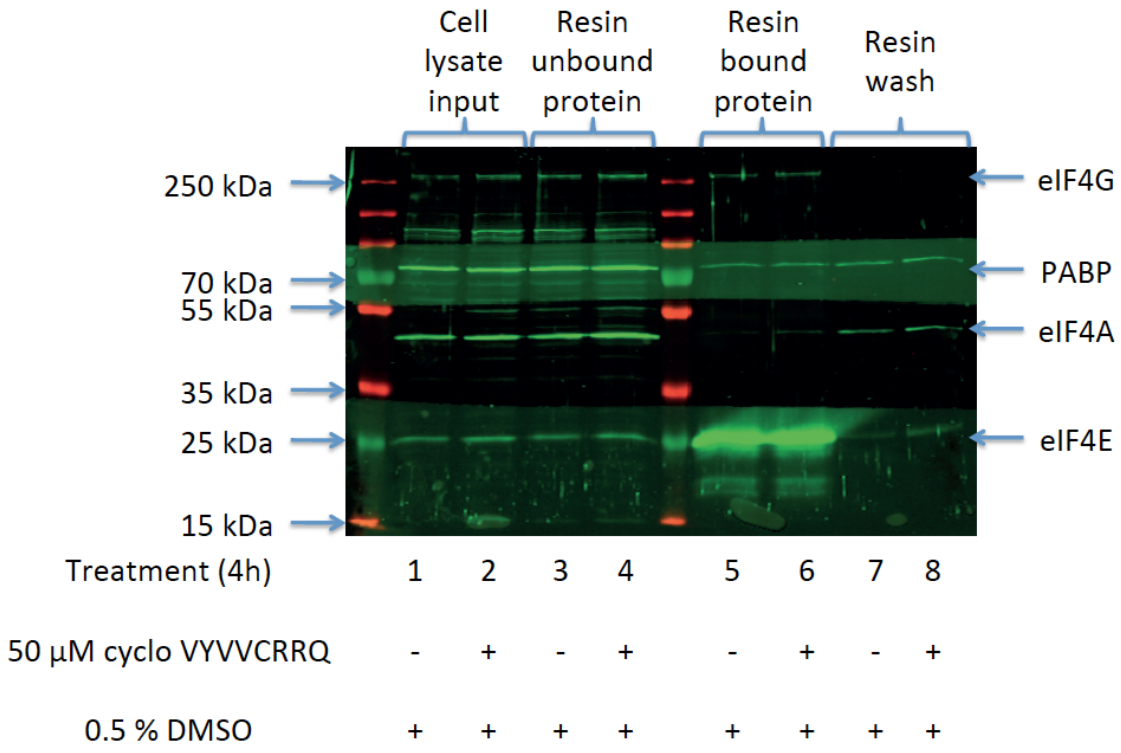

Figure 87: Representative western blot for eIF4G, PABP, eIF4A and eIF4E to analyze the effect of the treatment of HeLa cell lysate with 50 μM cyclo VYVVCRRQ on the assembly of the eIF4F complex. m^7 GTP sepharose pull-down products were separated on a 10 % SDS-PAGE gel against a Pageruler 10-250 kDa ladder. Equal quantities of vehicle alone treated (lane 1) and cyclic peptide treated (lane 2) cell lysate were loaded to provide an indication of protein levels in cell lysate. Equal quantities of m^7 GTP sepharose unbound protein for vehicle alone treated (lane 3) and cyclic peptide treated (lane 4) samples were loaded to visualize protein depletion via resin exposure. m^7 GTP sepharose bound protein for vehicle alone treated (lane 5) and cyclic peptide treated (lane 6) samples were loaded to visualize the effect of compound treatment on eIF4G, PABP, eIF4A and eIF4E resin association. Resin washings from vehicle alone treated (lane 7) and cyclic peptide treated (lane 8) samples were loaded to visualize protein dissociation during wash steps.

11 Conclusions and future work

The primary objective of this project was to develop novel inhibitors of cap-dependent translation by selectively targeting the oncogenic eIF4E / eIF4G PPI. SICLOPPS screening against the eIF4E / eIF4G RTHS isolated four potential inhibitors of the oncogenic PPI within *E. coli* (**Table 4**), which were subsequently synthesized by Fmoc SPPS. The MTT assay revealed that treatment with cyclo LFLFCRRQ (**Figure 57**) or cyclo VYVVCRRQ (**Figure 58**) elicited a dose-dependent reduction in the viability of MCF7 cells; an effect which is consistent with the inhibition of cap-dependent translation. The initial results from the luciferase assay were promising and indicated that cyclic peptide treatment inhibited the cap-dependent translation of Fluc from the PIC test reporter vector (**Figure 69**).

However testing of cyclic peptides against the control vectors PAT test (**Figure 70**) and CAT test (**Figure 71**), suggested that compound treatment also suppressed cap-independent translation to a minimal degree. Subsequent validation of these cyclic peptides by ^{35}S methionine incorporation assay (**Figure 74**) revealed that there was little significant impact of cyclic peptide treatment on translation. This finding is consistent with the failure of cyclic peptides to disrupt the eIF4E / eIF4G interaction within the malignant environment. m7 GTP pull-down assays revealed that treatment of intact HeLa cells with cyclo LFLFCRRQ (**Figure 80** and **Figure 81**) and cyclo VYVVCRRQ (**Figure 82** and **Figure 83**) did indeed fail to disrupt the oncogenic PPI. Similar experiments performed on HeLa cell lysate revealed that cyclo LFLFCRRQ (**Figure 84** and **Figure 85**) and cyclo VYVVCRRQ (**Figure 86** and **Figure 87**) failed to disrupt eIF4F complex formation, even when cell permeability was not a limiting factor. m7 GTP pull down assays therefore revealed that treatment with two of the SICLOPPS derived cyclic peptides had no impact on the integrity of the eIF4E / eIF4G interaction. This result is consistent with the corresponding failure of cyclo LFLFCRRQ and cyclo VYVVCRRQ to significantly reduce translation rates by ^{35}S methionine incorporation assay (**Figure 74**). It is therefore highly probable that the cyclic peptides isolated by SICLOPPS screening against the eIF4E / eIF4G RTHS, do not disrupt the oncogenic PPI. It is therefore probable that the eIF4E / eIF4G interaction within *E. coli* does not accurately mimic the PPI found within the malignant environment.

It is however conceivable that the failure of the Ssp inteins to efficiently splice cyclic peptides with the invariant 'CRRQ' motif (**Figure 48**) compromised the ability of SICLOPPS screening to isolate inhibitors of the eIF4E / eIF4G interaction. The failure of Ssp inteins to efficiently splice $CRRQX_4$ inhibitors resulted in the screening of a library of peptide extein loops, whose conformation was constrained by interaction of I_C and I_N (**Figure 48**). It is therefore conceivable that the conformation of the peptide extein loop was not accurately mimicked by the conformation of the cyclic peptide that was synthesized by SPPS. To circumvent this issue, it is plausible that the Npu* inteins could be substituted for their Ssp counterparts during the construction of SICLOPPS libraries. [342] [343] Chitin binding domain pull-down experiments have clearly demonstrated that the degree and rate of splicing of Npu* inteins is superior to that exhibited by Ssp inteins (**Figure 48**). During this project, it has also been shown that splicing of Npu* inteins is sufficient to restore RTHS colony viability on selective media (**Figure 50**). In addition, the degree of splicing of the Ssp intein has been shown to be greatly dependent on the extein sequence; a feature which is much less obvious for the Npu* intein (**Figure 48**). [342] The construction of pARCBD Npu* (Jaime Townend, unpublished work) therefore marks an advance towards the screening of cyclic peptide libraries that display reduced splicing bias depending on the sequence of the peptide extein.

The Ssp intein has previously been shown to exhibit conditional splicing depending on the amino acid sequences present at the N and C-terminal splice junctions. [342] By contrast, the Npu* intein has previously been shown to tolerate a wide range of amino acids at the splice junctions. [342] The application of the Npu* intein to SICLOPPS screening would therefore facilitate the splicing of cationic amino acids in cyclic peptides to promote water solubility and cell permeability of the therapeutic. The project would benefit from the systematic determination of a minimal amino acid motif to promote cell permeability that is also compatible with Npu* intein mediated cyclization. This could be achieved by the synthesis of a family of homologous cyclic peptides that incorporate different motifs derived from known cell permeable peptides. The family of cyclic peptides could be tagged via maleimide or iodoacetamide conjugation to fluorescent dyes. Immortalized cell lines could then be treated with fluorescently tagged cyclic peptides and subsequently visualized by microscopy. Once this minimal cell penetrating epitope has been determined, SICLOPPS screening with Npu* inteins could be used to develop cyclic peptide inhibitors of intracellular PPIs.

The interaction of eIF4G with eIF4E is mediated by the α helical $Y_0D_1R_2X_3F_4L_5X_6$ domain of the scaffolding protein (**Figure 7**). [163] [164] The evolution of the eIF4E binding helix into a peptide therapeutic has already been achieved via phage display and peptide stapling techniques. [170] [171] However, it would be of interest to explore the possibility of incorporating the eIF4E binding motif of eIF4G / 4EBPs ($Y_0D_1R_2X_3F_4L_5X_6$) into a cell permeable cyclic peptide. The incorporation of an α helix into a cyclic peptide ring introduces considerable strain, which may possibly reduce the percentage of peptide that displays the helical eIF4E binding motif. Reagrdless of this potential drawback, the comparison of the relative binding affinity of the linear $Y_0D_1R_2X_3F_4L_5X_6$ peptide against its cyclic counterpart could reveal if a slightly strained α helix might exhibit improved binding to eIF4E.

It may be relevant to pursue the development of a cyclic peptide inhibitor that incorporates the eIF4G derived 'SDVVL' motif that mediates a portion of the interaction of eIF4E with the scaffolding protein. [165] According to the published literature, the 'SDVVL' motif is unique to eIF4G, but is absent within 4EBPs. The selective inhibition of eIF4G binding to eIF4E with little or no impact on translational suppression by the 4EBPs represents a viable approach for the targeting of cap-dependent translation. This methodology would have the advantage of not only suppressing cap-dependent translation via the disruption of the eIF4E / eIF4G interaction; but also by promoting the association of the 4EBPs with eIF4E.

12 Experimental procedures

12.1 Preparation of molecular biology reagents

All salts, acids and bases were obtained from Fisher Scientific unless otherwise stated.

12.1.1 Antibiotics

Antibiotic	Master stock concentration	Working concentration
Carbenicillin	20 mg / ml	100 μg / ml
Spectinomycin	10 mg / ml	50 μg / ml
Kanamycin	10 mg / ml	50 μg / ml
Chloramphenicol	10 mg / ml	35 μg / ml

Table 5: Antibiotic stock solutions and final working concentrations used for selection against antibiotic resistance genes. Carbenicillin (Fisher Scientific, 12737149), spectinomycin (Sigma Aldrich, 85555) and kanamycin (Fisher Scientific, 10031553) were weighed separately and added to a pre-sterilized falcon tube under aseptic conditions, prior to dilution in sterilized, distilled water. Chloramphenicol (Fisher Scientific, 227920250) was diluted in molecular biology grade ethanol (Sigma Aldrich, E7023).

12.1.2 10 X Minimal media salts

Reagent	Quantity	Working concentration
Ammonium sulfate	10 g	76 mM
Potassium phosphate monobasic	45 g	0.33 M
Potassium phosphate dibasic	105 g	0.60 M
Sodium citrate dihydrate	5.0 g	17 mM
Sterile de-ionized water	To 1 L total volume	/

Table 6: Composition of 10 X minimal media salt master mix. All reagents were weighed separately and added to a pre-sterilized bottle under aseptic conditions, prior to dilution in sterilized, distilled water.

12.1.3 LB media

6.3 g of LB powder (Fisher Scientific, 10113293) was dissolved in 250 ml distilled water and autoclaved for 20 min at 115 °C.

12.1.4 LB agar plates

10 g of LB agar powder (Fisher Scientific, 12811660) was dissolved in 250 ml distilled water and autoclaved for 20 min at 115 °C. Allowed to cool to 50 °C prior to antibiotic addition and then swirled to ensure mixing. Poured into sterilized petri dishes and dried in an incubator for 30 - 60 min at 37 °C prior to use.

12.1.5 Super optimal culture (SOC) media

50 ml of LB media was supplemented with 0.50 ml of 1.0 M magnesium chloride / H_2O, 0.50 ml of 2.0 M magnesium sulfate / H_2O and 0.50 ml of 20 % sterile glucose (w/v) / H_2O (Invitrogen, 19002-013). The solution was mixed by inversion and filtered through a sterile filter into 3.0 ml aliquots and stored at 4 °C until needed.

12.1.6 Minimal media agar plates

3.8 g of agar powder (Fisher Scientific, 10548030) was dissolved in 200 ml distilled water and autoclaved for 20 min at 115 °C. 10 X minimal media salts (25 ml), 1.0 M $MgSO_4$ / H_2O (250 μl) and 50 % sterile glycerol (v:v) / H_2O (10 ml, Fisher Scientific, BP229) were added and used to cool the agar to 50 °C. Antibiotics, IPTG (Fisher Scientific, 10356553), arabinose (Sigma Aldrich, A3256) and 3-AT (Sigma Aldrich, A8056) were then added and sterile water used to bring the final volume to 250 ml. Poured into sterilized petri dishes and dried in an incubator for 30 - 60 min at 37 °C prior to use.

12.1.7 TBF1 buffer

Reagent	Quantity	Working concentration
Potassium acetate	0.59 g	30 mM
Rubidium chloride	2.4 g	0.10 M
Calcium chloride	0.29 g	10 mM
Manganese chloride	2.0 g	50 mM
Glycerol	30 ml	15 % v:v
1.0 % Acetic acid (v:v) / H_2O	To pH 5.8	/
Sterile de-ionized water	To 0.20 L total volume	/

Table 7: Composition of TBF1 buffer for chemically competent cell preparation. All reagents were weighed separately and added to a pre-sterilized bottle under aseptic conditions, prior to dilution in sterilized, distilled water. Solution was sterile filtered and 10 ml aliquots were frozen at -80 °C and thawed on ice for 15 min when needed. Reagents used were as follows: Glycerol (Fisher Scientific, BP229).

12.1.8 TBF2 buffer

Reagent	Quantity	Working concentration
MOPS	0.21 g	10 mM
Rubidium chloride	0.12 g	10 mM
Calcium chloride	1.1 g	75 mM
Glycerol	15 ml	15 % v:v
2.0 M NaOH / H_2O	To pH 6.5	/
Sterile de-ionized water	To 0.10 L total volume	/

Table 8: Composition of TBF2 buffer for chemically competent cell preparation. All reagents were weighed separately and added to a pre-sterilized bottle under aseptic conditions, prior to dilution in sterilized, distilled water. Solution was sterile filtered and 1.0 ml aliquots were frozen at -80 °C and thawed on ice for 15 min when needed. Reagents used were as follows: 4-morpholinepropanesulfonic acid (MOPS, Sigma Aldrich, M5162), Glycerol (Fisher Scientific, BP229).

12.1.9 SDS-PAGE 2 X loading buffer

Reagent	Quantity	Working concentration
Bromophenol blue	10 mg	0.34 mM
1.0 M Tris.HCl / H_2O pH 6.8	2.5 ml	60 mM
20 % SDS (v:v) / H_2O	5.0 ml	2.3 % (v:v)
50 % Glycerol (v:v) / H_2O	10 ml	11 % (v:v)
1.0 M DTT / H_2O	1.3 ml	30 mM
Water	25 ml	/

Table 9: Composition of 2 X sodium dodecyl sulfate polyacrylamide gel electrophoresis (SDS-PAGE) loading buffer. 10 % (v:v) of β-mercapto ethanol (BME, Sigma Aldrich, M6250) was added to 90 % (v:v) SDS-PAGE loading buffer, immediately prior to use. Reagents used were as follows: bromophenol blue (Sigma Aldrich, 114391), tris(hydroxymethyl)aminomethane hydrochloride (Tris.HCl, Fisher Scientific, 10060390), SDS (Fisher Scientific, 10607633), Glycerol (Fisher Scientific, BP229), dithiothreitol (DTT, Sigma Aldrich, 43816).

12.1.10 SDS-PAGE 5 X running buffer stock

Reagent	Quantity	Working concentration
Tris base	15 g	0.12 M
Glycine	94 g	1.3 M
10 % SDS (v:v) / H_2O	50 ml	0.50 % (v:v)
Water	To 1.0 L total volume	/

Table 10: Composition of 5 X sodium dodecyl sulfate polyacrylamide gel electrophoresis (SDS-PAGE) running buffer stock solution. 1 X SDS-PAGE running buffer was made via a one in five dilution of the stock solution with distilled water. Reagents used were as follows: tris(hydroxymethyl)aminomethane base (Tris base, Fisher Scientific, 10376743), glycine (Fisher Scientific, 10080160), SDS (Fisher Scientific, 10607633).

12.1.11 SDS-PAGE running gel

% gel	10 %	12 %	15 %
Reagent	Volume / ml	Volume / ml	Volume / ml
Water	12	10	7.2
1.5 M Tris.HCl / H_2O pH 8.8	7.5	7.5	7.5
20 % SDS (w/v) / H_2O	0.15	0.15	0.15
Acrylamide / Bis acrylamide (30 % / 0.80 % w/v)	9.9	12	15
10 % APS (w/v) / H_2O	0.15	0.15	0.15
TEMED	0.020	0.020	0.020

Table 11: Composition of sodium dodecyl sulfate polyacrylamide gel electrophoresis (SDS-PAGE) running gels. *N, N, N', N'*-tetramethylethylenediamine (TEMED) and ammonium persulfate (APS) were added last to initiate acrylamide polymerization and the gel was then immediately loaded onto the mould. The stacking gel was leveled via the addition of ~ 300 µl of isopropyl alcohol (IPA), before being left to set for 30 min. The unsolidified IPA / acrylamide top layer was removed with water. Reagents used were as follows: tris(hydroxymethyl)aminomethane hydrochloride (Tris.HCl, Fisher Scientific, 10060390), SDS (Fisher Scientific, 10607633), acrylamide / bis acrylamide (30 % / 0.80 % w/v, Fisher Scientific, 12381469), TEMED (Fisher Scientific, 10689543).

12.1.12 SDS-PAGE stacking gel

Reagent	Volume / ml
Water	4.8
0.50 M Tris.HCl / H_2O pH 6.8	2.0
10 % SDS (w/v)/ H_2O	0.16
Acrylamide/ Bis acrylamide (30 % / 0.80 % w/v)	1.0
10 % APS (w/v) / H_2O	0.080
TEMED	0.020

Table 12: Composition of sodium dodecyl sulfate polyacrylamide gel electrophoresis (SDS-PAGE) stacking gel. *N, N, N', N'*-tetramethylethylenediamine (TEMED) and ammonium persulfate (APS) were added last to initiate acrylamide polymerization and the gel was then immediately loaded onto the top of the running gel, prior to being left to set for 30 min with a 10 well comb. Reagents used were as follows: tris(hydroxymethyl)aminomethane hydrochloride (Tris.HCl, Fisher Scientific, 10060390), SDS (Fisher Scientific, 10607633), acrylamide / bis acrylamide (30 % / 0.80 % w/v, Fisher Scientific, 12381469), TEMED (Fisher Scientific, 10689543).

12.1.13 1 X Coomassie protein stain solution

Reagent	Quantity	Working concentration
Coomassie Brilliant Blue	1.0 g	1.2 mM
Acetic acid	0.10 L	10 % (v:v)
MeOH	0.50 L	50 % (v:v)
Water	To 1.0 L total volume	/

Table 13: Composition of 1 X sodium dodecyl sulfate polyacrylamide gel electrophoresis (SDS-PAGE) coomassie protein stain solution. Reagents used were as follows: coomassie brilliant blue (Sigma Aldrich, B0770), methanol (MeOH, Fisher Scientific, 10365710).

12.1.14 1 X Coomassie protein de-stain solution

Reagent	Quantity	Working concentration
Acetic acid	0.10 L	10 % (v:v)
MeOH	0.20 L	20 % (v:v)
Water	To 1.0 L total volume	/

Table 14: Composition of 1 X sodium dodecyl sulfate polyacrylamide gel electrophoresis (SDS-PAGE) coomassie protein de-stain solution. Reagents used were as follows: methanol (MeOH, Fisher Scientific, 10365710).

12.1.15 Z buffer

Reagent	Quantity	Working concentration
1.0 M Potassium Chloride / H_2O	0.50 ml	10 mM
Sodium phosphate monobasic	0.28 g	40 mM
Sodium phosphate dibasic	0.80 g	40 mM
1.0 M Magnesium sulfate / H_2O	50 μl	1.0 mM
BME	140 μl	40 mM
0.10 % SDS (w:v) / H_2O	2.5 ml	0.20 mM
Chloroform	2.5 ml	0.60 M
1.0 M HCl	To pH 7.0	/
Sterile de-ionized water	To 50 ml total volume	/

Table 15: Composition of Z buffer used for cell lysis during Ortho-nitrophenyl- β-galactoside (ONPG) assay. All reagents were measured separately and added to a pre-sterilized falcon tube under aseptic conditions, prior to dilution in sterilized, distilled water. Reagents used were as follows: β-mercapto ethanol (BME, Sigma Aldrich, M6250), sodium dodecyl sulfate (SDS, Fisher Scientific, 10607633), chloroform (Fisher Scientific, 10102190).

12.1.16 50 X TAE buffer

Reagent	Quantity	Working concentration
Tris base	0.24 kg	2.0 M
0.50 M EDTA / water	0.10 L	50 mM
Acetic acid	57 ml	1.0 M
NaOH	To pH 8.0	/
Sterile de-ionized water	To 1.0 L total volume	/

Table 16: Composition of agarose gel electrophoresis 50 X running buffer stock solution. 1 X TAE, agarose gel electrophoresis running buffer was made via a one in fifty dilution of the 50 X stock solution with distilled water. Reagents used were as follows: tris(hydroxymethyl)aminomethane base (Tris base, Fisher Scientific, 10376743), ethylenediaminetetraacetic acid (EDTA, Fisher Scientific, 10030140).

12.1.17 Chitin buffer

Reagent	Quantity	Working concentration
Tris.HCl	1.6 g	20 mM
Sodium chloride	15 mg	0.50 mM
TCEP	0.14 g	1.0 mM
NaOH	To pH 7.8	/
Sterile de-ionized water	To 0.50 L total volume	/

Table 17: Composition of chitin buffer used for purification and analysis of intein splicing. All reagents were weighed separately and added to a pre-sterilized bottle under aseptic conditions, prior to dilution in sterilized, distilled water. Reagents used were as follows: tris(hydroxymethyl)aminomethane hydrochloride (Tris.HCl, Fisher Scientific, 10060390), tris(2-carboxyethyl)phosphine hydrochloride (TCEP, Sigma Aldrich, C4706).

12.2 Preparation of competent cells

12.2.1 Preparation of chemically competent cells

Two 25 ml portions of freshly prepared LB media with antibiotics at appropriate concentrations (**Table 5**) were infected with two 250 μl aliquots (1.0 %) of an *E. coli* culture and subsequently incubated at 37 °C until an OD_{600} of between 0.50 and 0.70 was achieved. Cells were cooled on ice for 15 – 30 min and then pelleted via centrifugation for 15 min at 3100 rotations per minute (rpm) and the supernatant was discarded. Cell pellet was re-suspended in 1.0 ml TBF1 buffer (**Table 7**) per tube, followed by dilution via addition of another 4.0 ml TBF1 buffer (**Table 7**) each. Cells were pelleted via centrifugation for 15 min at 3100 rpm and the supernatant was discarded. During centrifugation, 25 PCR tubes were cooled on dry ice for 15 min. Cell pellet was carefully re-suspended in 1.0 ml TBF2 buffer (**Table 8**) per tube prior to combining the cells into one tube. Cells were snap frozen into 100 μl aliquots prior to cooling on dry ice for 15 min. Chemically competent cells were then frozen at -80 °C and thawed for 15 min on ice when needed.

12.2.2 Preparation of electro-competent cells

2.5 ml (1.0 %) of an *E. coli* culture was added to 250 ml L of sterile SOC media containing antibiotics at appropriate concentrations. The culture was incubated at 37 °C for 2 - 4 h until an OD_{600} of between 0.50 and 0.70 was achieved and then cooled on ice for 15 - 30 min. Cells were pelleted via centrifugation for 15 min at 3100 rpm and the supernatant was discarded. Cell pellet was re-suspended in 250 ml of ice cold 10 % Glycerol (v:v) / H_2O (Fisher Scientific, BP229) solution (v:v), then centrifuged at 4000 rpm for 15 min at 4 °C, prior to discarding the supernatant. This glycerol cycle was repeated with 125 ml, 50 ml, 25 ml and 10 ml washes. Cells were re-suspended in 2 ml of ice-cold glycerol and snap frozen into 100 μl aliquots as for the chemically competent cells. Electro-competent cells were then frozen at -80 °C and thawed on ice when needed.

12.3 Biochemical procedures

12.3.1 Plasmid mini-prep

LB liquid media (10 ml) was added to a falcon tube followed by addition of antibiotics at appropriate concentrations. A sterile micropipette tip was used to transfer cells from a stock culture maintained at -80 °C or from colonies on an agar plate, to the LB media. Strains were then cultured at an appropriate temperature (normally 37 °C, but 30 °C for strains carrying plasmids with temperature sensitive origins of replication) in the presence of antibiotics at appropriate concentrations (**Table 5**) for 16 h. Library stocks were obtained from these cultures via the addition of 0.90 ml of LB culture to 0.10 ml of DMSO (Fisher Scientific, BP231), prior to storage at -80 °C. *E. coli* cells containing vectors were pelleted via centrifugation for 15 min at 3100 rpm. The supernatant was discarded and plasmid DNA extracted using a plasmid miniprep kit (Genejet miniprep kit, Thermo Scientific, K0503) according to the manufacturers instructions. Plasmid elution was achieved via addition of 50 μl of molecular biology grade water (Fisher Scientific, BP28191) to the column, which was then left to elute for 30 min to 1 h. Centrifugation for 2.0 min at 13000 rpm yielded purified plasmid in water.

12.3.2 PCR [440]

Typically, PCR utilized an annealing temperature gradient to maximize the chances of gene amplification. Eight 50 μl PCR amplifications were set up on ice and mixed via gentle pipetting, each consisting of:

10 μl vortexed 5 X green GoTaq reaction buffer (Promega, M7911)
4.0 μl 10 mM 2'-Deoxynucleotide 5'-triphosphates (dNTPs, Promega, U1420)
2.0 μl forward primer (**Table 18**), 10 pmol / μl
2.0 μl reverse primer (**Table 18**), 10 pmol / μl
1.0 μl of DNA template (50 - 150 ng / μl)
31 μl molecular biology grade water (Fisher Scientific, BP28191)
0.50 μl GoTaq flexi DNA polymerase, 5.0 units / μl (Promega, M8295)

PCR samples were amplified according to the protocol below:

Heat initialization- 1 x 2.0 min at 95 °C

Followed by 40 cycles of:

Denaturation- 60 seconds (s) at 95 °C

Annealing- 60 s at 50 - 65 °C gradient over 8 samples

Extension- time dependent on amplicon length (1.0 min / 1.0 kb) at 72 °C

Followed by a final elongation of:

Final elongation- 5.0 min at 72 °C

Cooling- 60 min at 4 °C

PCR samples were analyzed via agarose gel electrophoresis and samples containing the expected PCR amplicons were combined and purified via spin column (Genejet PCR purification kit, Thermo Scientific, K0701) according to the manufacturers instructions.

12.3.3 REN digestions [441]

Digestions of vector and insert DNA were performed in parallel and set up on ice according to the following 50 μl NEB protocol:

1.0 mg of template DNA (vector or insert)

1.0 μl REN1 (10000-20000 units / ml, NEB)

1.0 μl REN2 (10000-20000 units / ml, NEB)

5.0 μl NEB buffer X (10 X buffer, NEB)

x μl molecular biology grade H_2O (to 50 μl total volume, Fisher Scientific, BP28191)

The NEB double digest finder was utilized to optimize buffers and REN compatibility (https://www.neb.com/tools-and-resources/interactive-tools/double-digest-finder) and high fidelity (HF) RENs were utilized when available. Digestions were performed 16 h at 37 °C in a warm water bath. Excess enzyme was added when RENs were not 100 % active in a given buffer. Digested products were then purified via either spin column (inserts) or via agarose gel electrophoresis (vector backbones) on a 0.80 - 1.0 % (w:v) agarose gel. In the latter case, digested DNA (50 μl) was applied to agarose gel wells with 10 μl of 5 X green GoTaq reaction buffer (Promega, M7911) for visualization. Discrete intense bands were visualized under ultra violet (UV) light and the gel excised with a razor blade. Agarose gel fragments were weighed and then solubilized in 2

equivalents of gel binding buffer (e.g. 100 mg : 200 μl) at 60 °C for 10 min with regular vortexing. Digested DNA was then purified via spin column (Genejet gel extraction kit, Thermo Scientific, K0691) and eluted in 35 μl of molecular biology grade water (Fisher Scientific, BP28191).

12.3.4 Agarose Gel electrophoresis [442]

Agarose powder (Fisher Scientific, BP160) was dissolved in 200 ml of 1 X TAE buffer (**Table 16**) by heating in a microwave and then 2 - 4 drops of ethidium bromide solution (Fisher Scientific, 10688294, 0.625 mg / ml) were mixed into the gel solution. Agarose gel was poured into a mould to set for 30 min with an appropriate comb to create sample wells. Samples were run against a log2 DNA ladder (NEB, N3200L) at 100 mV for 30 - 60 min.

12.3.5 Ligations [443]

Ligation mixtures (10 μl) were set up on ice as below and mixed by gentle pipetting.

1.5 μl vortexed T4 DNA ligase buffer (Promega, C1263)
100 ng Digested vector backbone DNA
X ng Digested insert DNA (variable molar insert : vector ratios, typically 3:1 and 6:1)
X μl molecular biology grade H_2O (to 10 μl total volume, Fisher Scientific, BP28191)
1.0 μl T4 DNA ligase (Promega, M1801)

Ligations were performed for 16 h at 16 °C, prior to transformation. Control ligations were performed with molecular biology grade water instead of insert DNA to establish the frequency of digested plasmid re-ligation. Insert quantities were calculated using the equation below:

$$\frac{(\text{ng of vector} \times \text{size of insert})}{\text{size of vector}} \times \text{molar ratio of insert : vector} = \text{ng of insert}$$

12.3.6 Transformation of chemically competent cells [444]

Plasmid transformation was achieved by defrosting 100 μl cell aliquots on ice for 15 min. 5.0 μl of purified plasmid, ligation mix or ligation control was then added to the cell aliquots. Cells were mixed via flicking, prior to incubation on ice for 30 min. Cells were then heat shocked at 42 °C for 40 s, prior to cooling on ice for 2.0 min. Cells were then added to 895 μl warmed SOC media (37 °C) and incubated at 37 °C with agitation for 60 min. 100 μl (10 %) of each SOC recovery culture was then plated on agar plates with appropriate antibiotic concentrations (**Table 5**) and incubated for 16 h at 37 °C.

12.3.7 Transformation of plasmids into electro-competent cells [224]

Plasmid transformation was achieved by defrosting 100 μl cell aliquots on ice for 15 min. 5.0 μl of purified plasmid, ligation mix or ligation control was then added to the cell aliquots. Cells were mixed via flicking, prior to electroporation using a Bio-Rad Micropulser. 895 μl ice-cold SOC media were immediately added and mixed by cautious micro pipetting. SOC recovery cultures were incubated at 37 °C with agitation for 60 min. 100 μl (10 %) of each SOC recovery culture was then plated on agar plates with appropriate antibiotic concentrations (**Table 5**) and incubated for 16 h at 37 °C.

12.3.8 Colony PCR

A colony PCR master mix was set up on ice by multiplying the number of colonies to be assessed by the single 9.8 μl mix below:

6.3 μl molecular biology grade H_2O (Fisher Scientific, BP28191)
2.0 μl vortexed 5 X green GoTaq reaction buffer (Promega, M7911)
1.0 μl fresh dNTPs, 10 mM (Promega, U1420)
0.25 μl forward primer (**Table 18**), 10 pmol / μl
0.25 μl reverse primer (**Table 18**), 10 pmol / μl
0.050 μl GoTaq flexi DNA polymerase, 5.0 units / μl (Promega, M8295)

The master mix was mixed by gentle pipetting and then aliquoted into 9.8 μl portions in PCR tubes. A single bacterial colony was then added to each PCR tube with a sterile micropipette tip from the agar plate. PCR samples were amplified according to the protocol below:

Heat initialization- 1 x 6.0 min at 94 °C

Followed by 35 cycles of:

Denaturation- 60 s at 94 °C

Annealing- 60 s at primer dependent temperature (50 - 65 °C)

Extension- time dependent on amplicon length (1.0 min / 1.0 kb) at 72 °C

Followed by a final elongation of:

Final elongation- 10 min at 72 °C

Cooling- 60 min at 4 °C

PCR samples were analyzed via agarose gel electrophoresis and samples containing the expected amplicons were sent for DNA sequencing (Eurofins) to confirm successful cloning of the desired construct.

12.3.9 SDS-PAGE [445]

SDS-PAGE gels were made in batches as previously described (**Table 11**, **Table 12**) and stored in cling film and wet paper towel at 4 °C until needed. Immediately prior to use, 10 % (v:v) of BME (Sigma Aldrich, M6250) was added to 90 % (v:v) SDS-PAGE loading buffer (**Table 9**), then 15 μl of each protein sample were mixed with 15 μl of 2 X SDS-PAGE loading buffer (**Table 9**). The mix was then heated in a PCR machine at 100 °C for 10 min to denature protein, prior to loading 25 μl of each mix to the wells of the SDS-PAGE gel. SDS-PAGE gels were loaded into a mini protean tetra cell (Bio Rad: 165-8000), which was then filled with SDS running buffer made via a one in five dilution of the 5 X stock (**Table 10**). Samples were then run at 150 V for 45 - 50 min (10 % gel) or 60 - 70 min (12 % gel) to separate proteins. Gels were then stained with Coomassie blue protein dye stain (**Table 13**) for 5.0 – 8.0 min with agitation and then rinsed with cold water and de-stained in 50 ml of Coomassie protein de-stain solution (**Table 14**) for 120 min. Gels were then washed repeatedly with water and visualized in a square petri dish, using an Epson scanner.

12.4 Peptide chemistry techniques

12.4.1 Fmoc SPPS

Pre loaded Fmoc-amino acid-Wang resins were purchased from Nova-Biochem or Matrix Innovation Inc. and pre swollen in 50 % DCM (v:v) / DMF for 30 min with agitation prior to synthesis. [294] [349] Fmoc α-amino protected amino acids were utilized with the following side chain protecting groups; Cys(StBu), His(Trt), Gln(Trt), Arg(Pbf), Tyr(tBu). [346] [357] [358] [359] [350] [360]

12.4.2 Peptide synthesis

Fmoc deprotection was achieved via exposure to 10 ml of 20 % piperidine (v:v) (Sigma Aldrich, 80640) / DMF at room temperature (RT) for 4.0 and 8.0 min respectively. Resin was then washed with 4 x 10 ml DMF (Fisher Scientific, D/3840/17) prior to coupling. Coupling was achieved using 3 molar equivalents (eq.) Fmoc-Nα protected amino acid (Nova-Biochem or Matrix Innovations Inc.), 3 eq. HOBt (Sigma Aldrich, 54802) and 3 eq. DIC (Sigma Aldrich, D125407, all eq. relative to 1 eq. of resin bound amine) dissolved in 3.0 – 5.0 ml DMF for 3 h at RT. [352] Resin was then washed with 4 x 10 ml DMF and coupling completion confirmed via free amine test.

12.4.3 Kaiser free amine test [354]

Following amino acid coupling, the resin was washed with 4 x 10 ml DMF and then a few resin beads (ca. 10) were transferred to a glass vial. 4 drops of 0.020 mM KCN (Sigma Aldrich, 207810) / pyridine (Sigma Aldrich, 270970) and 1 drop of 0.30 M ninhydrin (Sigma Aldrich, N4876) / ethanol (Sigma Aldrich, E7023) were then added and the mixture was heated at 140 °C for 4.0 min. Primary amines yield the characteristic deep blue colouration due to formation of Ruhemann's purple, in stark contrast to acylated amine groups that yield colourless to light yellow beads.

12.4.4 TNBS free amine test [355]

Following amino acid coupling, the resin was washed with 4 x 10 ml DMF and then a few resin beads (ca. 10) were transferred to a glass vial containing 10 drops of 10 % *N, N*-diisopropylethylamine (v:v) (DIPEA, Sigma Aldrich, 496219) / DMF. 1-2 drops of a

0.20 M solution of picrylsulfonic acid (Sigma Aldrich, 92822) in 20% H_2O (v:v) / DMF were then added and mixed for 2.0 min. Resin beads were then washed with DMF and visually inspected. Primary amines yield the red colouration of the conjugated trinitrophenylamine, in stark contrast to acylated amine groups that yield colourless to light yellow beads.

12.4.5 Peptide resin cleavage

Peptide resins were dried via 3 cycles of 1 x 10 ml DCM (Fisher Scientific, D/1850/17) followed by 1 x 10 ml Et_2O (Fisher Scientific, D/2400/17) washes. Resins were then exposed to 10 ml of cleavage cocktail consisting of 95 % TFA (Sigma Aldrich, T6508), 2.5 % TIS (Sigma Aldrich, 233781), 2.5 % H_2O (v:v:v) for 3 h at RT, prior to filtration to remove the resin from the peptide / TFA solution. TFA was rotary evaporated to minimum volume until a cloudy solution was obtained. The resulting suspension was then co-evaporated with 10 ml DCM x 3 and 10 ml MeOH x 3 (MeOH, Fisher Scientific, M/4056/17) prior to crashing the peptide from solution with Et_2O. Crude peptide was then washed with 3 x 25 ml Et_2O and frozen at -20 °C prior to analysis via MS.

12.4.6 Cys(StBu) deprotection

Cys(StBu) protected peptide (100 mg) was dissolved in DMF (3.0 ml) and 0.10 M $(NH_4)_2CO_3$ / H_2O (2.0 ml, Fisher Scientific, 10710292) was added and stirred under argon for 5.0 min to degas the solution. DTT (20 eq., Fisher Scientific, R0862) was dissolved in 0.10 M $(NH_4)_2CO_3$ / H_2O (1.0 ml) and added to the peptide solution. Solution was stirred under argon for 2 h and the final pH determined via pH paper (pH ~ 9). The pH was adjusted to pH ~ 3 with concentrated TFA and the solution volume reduced via rotary evaporation prior to purification by RP-HPLC.

12.4.7 Peptide cyclization in solution

Linear Cys(StBu) protected peptide (100 mg) was dissolved in DMF (100 ml) and stirred under argon. EDC (10 eq., Sigma Aldrich, 03450) with HOBt (10 eq.) in DMF (2.0 ml) was added drop wise to the stirred solution and left to react for 64 h. Water (2.0 ml) was then added and the solution was stirred for 30 min under argon to destroy excess carbodiimide. The resulting solution was rotary evaporated to dryness and the

peptide precipitated with three Et_2O washes. Peptide was dried under argon in preparation for Cys(StBu) deprotection.

12.4.8 Peptide cyclization on resin [369]

Fmoc-Glu(CO_2H)-ODmab (2 eq., Nova-Biochem, 852077) was added to (Benzotriazol-1yloxy)tripyrrolidinophosphonium hexafluorophosphate (PyBOP, 3 eq., Matrix Innovations Inc., 1-025-0001) and DIPEA (6 eq.) and then dissolved in DMF (4.0 ml). [368] The coupling solution was agitated via argon bubbling for 6 h with H-Rink amide Chemmatrix resin (Sigma Aldrich, 727768) and coupling completion was checked via TNBS test. Fmoc SPPS of the linear peptide was performed as previously described. H_2N-linear peptide-Glu(resin)-ODmab was swollen in a sinter funnel in DMF for 30 min. Resin was treated with 5 x 3.0 ml aliquots of 2.0 % hydrazine monohydrate (v:v) (Sigma Aldrich, 207942) / DMF for 3.0 min per aliquot. Resin was washed with 5 mM NaOH in 50 % water (v:v) / MeOH for 3 h to eliminate residual hydrazine. [370] Resin was washed for 1.0 min each with 5 x 10 ml aliquots of MeOH, followed by 5 x 10 ml aliquots of DMF. Resin was further washed for 1.0 min each with 5 x 10 ml aliquots of DCM, followed by 5 x 10 ml aliquots of DMF. H_2N-peptide-Glu(resin)-CO_2H was transferred to a round bottomed flask and EDC (10 eq.) with HOAt (10 eq., Carbosynth, FH14135) in DMF was added. Reaction was stirred for 18 h at RT, prior to washing for 1.0 min each with 4 x 10 ml DMF. Cyclisation was confirmed via TNBS test and the peptide was cleaved from the resin as previously described and purified via RP-HPLC.

12.4.9 Peptide purification via RP-HPLC

Peptides were dissolved in appropriate amounts of TFA, acetonitrile (MeCN, Fisher Scientific, A/0627/17), DMF and water prior to RP-HPLC purification. RP-HPLC utilized a binary solvent system consisting of solution A (0.1 % TFA / water) and B (0.1 % TFA / MeCN). Peptides were manually injected via the Waters Flex inject system into a RP-HPLC system consisting of a Waters 1525 binary pump coupled to a Waters 2998 photodiode array detector. Peptides were purified using a Waters Atlantis prep, T3, amide capped C18, 5 μm, 19 x 100 mm column at 17 ml / min for 20 min. Elution was monitored at 220 nm (peptide backbone) and 280 nm (aromatic amino acids, Trp and Tyr) and fractions were collected by hand and analyzed by ESI+ MS. Fractions were lyophilized and stored at -20°C.

12.5 Mammalian cell culture techniques

12.5.1 Passaging MCF-7 cells

Adherent MCF-7 cells were cultured in T75 tissue culture treated flasks (Fisher scientific: 10492371) in 12 ml Dulbecco's modified eagle medium (DMEM, Life technologies: 42430-025), supplemented with 1.0 % Penicillin / Streptomycin (v:v) (P/S, Life technologies: 15140-122) and 10 % Fetal bovine serum (v:v) (FBS, US origin, Life technologies: 10082-147) at 37 °C with 5.0 % CO_2 (Referred to as DMEM complete). Spent DMEM complete was removed from the T75 flask and discarded. Cell surface was washed with 10 ml PBS (Life technologies: 10010-015) and then the PBS was discarded. Adherent cells were suspended via the addition of 1.5 ml 0.050 % Trypsin (Life technologies: 25300054) and incubated at 37 °C with 5.0 % CO_2 for 5.0 min. Trypsin was neutralized via the addition of 10.5 ml DMEM complete and mixed with a stripette with tapping of the flask to loosen adherent cells. Cell clumps were separated via forceful stripette extrusion with rotation, which was repeated three times. Cells were diluted into fresh DMEM complete in a fresh T75 flask and mixed via rocking. The volume of DMEM complete in each T75 flask was maintained at a constant 12 ml and the cells were maintained at 37 °C with 5.0 % CO_2 in a Heracell 150i CO_2 incubator (Thermo Scientific: 51026280). Cells were manipulated in an Aura 2000 B.S. (Bioair instruments) material safety cabinet to maintain sterility.

12.5.2 Passaging HeLa cells

Adherent HeLa cells were cultured in T75 tissue culture treated flasks (Fisher scientific: 10492371) in 12 ml DMEM (Life technologies: 42430-025), supplemented with 10 % FBS (v:v) (South American origin, Fisher Scientific, Hyclone, SV30160.03) at 37 °C with 5.0 % CO_2 (Referred to as DMEM complete). Spent DMEM complete was removed from the T75 flask and discarded. Cell surface was washed with 10 ml PBS (Life technologies: 10010-015) and then the PBS was discarded. Adherent cells were suspended via the addition of 2.0 ml TrypLE (Life technologies: 12605-010) and incubated at 37 °C with 5.0 % CO_2 for 5.0 min. TrypLE was neutralized via the addition of 8.0 ml DMEM complete and mixed with a stripette with tapping of the flask to loosen adherent cells. Cell clumps were separated via forceful stripette extrusion with rotation, which was repeated three times. Cells were diluted into fresh DMEM complete

in a fresh T75 flask and mixed via rocking. The volume of DMEM complete in each T75 flask was maintained at a constant 12 ml and the cells were maintained at 37 °C with 5.0 % CO_2 in a Heracell 150i CO_2 incubator (Thermo Scientific: 51026280). Cells were manipulated in a Hera material safety cabinet to maintain sterility.

12.5.3 Cell counting

Washed and re-suspended cells were mixed thoroughly with a stripette and 200 μl of DMEM with cells were removed into an epindorf tube and mixed three times with a 1000 μl pipette tip. The cell suspension was further mixed 10 times with a 100 μl pipette tip, immediately prior to removal of 2 x 10 μl samples for cell counting. Cells were counted using a Neubauer improved bright line haemocytometer (0.0025 mm^2, Marienfeld, 06 400 30). All four counting grid corners were quantified for both counting grids, prior to determination of cell number/ml via the formula below:

$$\text{Number of cells per ml} = 10000 \times \frac{(\text{Average count of grids A and B})}{4}$$

12.5.4 Bradford assay [439]

A BSA standard curve was assembled via addition of 0, 3, 6, 12, 18 or 24 μl of 0.50 mg / ml BSA (made via a one in forty dilution of 20 mg / ml BSA, NEB, B9000S) to 600 μl of one in five diluted Bio-Rad protein assay dye concentrate (Bio-Rad, 5000006). BSA solutions equated to concentrations (c) of 0, 0.50, 1.0, 2.0, 3.0 and 4.0 mg / ml and were used as calibration standards to determine the molar extinction coefficient (ε) of the Bradford equation. 3.0 μl of treated or untreated cell lysate was then added to 600 μl of one in five diluted Bio-Rad protein assay dye concentrate and mixed via vortex. Protein samples or BSA standards (150 μl) were then added in triplicate to a clear colourless 96 well plate, maintaining a constant path length (l). Protein absorbance was measured at 630 nm (A_{630}) and background at 405 nm (A_{405}), which was used to correct samples for plate background. Protein concentration in treated and untreated cell lysates was determined according to the Bradford equation below:

$$A_{630} - A_{405} = \varepsilon \times c \times l$$

12.6 Experiment specific procedures

12.6.1 Primer list

	Primer name	5' to 3' sequence
A)	eIF4E XhoI Fw	GTTGTTCTCGAGATGGCGACTGTCGAACCGGAAACC
B)	eIF4E KpnI Rev	GTTGTTGGTACCTTAAACAACAAACCTATTTTTAG
C)	eIF4G SalI Fw	GTTGTTGTCGACATGGCCTTCAAGGAGGCGAACC
D)	eIF4G SacI Rev	GTTGTTGAGCTCTCATTCGGTCATTAACACTGTG
E)	C5X BglI Fw	GGAATTCGCCAATGGGGCGATCGCCCACAATTGC NNSNNSNNSNNSNNSTGCTTAAGTTTTGGC
F)	CRRQ5X BglI Fw	GGAATTCGCCAATGGGGCGATCGCCCACAATTGC CGCGCCAGNNSNNSNNSNNSNNSTGCTTAAGTTTTGGC
G)	CRRQ4X BglI Fw	GGAATTCGCCAATGGGGCGATCGCCCACAATTGC CGCCGCCAGNNSNNSNNSNNSTGCTTAAGTTTTGGC
H)	CBD HindIII Rev	GGAATTCAAGCTTTCATTGAAGCTGCCACA
I)	Zipper BglI Fw	GGAATTCGCCAATGGGGCGATCGCC
1)	P1	GGAATCAATGCCTGAGTG
2)	P2	ACTTAACGGCTGACATGG
3)	P3	ACGAGTATCGAGATGGCA
4)	P4	GGCATCAACAGCACATTC

Table 18: PCR primer table. REN sites are indicated in green, start and stop codons in blue with regions complementary to the target gene highlighted in red.

12.6.2 Construction of pTHCP14 eIF4E

eIF4E was amplified from a pcDNA eIF4E storage vector via extension PCR with primers A and B (**Table 18**), using an annealing temperature gradient of 50 – 65 °C and an extension time of 1.0 min. PCR products were analyzed via agarose gel electrophoresis on a 0.80 % gel and purified via spin column (Genejet gel extraction kit, Thermo Scientific, K0691) according to the manufacturers instructions. PCR products and pTHCP14 were subsequently digested with XhoI (1.0 μl, NEB, R0146S) and KpnI HF (1.0 μl, NEB, R3142S) in cut smart buffer (5.0 μl, 10 X, NEB, B7204S) for 2 h at 37 °C. Digested eIF4E insert and pTHCP14 backbone were purified via agarose gel electrophoresis on a 1.0 % gel as previously described. Digested eIF4E insert was ligated at insert : vector molar ratios of 4 : 1 and 7 : 1 between the XhoI and KpnI sites of pTHCP14 at 4 °C for 16 h. Ligation mixtures were transformed into chemically competent DH5α cells and plated onto LB agar plates with 100 μg / ml carbenicillin at 37 °C for 16 h. Carbenicllin resistant colonies containing the eIF4E gene were identified via colony PCR with primers A and B (**Table 18**), using an annealing temperature of 55 °C and an extension time of 1.0 min. Construction of pTHCP14 eIF4E was verified via DNA sequencing (Eurofins).

12.6.3 Construction of pTHCP14 eIF4E / eIF4G

eIF4G was amplified from a pcDNA eIF4G storage vector via extension PCR with primers C and D (**Table 18**), using an annealing temperature gradient of 50 – 65 °C and an extension time of 1.0 min. PCR products were analyzed via agarose gel electrophoresis on a 1.0 % gel and purified via spin column (Genejet gel extraction kit, Thermo Scientific, K0691) according to the manufacturers instructions. PCR products and pTHCP14 eIF4E were subsequently digested with SacI HF (1.0 μl, NEB, R3156S) and SalI HF (1.0 μl, NEB, R3138S) in cut smart buffer (5.0 μl, 10 X, NEB, B7204S) for 2 h at 37 °C. Digested eIF4G insert and pTHCP14 eIF4E backbone were purified via agarose gel electrophoresis on a 0.80 % gel as previously described. Digested eIF4G insert was ligated at insert : vector molar ratios of 3 : 1 and 6 : 1 between the SacI and SalI sites of pTHCP14 eIF4E at 4 °C for 16 h. Ligation mixtures were transformed into chemically competent DH5α cells and plated onto LB agar plates with 100 μg / ml carbenicillin at 37 °C for 16 h. Carbenicllin resistant colonies containing the eIF4E gene were identified via colony PCR with primers C and D (**Table 18**), using an annealing

temperature of 55 °C and an extension time of 1.0 min. Construction of pTHCP14 eIF4E / eIF4G was verified via DNA sequencing (Eurofins).

12.6.4 Construction of pAH68 eIF4E / eIF4G

pTHCP14 eIF4E / eIF4G was transformed into chemically competent GM2929 cells (methylation negative strain of *E. coli*) and re-extracted via plasmid mini prep to ensure non-methylated DNA for REN digestion. pTHCP14 eIF4E / eIF4G was subjected to a triple digest with SacI HF (1.0 μl, NEB, R3156S), BspHI (1.0 μl, NEB, R0517S) and MscI (1.0 μl, NEB, R0534S) in cut smart buffer (5.0 μl, 10 X, NEB, B7204S) for 2 h at 37 °C. BspHI was included to degrade the unwanted pTHCP14 vector backbone and enable separation of the desired insert from the pTHCP14 vector backbone. pAH68 was subjected to a sequential double digest in cut smart buffer (5.0 μl, 10 X, NEB, B7204S), initially with SmaI (1.0 μl, NEB, R0141S) at 25 °C for 2 h, followed by digestion at 37 °C for 2 h with SacI HF (1.0 μl, NEB, R3156S). Digested insert and pAH68 backbone were purified via agarose gel electrophoresis on a 0.80 % gel as previously described. Digested insert was ligated at insert : vector molar ratios of 1 : 1, 2 : 1 and 3 : 1 between the SmaI and SacI sites of pAH68 at 4 °C for 16 h. Ligation mixtures were transformed into chemically competent DH5α pir protein positive cells and plated onto LB agar plates with 100 μg / ml carbenicillin at 37 °C for 16 h. Carbenicllin resistant colonies containing the eIF4E (**Table 18:** primers A and B) and eIF4G (**Table 18:** primers C and D) genes were identified via colony PCR, using an annealing temperature of 50 °C and an extension time of 3.0 min. Construction of pAH68 eIF4E / eIF4G was verified via DNA sequencing (Eurofins).

12.6.5 Integration of pAH68 eIF4E / eIF4G into SNS126

pAH69 was transformed into electro-competent SNS126 cells and plated onto LB agar plates with 100 μg / ml carbenicillin and 25 μg / ml spectinomycin at 30 °C for 16 h. Freshly transformed pAH69 SNS126 cells were cultured in SOC media with 100 μg / ml carbenicillin and 25 μg / ml spectinomycin at 30 °C for 16 h. 2.5 ml (1.0 %) of the pAH69 SNS126 culture was added to 250 ml of sterile SOC media with 100 μg / ml carbenicillin and 25 μg / ml spectinomycin. The culture was incubated at 30 °C until an OD_{600} of ~ 0.30 was achieved, whereupon the culture was transferred to incubation in a 42 °C water bath for 30 min with agitation. It should be noted that the use of an air

incubator for this step provided poor heat transfer and insufficient expression of phage integrase for successful integration. Once an OD_{600} of ~ 0.70 was achieved, the cells were cooled on ice for 15 min. Cells were pelleted at 4 °C via centrifugation for 15 min at 3100 rpm and the supernatant was discarded. Cell pellet was re-suspended in 250 ml of ice cold 10 % Glycerol (v:v) / H_2O (Fisher Scientific, BP229) solution, then centrifuged at 4000 rpm for 15 min at 4 °C, prior to discarding the supernatant. This glycerol cycle was repeated with 125 ml, 50 ml, 25 ml and 10 ml washes. Cells were re-suspended in 2.0 ml of ice-cold glycerol and snap frozen into 100 μl aliquots as for the chemically competent cells. Electro-competent cells were then frozen at -80 °C and thawed on ice when needed.

pAH69 SNS126 electro-competent cells were defrosted on ice for 15 min and 2.0 μl of pAH68 or pAH68 eIF4E / eIF4G was then added to the cell aliquots. Cells were mixed via flicking, prior to electroporation using a Bio-Rad Micropulser. Ice cold SOC media (895 μl) was immediately added and mixed by cautious micro-pipetting. SOC recovery cultures were incubated at 32 °C with agitation for 1 h, followed by 42 °C with agitation for 1 h. Once again, the use of a warm water bath incubator was essential, as the use of an air incubator provided poor heat transfer and insufficient expression of phage integrase for successful integration. The previously constructed CtBP RTHS was recovered in tandem with pAH68 and pAH68 eIF4E / eIF4G integrations, as a positive control for colony PCR. 10 μl (1.0 %), 1.0 μl (0.10 %) or 0.10 μl (0.010 %) of each SOC recovery mixture was then plated on agar plates with 50 μg / ml carbenicillin, 25 μg / ml kanamycin and 25 μg / ml spectinomycin and incubated at 37 °C for 16 h. Colony PCR with primers 1, 2, 3 and 4 (**Table 18**), was used to identify single integrants of pAH68 derivatives into the HK022 site of SNS126. Colony PCR was performed with an annealing temperature of 59 °C and an extension time of 1.0 min and the resulting amplicons were analyzed via agarose gel electrophoresis on a 0.80 % gel. Colonies that exhibited amplicons indicative of integration were subsequently analyzed for eIF4E / eIF4G genes via colony PCR with primers A, B (**Table 18:** for eIF4E) and C, D (**Table 18:** for eIF4G). Colony PCR was performed with an annealing temperature of 59 °C and an extension time of 1.0 min and the resulting amplicons were analyzed via agarose gel electrophoresis on a 0.80 % gel.

12.6.6 Validation of the eIF4E / eIF4G RTHS via drop spotting

Colonies of the eIF4E / eIF4G RTHS that exhibited PCR amplicons consistent with successful integration were selected for validation. eIF4E / eIF4G RTHS candidates were cultured in LB media with 50 μg / ml carbenicillin, 25 μg / ml spectinomycin at 37 °C for 16 h. The previously constructed CtBP RTHS was cultured for 16 h in an identical manner, as a positive control. pAH69 SNS126 cells were cultured in LB media with 100 μg / ml carbenicillin, 25 μg / ml spectinomycin at 30 °C for 16 h, as a negative control. *E. coli* cultures (20 μl) were serially diluted into 10 % sterile glycerol (v:v) / H_2O (180 μl) to give 10^{-1}, 10^{-2}, 10^{-3}, 10^{-4}, $10^{-5}$and 10^{-6} dilutions of each culture. Serial dilutions (2.5 μl) were drop spotted onto minimal media agar containing a range of antibiotic, IPTG and 3-AT concentrations and incubated at 30 °C for 66 h.

12.6.7 ONPG assay

The eIF4E / eIF4G and the CtBP RTHS were cultured for 16 h at 37 °C in LB media with 50 μg / ml carbenicllin and 25 μg / ml spectinomycin. pAH69 SNS126 was cultured for 16 h at 30 °C in LB media with 100 μg / ml carbenicllin and 25 μg / ml spectinomycin to preserve pAH69. Six replicates of LB media (3.0 ml) with 50 μg / ml carbenicllin and 25 μg / ml spectinomycin were inoculated with 30 μl (1.0 %) of each *E. coli* culture (eIF4E / eIF4G RTHS, SNS126 pAH69 and CtBP RTHS, 18 x 3.0 ml cultures in total) and cultured at 30 °C until an OD_{600} ~ 0.40 was achieved. Each 3.0 ml culture was then sub-divided into three 1.0 ml cultures to provide three independent data points. Each set of three 1.0 ml cultures was induced with a different concentration of IPTG (0, 10, 25, 50, 100 and 250 μM) and cultured at 30 °C until an OD_{600} ~ 0.70 was achieved. All samples were placed on ice and the OD_{600} recorded.

0.30 ml of each induced culture was added to 0.40 ml Z buffer (**Table 15**) and vortexed for 10 s to ensure cell lysis. Samples were pre-incubated at 37 °C for 1.0 min prior to addition of ONPG (Sigma Aldrich, 73660, 4.0 mg / ml aqueous solution, 200 μl). Reactions were timed and allowed to proceed until visible yellow colouration developed, whereupon solutions were quenched with 1.0 M Na_2CO_3 (500 μl, aqueous) to denature β-galactosidase. OD_{420} (λ_{max} of ortho-nitrophenol) readings were recorded relative to an LB media alone blank and β-galactosidase activity was determined according to the Miller equation below:

$$\beta\text{-galactosidase activity} = \frac{1000 \times OD_{420}}{(\text{Reaction time} \times \text{Culture volume} \times OD_{600})}$$

12.6.8 Construction of pARCBD encoded SICLOPPS libraries

A portion of the intein pre-splicing construct (I_C-extein-I_N-CBD, lacking the N-terminus of I_C) was amplified from between the BglI and HindIII REN sites of pARCBD Ssp via PCR with forward primer E, F or G and reverse primer H (**Table 18**). The first PCR step of library construction was annealed at 55 °C for 60 s and elongated at 72 °C for 90 s. PCR products were analyzed via agarose gel electrophoresis on a 1.0 % gel and purified via spin column (Genejet gel extraction kit, Thermo Scientific, K0691) according to the manufacturers instructions. The second (zipper) PCR was performed in an identical fashion, except that forward primer I and reverse primer H were used (**Table 18**). Zipper PCR products were analyzed via agarose gel electrophoresis on a 1.0 % gel and purified via spin column (Genejet gel extraction kit, Thermo Scientific, K0691) according to the manufacturers instructions. It is important to note that a 55 °C annealing temperature for both PCR steps was found to be absolutely critical for the isolation of SICLOPPS libraries with sufficient diversity for screening.

pARCBD (42 μl, ~ 8000 ng) and zipper PCR products (42 μl, ~ 8000 ng) were subjected to REN digestion with BglI (2.0 μl, NEB, R0143S) and HindIII (1.0 μl , NEB, R0104S) in NEB buffer 2 (5.0 μl, 10 X, NEB, B7002S) at 37 °C for 16 h. RENs were inactivated via incubation at 80 °C for 20 min, prior to cooling on ice for 20 min. Thermostable alkaline phosphatase (TSAP, 2.0 μl, Promega, M9910) was added to the pARCBD digest and incubated at 37 °C for 1 h to dephosphorylate the digested plasmid backbone and minimize vector re-ligation. TSAP was inactivated via incubation at 80 °C for 20 min, prior to cooling on ice for 20 min. Digested zipper PCR products were analyzed via agarose gel electrophoresis on a 1.0 % gel and purified via spin column (Genejet gel extraction kit, Thermo Scientific, K0691) according to the manufacturers instructions. Digested pARCBD was purified via agarose gel electrophoresis on a 0.80 % gel as previously described.

Digested insert was ligated at insert : vector molar ratios of 3 : 1, 6 : 1, 9 : 1, 12 : 1 and 15 : 1 between the BglI and HindIII sites of pARCBD at 16 °C for 16 h. T4 DNA ligase (Promega, M1801) was inactivated via incubation at 70 °C for 10 min, prior to cooling

on ice for 20 min. Ligations were combined and dialyzed against sterile molecular biology grade water (200 ml, Fisher Scientific, BP28191) using V-series drop dialysis membranes (Merck Millipore, VSWP02500) for 3 – 6 h. It should be noted that failure to dialyze ligation mixtures severely impaired transformation efficiency due to arching of electric current during transformation into electro-competent cells. The reduction of salt concentration in ligation mixtures was found to be absolutely essential for obtaining SICLOPPS libraries with sufficient diversity for screening.

Minimal media SICLOPPS library construction plates containing 5.0 mM 3-AT, 50 μg / ml kanamycin, 25 μg / ml spectinomycin, 35 μg /ml chloramphenicol, 50 μM IPTG and 6.5 μM arabinose were prepared in advance. Dialyzed ligation mixture was transformed into electro-competent eIF4E / eIF4G RTHS cells and recovered in SOC media (1.0 ml) in a warm water bath incubator at 37 °C for 1 h 15 min. A sample of SOC recovery culture (20 μl) was serially diluted with sterile SOC media to give solutions representing 10^{-4}, 10^{-5}, 10^{-6} and 10^{-7} dilutions of the recovery culture. The remaining SOC recovery culture (980 μl) was pelleted via centrifugation at 3100 rpm for 15 min and ~ 900 μl of the supernatant was removed. Meanwhile, LB agar plates with 35 μg / ml chloramphenicol and SICLOPPS library plates were pre-warmed at 37 °C for 10 min prior to plating. Pelleted cells were re-suspended in the remaining ~ 100 μl of SOC media, plated onto SILCOPPS library construction plates and incubated at 37 °C for 90 h. Each SOC recovery culture dilution was plated onto LB agar plates with 35 μg / ml chloramphenicol and incubated at 37 °C for 16 h. The number of colonies on each dilution plate provided an estimate of the diversity of the SICLOPPS library and hence the percentage of theoretically possible cyclic peptides that had been successfully encoded into pARCBD Ssp.

12.6.9 Screening of pARCBD encoded SICLOPPS libraries

96 colonies were picked from SICLOPPS library construction plates and cultured in LB media with 35 μg /ml chloramphenicol in a 96 well plate (Greiner, 655180) at 37 °C for 16 h. *E. coli* cultures (20 μl) were serially diluted into 10 % sterile glycerol (v:v) / H_2O (180 μl) to give 10^{-1}, 10^{-2}, 10^{-3}, 10^{-4}, 10^{-5} and 10^{-6} dilutions of each culture. Four minimal media agar SICLOPPS screening plates were prepared with 5.0 mM 3-AT, 50 μg / ml kanamycin, 25 μg / ml spectinomycin, 35 μg /ml chloramphenicol and varying concentrations of IPTG and arabinose. Plate 1 lacked both IPTG and arabinose and

functioned as a control plate in which both expression of RTHS repressor fusion proteins and expression of the pARCBD Ssp encoded cyclic peptides was repressed. Plate 2 contained 50 μM IPTG but lacked arabinose and functioned as a control plate in which expression of RTHS repressor fusion proteins was induced. Plate 3 contained 6.5 μM arabinose but lacked IPTG and functioned as a control plate in which expression of the pARCBD Ssp encoded cyclic peptides was induced. Plate 4 contained both 50 μM IPTG and 6.5 μM arabinose and functioned as a test plate to determine the dependence of the growth of the eIF4E / eIF4G RTHS on the presence of a functional cyclic peptide inhibitor of the PPI. Serial dilutions (2.5 μl) were drop spotted onto four minimal media agar plates containing a range of IPTG and arabinose concentrations and incubated at 37 °C for 90 h.

Colony growth of serial dilutions on plate 2 (50 μM IPTG, 0 μM arabinose) was compared to the corresponding growth of dilutions on plate 1 (0 μM IPTG, 0 μM arabinose) to confirm inhibition of growth of the eIF4E / eIF4G RTHS upon exposure to IPTG. Colony growth of serial dilutions on plate 3 (0 μM IPTG, 6.5 μM arabinose) was compared to the corresponding growth of dilutions on plate 1 (0 μM IPTG, 0 μM arabinose) to confirm that the arabinose induced expression of cyclic peptides from pARCBD Ssp was not toxic to *E. coli* Colony growth of serial dilutions on plate 2 (50 μM IPTG, 0 μM arabinose) was compared to the corresponding growth of dilutions on plate 4 (50 μM IPTG, 6.5 μM arabinose). SICLOPPS screening candidates exhibited arabinose induced restoration of colony growth in the presence of IPTG. SICLOPPS candidates were cultured in LB media (10 ml) with 35 μg / ml chloramphenicol at 37 °C for 16 h and the pARCBD plasmid extracted via mini prep.

12.6.10 Secondary screening of SICLOPPS candidates

SICLOPPS screening candidates were re-transformed into the eIF4E / eIF4G RTHS and drop spotting repeated on SICLOPPS screening plates to confirm phenotypic retention. Identical SICLOPPS candidates were transformed in parallel into a previously constructed heterodimeric control RTHS. pARCBD vectors in the heterodimeric control RTHS were drop spotted onto SICLOPPS screening plates in an identical fashion to those re-transformed into the eIF4E / eIF4G RTHS.

Colonies that displayed phenotypic retention in the eIF4E / eIF4G RTHS were hypothesized to contain pARCBD derivatives that encoded potential cyclic peptide inhibitors of the eIF4E / eIF4G interaction and were identified as secondary screening candidates. SICLOPPS secondary screening candidates were further refined as those that exhibited arabinose induced restoration of growth in the presence of IPTG; specifically in the eIF4E / eIF4G RTHS, but not in the control RTHS. This back screening procedure helped to eliminate false positives caused by pARCBD derivatives that encoded inhibitors of the interaction of 'P22' or 434 with the chimeric DNA operator. Such false positives exhibited arabinose dependent growth restoration in the presence of IPTG, in both the control and the eIF4E / eIF4G RTHS. Secondary screening candidates from all library screens were ranked via drop spotting onto SICLOPPS screening plates followed by incubation at 37 °C for 90 h.

12.6.11 Chitin bead pull-down intein splicing assay

pARCBD derivatives encoding potential cyclic peptide inhibitors of the eIF4E / eIF4G interaction were isolated via mini prep and re-transformed into the eIF4E / eIF4G RTHS. pARCBD derivatives in the eIF4E / eIF4G RTHS were cultured in LB media with 25 μg / ml spectinomycin and 35 μg / ml chloramphenicol at 37 °C for 16 h. In parallel pARCBD Ssp and pARCBD Npu* derivatives encoding the Hypoxia inducible factor (HIF) inhibitor (P1) and cyclo CRRQVYVH were cultured identically in the HIF RTHS or the eIF4E / eIF4G RTHS respectively. 250 ml of LB media with 25 μg / ml spectinomycin and 35 μg / ml chloramphenicol was inoculated with 2.5 ml (1.0 %) of each *E. coli* culture and cultured at 37 °C until an OD_{600} = 0.50 - 0.70 was achieved. Expression of the intein pre-splicing construct (I_C-extein-I_N-CBD), was induced with arabinose (3.3 mM) and cultures were incubated at 37 °C for 3 h. Cells were harvested by centrifugation at 3100 rpm for 15 min at 4 °C and then frozen at -80 °C. Cell pellets were thawed on ice for 15 min, re-suspended in chitin buffer (**Table 17:** 5.0 ml) and incubated at 4 °C for 15 min. Cell lysis was completed via three 1.0 min sonication cycles and insoluble lysate was separated by centrifugation at 8000 rpm for 45 min at 4 °C. Soluble cell lysate was filtered through 0.22 μm sterile syringe filters (Fisher Scientific, 10565022) and kept on ice. Soluble cell lysate was loaded to chitin beads (200 μl, NEB, S6651S, pre-equilibrated with chitin buffer, **Table 17:** 2 x 5.0 ml) at 4 °C for 2 h with agitation. Beads were washed with chitin buffer (**Table 17:** 4 x 5.0 ml, 15 min per aliquot) and pelleted by centrifugation at 2500 rpm for 15 min at 4 °C.

Supernatant washings were discarded and intein splicing was allowed to proceed on the affinity beads at 25 °C for 16 h. Resin bound proteins were eluted in SDS-PAGE loading buffer (**Table 9**) at 100 °C and analyzed on a 15 % gel.

12.6.12 MTT assay [376]

MCF-7 cells were trypsinized and re-suspended as previously described and counted as above. Cells were appropriately diluted with DMEM complete to yield stock solutions of the required concentrations (25000 cells / ml). Cell dilutions (200 μl, 5000 cells per well) were mixed with a strippette immediately prior to plating. Cells were plated in triplicate for all samples in addition to the vehicle alone controls. 96 well plates plate (Corning: 3596, VWR: 734-1794) were incubated at 37 °C with 5.0 % CO_2 for 24 h to allow cells to adhere to the plate. Spent DMEM complete was removed with a P1000 and replaced with fresh DMEM complete (198 μl), to which was added 50 % DMSO / water (vehicle alone control, 2.0 μl, final DMSO concentration ~ 0.5 %) or peptide dissolved in 50 % DMSO / water (test compound, 2.0 μl, final DMSO concentration ~ 0.5 %). 96 well plates were incubated at 37 °C with 5.0 % CO_2 for 24 h to allow cell dosage. Spent DMEM complete was removed with a P1000 and the cells were washed with ~ 200 μl PBS. DMEM without phenol red (Clear DMEM, Life technologies: 21063-029) was supplemented with 1.0 % P/S (v:v) (Life technologies: 15140-122) and 10 % FBS (v:v) (US origin, Life technologies: 10082-147) to generate clear DMEM complete. 100 μl of clear DMEM complete was added to all cell wells. 4.0 mg of MTT (Sigma Aldrich: M5655-100 mg) was weighed into a sterile epindorf tube (covered in foil as MTT is light sensitive) and 0.80 ml PBS (37 °C) was added. MTT was dissolved by pipetting up and down ten times followed by a 2.0 – 5.0 min vortex, which yielded a 12 mM solution. 10 μl of 12 mM MTT / PBS solution was then added to all wells and mixed via agitation. 96 well plates were incubated in the dark at 37 °C with 5.0 % CO_2 for 4 h to allow dosage of cells with MTT and metabolism to insoluble purple formazan. Cells were visualized under a microscope after MTT treatment to ensure formation of purple precipitate. Spent clear DMEM complete with MTT was removed, prior to solubilisation of formazan with 100 μl of DMSO. [380] The 96 well plate was wrapped in foil to protect the MTT assay from light, prior to quantification on an Infinite M200 Pro (Tecan) plate reader.

12.6.13 Construction of luciferase assay vectors

pRAF (Apaf-1 IRES source, 5000 ng), pRMF (c-Myc IRES source, 5000 ng), pRemcvF (EMCV IRES source, 5000 ng) and pRhrvF (HRV IRES source, 5000 ng) were subjected to REN digestion with SpeI HF (1.0 μl, NEB, R3133S) and SgrAI (1.0 μl, NEB, R0603S) in cut smart buffer (6.0 μl, 10 X, NEB, B7204S) for 3 h 30 min at 37 °C. RENs were inactivated via incubation at 80 °C for 20 min, prior to cooling on ice for 20 min. Excised SpeI / IRES / Fluc / SgrAI DNA fragments were purified via agarose gel electrophoresis on a 1.0 % gel as previously described. Four PIC test (5000 ng) digests were performed in parallel with SpeI HF (1.0 μl, NEB, R3133S) and SgrAI (1.0 μl, NEB, R0603S) in cut smart buffer (6.0 μl, 10 X, NEB, B7204S) for 3 h 30 min at 37 °C. RENs were inactivated via incubation at 80 °C for 20 min, cooled on ice for 20 min and then purified via agarose gel electrophoresis on a 1.0 % gel as previously described. Digested SpeI / IRES / Fluc / SgrAI inserts were ligated at insert : vector molar ratios of 3 : 1 and 6 : 1 between the SpeI and SgrAI sites of PIC test at 16 °C for 16 h. Ligation mixtures were transformed into chemically competent DH5α cells and plated onto LB agar plates with 100 μg / ml carbenicillin at 37 °C for 16 h. Carbenicllin resistant colonies containing the desired SpeI / IRES / Fluc / SgrAI inserts were identified by test digestion for REN sites within IRES sequences, which was performed as follows. Four colonies of each IRES containing PIC test vector derivative were cultured with 100 μg / ml carbenicillin at 37 °C for 16 h and the plasmid extracted by miniprep as previously described. PAT test (Apaf-1 IRES, 2500 ng) was subjected to REN digestion with BglII (0.25 μl, NEB, R0144S) in NEB buffer 3.1 (1.5 μl, 10 X, NEB, B7203S) with molecular biology grade H_2O (to 6 μl total volume, Fisher Scientific, BP28191) for 3 h 45 min at 37 °C. CAT test (c-Myc IRES, 2500 ng) was subjected to REN digestion with BamHI (0.25 μl, NEB, R0136S) in NEB buffer 3.1 (1.5 μl, 10 X, NEB, B7203S) with molecular biology grade H_2O (to 6 μl total volume, Fisher Scientific, BP28191) for 3 h 45 min at 37 °C. MAT test (HRV IRES, 2500 ng) or HAT test (HRV IRES, 2500 ng) were subjected to REN digestion with HindIII (0.25 μl, NEB, R0104S) in NEB buffer 2.1 (1.5 μl, 10 X, NEB, B7202S) with molecular biology grade H_2O (to 6 μl total volume, Fisher Scientific, BP28191) for 3 h 45 min at 37 °C. REN test digestion samples were subsequently analyzed by agarose gel electrophoresis on a 1.0 % gel to identify colonies that contained PIC test vectors with the desired IRES candidates inserted 5' to the Fluc gene. Construction of PAT test (Apaf-1 IRES), CAT

test (c-Myc IRES), MAT test (EMCV IRES) and HAT test (HRV IRES) was verified via DNA sequencing (Eurofins).

12.6.14 Luciferase assay

HeLa cells were trypsinized and re-suspended as previously described and counted as above. Cells were appropriately diluted with DMEM complete to yield stock solutions of the required concentrations (25000 cells / ml). 200 μl of this cell stock (5000 cells) was then plated in triplicate for each treatment in a 96 well plate (Corning: 3596, VWR: 734-1794). 96 well plates were incubated at 37 °C with 5.0 % CO_2 for 16 h to allow cells to adhere to the plate.

Plasmids for transfection (PIC test, PAT test, CAT test, MAT test and HAT test) were isolated via maxi-prep (Genejet maxiprep kit, Fisher Scientific, 11551645) and the DNA eluted in filter sterilized, molecular biology grade water (Fisher Scientific, BP28191). [394] 1.0 μg of plasmid was needed to transfect 100000 cells, so each well (5000 cells) required 50 ng of plasmid for effective transfection. Briefly, sufficient plasmid to transfect all required wells was added to a sterile epindorf tube, diluted to < 100 ng / μl with sterile, molecular biology grade water (to ensure that the DNA would not precipitate upon addition to transfection reagent) and mixed via gentle pipetting. For every μg of DNA, 3.0 μl of Genejuice transfection reagent (Merck, 70967-3) were required. A sterile epindorf was set up in the flow hood and (100-X) μl of DMEM (without FBS or P/S as they interfere with transfection complex formation) was added. X μl of Genejuice (3.0 μl per μg of DNA) was then carefully added, without touching the sides of the epindorf tube (as plastic inactivates transfection reagents) and mixed via a 3 s vortex, prior to a 5.0 min incubation at RT. Premixed plasmid DNA solution was then added to the tube, mixed carefully by pipetting and incubated for 40 min at RT.

Meanwhile spent DMEM complete was removed from the 96 well plate using a one tip per well rule, to minimize cross well contamination. The total volume of the transfection master mix was then made up to 5.0 μl per well (for example 40 wells requires a total volume of 200 μl) by adding DMEM (without FBS or P/S) to the epindorf tube followed by careful pipette mixing. Diluted transfection mix (5.0 μl) was then added to each well and mixed via a gentle north, south, east, west (NSEW) motion. 96 well plates were incubated at 37 °C with 5.0 % CO_2 for 48 h to allow plasmid

transfection. Spent transfection mix was removed (using a one tip per well rule) and the cell monolayer washed with PBS. Fresh DMEM complete (200 μl per treated well) was supplemented with vehicle alone control (0.50 % DMSO), 5.0 μM PP242, 500 nM rapamycin, 500 μM 4EGi, 35 μM cycloheximide, 1.0 μM thapsigargin or 50 μM cyclic peptide and then added to treated wells in triplicate. Inhibitor dosage was performed over four hours during which 96 well plates were incubated at 37 °C with 5.0 % CO_2. Spent DMEM complete was removed (using a one tip per well rule) and the cell monolayer washed once with PBS (~ 200 μl). Spent PBS was removed and discarded (using a one tip per well rule). Cells were lysed via addition of 20 μl of 1X Passive Lysis Buffer (PLB, Promega, E194, using a one tip per well rule) to each well of the 96 well plate followed by lysis on ice on a rocker for 15 min. 5.0 μl of each well's cell lysate was transferred to an opaque white 96 well plate and quantified on a Glomax multi detection system luminometer (Promega) using a Dual luciferase reporter assay system kit (Promega, E1980). 25 μl of each reagent was used to quantify each well, using a 2 s delay and a 10 s read time.

Data points were corrected for plate background by subtracting readings for wells containing lysed non-transfected cells. The ratio of background corrected Firefly to Renilla luciferase signal is calculated in isolation to correct for differing plasmid transfection efficiencies. The ratios of Fluc to Rluc were averaged over triplicate treatment repeats within each experiment and then normalized to the average of triplicate vehicle alone controls. Triplicate averages from each of three experimental repeats were then averaged and the standard deviation of the repeats determined.

12.6.15 ^{35}S Methionine / Cysteine Incorporation assay

HeLa cells were trypsinized and re-suspended as previously described and counted as above. Cells were appropriately diluted with DMEM complete to yield stock solutions of the required concentrations (80 000 cells / ml). 5.0 ml of this cell stock (400 000 cells) was then plated in a tissue culture treated 6.0 cm dish. The dish was mixed via a gentle north, south, east, west (NSEW) motion (to ensure even cell monolayer) and then incubated at 37 °C with 5.0 % CO_2 24 h to allow cells to adhere to the dish. Spent DMEM complete was removed and the cell monolayer washed once with PBS (~ 10 ml). Fresh DMEM complete (5.0 ml) was supplemented with vehicle alone control (0.50 % DMSO), 5.0 μM PP242, 500 nM rapamycin, 500 μM 4EGi, 35 μM

cycloheximide, 1.0 μM thapsigargin or 50 μM cyclic peptide and then added to the dish prior to incubation at 37 °C with 5.0 % CO_2 for 4 h. All treatments were staggered by exactly 90 s to allow pulse labeling of each dish with ^{35}S Methionine for exactly 30 min. After 3 h 30 min of the 4 h treatment, 3.5 ml of conditioned treated media was removed and mixed with 5.0 μl of ^{35}S Methionine / Cysteine solution (Perkin Elmer, Expre^{35}S^{35}S protein labeling mix, NEG072). The remaining 1.5 ml of conditioned treated media was removed from the dish and discarded. 3.2 ml of conditioned treated media supplemented with ^{35}S Methionine / Cysteine was then returned to the appropriate 6.0 cm dish and incubated at 37 °C with 5.0 % CO_2 for 30 min. Spent media was then removed and the cell monolayer washed with 800 μl PBS. Cell monolayer in PBS was rapidly placed on ice to terminate translation, until all treatments were ready for harvest. Cells were scraped into an epindorf and separated via centrifugation for 5.0 min at 2000 g at 4 °C. The supernatant was discarded and cells were lysed in 100 μl of ice cold MPER (Thermo Scientific, 78505). Insoluble lysate was separated via centrifugation for 15 min at 14000 g at 4 °C.

12.6.16 Scintillation counting procedure for ^{35}S Methionine / Cysteine incorporation assay

5 μl of cell lysate was spotted in triplicate onto filter paper discs (Whatmann, 1001030) and left to dry for 20 min. Protein was precipitated by placing the filter paper discs into 100 ml 10 % TCA (w:v) supplemented with unlabeled L Methionine (5 mM, M5308, Sigma Aldrich) for 20 min. 10 % TCA solution was then discarded and 100 ml 5.0 % TCA added, prior to heating to 90 °C to degrade aminoacyl tRNAs. The solution was then left to cool (15 - 20 min) and the discs were washed with 70 % ethanol and then acetone. Discs were left to dry on Aluminum foil and scintillation vials were prepared in triplicate. One disc was added to each scintillation vial and 1.0 ml scintillation fluid (Fisher Scientific, Scintisafe 2, SC/9195/21) was added to each vial. Radioactive counts per minute were obtained over a three minute period and averaged to give counts per min for each triplicate data point. Cell lysate concentration was determined via Bradford assay and used to correct observed readings per μg of protein.

12.6.17 m^7 GTP resin pull-down

HeLa cells were trypsinized and re-suspended as previously described and counted as above. Cells were appropriately diluted with DMEM complete to yield stock solutions of the required concentrations (100 000 cells / ml). 10 ml of this cell stock (1 000 000 cells) was then plated in a tissue culture treated 10 cm dish. The dish was mixed via a gentle north, south, east, west (NSEW) motion (to ensure even cell monolayer) and then incubated at 37 °C with 5.0 % CO_2 for 24 h to allow cells to adhere to the dish. Spent DMEM complete was removed and the cell monolayer washed once with PBS (~ 10 ml). Fresh DMEM complete (~ 10 ml) was then added to the dish prior to incubation at 37 °C with 5. % CO_2 for 24 h. Compound treatments were performed against either intact cells, or against freshly prepared cell lysate to elucidate the influence of cell permeability on the efficacy of cyclic peptides. Intact cell treatments were performed by incubating cells with fresh DMEM complete media supplemented with vehicle alone control (0.5 % DMSO), rapamycin (500 nM) or cyclic peptides (50 μM) for 4 h. Samples for cell lysate treatment were not treated at this stage and were therefore immediately subjected to cell lysis via the following procedure.

To prevent degradation of protein in the lysate, all steps from cell lysis (including pre-equilibration of resin) up to making SDS-PAGE samples in SDS-PAGE loading buffer, were performed in a cold room ON THE SAME DAY. The resin and samples were EXTREMELY sensitive to heat and degraded rapidly even upon touching with gloved hands, so handling was minimized. The pull-down was performed as rapidly as possible and with pre chilled tubes, reagents, containers and pipettes/tips. All items used for the pull-down were pre-chilled in a cold room for 16 h. Whenever a sample was vortexed, a continuous vortex was used to minimize friction between the sample and the vortex.

Either m^7 GTP agarose (Jena Bioscience, AC-155) or m^7 GTP sepharose (GE healthcare, discontinued) was vortexed (in a cold room) to re-suspend beads and 30 μl was removed into a pre-chilled epindorf tube with a wide bore pipette tip. Beads in 20 % EtOH / H_2O were washed (no more than 30 min prior to cell lysis) twice with 300 μl of PBS. Resin was isolated via centrifugation at 10000 g for 2.0 min at 4 °C (in a pre chilled centrifuge) and the washings discarded.

Spent DMEM complete was removed from the 10 cm dish and the cell monolayer washed once with 10 ml PBS. 400 μl of MPER (Thermo Scientific: 78505) supplemented with 1.0 % Halt protease and phosphatase inhibitor cocktail (Life technologies: 78440) was added to each dish. Dishes were agitated on a rocker (in a cold room) on ice for 10 min. Cells were detached on ice (covered with foil, helps to prevent ice contaminating the lysate) using a cell scraper and transferred to a sterile epindorf. Cell lysis was completed via a 10 s continuous vortex. Soluble lysate was separated by centrifugation at 14000 g for 10 min at 4 °C and transferred to a separate epindorf via pipetting. Lysate concentration was determined via Bradford assay at 630 nm against a background wavelength of 405 nm.

Cell lysate treatments were performed by incubating soluble cell lysate in MPER with vehicle alone control (0.5 % DMSO) or cyclic peptides (50 μM) for 4 h. Samples derived from compound treatment of whole cells were not treated at this stage and were loaded to m^7 GTP affinity resin as follows. ~ 1000 μg of vehicle alone or compound treated cell lysate in MPER was added to m^7 GTP sepharose resin. A 100 μl sample of each cell lysate was removed and added to 100 μl of 2X SDS-PAGE loading buffer (**Table 9:** 900 μl of loading buffer + 100 μl of BME), vortexed and kept on ice. Cell lysate (~ 1000 μg) and m^7 GTP affinity resin (30 μl) were packed tightly into a falcon tube and agitated end over end at 4 °C (in a cold room) for 30 min. Samples were then spun down in a pre chilled centrifuge at 10000 g for 2.0 min at 4 °C. 100 μl of each supernatant (resin flow through containing unbound protein) was then removed and added to 100 μl of 2X SDS-PAGE loading buffer (**Table 9:** 900 μl of loading buffer + 100 μl of BME), vortexed and kept on ice. The remaining supernatant was removed to a separate epindorf and kept on ice. Beads were then washed with 300 μl of PBS three times (add PBS, vortex 3s, centrifuge at 10000 g for 2.0 min at 4 °C, then pipette off supernatant). The remaining beads were re-suspended in 80 μl of 2X SDS-PAGE loading buffer (**Table 9:** 900 μl of loading buffer + 100 μl of BME), vortexed and heated to 70 °C for 5.0 min. Beads were then isolated via centrifugation at 11000 g for 5.0 min at 4 °C. Crude cell lysate, resin unbound protein, resin wash and thermally eluted protein samples were frozen at -20 °C until needed.

12.6.18 Western blotting of m7 GTP pull-down experiments [446]

A 10 % (probed for eIF4G, PABP, eIF4A and eIF4E) and a 12 % (to blot for eIF4G, PABP, eIF4A and 4EBPs) SDS-PAGE were assembled (**Table 11**, **Table 12**). 15 μl of each sample was loaded to each gel lane and the SDS - PAGE gels were run at 120 V for 75 - 90 min to separate proteins in a mini protean tetra cell (Bio Rad: 165-8000). Transfer of proteins to nitrocellulose membranes was achieved using a mini trans-blot electrophoretic transfer cell (Bio-Rad: 170-3930) in combination with transfer buffer (made via 1 / 10 dilution of 10 X transfer buffer, Bio Rad: 161-0732, as per the manufacturers instructions, with 20 % MeOH added). Blotting card, nitro-cellulose transfer membrane and transfer sponges were soaked in transfer buffer at RT for 15 min prior to use. Transfer of the 10 % SDS-PAGE to 0.45 μm nitrocellulose membrane (Bio rad: 162-0115) and the 12 % gel to 0.20 μm Whatman Protran nitrocellulose (GE healthcare: 10401396) was achieved at constant current (250 mA) at 100 V for 60 min. The tank contained an ice pack and was submerged in an ice bucket during transfer to dissipate excess heat generated upon electrophoretic transfer. Membranes were blocked with 3.0 % BSA / TBST for 1 h at RT on a rocker. Blocking solution was then discarded and the membranes were exposed to primary antibodies at appropriate dilutions in 3.0 % BSA / TBST at 4 °C for 16 h (**Table 19**). Membranes were washed with 3 x 10 ml, 10 min TBST at RT on a rocker. Secondary antibodies directly conjugated to fluorophores (Anti Rabbit, Dylight, 800 nm, Thermo Scientific: SA5-10036) were prepared at 1 / 15000 dilution in 15 ml 3.0 % BSA / TBST per membrane. Membranes were exposed to secondary antibodies in opaque black boxes (to prevent photobleaching) for 1 h at RT on a rocker. Membrane segments were then washed with 1 x TBST, 10 ml, 1.0 min followed by 1 x TBST, 10 ml, 5.0 min. Then traces of Tween were removed by washing membrane segments with 1 x PBS, 10 ml, 5.0 min, prior to imaging on an Odyssey scanner (Li-cor).

Antibodies	Species raised within	Primary or secondary antibody	Company	Dilution (v:v) factor in 3 % BSA / TBST
Anti eIF4G1, 'Edith'	Rabbit	Primary	In house	1 / 1000
Anti PABP, 'Red 2'	Rabbit	Primary	In house	1 / 2500
Anti eIF4A, 'BLOO4A'	Rabbit	Primary	In house	1 / 5000
Anti eIF4E, 'Xavier'	Rabbit	Primary	In house	1 / 2000
Anti 4EBP, '♯9644-5, 53H11'	Rabbit	Primary	Cell signaling	1 / 1000
Dylight 800nm, 'SA5-10036'	Goat (anti Rabbit IgG)	Secondary	Thermo Scientific	1 / 15000

Table 19: Dilutions of antibodies used during m^7 GTP pull-down experiments. In house antibodies were kindly provided by Dr. S. J. Morley, University of Sussex.

13 Peptide characterization

13.1 Characterization methodology and instrumentation

13.1.1 Analytical RP-HPLC

Peptides were dissolved in TFA / water prior to analytical RP-HPLC. RP-HPLC utilized a binary solvent system consisting of solution A (0.1 %TFA/water) and B (0.1 % TFA/ MeCN). Peptides were analyzed using a Atlantis T3, amide capped C18, 5 um, 6 x100 mm column (Waters) at a flow rate of 1.0 ml/min. The analytical program utilized a gradient from 5-95 % solution B over 30 min. Elution was monitored at 220 (peptide backbone) and 280 nm (aromatic amino acids, Trp and Tyr). Analytical RP-HPLC data is reported as column retention time (t_R) / min, quoted as a range of peak width at half height.

13.1.2 ESI$^+$ MS

Spectra were recorded on an Acquity UPLC H-class system (Waters) coupled to a triple quadrupole mass spectrometer as solutions in HPLC grade MeOH. MS data is reported as mass to charge ratio (m/z) / Dalton (Da, assignment, expected m/z / Da).

13.1.3 UV-vis spectroscopy

Spectra were recorded on a Cary 100 Bio spectrophotometer (Varian) as solutions in HPLC grade MeOH against a MeOH blank. MeOH solutions were scanned from 800 to 200nm to identify unique absorptions due to specific amino acids. Spectra were collected and analyzed using Cary Win UV-Scan software. UV-vis data is reported as λ_{max} / nm (assignment).

13.1.4 IR spectroscopy

Spectra were recorded on a golden gate Nicolet 380 FT-IR system (Thermo scientific) as solid powders. A 32 scan program from 4000 to 400 cm^{-1} was used to identify bond stretches and bends in peptide samples, measured against a 32 scan background. Spectra were collected and analyzed using OMNIC software. IR data is reported as wavenumber (ν) / cm^{-1} (assignment).

13.1.5 NMR spectroscopy

^{1}H 1D, ^{1}H COSY and ^{1}H TOCSY spectra were recorded on a Bruker 600 MHz spectrometer in d^{6} DMSO by Dr. Stewart Findlow. Spectra were analyzed using ACD labs software, ACD Spectrus Processor, normalized to 2.50 ppm (DMSO) and the ^{1}H NMR spectra assigned from COSY and TOCSY coupling patterns. NMR data is reported as chemical shift (δ) / ppm (Integral, multiplicity, coupling constant / Hz, assignment).

13.2 Characterization of peptides

13.2.1 AEG001: H_2N-VYVVC(StBu)RRQ-CO_2H

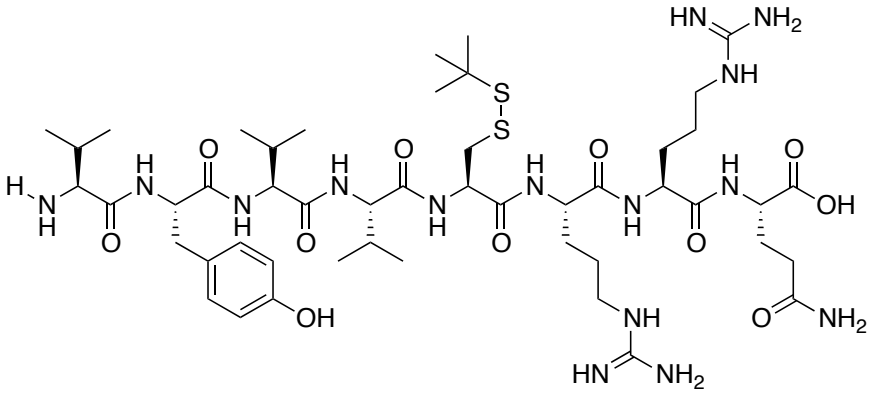

Peptide was cleaved from the resin and purified via preparative RP-HPLC as described above. Purified fractions were frozen at -80 °C and lyophilized to give a white powder (343 mg, 62 %). Analytical RP-HPLC retention time (t_R) = 14.1 - 14.5 min. m/z (ESI^+): 1110.9 ($[M+H]^+$, 1110.4), 556.0 ($[M+2H]^{2+}$, 556.2), 371.0 ($[M+3H]^{3+}$, 371.1). λ_{max} / nm, 274 (Tyrosine π-π*). ν / cm^{-1}, 3270.5 (Amine N-H stretch), 1625.1 (Amide C=O stretch), 1515.5 (Aromatic C=C bend). δ / ppm (600 MHz, d^6 DMSO), 8.45 (1H, d, 8.24 Hz, Cys / Tyr amide), 8.25 (2H, br d, 6.71 Hz, Gln amide, Cys / Tyr amide), 8.17 (1H, br d, 8.54 Hz, Val amide), 8.04 (2H, br d, 4.58 Hz, Arg amide x 2), 7.98 (1H, br s, Arg η C=N-H), 7.97 (1H, br s, Arg η C=N-H), 7.88 (1H, br d, 8.85 Hz, Val amide), 7.57 (1H, t, 5.38 Hz, 5.38 Hz, Arg ε N-H), 7.53 (1H, t, 5.38 Hz, 5.38 Hz, Arg ε N-H), 7.28 (2H, br s, Gln δ amide), 7.06 (2H, d, 8.24 Hz, Tyr ortho Ar-H x 2), 6.84 (1H, br s, Gln δ amide), 6.63 (2H, d, 8.24 Hz, Tyr meta Ar-H x 2), 4.63 (1H, ddd, 8.54 Hz, 8.54 Hz, 4.88 Hz, Cys / Tyr α C-H), 4.53 (1H, ddd, 8.24 Hz, 8.24 Hz, 5.49 Hz, Cys / Tyr α C-H), 4.28 (2H, m, Arg α C-H x 2), 4.24 (1H, dd, 8.54 Hz, 7.63 Hz, Val α C-H), 4.20 (1H, dd, 9.16 Hz, 8.20 Hz, Val α C-H), 4.14 (1H, ddd, 7.60 Hz, 7.60 Hz, 5.80 Hz, Gln α C-H), 3.06 (5H, m, Cys / Tyr β C-H, Arg δ C-H x 4), 2.90 (1H, dd, 13.73 Hz, 8.85 Hz, Cys / Tyr β C-H), 2.85 (1H, dd, 14.65 Hz, 3.97 Hz, Cys / Tyr β C-H), 2.68 (1H, dd, 14.04 Hz, 9.77 Hz, Cys / Tyr β C-H), 2.12 (3H, m, Gln γ C-H x 2, N terminal Val β C-H), 1.94 (3H, m, Val β C-H x 2, Gln β C-H), 1.79 (1H, m, Gln β C-H), 1.66 (2H, m, Arg β C-H x 2), 1.49 (6H, m, Arg β C-H x 2, Arg γ C-H x 4), 1.27 (9H, s, Cys $C(CH_3)_3$), 0.93 (3H, d, 6.71 Hz, N terminal Val γ CH_3), 0.84 (15H, m, N terminal Val γ CH_3, Val γ CH_3 x 4).

13.2.2 AEG002: H_2N-VYVHC(StBu)RRQ-CO_2H

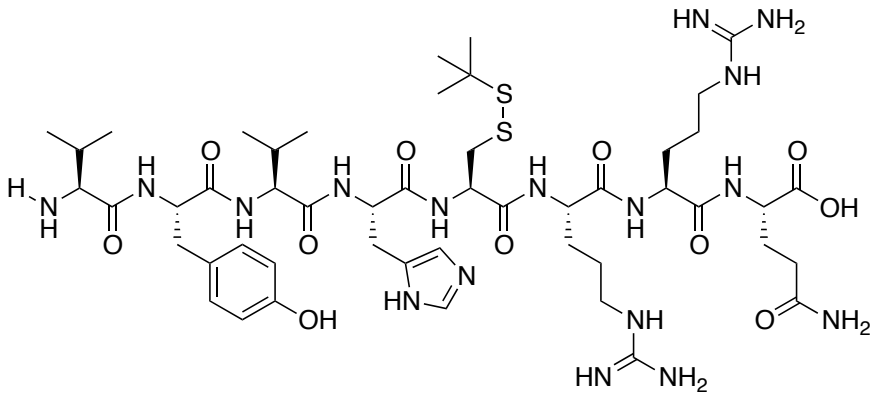

Peptide was cleaved from the resin and purified via preparative RP-HPLC as described above. Purified fractions were frozen at -80 °C and lyophilized to give a white powder (149 mg, 26 %). Analytical RP-HPLC retention time (t_R) = 12.2 - 12.9 min. m/z (ESI^+): 575.1 ($[M+2H]^{2+}$, 575.2), 383.6 ($[M+3H]^{3+}$, 383.6), 288.0 ($[M+4H]^{4+}$, 288.1). λ_{max} / nm, 277 (Tyrosine π-π*). ν / cm^{-1}, 3279.1 (Amine N-H stretch), 1632.9 (Amide C=O stretch), 1515.9 (Aromatic C=C bend). δ / ppm (600 MHz, d^6 DMSO), 9.24 (1H, br s, His δ N-H), 8.93 (1H, br s, His ε N=C-H), 8.43 (1H, d, 7.93 Hz, Cys / His / Tyr amide), 8.31 (1H, m, Cys / His / Tyr amide), 8.26 (1H, d, 7.32 Hz, Gln amide), 8.23 (1H, d, 7.63 Hz, Cys / His / Tyr amide), 8.19 (1H, br d, 8.24 Hz, Val amide), 8.01 (2H, br d, 7.63 Hz, Arg amide x 2), 7.97 (2H, br s, Arg η C=N-H x 2), 7.61 (2H, m, Arg ε N-H x 2), 7.30 (3H, m, Gln δ amide, Cys / His / Tyr amide, His δ C=C-H), 7.08 (2H, d, 8.24 Hz, Tyr ortho Ar-H x 2), 6.84 (1H, br s, Gln δ amide), 6.64 (2H, d, 8.24 Hz, Tyr meta Ar-H x 2), 4.70 (1H, ddd, 8.54 Hz, 7.63 Hz, 6.41 Hz, Cys / His / Tyr α C-H), 4.62 (1H, ddd, 13.43 Hz, 5.49 Hz, 3.97 Hz, Cys / His / Tyr α C-H), 4.52 (1H, ddd, 7.63 Hz, 7.63 Hz, 5.49 Hz, Cys / His / Tyr α C-H), 4.28 (2H, ddd, 19.84 Hz, 7.93 Hz, 7.02 Hz, Arg α C-H x 2), 4.15 (1H, ddd, 8.54 Hz, 7.32 Hz, 7.32 Hz, Gln α C-H), 3.08 (6H, m, Cys / His / Tyr β C-H x 2, Arg δ C-H x 4), 2.93 (2H, dd, 14.34 Hz, 8.85 Hz, Cys / His / Tyr β C-H x 2), 2.82 (1H, dd, 14.34 Hz, 3.05 Hz, Cys / His / Tyr β C-H), 2.65 (1H, dd, 14.65 Hz, 10.38 Hz, Cys / His / Tyr β C-H), 2.12 (3H, m, Gln γ C-H x 2, N terminal Val β C-H), 1.94 (2H, dq, 13.77 Hz, 6.9 Hz, 6.9 Hz, 6.9 Hz, Val β C-H, Gln β C-H), 1.79 (1H, m, Gln β C-H), 1.67 (2H, m, Arg β C-H x 2), 1.50 (6H, m, Arg β C-H x 2, Arg γ C-H x 4), 1.27 (9H, s, Cys $C(CH_3)_3$), 0.92 (2H, d, 7.02 Hz, N terminal Val γ C-H x 2), 0.88 (1H, br d, 7.02 Hz, N terminal Val γ C-H), 0.85 (3H, d, 6.71 Hz, N terminal Val γ CH_3), 0.81 (6H, br d, 5.49 Hz, Val γ CH_3 x 2).

13.2.3 AEG003: H_2N-IHRYC(StBu)RRQ-CO_2H

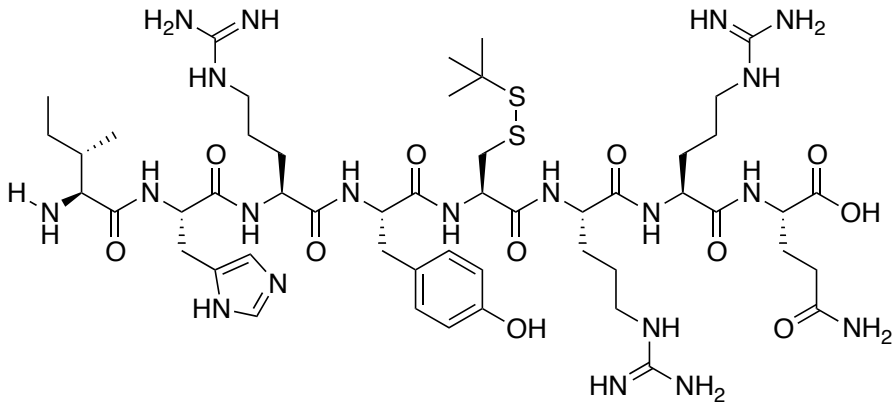

Peptide was cleaved from the resin and purified via preparative RP-HPLC as described above. Purified fractions were frozen at -80 °C and lyophilized to give a white powder (334 mg, 55 %). Analytical RP-HPLC retention time (t_R) = 12.5 - 12.8 min. m/z (ESI^+): 610.5 ($[M+2H]^{2+}$, 610.8), 407.3 ($[M+3H]^{3+}$, 407.5), 305.8 ($[M+4H]^{4+}$, 305.9). λ_{max} / nm, 274 (Tyrosine π-π*). ν / cm^{-1}, 3279.8 (Amine N-H stretch), 1621.8 (Amide C=O stretch), 1515.5 (Aromatic C=C bend). δ / ppm (600 MHz, d^6 DMSO), 9.21 (1H, br s, His δ N-H), 8.95 (1H, br s, His ε N=C-H), 8.70 (1H, d, 7.93 Hz, Cys / His / Tyr amide), 8.42 (1H, br d, 7.94 Hz, Cys / His / Tyr amide), 8.27 (1H, br d, 7.02 Hz, Gln amide), 8.22 (1H, d, 7.32 Hz, Arg amide), 8.15 (1H, d, 7.63 Hz, Arg amide), 8.10 (3H, m, Arg η C=N-H x 3), 8.05 (1H, d, 7.32 Hz, Arg amide), 7.66 (1H, br t, 5.19 Hz, 5.19 Hz, Arg ε N-H), 7.62 (2H, m, Arg ε N-H x 2), 7.29 (3H, m, Gln δ amide, Cys / His / Tyr amide, His δ C=C-H), 7.01 (2H, d, 8.24 Hz, Tyr ortho Ar-H x 2), 6.84 (1H, br s, Gln δ amide), 6.60 (2H, d, 8.24 Hz, Tyr meta Ar-H x 2), 4.69 (1H, ddd, 7.32 Hz, 7.32 Hz, 6.10 Hz, Cys / His / Tyr α C-H), 4.53 (2H, ddd, 12.51 Hz, 9.77 Hz, 7.93 Hz, Cys / His / Tyr α C-H x 2), 4.29 (3H, m, Arg α C-H x 3), 4.14 (1H, ddd, 8.24 Hz, 7.32 Hz, 6.41 Hz, Gln α C-H), 3.06 (8H, m, Cys / His / Tyr β C-H x 2, Arg δ C-H x 6), 2.94 (3H, m, Cys / His / Tyr β C-H x 3), 2.69 (1H, dd, 14.95 Hz, 9.46 Hz, Cys / His / Tyr β C-H), 2.10 (3H, m, Gln γ C-H x 2), 1.93 (1H, m, Gln β C-H), 1.79 (2H, m, Gln β C-H, N terminal Ile β C-H), 1.67 (3H, m, Arg β C-H x 3), 1.49 (10H, m, Arg β C-H x 3, Arg γ C-H x 6, N terminal Ile γ C-H), 1.27 (9H, s, Cys $C(CH_3)_3$), 1.11 (1H, m, N terminal Ile γ C-H), 0.85 (6H, m, N terminal Ile γ CH_3, N terminal Ile δ CH_3).

13.2.4 AEG004: H_2N-LFLFC(StBu)RRQ-CO_2H

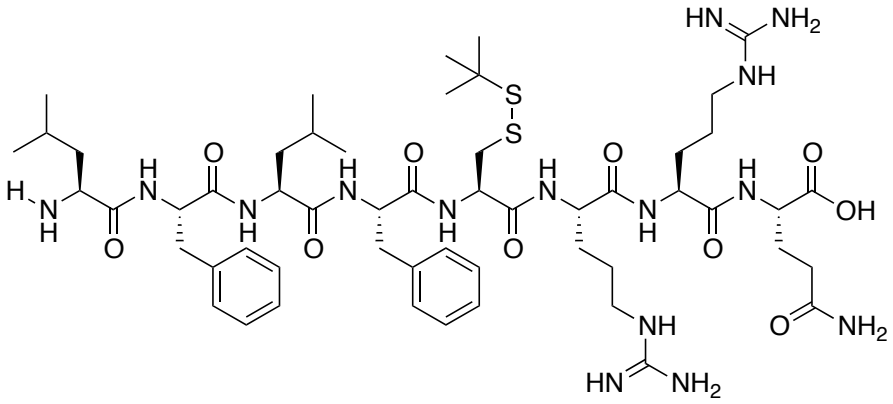

Peptide was cleaved from the resin and purified via preparative RP-HPLC as described above. Purified fractions were frozen at -80 °C and lyophilized to give a white powder (396 mg, 68 %). Analytical RP-HPLC retention time (t_R) = 16.8 - 17.1 min. m/z (ESI^+): 1171.8 ($[M+H]^+$, 1171.5), 586.1 ($[M+2H]^{2+}$, 586.3), 391.0 ($[M+3H]^{3+}$, 391.2) . λ_{max} / nm, 258 (Phenylalanine π-π*). ν / cm^{-1}, 3274.7 (Amine N-H stretch), 1629.0 (Amide C=O stretch), 1527.7 (Aromatic C=C bend). δ / ppm (600 MHz, d^6 DMSO), 8.67 (1H, d, 8.24 Hz, Cys / Phe amide), 8.34 (1H, br d, 7.93 Hz, Cys / Phe amide), 8.26 (1H, br d, 7.02 Hz, Gln amide), 8.20 (1H, br d, 8.24 Hz, Leu amide), 8.12 (1H, br d, 7.93 Hz, Arg amide), 8.02 (4H, m, Arg amide, Cys / Phe amide, Arg η C=N-H x 2), 7.55 (2H, t, 5.49 Hz, 5.49 Hz, Arg ε N-H x 2), 7.28 (1H, br s, Gln δ amide), 7.22 (10H, m, Phe Ar-H x 10), 6.84 (2H, br s, Gln δ amide), 4.60 (2H, m, Cys / Phe α C-H x 2), 4.53 (1H, ddd, 8.20 Hz, 5.20 Hz, 5.20 Hz, Cys / Phe α C-H), 4.30 (3H, m, Arg α C-H x 2, Leu α C-H,), 4.14 (1H, ddd, 8.24 Hz, 7.32 Hz, 6.10 Hz, Gln α C-H), 3.08 (5H, m, Cys / Phe β C-H, Arg δ C-H x 4), 3.02 (1H, dd, 14.34 Hz, 4.27 Hz, Cys / Phe β C-H), 2.93 (2H, m, Cys / Phe β C-H x 2), 2.80 (1H, dd, 14.34 Hz, 9.16 Hz, Cys / Phe β C-H), 2.75 (1H, dd, 14.04 Hz, 9.16 Hz, Cys / Phe β C-H), 2.13 (2H, m, Gln γ C-H x 2), 1.94 (1H, m, Gln β C-H), 1.79 (1H, m, Gln β C-H), 1.64 (3H, m, Arg β C-H x 2, Leu β C-H), 1.50 (9H, m, Arg β C-H x 2, Arg γ C-H x 4, Leu β C-H x 3), 1.38 (2H, m, Leu γ C-H x 2), 1.27 (9H, s, Cys $C(CH_3)_3$), 0.86 (9H, m, Leu δ CH_3 x 3), 0.80 (3H, d, 6.41 Hz, Leu δ CH_3,).

13.2.5 AEG005: H_2N-VYVVC(SH)RRQ-CO_2H

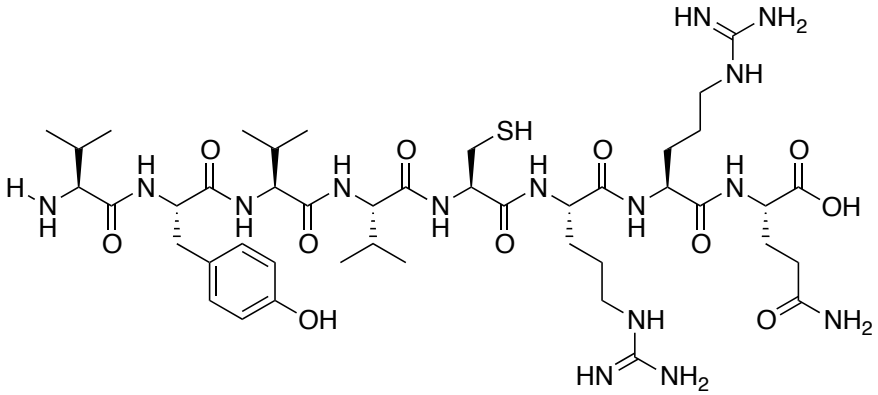

Peptide was prepared from the Cys(StBu) protected precursor via cleavage of the StBu protecting group and subsequent RP-HPLC purification as outlined in experimental procedures. Purified fractions were frozen at -80 °C and lyophilized to give a white powder (27 mg, 54 %). Analytical RP-HPLC retention time (t_R) = 11.7 - 12.0 min. m/z (ESI^+): 511.9 ($[M+2H]^{2+}$, 512.1), 341.7 ($[M+3H]^{3+}$, 341.8) . λ_{max} / nm, 274 (Tyrosine π-π*). ν / cm^{-1}, 3271.5 (Amine N-H stretch), 2965.9 (alkyl C-H stretch), 1632.7 (Amide C=O stretch), 1515.8 (Aromatic C=C bend). δ / ppm (600 MHz, d^6 DMSO), 8.45 (1H, br d, 7.94 Hz, Cys / Tyr amide), 8.26 (1H, br d, 7.02 Hz, Gln amide), 8.18 (1H, br d, 8.85 Hz, Val amide), 8.09 (2H, m, Arg amide, Cys / Tyr amide), 8.05 (1H, d, 7.32 Hz, Arg amide), 7.97 (1H, br s, Arg η C=N-H), 7.96 (1H, br s, Arg η C=N-H), 7.91 (1H, br d, 8.54 Hz, Val amide), 7.53 (2H, m, Arg ε N-H x 2), 7.28 (2H, br s, Gln δ amide), 7.06 (3H, br d, 8.24 Hz, Tyr ortho Ar-H x 2), 6.84 (2H, br s, Gln δ amide), 6.63 (2H, d, 8.24 Hz, Tyr meta Ar-H x 2), 4.63 (1H, ddd, 10.68 Hz, 4.58 Hz, 4.58 Hz, Cys / Tyr α C-H), 4.42 (1H, ddd, 10.38 Hz, 7.32 Hz, 5.80 Hz, Cys / Tyr α C-H), 4.29 (2H, m, Arg α C-H x 2), 4.24 (1H, dd, 8.85 Hz, 7.93 Hz, Val α C-H), 4.18 (1H, dd, 9.16 Hz, 7.93 Hz, Val α C-H), 4.13 (1H, ddd, 7.93 Hz, 7.93 Hz, 5.8 Hz, Gln α C-H), 3.08 (5H, m, Arg δ C-H x 4), 2.85 (1H, dd, 16.48 Hz, 3.97 Hz, Cys / Tyr β C-H), 2.74 (1H, m, Cys / Tyr β C-H), 2.67 (2H, m, Cys / Tyr β C-H), 2.35 (1H, dd, 8.5 Hz, 8.5 Hz, Cys / Tyr β C-H), 2.12 (3H, m, Gln γ C-H x 2, N terminal Val β C-H), 1.94 (3H, m, Val β C-H x 2, Gln β C-H), 1.78 (1H, m, Gln β C-H), 1.67 (2H, m, Arg β C-H x 2), 1.50 (7H, m, Arg β C-H x 2, Arg γ C-H x 4), 0.92 (4H, d, 6.71 Hz, N terminal Val γ CH_3), 0.84 (18H, m, N terminal Val γ CH_3, Val γ CH_3 x 4).

13.2.6 AEG006: H_2N-VYVHC(SH)RRQ-CO_2H

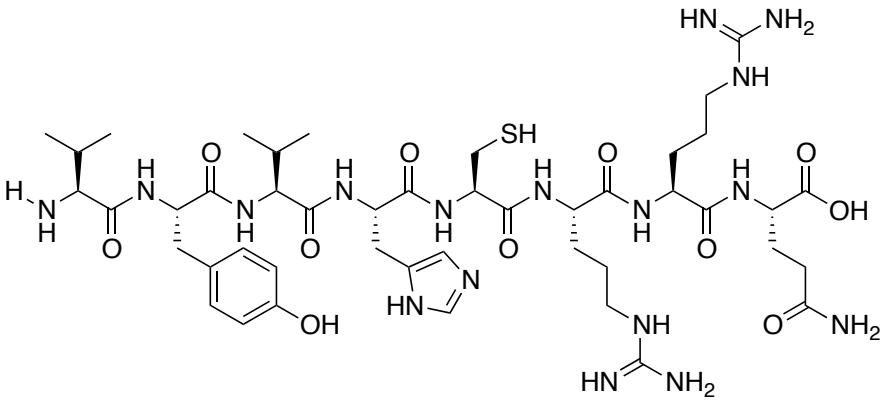

Peptide was prepared from the Cys(StBu) protected precursor via cleavage of the StBu protecting group and subsequent RP-HPLC purification as outlined in experimental procedures. Purified fractions were frozen at -80 °C and lyophilized to give a white powder (38 mg, 77 %). Analytical RP-HPLC retention time (t_R) = 10.6 - 10.8 min. m/z (ESI^+): 531.0 ($[M+2H]^{2+}$, 531.1), 354.2 ($[M+3H]^{3+}$, 354.4), 266.0 ($[M+4H]^{4+}$, 266.1). λ_{max} / nm, 275 (Tyrosine π-π*). ν / cm^{-1}, 3273.6 (Amine N-H stretch), 1629.5 (Amide C=O stretch), 1515.8 (Aromatic C=C bend). δ / ppm (600 MHz, d^6 DMSO), 9.24 (1H, br s, His δ N-H), 8.95 (1H, br s, His ε N=C-H), 8.44 (1H, d, 7.69 Hz, Cys / His / Tyr amide), 8.36 (1H, br d, 7.69 Hz, Cys / His / Tyr amide), 8.30 (1H, d, 7.32 Hz, Arg amide), 8.27 (1H, d, 7.69 Hz, Gln amide), 8.20 (1H, br d, 8.42 Hz, Val amide), 8.06 (1H, br d, 7.32 Hz, Cys / His / Tyr amide), 8.03 (1H, br d, 7.32 Hz, Arg amide), 7.97 (3H, br s, Arg η C=N-H x 2), 7.60 (2H, m, Arg ε N-H x 2), 7.33 (1H, br s, His δ C=C-H), 7.29 (1H, br s, Gln δ amide), 7.08 (2H, d, 8.42 Hz, Tyr ortho Ar-H x 2), 6.85 (2H, br s, Gln δ amide), 6.64 (2H, d, 8.42 Hz, Tyr meta Ar-H x 2), 4.66 (1H, ddd, 10.6 Hz, 6.6 Hz, 6.6 Hz, Cys / His / Tyr α C-H), 4.62 (1H, m, Cys / His / Tyr α C-H), 4.44 (1H, ddd, 9.5 Hz, 6.6 Hz, 6.6 Hz, Cys / His / Tyr α C-H), 4.28 (2H, m, Arg α C-H x 2), 4.15 (2H, m, Gln α C-H, Val α C-H), 3.08 (7H, m, Cys / His / Tyr β C-H, Arg δ C-H x 4), 2.96 (1H, dd, 19.4 Hz, 8.1 Hz, Cys / His / Tyr β C-H), 2.81 (1H, dd, 14.3 Hz, 3.3 Hz, Cys / His / Tyr β C-H), 2.74 (2H, m, Cys / His / Tyr β C-H), 2.64 (1H, dd, 14.7 Hz, 10.3 Hz, Cys / His / Tyr β C-H), 2.36 (1H, dd, 9.5 Hz, 8.4 Hz, Cys / His / Tyr β C-H), 2.12 (3H, m, Gln γ C-H x 2, N terminal Val β C-H), 1.93 (2H, m, Val β C-H, Gln β C-H), 1.79 (1H, m, Gln β C-H), 1.68 (2H, m, Arg β C-H x 2), 1.51 (7H, m, Arg β C-H x 2, Arg γ C-H x 4), 0.92 (4H, d, 6.96 Hz, N terminal Val γ CH_3), 0.85 (4H, d, 6.96 Hz, N terminal Val γ CH_3), 0.82 (3H, d, 6.59 Hz, Val γ CH_3), 0.81 (3H, d, 6.59 Hz, Val γ CH_3),

13.2.7 AEG007: H_2N-IHRYC(SH)RRQ-CO_2H

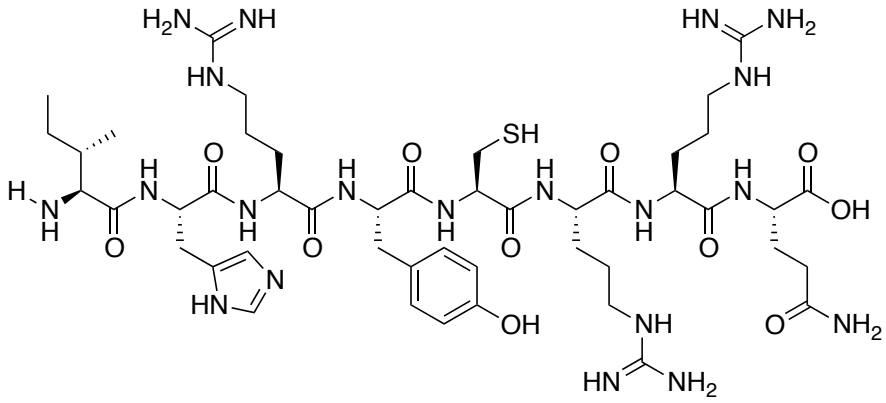

Peptide was prepared from the Cys(StBu) protected precursor via cleavage of the StBu protecting group and subsequent RP-HPLC purification as outlined in experimental procedures. Purified fractions were frozen at -80 °C and lyophilized to give a white powder (27 mg, 58 %). Analytical RP-HPLC retention time (t_R) = 10.6 - 10.9 min. m/z (ESI^+): 566.4 ($[M+2H]^{2+}$, 566.7), 378.0 ($[M+3H]^{3+}$, 378.1), 283.8 ($[M+4H]^{4+}$, 283.8). λ_{max} / nm, 277 (Tyrosine π-π*). ν / cm^{-1}, 3203.0 (Amine N-H stretch), 1633.7 (Amide C=O stretch), 1515.3 (Aromatic C=C bend). δ / ppm (600 MHz, d^6 DMSO), 9.21 (1H, br s, His δ N-H), 8.97 (1H, br s, His ε N=C-H), 8.70 (1H, br d, 7.94 Hz, Cys / His / Tyr amide), 8.27 (1H, d, 7.63 Hz, Gln amide), 8.26 (1H, d, 8.24 Hz, Cys / His / Tyr amide), 8.22 (1H, br d, 7.32 Hz, Arg amide), 8.18 (1H, br d, 7.32 Hz, Arg amide), 8.12 (5H, m, Cys / His / Tyr amide, Arg η C=N-H x 3), 8.06 (1H, br d, 7.32 Hz, Arg amide), 7.65 (1H, br t, 5.19 Hz, 5.19 Hz, Arg ε N-H), 7.60 (2H, br t, 5.49 Hz, 5.49 Hz, Arg ε N-H x 2), 7.29 (3H, s, Gln δ amide, His δ C=C-H), 7.02 (4H, br d, 8.24 Hz, Tyr ortho Ar-H x 2), 6.84 (1H, br s, Gln δ amide), 6.61 (2H, d, 8.24 Hz, Tyr meta Ar-H x 2), 4.69 (1H, ddd, 10.38 Hz, 7.63 Hz, 6.10 Hz, Cys / His / Tyr α C-H), 4.52 (1H, ddd, 10.07 Hz, 7.93 Hz, 4.58 Hz, Cys / His / Tyr α C-H), 4.44 (1H, ddd, 10.1 Hz, 7.0 Hz, 7.0 Hz, Cys / His / Tyr α C-H), 4.28 (4H, m, Arg α C-H x 3), 4.15 (1H, ddd, 10.68 Hz, 7.93 Hz, 6.10 Hz, Gln α C-H), 3.07 (10H, m, Cys / His / Tyr β C-H, Arg δ C-H x 6), 2.96 (1H, dd, 15.26 Hz, 7.63 Hz, Cys / His / Tyr β C-H), 2.90 (1H, dd, 14.95 Hz, 3.97 Hz, Cys / His / Tyr β C-H), 2.72 (4H, m, Cys / His / Tyr β C-H x 2), 2.35 (1H, dd, 8.5 Hz, 8.5 Hz, Cys / His / Tyr β C-H), 2.12 (2H, m, Gln γ C-H x 2), 1.93 (1H, m, Gln β C-H), 1.79 (2H, m, Gln β C-H, N terminal Ile β C-H), 1.67 (4H, m, Arg β C-H x 3), 1.47 (13H, m, Arg β C-H x 3, Arg γ C-H x 6, N terminal Ile γ C-H), 1.11 (1H, m, N terminal Ile γ C-H), 0.86 (4H, d, 6.71 Hz, N terminal Ile γ CH_3), 0.83 (4H, dd, 7.32 Hz, 7.32 Hz, N terminal Ile δ CH_3).

13.2.8 AEG008: H_2N-LFLFC(SH)RRQ-CO_2H

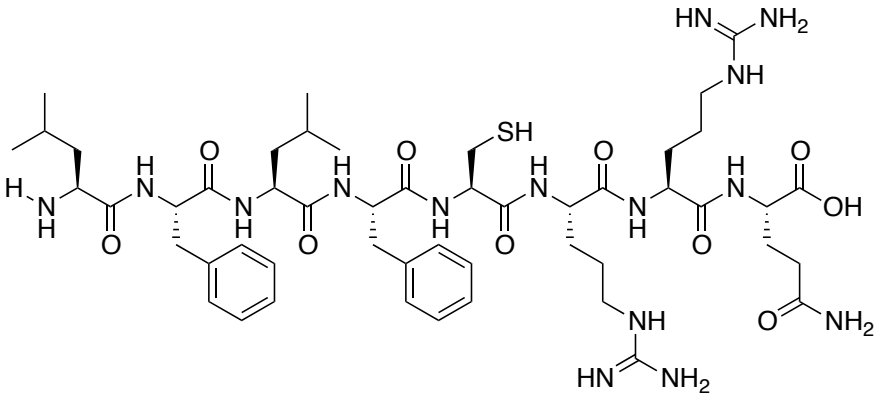

Peptide was prepared from the Cys(StBu) protected precursor via cleavage of the StBu protecting group and subsequent RP-HPLC purification as outlined in experimental procedures. Purified fractions were frozen at -80 °C and lyophilized to give a white powder (16 mg, 16 %). Analytical RP-HPLC retention time (t_R) = 15.2 - 15.6 min. m/z (ESI^+): 542.0 ($[M+2H]^{2+}$, 542.2), 361.7 ($[M+3H]^{3+}$, 361.8) . λ_{max} / nm, 257 (Phenylalanine π-π*). ν / cm^{-1}, 3269.9 (Amine N-H stretch), 2956.5 (alkyl C-H stretch), 1626.1 (Amide C=O stretch), 1537.7 (Aromatic C=C bend). δ / ppm (600 MHz, d^6 DMSO), 8.67 (1H, d, 8.24 Hz, Cys / Phe amide), 8.26 (1H, br d, 5.49 Hz, Gln amide), 8.21 (1H, d, 8.24 Hz, Leu amide), 8.19 (1H, d, 7.93 Hz, Cys / Phe amide), 8.16 (1H, br d, 7.63 Hz, Arg amide), 8.07 (1H, br d, 7.32 Hz, Arg amide), 8.02 (5H, m, Cys / Phe amide, Arg η C=N-H x 2), 7.54 (2H, t, 5.49 Hz, 5.49 Hz, Arg ε N-H x 2), 7.28 (2H, br s, Gln δ amide), 7.24 (10H, m, Phe Ar-H x 10), 6.84 (2H, br s, Gln δ amide), 4.60 (2H, m, Cys / Phe α C-H x 2), 4.44 (1H, ddd, 7.93 Hz, 7.02 Hz, 6.10 Hz, Cys / Phe α C-H), 4.30 (4H, m, Arg α C-H x 2, Leu α C-H), 4.14 (1H, ddd, 10.40 Hz, 7.0 Hz, 7.0 Hz, Gln α C-H), 3.09 (5H, m, Arg δ C-H x 4), 3.02 (1H, dd, 14.19 Hz, 4.12 Hz, Cys / Phe β C-H), 2.94 (1H, dd, 14.19 Hz, 4.12 Hz, Cys / Phe β C-H), 2.81 (1H, dd, 18.92 Hz, 9.46 Hz, Cys / Phe β C-H), 2.73 (3H, m, Cys / Phe β C-H x 2), 2.35 (1H, dd, 8.5 Hz, 8.5 Hz, Cys / Phe β C-H), 2.13 (2H, m, Gln γ C-H x 2), 1.93 (1H, m, Gln β C-H), 1.79 (1H, m, Gln β C-H), 1.68 (2H, m, Arg β C-H x 2), 1.51 (11H, m, Arg β C-H x 2, Arg γ C-H x 4, Leu β C-H x 4), 1.37 (2H, m, Leu γ C-H x 2), 0.86 (12H, m, Leu δ CH_3 x 3), 0.80 (4H, d, 6.41 Hz, Leu δ CH_3).

13.2.9 AEG009: Cyclo VYVVC(SH)RRQ

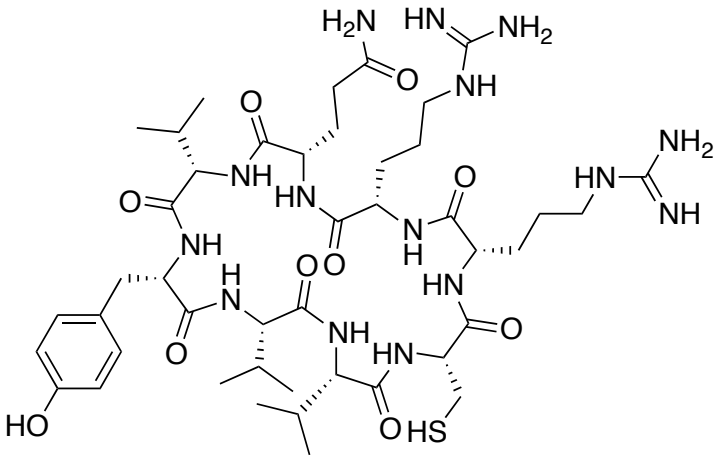

Peptide was cyclized in solution, and then the Cys(StBu) protecting group was removed as outlined in experimental procedures. Peptide was purified via RP-HPLC, then purified fractions were frozen at -80 °C and lyophilized to give a white powder (40 mg, 22 %). Analytical RP-HPLC retention time (t_R) = 13.0 - 13.4 min. m/z (ESI^+): 1004.6 ($[M+H]^+$, 1005.2), 502.9 ($[M+2H]^{2+}$, 503.1). λ_{max} / nm, 278 (Tyrosine π-π*). ν / cm^{-1}, 3294.6 (Amine N-H stretch), 2971.4 (alkyl C-H stretch), 1651.1 (Amide C=O stretch), 1515.3 (Aromatic C=C bend). δ / ppm (600 MHz, d^6 DMSO), 7.53 (1H, br t, 5.34 Hz, 5.34 Hz, Arg ε N-H), 7.47 (1H, t, 4.90 Hz, 4.90 Hz, Arg ε N-H), 7.35 (2H, br s, Gln δ amide), 6.97 (3H, br d, 8.54 Hz, Tyr ortho Ar-H x 2), 6.89 (1H, br s, Gln δ amide), 6.63 (2H, d, 8.54 Hz, Tyr meta Ar-H x 2), 3.08 (5H, m, Arg δ C-H x 4), 3.01 (2H, m, Cys / Tyr β C-H x 2), 2.15 (2H, m, Gln γ C-H x 2), 1.98 (4H, m, Val β C-H x 3, Gln β C-H), 1.79 (2H, m, Gln β C-H), 1.62 (2H, m, Arg β C-H x 2), 1.45 (5H, m, Arg β C-H x 2, Arg γ C-H x 4), 0.97 (3H, d, 6.71 Hz, Val γ CH_3), 0.95 (3H, d, 6.71 Hz, Val γ CH_3), 0.89 (3H, br d, 6.41 Hz, Val γ CH_3), 0.82 (4H, br d, 6.41 Hz, Val γ CH_3), 0.75 (3H, d, 6.71 Hz, Val γ CH_3), 0.68 (2H, br d, 6.10 Hz, Val γ CH_3).

13.2.10 AEG010: Cyclo VYVHC(SH)RRQ

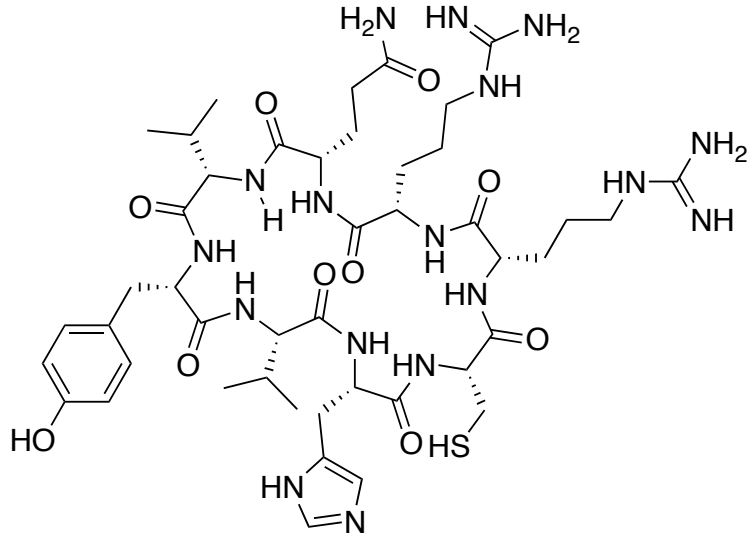

Peptide was cyclized on resin, then cleaved from the resin and purified via RP-HPLC as outlined in experimental procedures. Purified fractions were frozen at -80 °C and lyophilized to give a white powder (20 mg, 8 %). Analytical RP-HPLC retention time (t_R) = 13.2 - 13.9 min. m/z (ESI$^+$): 521.9 ([M+2H]$^{2+}$, 522.1), 348.2 ([M+3H]$^{3+}$, 348.4). λ_{max} / nm, 277 (Tyrosine π-π*). ν / cm^{-1}, 3271.9 (Amine N-H stretch), 1651.3 (Amide C=O stretch), 1515.6 (Aromatic C=C bend). δ / ppm (600 MHz, d^6 DMSO), 9.20 (1H, br s, His δ N-H), 8.98 (1H, br s, His ε N=C-H), 7.61 (4H, m, Arg ε N-H x 2), 7.39 (4H, m, Gln δ amide, His δ C=C-H), 7.04 (2H, br d, 8.42 Hz, Tyr ortho Ar-H x 2), 6.93 (1H, br s, Gln δ amide), 6.65 (2H, br d, 8.42 Hz, Tyr meta Ar-H x 2), 3.08 (9H, m, Cys / His / Tyr β C-H x 3, Arg δ C-H x 4), 2.17 (3H, m, Gln γ C-H x 2), 2.01 (1H, m, Val β C-H), 1.89 (3H, m, Val β C-H, Gln β C-H), 1.74 (3H, m, Gln β C-H), 1.62 (2H, m, Arg β C-H x 2), 1.48 (8H, m, Arg β C-H x 2, Arg γ C-H x 4), 0.80 (7H, m, Val γ CH_3 x 2), 0.73 (4H, d, 7.32 Hz, Val γ CH_3). 0.71 (4H, d, 6.59 Hz, Val γ CH_3).

13.2.11 AEG011: Cyclo IHRYC(SH)RRQ

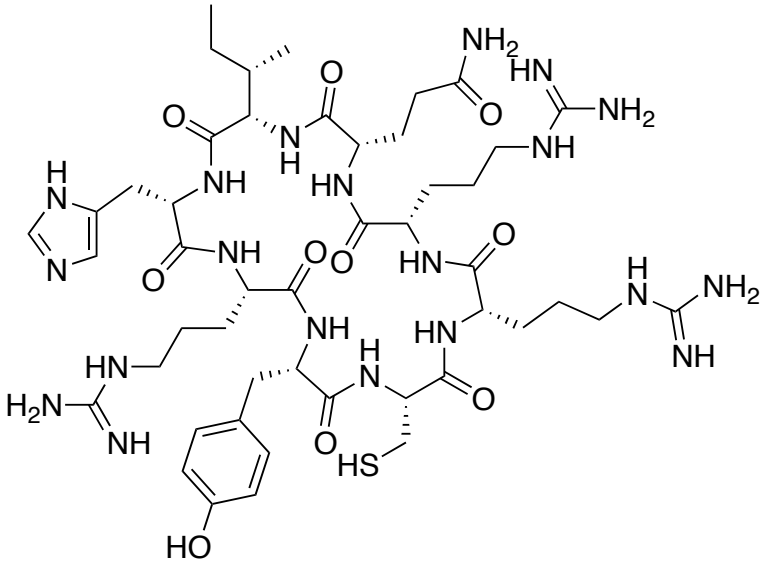

Peptide was cyclized on resin, then cleaved from the resin and purified via RP-HPLC as outlined in experimental procedures. Purified fractions were frozen at -80 °C and lyophilized to give a white powder (30 mg, 11%). Analytical RP-HPLC retention time (t_R) = 11.4 - 11.8 min. m/z (ESI$^+$): 557.4 ([M+2H]$^{2+}$, 557.7), 371.9 ([M+3H]$^{3+}$, 372.1), 279.2 ([M+4H]$^{4+}$, 279.3). λ_{max} / nm, 277 (Tyrosine π-π*). ν / cm^{-1}, 1651.1 (Amide C=O stretch), 1515.7 (Aromatic C=C bend). δ / ppm (600 MHz, d^6 DMSO), 9.24 (1H, br s, His δ N-H), 8.00 (1H, br s, His ε N=C-H), 7.65 (2H, m, Arg ε N-H), 7.57 (2H, m, Arg ε N-H x 2), 7.38 (2H, m, Gln δ amide, His δ C=C-H), 7.01 (2H, d, 8.42 Hz, Tyr ortho Ar-H x 2), 6.68 (2H, d, 8.42 Hz, Tyr meta Ar-H x 2), 3.06 (11H, m, Arg δ C-H x 6), 2.17 (2H, m, Gln γ C-H x 2), 1.79 (6H, m, Gln β C-H x 2), 1.65 (3H, m, Arg β C-H x 3), 1.47 (11H, m, Arg β C-H x 3, Arg γ C-H x 6), 1.27 (1H, m, Ile γ C-H), 0.76 (4H, dd, 8.42 Hz, 7.32 Hz, Ile δ CH_3), 0.68 (3H, br d, 4.39 Hz, Ile γ CH_3).

13.2.12 AEG012: Cyclo LFLFC(SH)RRQ

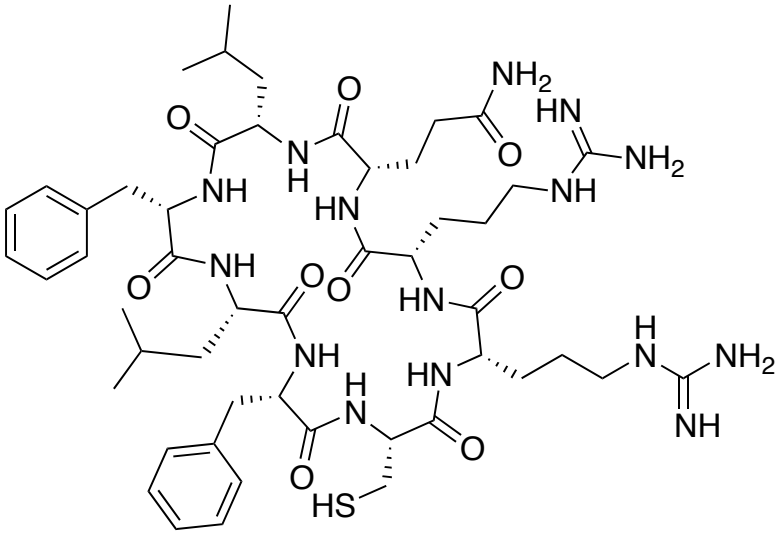

Peptide was cyclized in solution, and then the Cys(StBu) protecting group was removed as outlined in experimental procedures. Peptide was purified via RP-HPLC, then purified fractions were frozen at -80 °C and lyophilized to give a white powder (41 mg, 24 %). Analytical RP-HPLC retention time (t_R) = 17.6 - 18.1 min. m/z (ESI^+): 1064.6 ($[M+H]^+$, 1065.3), 533.0 ($[M+2H]^{2+}$, 533.2). λ_{max} / nm, 258 (Phenylalanine π-π*). ν / cm^{-1}, 3305.5 (Amine N-H stretch), 2960.3 (alkyl C-H stretch), 1650.8 (Amide C=O stretch), 1519.6 (Aromatic C=C bend). δ / ppm (600 MHz, d^6 DMSO), 7.52 (1H, br t, 5.49 Hz, 5.49 Hz, Arg ε N-H), 7.49 (1H, m, Arg ε N-H), 7.37 (1H, br s, Gln δ amide), 7.24 (9H, m, Phe Ar-H x 10), 6.92 (1H, br s, Gln δ amide), 3.07 (4H, m, Arg δ C-H x 4), 2.96 (1H, m, Cys / Phe β C-H), 2.87 (1H, dd, 7.93 Hz, 7.93 Hz, Cys / Phe β C-H), 2.39 (1H, m, Cys / Phe β C-H), 2.15 (2H, m, Gln γ C-H x 2), 1.95 (1H, m, Gln β C-H), 1.79 (2H, m, Gln β C-H), 1.62 (2H, m, Arg β C-H x 2), 1.46 (7H, m, Arg β C-H x 2, Arg γ C-H x 4), 0.81 (7H, m, Leu δ CH_3 x 3), 0.75 (3H, d, 5.49 Hz, Leu δ CH_3).

14 References

1. Scott, D. E., Coyne, A. G., Hudson, S. A., Abell, C., Fragment-based approaches in drug discovery and chemical biology. *Biochemistry,* **2012,** *51* (25), 4990-5003.

2. Lipinski, C. A., Lombardo, F., Dominy, B. W., Feeney, P. J., Experimental and computational approaches to estimate solubility and permeability in drug discovery and development settings. *Adv Drug Deliver Rev,* **1997,** *23* (1-3), 3-25.

3. Lipinski, C. A., Drug-like properties and the causes of poor solubility and poor permeability. *J Pharmacol Toxicol,* **2000,** *44* (1), 235-249.

4. Smith, G. P., Filamentous fusion phage: novel expression vectors that display cloned antigens on the virion surface. *Science,* **1985,** *228* (4705), 1315-1317.

5. Lo Conte, L., Chothia, C., Janin, J., The atomic structure of protein-protein recognition sites. *J Mol Biol,* **1999,** *285* (5), 2177-2198.

6. Moreira, I. S., Fernandes, P. A., Ramos, M. J., Hot spots--a review of the protein-protein interface determinant amino-acid residues. *Proteins,* **2007,** *68* (4), 803-812.

7. Clackson, T., Wells, J. A., A hot spot of binding energy in a hormone-receptor interface. *Science,* **1995,** *267* (5196), 383-386.

8. Thorn, K. S., Bogan, A. A., ASEdb: a database of alanine mutations and their effects on the free energy of binding in protein interactions. *Bioinformatics,* **2001,** *17* (3), 284-285.

9. Bogan, A. A., Thorn, K. S., Anatomy of hot spots in protein interfaces. *J Mol Biol,* **1998,** *280* (1), 1-9.

10. Wells, J. A., McClendon, C. L., Reaching for high-hanging fruit in drug discovery at protein-protein interfaces. *Nature,* **2007,** *450* (7172), 1001-1009.

11. Buchwald, P., Small-molecule protein-protein interaction inhibitors: therapeutic potential in light of molecular size, chemical space, and ligand binding efficiency considerations. *IUBMB life,* **2010,** *62* (10), 724-731.

12. Livnah, O., Stura, E. A., Johnson, D. L., Middleton, S. A., Mulcahy, L. S., Wrighton, N. C., Dower, W. J., Jolliffe, L. K., Wilson, I. A., Functional mimicry of a protein hormone by a peptide agonist: the EPO receptor complex at 2.8 A. *Science,* **1996,** *273* (5274), 464-471.

13. Hanahan, D., Weinberg, R. A., The hallmarks of cancer. *Cell,* **2000,** *100* (1), 57-70.

14. Cencic, R., Hall, D. R., Robert, F., Du, Y., Min, J., Li, L., Qui, M., Lewis, I., Kurtkaya, S., Dingledine, R., Fu, H., Kozakov, D., Vajda, S., Pelletier, J., Reversing chemoresistance by small molecule inhibition of the translation initiation complex eIF4F. *P Natl Acad Sci USA,* **2011,** *108* (3), 1046-1051.

15. Cencic, R., Desforges, M., Hall, D. R., Kozakov, D., Du, Y., Min, J., Dingledine, R., Fu, H., Vajda, S., Talbot, P. J., Pelletier, J., Blocking eIF4E-eIF4G interaction as a strategy to impair coronavirus replication. *J Virol,* **2011,** *85* (13), 6381-6389.

16. Miranda, E., Nordgren, I. K., Male, A. L., Lawrence, C. E., Hoakwie, F., Cuda, F., Court, W., Fox, K. R., Townsend, P. A., Packham, G. K., Eccles, S. A., Tavassoli, A., A cyclic peptide inhibitor of HIF-1 heterodimerization that inhibits hypoxia signaling in cancer cells. *J Am Chem Soc,* **2013,** *135* (28), 10418-10425.

17. Graff, J. R., Konicek, B. W., Vincent, T. M., Lynch, R. L., Monteith, D., Weir, S. N., Schwier, P., Capen, A., Goode, R. L., Dowless, M. S., Chen, Y., Zhang, H., Sissons, S., Cox, K., McNulty, A. M., Parsons, S. H., Wang, T., Sams, L., Geeganage, S., Douglass, L. E., Neubauer, B. L., Dean, N. M., Blanchard, K., Shou, J., Stancato, L. F., Carter, J. H., Marcusson, E. G., Therapeutic suppression of translation initiation factor eIF4E expression reduces tumor growth without toxicity. *J Clin Invest,* **2007,** *117* (9), 2638-2648.

18. Furuichi, Y., Morgan, M., Shatkin, A. J., Jelinek, W., Salditt-Georgieff, M., Darnell, J. E., Methylated, blocked 5 termini in HeLa cell mRNA. *P Natl Acad Sci USA,* **1975,** *72* (5), 1904-1908.

19. Fabrega, C., Hausmann, S., Shen, V., Shuman, S., Lima, C. D., Structure and mechanism of mRNA cap (guanine-N7) methyltransferase. *Mol Cell,* **2004,** *13* (1), 77-89.

20. Bienroth, S., Keller, W., Wahle, E., Assembly of a processive messenger RNA polyadenylation complex. *EMBO J,* **1993,** *12* (2), 585-594.

21. Kapp, L. D., Lorsch, J. R., GTP-dependent recognition of the methionine moiety on initiator tRNA by translation factor eIF2. *J Mol Biol,* **2004,** *335* (4), 923-936.

22. Dettman, G. L., Stanley, W. M., Jr., Recognition of eukaryotic initiator tRNA by an initiation factor and the transfer of the methionine moiety into peptide linkage. *Biochim Biophys Acta,* **1972,** *287* (1), 124-133.

23. Schreier, M. H., Staehelin, T., Initiation of eukaryotic protein synthesis: (Met-tRNA f -40S ribosome) initiation complex catalysed by purified initiation factors in the absence of mRNA. *Nat New Biol,* **1973,** *242* (115), 35-38.

24. Darnbrough, C., Legon, S., Hunt, T., Jackson, R. J., Initiation of protein synthesis: evidence for messenger RNA-independent binding of methionyl-transfer RNA to the 40 S ribosomal subunit. *J Mol Biol,* **1973,** *76* (3), 379-403.

25. Levin, D. H., Kyner, D., Acs, G., Protein initiation in eukaryotes: formation and function of a ternary complex composed of a partially purified ribosomal factor, methionyl transfer RNA, and guanosine triphosphate. *P Natl Acad Sci USA,* **1973,** *70* (1), 41-45.

26. Singh, C. R., He, H., Ii, M., Yamamoto, Y., Asano, K., Efficient incorporation of eukaryotic initiation factor 1 into the multifactor complex is critical for formation of functional ribosomal preinitiation complexes in vivo. *J Biol Chem,* **2004,** *279* (30), 31910-31920.

27. Maag, D., Lorsch, J. R., Communication between eukaryotic translation initiation factors 1 and 1A on the yeast small ribosomal subunit. *J Mol Biol,* **2003,** *330* (5), 917-924.

28. Chaudhuri, J., Si, K., Maitra, U., Function of eukaryotic translation initiation factor 1A (eIF1A) (formerly called eIF-4C) in initiation of protein synthesis. *J Biol Chem,* **1997,** *272* (12), 7883-7891.

29. Pestova, T. V., Kolupaeva, V. G., The roles of individual eukaryotic translation initiation factors in ribosomal scanning and initiation codon selection. *Genes Dev,* **2002,** *16* (22), 2906-2922.

30. Algire, M. A., Maag, D., Savio, P., Acker, M. G., Tarun, S. Z., Jr., Sachs, A. B., Asano, K., Nielsen, K. H., Olsen, D. S., Phan, L., Hinnebusch, A. G., Lorsch, J. R., Development and characterization of a reconstituted yeast translation initiation system. *RNA,* **2002,** *8* (3), 382-397.

31. Majumdar, R., Bandyopadhyay, A., Maitra, U., Mammalian translation initiation factor eIF1 functions with eIF1A and eIF3 in the formation of a stable 40 S preinitiation complex. *J Biol Chem,* **2003,** *278* (8), 6580-6587.

32. Trachsel, H., Erni, B., Schreier, M. H., Staehelin, T., Initiation of mammalian protein synthesis. II. The assembly of the initiation complex with purified initiation factors. *J Mol Biol,* **1977,** *116* (4), 755-767.

33. Pelletier, J., Kaplan, G., Racaniello, V. R., Sonenberg, N., Cap-independent translation of poliovirus mRNA is conferred by sequence elements within the 5' noncoding region. *Mol Cell Biol,* **1988,** *8* (3), 1103-1112.

34. Pelletier, J., Sonenberg, N., Internal initiation of translation of eukaryotic mRNA directed by a sequence derived from poliovirus RNA. *Nature,* **1988,** *334* (6180), 320-325.

35. Hunter, A. R., Jackson, R. J., Hunt, T., The role of complexes between the 40-S ribosomal subunit and Met-tRNA-Met-f in the initiation of protein synthesis in the wheat-germ system. *Eur J Biochem,* **1977,** *75* (1), 159-170.

36. Kozak, M., Nucleotide sequences of 5'-terminal ribosome-protected initiation regions from two reovirus messages. *Nature,* **1977,** *269* (5627), 391-394.

37. Kozak, M., Shatkin, A. J., Migration of 40 S ribosomal subunits on messenger RNA in the presence of edeine. *J Biol Chem,* **1978,** *253* (18), 6568-6577.

38. Kozak, M., Migration of 40 S ribosomal subunits on messenger RNA when initiation is perturbed by lowering magnesium or adding drugs. *J Biol Chem,* **1979,** *254* (11), 4731-4738.

39. Kozak, M., Binding of wheat germ ribosomes to bisulfite-modified reovirus messenger RNA: evidence for a scanning mechanism. *J Mol Biol,* **1980,** *144* (3), 291-304.

40. Kozak, M., Influence of mRNA secondary structure on binding and migration of 40S ribosomal subunits. *Cell,* **1980,** *19* (1), 79-90.

41. Kozak, M., Influences of mRNA secondary structure on initiation by eukaryotic ribosomes. *P Natl Acad Sci USA,* **1986,** *83* (9), 2850-2854.

42. Kozak, M., Compilation and analysis of sequences upstream from the translational start site in eukaryotic mRNAs. *Nucleic Acids Res,* **1984,** *12* (2), 857-872.

43. Kozak, M., An analysis of 5'-noncoding sequences from 699 vertebrate messenger RNAs. *Nucleic Acids Res,* **1987,** *15* (20), 8125-8148.

44. Kozak, M., Circumstances and mechanisms of inhibition of translation by secondary structure in eucaryotic mRNAs. *Mol Cell Biol,* **1989,** *9* (11), 5134-5142.

45. Kevil, C., Carter, P., Hu, B., DeBenedetti, A., Translational enhancement of FGF-2 by eIF-4 factors, and alternate utilization of CUG and AUG codons for translation initiation. *Oncogene,* **1995,** *11* (11), 2339-2348.

46. Nathan, C. O., Carter, P., Liu, L., Li, B. D., Abreo, F., Tudor, A., Zimmer, S. G., De Benedetti, A., Elevated expression of eIF4E and FGF-2 isoforms during vascularization of breast carcinomas. *Oncogene,* **1997,** *15* (9), 1087-1094.

47. Crew, J. P., Fuggle, S., Bicknell, R., Cranston, D. W., de Benedetti, A., Harris, A. L., Eukaryotic initiation factor-4E in superficial and muscle invasive bladder cancer and its correlation with vascular endothelial growth factor expression and tumour progression. *Br J Cancer,* **2000,** *82* (1), 161-166.

48. Kevil, C. G., De Benedetti, A., Payne, D. K., Coe, L. L., Laroux, F. S., Alexander, J. S., Translational regulation of vascular permeability factor by eukaryotic initiation factor 4E: implications for tumor angiogenesis. *Int J Cancer,* **1996,** *65* (6), 785-790.

49. Kozak, M., Possible role of flanking nucleotides in recognition of the AUG initiator codon by eukaryotic ribosomes. *Nucleic Acids Res,* **1981,** *9* (20), 5233-5252.

50. Kozak, M., Point mutations close to the AUG initiator codon affect the efficiency of translation of rat preproinsulin in vivo. *Nature,* **1984,** *308* (5956), 241-246.

51. Kozak, M., Point mutations define a sequence flanking the AUG initiator codon that modulates translation by eukaryotic ribosomes. *Cell,* **1986,** *44* (2), 283-292.

52. Kozak, M., Recognition of AUG and alternative initiator codons is augmented by G in position +4 but is not generally affected by the nucleotides in positions +5 and +6. *EMBO J,* **1997,** *16* (9), 2482-2492.

53. Maag, D., Fekete, C. A., Gryczynski, Z., Lorsch, J. R., A conformational change in the eukaryotic translation preinitiation complex and release of eIF1 signal recognition of the start codon. *Mol Cell,* **2005,** *17* (2), 265-275.

54. Maag, D., Algire, M. A., Lorsch, J. R., Communication between eukaryotic translation initiation factors 5 and 1A within the ribosomal pre-initiation complex plays a role in start site selection. *J Mol Biol,* **2006,** *356* (3), 724-737.

55. Lomakin, I. B., Kolupaeva, V. G., Marintchev, A., Wagner, G., Pestova, T. V., Position of eukaryotic initiation factor eIF1 on the 40S ribosomal subunit determined by directed hydroxyl radical probing. *Genes Dev,* **2003,** *17* (22), 2786-2797.

56. Loughran, G., Sachs, M. S., Atkins, J. F., Ivanov, I. P., Stringency of start codon selection modulates autoregulation of translation initiation factor eIF5. *Nucleic Acids Res,* **2012,** *40* (7), 2898-2906.

57. Pestova, T. V., Borukhov, S. I., Hellen, C. U., Eukaryotic ribosomes require initiation factors 1 and 1A to locate initiation codons. *Nature,* **1998,** *394* (6696), 854-859.

58. Fekete, C. A., Applefield, D. J., Blakely, S. A., Shirokikh, N., Pestova, T., Lorsch, J. R., Hinnebusch, A. G., The eIF1A C-terminal domain promotes initiation complex assembly, scanning and AUG selection in vivo. *EMBO J,* **2005,** *24* (20), 3588-3601.

59. Cheung, Y. N., Maag, D., Mitchell, S. F., Fekete, C. A., Algire, M. A., Takacs, J. E., Shirokikh, N., Pestova, T., Lorsch, J. R., Hinnebusch, A. G., Dissociation of eIF1 from the 40S ribosomal subunit is a key step in start codon selection in vivo. *Genes Dev,* **2007,** *21* (10), 1217-1230.

60. Passmore, L. A., Schmeing, T. M., Maag, D., Applefield, D. J., Acker, M. G., Algire, M. A., Lorsch, J. R., Ramakrishnan, V., The eukaryotic translation initiation factors eIF1 and eIF1A induce an open conformation of the 40S ribosome. *Mol Cell,* **2007,** *26* (1), 41-50.

61. Rabl, J., Leibundgut, M., Ataide, S. F., Haag, A., Ban, N., Crystal structure of the eukaryotic 40S ribosomal subunit in complex with initiation factor 1. *Science,* **2011,** *331* (6018), 730-736.

62. Weisser, M., Voigts-Hoffmann, F., Rabl, J., Leibundgut, M., Ban, N., The crystal structure of the eukaryotic 40S ribosomal subunit in complex with eIF1 and eIF1A. *Nat Struct Mol Biol,* **2013,** *20* (8), 1015-1017.

63. Cigan, A. M., Feng, L., Donahue, T. F., tRNAi(met) functions in directing the scanning ribosome to the start site of translation. *Science,* **1988,** *242* (4875), 93-97.

64. Unbehaun, A., Borukhov, S. I., Hellen, C. U., Pestova, T. V., Release of initiation factors from 48S complexes during ribosomal subunit joining and the link between establishment of codon-anticodon base-pairing and hydrolysis of eIF2-bound GTP. *Genes Dev,* **2004,** *18* (24), 3078-3093.

65. Olsen, D. S., Savner, E. M., Mathew, A., Zhang, F., Krishnamoorthy, T., Phan, L., Hinnebusch, A. G., Domains of eIF1A that mediate binding to eIF2, eIF3 and eIF5B and promote ternary complex recruitment in vivo. *EMBO J,* **2003,** *22* (2), 193-204.

66. Nanda, J. S., Cheung, Y. N., Takacs, J. E., Martin-Marcos, P., Saini, A. K., Hinnebusch, A. G., Lorsch, J. R., eIF1 controls multiple steps in start codon recognition during eukaryotic translation initiation. *J Mol Biol,* **2009,** *394* (2), 268-285.

67. Das, S., Ghosh, R., Maitra, U., Eukaryotic translation initiation factor 5 functions as a GTPase-activating protein. *J Biol Chem,* **2001,** *276* (9), 6720-6726.

68. Das, S., Maitra, U., Functional significance and mechanism of eIF5-promoted GTP hydrolysis in eukaryotic translation initiation. *Prog Nucleic Acid Res Mol Biol,* **2001,** *70* (1), 207-231.

69. Paulin, F. E., Campbell, L. E., O'Brien, K., Loughlin, J., Proud, C. G., Eukaryotic translation initiation factor 5 (eIF5) acts as a classical GTPase-activator protein. *Curr Biol,* **2001,** *11* (1), 55-59.

70. Pestova, T. V., Lomakin, I. B., Lee, J. H., Choi, S. K., Dever, T. E., Hellen, C. U., The joining of ribosomal subunits in eukaryotes requires eIF5B. *Nature,* **2000,** *403* (6767), 332-335.

71. Lee, J. H., Pestova, T. V., Shin, B. S., Cao, C., Choi, S. K., Dever, T. E., Initiation factor eIF5B catalyzes second GTP-dependent step in eukaryotic translation initiation. *P Natl Acad Sci USA,* **2002,** *99* (26), 16689-16694.

72. Acker, M. G., Shin, B. S., Dever, T. E., Lorsch, J. R., Interaction between eukaryotic initiation factors 1A and 5B is required for efficient ribosomal subunit joining. *J Biol Chem,* **2006,** *281* (13), 8469-8475.

73. Fringer, J. M., Acker, M. G., Fekete, C. A., Lorsch, J. R., Dever, T. E., Coupled release of eukaryotic translation initiation factors 5B and 1A from 80S ribosomes following subunit joining. *Mol Cell Biol,* **2007,** *27* (6), 2384-2397.

74. Crick, F. H., Codon--anticodon pairing: the wobble hypothesis. *J Mol Biol,* **1966,** *19* (2), 548-555.

75. Rheinberger, H. J., Sternbach, H., Nierhaus, K. H., Codon-anticodon interaction at the ribosomal E site. *J Biol Chem,* **1986,** *261* (20), 9140-9143.

76. Moon, H. M., Redfield, B., Millard, S., Vane, F., Weissbach, H., Multiple forms of elongation factor 1 from calf brain. *P Natl Acad Sci USA,* **1973,** *70* (12), 3282-3286.

77. Nombela, C., Ochoa, S., Conformational control of the interaction of eukaryotic elongation factors EF-1 and EF-2 with ribosomes. *P Natl Acad Sci USA,* **1973,** *70* (12), 3556-3560.

78. Nolan, R. D., Grasmuk, H., Drews, J., The binding of tritiated elongation factors 1 and 2 to ribosomes from Krebs II mouse ascites tumor cells. *Eur J Biochem,* **1975,** *50* (2), 391-402.

79. Nagata, S., Iwasaki, K., Kaziro, Y., Interaction of the low molecular weight form of elongation factor 1 with guanine nucleotides and aminoacyl-tRNA. *Arch Biochem Biophys,* **1976,** *172* (1), 168-177.

80. Moon, H. M., Redfield, B., Weissbach, H., Interaction of eukaryote elongation factor EF 1 with guanosine nucleotides and aminoacyl-tRNA. *P Natl Acad Sci USA,* **1972,** *69* (5), 1249-1252.

81. Weissbach, H., Redfield, B., Moon, H. M., Further studies on the interactions of elongation factor 1 from animal tissues. *Arch Biochem Biophys,* **1973,** *156* (1), 267-275.

82. Trupin, J. S., Rottman, F. M., Brimacombe, R. L., Leder, P., Bernfield, M. R., Nirenberg, M. W., Rna Codewords and Protein Synthesis, Vi. On the Nucleotide Sequences of Degenerate Codeword Sets for Isoleucine, Tyrosine, Asparagine, and Lysine. *P Natl Acad Sci USA,* **1965,** *53* (4), 807-811.

83. Robertus, J. D., Ladner, J. E., Finch, J. T., Rhodes, D., Brown, R. S., Clark, B. F., Klug, A., Correlation between three-dimensional structure and chemical reactivity of transfer RNA. *Nucleic Acids Res,* **1974,** *1* (7), 927-932.

84. Wettstein, F. O., Noll, H., Binding of Transfer Ribonucleic Acid to Ribosomes Engaged in Protein Synthesis: Number and Properties of Ribosomal Binding Sites. *J Mol Biol,* **1965,** *11* (1), 35-53.

85. Rodnina, M. V., El'skaya, A. V., Semenkov Yu, P., Kirillov, S. V., Number of tRNA binding sites on 80 S ribosomes and their subunits. *FEBS Lett,* **1988,** *231* (1), 71-74.

86. Rheinberger, H. J., Nierhaus, K. H., Testing an alternative model for the ribosomal peptide elongation cycle. *P Natl Acad Sci USA,* **1983,** *80* (14), 4213-4217.

87. Geigenmuller, U., Hausner, T. P., Nierhaus, K. H., Analysis of the puromycin reaction. The ribosomal exclusion principle for AcPhe-tRNA binding re-examined. *Eur J Biochem,* **1986,** *161* (3), 715-721.

88. Rheinberger, H. J., Nierhaus, K. H., Allosteric interactions between the ribosomal transfer RNA-binding sites A and E. *J Biol Chem,* **1986,** *261* (20), 9133-9139.

89. Rheinberger, H. J., Sternbach, H., Nierhaus, K. H., Three tRNA binding sites on Escherichia coli ribosomes. *P Natl Acad Sci USA,* **1981,** *78* (9), 5310-5314.

90. Gnirke, A., Geigenmuller, U., Rheinberger, H. J., Nierhaus, L. H., The allosteric three-site model for the ribosomal elongation cycle. Analysis with a heteropolymeric mRNA. *J Biol Chem,* **1989,** *264* (13), 7291-7301.

91. Nierhaus, K. H., The allosteric three-site model for the ribosomal elongation cycle: features and future. *Biochemistry,* **1990,** *29* (21), 4997-5008.

92. Dever, T. E., Green, R., The elongation, termination, and recycling phases of translation in eukaryotes. *Cold Spring Harb Perspect Biol,* **2012,** *4* (7), a013706.

93. Baliga, B. S., Munro, H. N., Evidence of formation of a complex between GTP and elongation factor two and the binding of the complex to a specific site on mammalian ribosomes. *Biochim Biophys Acta,* **1972,** *277* (2), 368-383.

94. Nygard, O., Nilsson, L., Nucleotide-mediated interactions of eukaryotic elongation factor EF-2 with ribosomes. *Eur J Biochem,* **1984,** *140* (1), 93-96.

95. Skogerson, L., Moldave, K., The binding of aminoacyl transferase II to ribosomes. *Biochem Biophys Res Commun,* **1967,** *27* (5), 568-572.

96. Nygard, O., Nilsson, L., Characterization of the ribosomal properties required for formation of a GTPase active complex with the eukaryotic elongation factor 2. *Eur J Biochem,* **1989,** *179* (3), 603-608.

97. Skogerson, L., Moldave, K., Characterization of the interaction of aminoacyltransferase II with ribosomes. Binding of transferase II and translocation of peptidyl transfer ribonucleic acid. *J Biol Chem,* **1968,** *243* (20), 5354-5360.

98. Nilsson, L., Nygard, O., Affinity labelling of the eukaryotic elongation factor EF-2 with the guanosine nucleotide analogue 5'-p-fluorosulfonylbenzoylguanosine. *Biochim Biophys Acta,* **1984,** *782* (1), 49-54.

99. Mizumoto, K., Iwasaki, K., Kaziro, Y., Studies on polypeptide elongation factor 2 from pig liver. III. Interaction with guanine nucleotides in the presence and absence of ribosomes. *J Biochem,* **1974,** *76* (6), 1269-1280.

100. Henriksen, O., Robinson, E. A., Maxwell, E. S., Interaction of guanosine nucleotides with elongation factor 2. I. Equilibrium dialysis studies. *J Biol Chem,* **1975,** *250* (2), 720-724.

101. Nilsson, L., Nygard, O., The mechanism of the protein-synthesis elongation cycle in eukaryotes. Effect of ricin on the ribosomal interaction with elongation factors. *Eur J Biochem,* **1986,** *161* (1), 111-117.

102. Lill, R., Wintermeyer, W., Destabilization of codon-anticodon interaction in the ribosomal exit site. *J Mol Biol,* **1987,** *196* (1), 137-148.

103. Rheinberger, H. J., Nierhaus, K. H., Adjacent codon-anticodon interactions of both tRNAs present at the ribosomal A and P or P and E sites. *FEBS Lett,* **1986,** *204* (1), 97-99.

104. Goldstein, J. L., Beaudet, A. L., Caskey, C. T., Peptide chain termination with mammalian release factor. *P Natl Acad Sci USA,* **1970,** *67* (1), 99-106.

105. Konecki, D. S., Aune, K. C., Tate, W., Caskey, C. T., Characterization of reticulocyte release factor. *J Biol Chem,* **1977,** *252* (13), 4514-4520.

106. Frolova, L., Le Goff, X., Rasmussen, H. H., Cheperegin, S., Drugeon, G., Kress, M., Arman, I., Haenni, A. L., Celis, J. E., Philippe, M., et al., A highly conserved eukaryotic protein family possessing properties of polypeptide chain release factor. *Nature,* **1994,** *372* (6507), 701-703.

107. Cheng, Z., Saito, K., Pisarev, A. V., Wada, M., Pisareva, V. P., Pestova, T. V., Gajda, M., Round, A., Kong, C., Lim, M., Nakamura, Y., Svergun, D. I., Ito, K., Song, H., Structural insights into eRF3 and stop codon recognition by eRF1. *Genes Dev,* **2009,** *23* (9), 1106-1118.

108. Song, H., Mugnier, P., Das, A. K., Webb, H. M., Evans, D. R., Tuite, M. F., Hemmings, B. A., Barford, D., The crystal structure of human eukaryotic release factor eRF1--mechanism of stop codon recognition and peptidyl-tRNA hydrolysis. *Cell,* **2000,** *100* (3), 311-321.

109. Holley, R. W., Structure of an alanine transfer ribonucleic acid. *JAMA,* **1965,** *194* (8), 868-871.

110. Holley, R. W., Apgar, J., Everett, G. A., Madison, J. T., Marquisee, M., Merrill, S. H., Penswick, J. R., Zamir, A., Structure of a Ribonucleic Acid. *Science,* **1965,** *147* (3664), 1462-1465.

111. Inagaki, Y., Blouin, C., Doolittle, W. F., Roger, A. J., Convergence and constraint in eukaryotic release factor 1 (eRF1) domain 1: the evolution of stop codon specificity. *Nucleic Acids Res,* **2002,** *30* (2), 532-544.

112. Fan-Minogue, H., Du, M., Pisarev, A. V., Kallmeyer, A. K., Salas-Marco, J., Keeling, K. M., Thompson, S. R., Pestova, T. V., Bedwell, D. M., Distinct eRF3 requirements suggest alternate eRF1 conformations mediate peptide release during eukaryotic translation termination. *Mol Cell,* **2008,** *30* (5), 599-609.

113. Chavatte, L., Seit-Nebi, A., Dubovaya, V., Favre, A., The invariant uridine of stop codons contacts the conserved NIKSR loop of human eRF1 in the ribosome. *EMBO J,* **2002,** *21* (19), 5302-5311.

114. Bulygin, K. N., Khairulina, Y. S., Kolosov, P. M., Ven'yaminova, A. G., Graifer, D. M., Vorobjev, Y. N., Frolova, L. Y., Kisselev, L. L., Karpova, G. G., Three

distinct peptides from the N domain of translation termination factor eRF1 surround stop codon in the ribosome. *RNA,* **2010,** *16* (10), 1902-1914.

115. Bertram, G., Bell, H. A., Ritchie, D. W., Fullerton, G., Stansfield, I., Terminating eukaryote translation: domain 1 of release factor eRF1 functions in stop codon recognition. *RNA,* **2000,** *6* (9), 1236-1247.

116. Zhouravleva, G., Frolova, L., Le Goff, X., Le Guellec, R., Inge-Vechtomov, S., Kisselev, L., Philippe, M., Termination of translation in eukaryotes is governed by two interacting polypeptide chain release factors, eRF1 and eRF3. *EMBO J,* **1995,** *14* (16), 4065-4072.

117. Merkulova, T. I., Frolova, L. Y., Lazar, M., Camonis, J., Kisselev, L. L., C-terminal domains of human translation termination factors eRF1 and eRF3 mediate their in vivo interaction. *FEBS Lett,* **1999,** *443* (1), 41-47.

118. Kisselev, L. L., Frolova, L., Termination of translation in eukaryotes. *Biochem Cell Biol,* **1995,** *73* (11-12), 1079-1086.

119. Frolova, L. Y., Tsivkovskii, R. Y., Sivolobova, G. F., Oparina, N. Y., Serpinsky, O. I., Blinov, V. M., Tatkov, S. I., Kisselev, L. L., Mutations in the highly conserved GGQ motif of class 1 polypeptide release factors abolish ability of human eRF1 to trigger peptidyl-tRNA hydrolysis. *RNA,* **1999,** *5* (8), 1014-1020.

120. Alkalaeva, E. Z., Pisarev, A. V., Frolova, L. Y., Kisselev, L. L., Pestova, T. V., In vitro reconstitution of eukaryotic translation reveals cooperativity between release factors eRF1 and eRF3. *Cell,* **2006,** *125* (6), 1125-1136.

121. Frolova, L., Le Goff, X., Zhouravleva, G., Davydova, E., Philippe, M., Kisselev, L., Eukaryotic polypeptide chain release factor eRF3 is an eRF1- and ribosome-dependent guanosine triphosphatase. *RNA,* **1996,** *2* (4), 334-341.

122. Sonenberg, N., Guertin, D., Lee, K. A., Capped mRNAs with reduced secondary structure can function in extracts from poliovirus-infected cells. *Mol Cell Biol,* **1982,** *2* (12), 1633-1638.

123. Svitkin, Y. V., Pause, A., Haghighat, A., Pyronnet, S., Witherell, G., Belsham, G. J., Sonenberg, N., The requirement for eukaryotic initiation factor 4A (elF4A) in translation is in direct proportion to the degree of mRNA 5' secondary structure. *RNA,* **2001,** *7* (3), 382-394.

124. Grens, A., Scheffler, I. E., The 5'- and 3'-untranslated regions of ornithine decarboxylase mRNA affect the translational efficiency. *J Biol Chem,* **1990,** *265* (20), 11810-11816.

125. Manzella, J. M., Blackshear, P. J., Regulation of rat ornithine decarboxylase mRNA translation by its 5'-untranslated region. *J Biol Chem,* **1990,** *265* (20), 11817-11822.

126. Lee, K. A., Guertin, D., Sonenberg, N., mRNA secondary structure as a determinant in cap recognition and initiation complex formation. ATP-Mg2+ independent cross-linking of cap binding proteins to m7I-capped inosine-substituted reovirus mRNA. *J Biol Chem,* **1983,** *258* (2), 707-710.

127. Sonenberg, N., ATP/Mg++-dependent cross-linking of cap binding proteins to the 5' end of eukaryotic mRNA. *Nucleic Acids Res,* **1981,** *9* (7), 1643-1656.

128. Nathan, C. O., Franklin, S., Abreo, F. W., Nassar, R., de Benedetti, A., Williams, J., Stucker, F. J., Expression of eIF4E during head and neck tumorigenesis: possible role in angiogenesis. *Laryngoscope,* **1999,** *109* (8), 1253-1258.

129. Flowers, A., Chu, Q. D., Panu, L., Meschonat, C., Caldito, G., Lowery-Nordberg, M., Li, B. D., Eukaryotic initiation factor 4E overexpression in triple-negative breast cancer predicts a worse outcome. *Surgery,* **2009,** *146* (2), 220-226.

130. Miyagi, Y., Sugiyama, A., Asai, A., Okazaki, T., Kuchino, Y., Kerr, S. J., Elevated levels of eukaryotic translation initiation factor eIF-4E, mRNA in a broad spectrum of transformed cell lines. *Cancer Lett,* **1995,** *91* (2), 247-252.

131. Lazaris-Karatzas, A., Montine, K. S., Sonenberg, N., Malignant transformation by a eukaryotic initiation factor subunit that binds to mRNA 5' cap. *Nature,* **1990,** *345* (6275), 544-547.

132. Sorrells, D. L., Meschonat, C., Black, D., Li, B. D., Pattern of amplification and overexpression of the eukaryotic initiation factor 4E gene in solid tumor. *J Surg Res,* **1999,** *85* (1), 37-42.

133. Polunovsky, V. A., Rosenwald, I. B., Tan, A. T., White, J., Chiang, L., Sonenberg, N., Bitterman, P. B., Translational control of programmed cell death: eukaryotic translation initiation factor 4E blocks apoptosis in growth-factor-restricted fibroblasts with physiologically expressed or deregulated myc. *Mol Cell Biol,* **1996,** *16* (11), 6573-6581.

134. Jia, Y., Polunovsky, V., Bitterman, P. B., Wagner, C. R., Cap-dependent translation initiation factor eIF4E: an emerging anticancer drug target. *Med Res Rev,* **2012,** *32* (4), 786-814.

135. Grifo, J. A., Tahara, S. M., Morgan, M. A., Shatkin, A. J., Merrick, W. C., New initiation factor activity required for globin mRNA translation. *J Biol Chem,* **1983,** *258* (9), 5804-5810.

136. Etchison, D., Milburn, S. C., Edery, I., Sonenberg, N., Hershey, J. W., Inhibition of HeLa cell protein synthesis following poliovirus infection correlates with the proteolysis of a 220,000-dalton polypeptide associated with eucaryotic initiation factor 3 and a cap binding protein complex. *J Biol Chem,* **1982,** *257* (24), 14806-14810.

137. Edery, I., Humbelin, M., Darveau, A., Lee, K. A., Milburn, S., Hershey, J. W., Trachsel, H., Sonenberg, N., Involvement of eukaryotic initiation factor 4A in the cap recognition process. *J Biol Chem,* **1983,** *258* (18), 11398-11403.

138. Rozen, F., Edery, I., Meerovitch, K., Dever, T. E., Merrick, W. C., Sonenberg, N., Bidirectional RNA helicase activity of eucaryotic translation initiation factors 4A and 4F. *Mol Cell Biol,* **1990,** *10* (3), 1134-1144.

139. Lamphear, B. J., Kirchweger, R., Skern, T., Rhoads, R. E., Mapping of functional domains in eukaryotic protein synthesis initiation factor 4G (eIF4G) with picornaviral proteases. Implications for cap-dependent and cap-independent translational initiation. *J Biol Chem,* **1995,** *270* (37), 21975-21983.

140. Rozen, F., Pelletier, J., Trachsel, H., Sonenberg, N., A lysine substitution in the ATP-binding site of eucaryotic initiation factor 4A abrogates nucleotide-binding activity. *Mol Cell Biol,* **1989,** *9* (9), 4061-4063.

141. Abramson, R. D., Dever, T. E., Lawson, T. G., Ray, B. K., Thach, R. E., Merrick, W. C., The ATP-dependent interaction of eukaryotic initiation factors with mRNA. *J Biol Chem,* **1987,** *262* (8), 3826-3832.

142. Pause, A., Sonenberg, N., Mutational analysis of a DEAD box RNA helicase: the mammalian translation initiation factor eIF-4A. *EMBO J,* **1992,** *11* (7), 2643-2654.

143. Pause, A., Methot, N., Sonenberg, N., The HRIGRXXR region of the DEAD box RNA helicase eukaryotic translation initiation factor 4A is required for RNA binding and ATP hydrolysis. *Mol Cell Biol,* **1993,** *13* (11), 6789-6798.

144. Imataka, H., Sonenberg, N., Human eukaryotic translation initiation factor 4G (eIF4G) possesses two separate and independent binding sites for eIF4A. *Mol Cell Biol,* **1997,** *17* (12), 6940-6947.

145. Imataka, H., Gradi, A., Sonenberg, N., A newly identified N-terminal amino acid sequence of human eIF4G binds poly(A)-binding protein and functions in poly(A)-dependent translation. *EMBO J,* **1998,** *17* (24), 7480-7489.

146. Korneeva, N. L., Lamphear, B. J., Hennigan, F. L., Rhoads, R. E., Mutually cooperative binding of eukaryotic translation initiation factor (eIF) 3 and eIF4A to human eIF4G-1. *J Biol Chem,* **2000,** *275* (52), 41369-41376.

147. LeFebvre, A. K., Korneeva, N. L., Trutschl, M., Cvek, U., Duzan, R. D., Bradley, C. A., Hershey, J. W. B., Rhoads, R. E., Translation initiation factor eIF4G-1 binds to eIF3 through the eIF3e subunit. *J Biol Chem,* **2006,** *281* (32), 22917-22932.

148. Pyronnet, S., Imataka, H., Gingras, A. C., Fukunaga, R., Hunter, T., Sonenberg, N., Human eukaryotic translation initiation factor 4G (eIF4G) recruits mnk1 to phosphorylate eIF4E. *EMBO J,* **1999,** *18* (1), 270-279.

149. Ray, B. K., Lawson, T. G., Kramer, J. C., Cladaras, M. H., Grifo, J. A., Abramson, R. D., Merrick, W. C., Thach, R. E., ATP-dependent unwinding of messenger RNA structure by eukaryotic initiation factors. *J Biol Chem,* **1985,** *260* (12), 7651-7658.

150. Sonenberg, N., Morgan, M. A., Merrick, W. C., Shatkin, A. J., A polypeptide in eukaryotic initiation factors that crosslinks specifically to the 5'-terminal cap in mRNA. *P Natl Acad Sci USA,* **1978,** *75* (10), 4843-4847.

151. Sonenberg, N., Guertin, D., Cleveland, D., Trachsel, H., Probing the function of the eucaryotic 5' cap structure by using a monoclonal antibody directed against cap-binding proteins. *Cell,* **1981,** *27* (3), 563-572.

152. Sonenberg, N., Trachsel, H., Hecht, S., Shatkin, A. J., Differential stimulation of capped mRNA translation in vitro by cap binding protein. *Nature,* **1980,** *285* (5763), 331-333.

153. von Der Haar, T., Ball, P. D., McCarthy, J. E., Stabilization of eukaryotic initiation factor 4E binding to the mRNA 5'-Cap by domains of eIF4G. *J Biol Chem,* **2000,** *275* (39), 30551-30555.

154. Shveygert, M., Kaiser, C., Bradrick, S. S., Gromeier, M., Regulation of eukaryotic initiation factor 4E (eIF4E) phosphorylation by mitogen-activated protein kinase occurs through modulation of Mnk1-eIF4G interaction. *Mol Cell Biol,* **2010,** *30* (21), 5160-5167.

155. Waskiewicz, A. J., Johnson, J. C., Penn, B., Mahalingam, M., Kimball, S. R., Cooper, J. A., Phosphorylation of the cap-binding protein eukaryotic translation initiation factor 4E by protein kinase Mnk1 in vivo. *Mol Cell Biol,* **1999,** *19* (3), 1871-1880.

156. Flynn, A., Proud, C. G., Serine 209, not serine 53, is the major site of phosphorylation in initiation factor eIF-4E in serum-treated Chinese hamster ovary cells. *J Biol Chem,* **1995,** *270* (37), 21684-21688.

157. Joshi, B., Cai, A. L., Keiper, B. D., Minich, W. B., Mendez, R., Beach, C. M., Stepinski, J., Stolarski, R., Darzynkiewicz, E., Rhoads, R. E., Phosphorylation of eukaryotic protein synthesis initiation factor 4E at Ser-209. *J Biol Chem,* **1995,** *270* (24), 14597-14603.

158. Ueda, H., Iyo, H., Doi, M., Inoue, M., Ishida, T., Morioka, H., Tanaka, T., Nishikawa, S., Uesugi, S., Combination of Trp and Glu residues for recognition of mRNA cap structure. Analysis of m7G base recognition site of human cap binding protein (IF-4E) by site-directed mutagenesis. *FEBS Lett,* **1991,** *280* (2), 207-210.

159. Matsuo, H., Li, H., McGuire, A. M., Fletcher, C. M., Gingras, A. C., Sonenberg, N., Wagner, G., Structure of translation factor eIF4E bound to m7GDP and interaction with 4E-binding protein. *Nat Struct Biol,* **1997,** *4* (9), 717-724.

160. Tomoo, K., Shen, X., Okabe, K., Nozoe, Y., Fukuhara, S., Morino, S., Ishida, T., Taniguchi, T., Hasegawa, H., Terashima, A., Sasaki, M., Katsuya, Y., Kitamura, K., Miyoshi, H., Ishikawa, M., Miura, K., Crystal structures of 7-methylguanosine 5'-triphosphate (m(7)GTP)- and P(1)-7-methylguanosine-P(3)-adenosine-5',5'-triphosphate (m(7)GpppA)-bound human full-length eukaryotic initiation factor 4E: biological importance of the C-terminal flexible region. *Biochem J,* **2002,** *362* (3), 539-544.

161. Marcotrigiano, J., Gingras, A. C., Sonenberg, N., Burley, S. K., Cocrystal structure of the messenger RNA 5' cap-binding protein (eIF4E) bound to 7-methyl-GDP. *Cell,* **1997,** *89* (6), 951-961.

162. Niedzwiecka, A., Marcotrigiano, J., Stepinski, J., Jankowska-Anyszka, M., Wyslouch-Cieszynska, A., Dadlez, M., Gingras, A.-C., Mak, P., Darzynkiewicz, E., Sonenberg, N., Burley, S. K., Stolarski, R., Biophysical Studies of eIF4E Cap-binding Protein: Recognition of mRNA 5′ Cap Structure and Synthetic Fragments of eIF4G and 4E-BP1 Proteins. *J Mol Biol,* **2002,** *319* (3), 615-635.

163. Mader, S., Lee, H., Pause, A., Sonenberg, N., The translation initiation factor eIF-4E binds to a common motif shared by the translation factor eIF-4 gamma and the translational repressors 4E-binding proteins. *Mol Cell Biol,* **1995,** *15* (9), 4990-4997.

164. Marcotrigiano, J., Gingras, A., Sonenberg, N., Burley, S., Cap-dependent translation initiation in eukaryotes is regulated by a molecular mimic of eIF4G. *Mol Cell,* **1999,** *3* (6), 707-716.

165. Umenaga, Y., Paku, K. S., In, Y., Ishida, T., Tomoo, K., Identification and function of the second eIF4E-binding region in N-terminal domain of eIF4G: comparison with eIF4E-binding protein. *Biochem Bioph Res Co,* **2011,** *414* (3), 462-467.

166. Siddiqui, N., Tempel, W., Nedyalkova, L., Volpon, L., Wernimont, A. K., Osborne, M. J., Park, H. W., Borden, K. L., Structural insights into the allosteric effects of 4EBP1 on the eukaryotic translation initiation factor eIF4E. *J Mol Biol,* **2012,** *415* (5), 781-792.

167. Dostie, J., Ferraiuolo, M., Pause, A., Adam, S. A., Sonenberg, N., A novel shuttling protein, 4E-T, mediates the nuclear import of the mRNA 5' cap-binding protein, eIF4E. *EMBO J,* **2000,** *19* (12), 3142-3156.

168. Brown, C. J., Verma, C. S., Walkinshaw, M. D., Lane, D. P., Crystallization of eIF4E complexed with eIF4GI peptide and glycerol reveals distinct structural differences around the cap-binding site. *Cell Cycle,* **2009,** *8* (12), 1905-1911.

169. Herbert, T. P., Fahraeus, R., Prescott, A., Lane, D. P., Proud, C. G., Rapid induction of apoptosis mediated by peptides that bind initiation factor eIF4E. *Curr Biol,* **2000,** *10* (13), 793-796.

170. Zhou, W., Quah, S. T., Verma, C. S., Liu, Y., Lane, D. P., Brown, C. J., Improved eIF4E binding peptides by phage display guided design: plasticity of interacting surfaces yield collective effects. *PLOS One,* **2012,** *7* (10), e47235.

171. Lama, D., Quah, S. T., Verma, C. S., Lakshminarayanan, R., Beuerman, R. W., Lane, D. P., Brown, C. J., Rational optimization of conformational effects induced by hydrocarbon staples in peptides and their binding interfaces. *Sci Rep,* **2013,** *3*, 3451.

172. Danho, W., Fotouhi, N., Han, Y., Khan, W., Milletti, F., Nui, H., Cell penetrating peptides to target eIF4E. *WO2014009259 A1 (patent),* **2014**.

173. Brown, C. J., Chia, C. S. B., Eif4e binding peptides. *WO2011136744 A1 (patent),* **2011**.

174. Naora, H., Peptides that bind eukaryotic translation initiation factor 4e. *US20110319338 A1 (patent),* **2011**.

175. Jacobson, B. A., Alter, M. D., Kratzke, M. G., Frizelle, S. P., Zhang, Y., Peterson, M. S., Avdulov, S., Mohorn, R. P., Whitson, B. A., Bitterman, P. B., Polunovsky, V. A., Kratzke, R. A., Repression of cap-dependent translation attenuates the transformed phenotype in non-small cell lung cancer both in vitro and in vivo. *Cancer Res,* **2006,** *66* (8), 4256-4262.

176. Pause, A., Belsham, G. J., Gingras, A. C., Donze, O., Lin, T. A., Lawrence, J. C., Jr., Sonenberg, N., Insulin-dependent stimulation of protein synthesis by phosphorylation of a regulator of 5'-cap function. *Nature,* **1994,** *371* (6500), 762-767.

177. Gingras, A. C., Gygi, S. P., Raught, B., Polakiewicz, R. D., Abraham, R. T., Hoekstra, M. F., Aebersold, R., Sonenberg, N., Regulation of 4E-BP1 phosphorylation: a novel two-step mechanism. *Genes Dev,* **1999,** *13* (11), 1422-1437.

178. Poulin, F., Gingras, A. C., Olsen, H., Chevalier, S., Sonenberg, N., 4E-BP3, a new member of the eukaryotic initiation factor 4E-binding protein family. *J Biol Chem,* **1998,** *273* (22), 14002-14007.

179. Haghighat, A., Mader, S., Pause, A., Sonenberg, N., Repression of cap-dependent translation by 4E-binding protein 1: competition with p220 for binding to eukaryotic initiation factor-4E. *EMBO J,* **1995,** *14* (22), 5701-5709.

180. Feigenblum, D., Schneider, R. J., Cap-binding protein (eukaryotic initiation factor 4E) and 4E-inactivating protein BP-1 independently regulate cap-dependent translation. *Mol Cell Biol,* **1996,** *16* (10), 5450-5457.

181. Schalm, S. S., Fingar, D. C., Sabatini, D. M., Blenis, J., TOS motif-mediated raptor binding regulates 4E-BP1 multisite phosphorylation and function. *Curr Biol,* **2003,** *13* (10), 797-806.

182. Martineau, Y., Azar, R., Muller, D., Lasfargues, C., El Khawand, S., Anesia, R., Pelletier, J., Bousquet, C., Pyronnet, S., Pancreatic tumours escape from translational control through 4E-BP1 loss. *Oncogene,* **2013,** *5* (6), 1-8.

183. Gingras, A. C., Raught, B., Gygi, S. P., Niedzwiecka, A., Miron, M., Burley, S. K., Polakiewicz, R. D., Wyslouch-Cieszynska, A., Aebersold, R., Sonenberg, N., Hierarchical phosphorylation of the translation inhibitor 4E-BP1. *Genes Dev,* **2001,** *15* (21), 2852-2864.

184. Martín, M. E., Pérez, M. I., Redondo, C., Álvarez, M. I., Saklinas, M., Fando, J. L., 4E binding protein 1 expression is inversely correlated to the progression of gastrointestinal cancers. *Int J Biochem Cell B,* **2000,** *32* (6), 633-642.

185. Coleman, L. J., Peter, M. B., Teall, T. J., Brannan, R. A., Hanby, A. M., Honarpisheh, H., Shaaban, A. M., Smith, L., Speirs, V., Verghese, E. T., McElwaine, J. N., Hughes, T. A., Combined analysis of eIF4E and 4E-binding protein expression predicts breast cancer survival and estimates eIF4E activity. *Br J Cancer,* **2009,** *100* (9), 1393-1399.

186. Spoerner, M., Hozsa, C., Poetzl, J. A., Reiss, K., Ganser, P., Geyer, M., Kalbitzer, H. R., Conformational states of human rat sarcoma (Ras) protein complexed with its natural ligand GTP and their role for effector interaction and GTP hydrolysis. *J Biol Chem,* **2010,** *285* (51), 39768-39778.

187. Lazaris-Karatzas, A., Smith, M. R., Frederickson, R. M., Jaramillo, M. L., Liu, Y. L., Kung, H. F., Sonenberg, N., Ras mediates translation initiation factor 4E-induced malignant transformation. *Genes Dev,* **1992,** *6* (9), 1631-1642.

188. Waskiewicz, A. J., Flynn, A., Proud, C. G., Cooper, J. A., Mitogen-activated protein kinases activate the serine/threonine kinases Mnk1 and Mnk2. *EMBO J,* **1997,** *16* (8), 1909-1920.

189. Fukunaga, R., Hunter, T., MNK1, a new MAP kinase-activated protein kinase, isolated by a novel expression screening method for identifying protein kinase substrates. *EMBO J,* **1997,** *16* (8), 1921-1933.

190. Brunet, A., Pages, G., Pouyssegur, J., Constitutively active mutants of MAP kinase kinase (MEK1) induce growth factor-relaxation and oncogenicity when expressed in fibroblasts. *Oncogene,* **1994,** *9* (11), 3379-3387.

191. Minich, W. B., Balasta, M. L., Goss, D. J., Rhoads, R. E., Chromatographic resolution of in vivo phosphorylated and nonphosphorylated eukaryotic translation initiation factor eIF-4E: increased cap affinity of the phosphorylated form. *P Natl Acad Sci USA,* **1994,** *91* (16), 7668-7672.

192. Yoshizawa, A., Fukuoka, J., Shimizu, S., Shilo, K., Franks, T. J., Hewitt, S. M., Fujii, T., Cordon-Cardo, C., Jen, J., Travis, W. D., Overexpression of phospho-eIF4E is associated with survival through AKT pathway in non-small cell lung cancer. *Clin Cancer Res,* **2010,** *16* (1), 240-248.

193. Frederickson, R. M., Montine, K. S., Sonenberg, N., Phosphorylation of eukaryotic translation initiation factor 4E is increased in Src-transformed cell lines. *Mol Cell Biol,* **1991,** *11* (5), 2896-2900.

194. Topisirovic, I., Ruiz-Gutierrez, M., Borden, K. L., Phosphorylation of the eukaryotic translation initiation factor eIF4E contributes to its transformation and mRNA transport activities. *Cancer Res,* **2004,** *64* (23), 8639-8642.

195. Furic, L., Rong, L., Larsson, O., Koumakpayi, I. H., Yoshida, K., Brueschke, A., Petroulakis, E., Robichaud, N., Pollak, M., Gaboury, L. A., Pandolfi, P. P., Saad, F., Sonenberg, N., eIF4E phosphorylation promotes tumorigenesis and is associated with prostate cancer progression. *P Natl Acad Sci USA,* **2010,** *107* (32), 14134-14139.

196. Gu, Y., Zhou, H., Gan, Y., Zhang, J., Chen, J., Gan, X., Li, H., Zheng, W., Meng, Z., Ma, X., Wang, X., Xu, X., Xu, G., Lu, X., Liang, Y., Zhang, X., Lu, X., Huang, W., Xu, R., Small-molecule induction of phospho-eIF4E sumoylation and degradation via targeting its phosphorylated serine 209 residue. *Oncotarget,* **2015,** *6* (17), 15111-15121.

197. Konicek, B. W., Stephens, J. R., McNulty, A. M., Robichaud, N., Peery, R. B., Dumstorf, C. A., Dowless, M. S., Iversen, P. W., Parsons, S., Ellis, K. E., McCann, D. J., Pelletier, J., Furic, L., Yingling, J. M., Stancato, L. F., Sonenberg, N., Graff, J. R., Therapeutic inhibition of MAP kinase interacting kinase blocks eukaryotic initiation factor 4E phosphorylation and suppresses outgrowth of experimental lung metastases. *Cancer Res,* **2011,** *71* (5), 1849-1857.

198. Pons, B., Peg, V., Vazquez-Sanchez, M. A., Lopez-Vicente, L., Argelaguet, E., Coch, L., Martinez, A., Hernandez-Losa, J., Armengol, G., Ramon, Y. C. S., The effect of p-4E-BP1 and p-eIF4E on cell proliferation in a breast cancer model. *Int J Oncol,* **2011,** *39* (5), 1337-1345.

199. Wheater, M. J., Johnson, P. W., Blaydes, J. P., The role of MNK proteins and eIF4E phosphorylation in breast cancer cell proliferation and survival. *Cancer Biol Ther,* **2010,** *10* (7), 728-735.

200. Ueda, T., Watanabe-Fukunaga, R., Fukuyama, H., Nagata, S., Fukunaga, R., Mnk2 and Mnk1 are essential for constitutive and inducible phosphorylation of eukaryotic initiation factor 4E but not for cell growth or development. *Mol Cell Biol,* **2004,** *24* (15), 6539-6549.

201. Inoki, K., Zhu, T., Guan, K. L., TSC2 mediates cellular energy response to control cell growth and survival. *Cell,* **2003,** *115* (5), 577-590.

202. Mendez, R., Myers, M. G., Jr., White, M. F., Rhoads, R. E., Stimulation of protein synthesis, eukaryotic translation initiation factor 4E phosphorylation, and PHAS-I phosphorylation by insulin requires insulin receptor substrate 1 and phosphatidylinositol 3-kinase. *Mol Cell Biol,* **1996,** *16* (6), 2857-2864.

203. Dufner, A., Andjelkovic, M., Burgering, B. M., Hemmings, B. A., Thomas, G., Protein kinase B localization and activation differentially affect S6 kinase 1 activity and eukaryotic translation initiation factor 4E-binding protein 1 phosphorylation. *Mol Cell Biol,* **1999,** *19* (6), 4525-4534.

204. Manning, B. D., Tee, A. R., Logsdon, M. N., Blenis, J., Cantley, L. C., Identification of the tuberous sclerosis complex-2 tumor suppressor gene product

tuberin as a target of the phosphoinositide 3-kinase/akt pathway. *Mol Cell,* **2002,** *10* (1), 151-162.

205. Troppmair, J., Bruder, J. T., Munoz, H., Lloyd, P. A., Kyriakis, J., Banerjee, P., Avruch, J., Rapp, U. R., Mitogen-activated protein kinase/extracellular signal-regulated protein kinase activation by oncogenes, serum, and 12-O-tetradecanoylphorbol-13-acetate requires Raf and is necessary for transformation. *J Biol Chem,* **1994,** *269* (9), 7030-7035.

206. Avruch, J., Zhang, X. F., Kyriakis, J. M., Raf meets Ras: completing the framework of a signal transduction pathway. *Trends Biochem Sci,* **1994,** *19* (7), 279-283.

207. Gardner, A. M., Vaillancourt, R. R., Lange-Carter, C. A., Johnson, G. L., MEK-1 phosphorylation by MEK kinase, Raf, and mitogen-activated protein kinase: analysis of phosphopeptides and regulation of activity. *Mol Biol Cell,* **1994,** *5* (2), 193-201.

208. Scheper, G. C., van Kollenburg, B., Hu, J., Luo, Y., Goss, D. J., Proud, C. G., Phosphorylation of eukaryotic initiation factor 4E markedly reduces its affinity for capped mRNA. *J Biol Chem,* **2002,** *277* (5), 3303-3309.

209. Slepenkov, S. V., Darzynkiewicz, E., Rhoads, R. E., Stopped-flow kinetic analysis of eIF4E and phosphorylated eIF4E binding to cap analogs and capped oligoribonucleotides: evidence for a one-step binding mechanism. *J Biol Chem,* **2006,** *281* (21), 14927-14938.

210. Rousseau, D., Kaspar, R., Rosenwal, I., Gehrke, L., Sonenberg, N., Translation initiation of ornithine decarboxylase and nucleocytoplasmic transport of cyclin D1 mRNA are increased in cells overexpressing eukaryotic initiation factor 4E. *P Natl Acad Sci USA,* **1996,** *93* (3), 1065-1070.

211. Rosenwald, I. B., Kaspar, R., Rousseau, D., Gehrke, L., Leboulch, P., Chen, J. J., Schmidt, E. V., Sonenberg, N., London, I. M., Eukaryotic translation initiation factor 4E regulates expression of cyclin D1 at transcriptional and post-transcriptional levels. *J Biol Chem,* **1995,** *270* (36), 21176-21180.

212. Culjkovic, B., Topisirovic, I., Skrabanek, L., Ruiz-Gutierrez, M., Borden, K. L., eIF4E promotes nuclear export of cyclin D1 mRNAs via an element in the 3'UTR. *J Cell Biol,* **2005,** *169* (2), 245-256.

213. Culjkovic, B., Topisirovic, I., Skrabanek, L., Ruiz-Gutierrez, M., Borden, K. L., eIF4E is a central node of an RNA regulon that governs cellular proliferation. *J Cell Biol,* **2006,** *175* (3), 415-426.

214. Martinez, A., Sese, M., Losa, J. H., Robichaud, N., Sonenberg, N., Aasen, T., Ramon, Y. C. S., Phosphorylation of eIF4E Confers Resistance to Cellular Stress and DNA-Damaging Agents through an Interaction with 4E-T: A Rationale for Novel Therapeutic Approaches. *PLOS One,* **2015,** *10* (4), e0123352.

215. Park, S. H., Raines, R. T., Genetic selection for dissociative inhibitors of designated protein-protein interactions. *Nat Biotechnol,* **2000,** *18* (8), 847-851.

216. Joung, J. K., Ramm, E. I., Pabo, C. O., A bacterial two-hybrid selection system for studying protein-DNA and protein-protein interactions. *P Natl Acad Sci USA,* **2000,** *97* (13), 7382-7387.

217. Scott, C. P., Abel-Santos, E., Wall, M., Wahnon, D. C., Benkovic, S. J., Production of cyclic peptides and proteins in vivo. *P Natl Acad Sci USA,* **1999,** *96* (24), 13638-13643.

218. Chien, C. T., Bartel, P. L., Sternglanz, R., Fields, S., The two-hybrid system: a method to identify and clone genes for proteins that interact with a protein of interest. *P Natl Acad Sci USA,* **1991,** *88* (21), 9578-9582.

219. Dombroski, A. J., Walter, W. A., Record, M. T., Jr., Siegele, D. A., Gross, C. A., Polypeptides containing highly conserved regions of transcription initiation factor sigma 70 exhibit specificity of binding to promoter DNA. *Cell,* **1992,** *70* (3), 501-512.

220. Poustovoitov, M., Serebriiskii, I., Adams, P. D., A two-step two-hybrid system to identify functionally significant protein-protein interactions. *Methods,* **2004,** *32* (4), 371-380.

221. Pan, T., Coleman, J. E., Structure and function of the Zn(II) binding site within the DNA-binding domain of the GAL4 transcription factor. *P Natl Acad Sci USA,* **1989,** *86* (9), 3145-3149.

222. Keegan, L., Gill, G., Ptashne, M., Separation of DNA binding from the transcription-activating function of a eukaryotic regulatory protein. *Science,* **1986,** *231* (4739), 699-704.

223. Delorme, E., Transformation of Saccharomyces cerevisiae by electroporation. *Appl Environ Microb,* **1989,** *55* (9), 2242-2246.

224. Dower, W. J., Miller, J. F., Ragsdale, C. W., High efficiency transformation of E. coli by high voltage electroporation. *Nucleic Acids Res,* **1988,** *16* (13), 6127-6145.

225. Hu, J. C., O'Shea, E. K., Kim, P. S., Sauer, R. T., Sequence requirements for coiled-coils: analysis with lambda repressor-GCN4 leucine zipper fusions. *Science,* **1990,** *250* (4986), 1400-1403.

226. Longo, F., Marchetti, M. A., Castagnoli, L., Battaglia, P. A., Gigliani, F., A novel approach to protein-protein interaction: complex formation between the p53 tumor suppressor and the HIV Tat proteins. *Biochem Biophys Res Commun,* **1995,** *206* (1), 326-334.

227. Pabo, C. O., Sauer, R. T., Sturtevant, J. M., Ptashne, M., The lambda repressor contains two domains. *P Natl Acad Sci USA,* **1979,** *76* (4), 1608-1612.

228. Ptashne, M., Backman, K., Humayun, M. Z., Jeffrey, A., Maurer, R., Meyer, B., Sauer, R. T., Autoregulation and function of a repressor in bacteriophage lambda. *Science,* **1976,** *194* (4261), 156-161.

229. Dove, S. L., Joung, J. K., Hochschild, A., Activation of prokaryotic transcription through arbitrary protein-protein contacts. *Nature,* **1997,** *386* (6625), 627-630.

230. Sauer, R. T., Yocum, R. R., Doolittle, R. F., Lewis, M., Pabo, C. O., Homology among DNA-binding proteins suggests use of a conserved super-secondary structure. *Nature,* **1982,** *298* (5873), 447-451.

231. Pabo, C. O., Lewis, M., The operator-binding domain of lambda repressor: structure and DNA recognition. *Nature,* **1982,** *298* (5873), 443-447.

232. Beamer, L. J., Pabo, C. O., Refined 1.8 A crystal structure of the lambda repressor-operator complex. *J Mol Biol,* **1992,** *227* (1), 177-196.

233. Johnson, A. D., Meyer, B. J., Ptashne, M., Interactions between DNA-bound repressors govern regulation by the lambda phage repressor. *P Natl Acad Sci USA,* **1979,** *76* (10), 5061-5065.

234. Sauer, R. T., Pabo, C. O., Meyer, B. J., Ptashne, M., Backman, K. C., Regulatory functions of the lambda repressor reside in the amino-terminal domain. *Nature,* **1979,** *279* (5712), 396-400.

235. Pribnow, D., Nucleotide sequence of an RNA polymerase binding site at an early T7 promoter. *P Natl Acad Sci USA,* **1975,** *72* (3), 784-788.

236. Schaller, H., Gray, C., Herrmann, K., Nucleotide sequence of an RNA polymerase binding site from the DNA of bacteriophage fd. *P Natl Acad Sci USA,* **1975,** *72* (2), 737-741.

237. Hawley, D. K., McClure, W. R., Compilation and analysis of Escherichia coli promoter DNA sequences. *Nucleic Acids Res,* **1983,** *11* (8), 2237-2255.

238. Siebenlist, U., Simpson, R. B., Gilbert, W., E. coli RNA polymerase interacts homologously with two different promoters. *Cell,* **1980,** *20* (2), 269-281.

239. Di Lallo, G., Anderluzzi, D., Ghelardini, P., Paolozzi, L., FtsZ dimerization in vivo. *Mol Microbiol,* **1999,** *32* (2), 265-274.

240. Di Lallo, G., Ghelardini, P., Paolozzi, L., Two-hybrid assay: construction of an Escherichia coli system to quantify homodimerization ability in vivo. *Microbiology,* **1999,** *145* (6), 1485-1490.

241. Dmitrova, M., Younes-Cauet, G., Oertel-Buchheit, P., Porte, D., Schnarr, M., Granger-Schnarr, M., A new LexA-based genetic system for monitoring and analyzing protein heterodimerization in Escherichia coli. *Mol Gen Genet,* **1998,** *257* (2), 205-212.

242. Hays, L. B., Chen, Y. S., Hu, J. C., Two-hybrid system for characterization of protein-protein interactions in E. coli. *BioTechniques,* **2000,** *29* (2), 288-294.

243. Karimova, G., Pidoux, J., Ullmann, A., Ladant, D., A bacterial two-hybrid system based on a reconstituted signal transduction pathway. *P Natl Acad Sci USA,* **1998,** *95* (10), 5752-5756.

244. Di Lallo, G., Castagnoli, L., Ghelardini, P., Paolozzi, L., A two-hybrid system based on chimeric operator recognition for studying protein homo/heterodimerization in Escherichia coli. *Microbiology,* **2001,** *147* (6), 1651-1656.

245. Bushman, F. D., Ptashne, M., Activation of transcription by the bacteriophage 434 repressor. *P Natl Acad Sci USA,* **1986,** *83* (24), 9353-9357.

246. Xu, J., Koudelka, G. B., Mutually Exclusive Utilization of PR and PRM Promoters in Bacteriophage 434 OR. *J Bacteriol,* **2000,** *182* (11), 3165-3174.

247. Valenzuela, D., Ptashne, M., P22 repressor mutants deficient in co-operative binding and DNA loop formation. *EMBO J,* **1989,** *8* (13), 4345-4350.

248. Anderson, J., Ptashne, M., Harrison, S. C., Cocrystals of the DNA-binding domain of phage 434 repressor and a synthetic phage 434 operator. *P Natl Acad Sci USA,* **1984,** *81* (5), 1307-1311.

249. Anderson, J. E., Ptashne, M., Harrison, S. C., A phage repressor-operator complex at 7 A resolution. *Nature,* **1985,** *316* (6029), 596-601.

250. Anderson, J. E., Ptashne, M., Harrison, S. C., Structure of the repressor-operator complex of bacteriophage 434. *Nature,* **1987,** *326* (6116), 846-852.

251. Aggarwal, A. K., Rodgers, D. W., Drottar, M., Ptashne, M., Harrison, S. C., Recognition of a DNA operator by the repressor of phage 434: a view at high resolution. *Science,* **1988,** *242* (4880), 899-907.

252. Harrison, S. C., Anderson, J. E., Koudelka, G. B., Mondragon, A., Subbiah, S., Wharton, R. P., Wolberger, C., Ptashne, M., Recognition of DNA sequences by the repressor of bacteriophage 434. *Biophys Chem,* **1988,** *29* (1), 31-37.

253. Di Lallo, G., Castagnoli, L., Ghelardini, P., Paolozzi, L., A two-hybrid system based on chimeric operator recognition for studying protein homo/heterodimerization in Escherichia coli. *Microbiology,* **2001,** *147* (6), 1651-1656.

254. Wharton, R. P., Ptashne, M., A new-specificity mutant of 434 repressor that defines an amino acid-base pair contact. *Nature,* **1987,** *326* (6116), 888-891.

255. De Anda, J., Poteete, A. R., Sauer, R. T., P22 c2 repressor. Domain structure and function. *J Biol Chem,* **1983,** *258* (17), 10536-10542.

256. Watkins, D., Hsiao, C., Woods, K. K., Koudelka, G. B., Williams, L. D., P22 c2 repressor-operator complex: mechanisms of direct and indirect readout. *Biochemistry,* **2008,** *47* (8), 2325-2338.

257. Sauer, R. T., Ross, M. J., Ptashne, M., Cleavage of the lambda and P22 repressors by recA protein. *J Biol Chem,* **1982,** *257* (8), 4458-4462.

258. Wharton, R. P., Brown, E. L., Ptashne, M., Substituting an alpha-helix switches the sequence-specific DNA interactions of a repressor. *Cell,* **1984,** *38* (2), 361-369.

259. Bushman, F. D., The bacteriophage 434 right operator. Roles of O(R)1, O(R)2 and O(R)3. *J Mol Biol,* **1993,** *230* (1), 28-40.

260. Poteete, A. R., Ptashne, M., Ballivet, M., Eisen, H., Operator sequences of bacteriophages P22 and 21. *J Mol Biol,* **1980,** *137* (1), 81-91.

261. Pirrotta, V., Sequence of the OR operator of phage lambda. *Nature,* **1975,** *254* (5496), 114-117.

262. Hollis, M., Valenzuela, D., Pioli, D., Wharton, R., Ptashne, M., A repressor heterodimer binds to a chimeric operator. *P Natl Acad Sci USA,* **1988,** *85* (16), 5834-5838.

263. Webster, C., Merryweather, A., Brammar, W., Efficient repression by a heterodimeric repressor in Escherichia coli. *Mol Microbiol,* **1992,** *6* (3), 371-377.

264. Sauer, R. T., Pan, J., Hopper, P., Hehir, K., Brown, J., Poteete, A. R., Primary structure of the phage P22 repressor and its gene c2. *Biochemistry,* **1981,** *20* (12), 3591-3598.

265. Sanger, F., Coulson, A. R., Hong, G. F., Hill, D. F., Petersen, G. B., Nucleotide sequence of bacteriophage lambda DNA. *J Mol Biol,* **1982,** *162* (4), 729-773.

266. Horswill, A. R., Savinov, S. N., Benkovic, S. J., A systematic method for identifying small-molecule modulators of protein-protein interactions. *P Natl Acad Sci USA,* **2004,** *101* (44), 15591-15596.

267. Struhl, K., Cameron, J. R., Davis, R. W., Functional genetic expression of eukaryotic DNA in Escherichia coli. *P Natl Acad Sci USA,* **1976,** *73* (5), 1471-1475.

268. Struhl, K., Davis, R. W., Production of a functional eukaryotic enzyme in Escherichia coli: cloning and expression of the yeast structural gene for imidazole-glycerolphosphate dehydratase (his3). *P Natl Acad Sci USA,* **1977,** *74* (12), 5255-5259.

269. de Boer, H. A., Comstock, L. J., Vasser, M., The tac promoter: a functional hybrid derived from the trp and lac promoters. *P Natl Acad Sci USA,* **1983,** *80* (1), 21-25.

270. Datsenko, K. A., Wanner, B. L., One-step inactivation of chromosomal genes in Escherichia coli K-12 using PCR products. *P Natl Acad Sci USA,* **2000,** *97* (12), 6640-6645.

271. Platt, R., Drescher, C., Park, S. K., Phillips, G. J., Genetic system for reversible integration of DNA constructs and lacZ gene fusions into the Escherichia coli chromosome. *Plasmid,* **2000,** *43* (1), 12-23.

272. Haldimann, A., Wanner, B. L., Conditional-replication, integration, excision, and retrieval plasmid-host systems for gene structure-function studies of bacteria. *J Bacteriol,* **2001,** *183* (21), 6384-6393.

273. Jacob, F., Monod, J., Genetic regulatory mechanisms in the synthesis of proteins. *J Mol Biol,* **1961,** *3* (3), 318-356.

274. Hirata, R., Ohsumk, Y., Nakano, A., Kawasaki, H., Suzuki, K., Anraku, Y., Molecular structure of a gene, VMA1, encoding the catalytic subunit of H(+)-translocating adenosine triphosphatase from vacuolar membranes of Saccharomyces cerevisiae. *J Biol Chem,* **1990,** *265* (12), 6726-6733.

275. Kane, P. M., Yamashiro, C. T., Wolczyk, D. F., Neff, N., Goebl, M., Stevens, T. H., Protein splicing converts the yeast TFP1 gene product to the 69-kD subunit of the vacuolar H(+)-adenosine triphosphatase. *Science,* **1990,** *250* (4981), 651-657.

276. Wu, H., Hu, Z., Liu, X. Q., Protein trans-splicing by a split intein encoded in a split DnaE gene of Synechocystis sp. PCC6803. *P Natl Acad Sci USA,* **1998,** *95* (16), 9226-9231.

277. Sun, P., Ye, S., Ferrandon, S., Evans, T. C., Xu, M. Q., Rao, Z., Crystal structures of an intein from the split dnaE gene of Synechocystis sp. PCC6803 reveal

the catalytic model without the penultimate histidine and the mechanism of zinc ion inhibition of protein splicing. *J Mol Biol,* **2005,** *353* (5), 1093-1105.

278. Xu, M. Q., Comb, D. G., Paulus, H., Noren, C. J., Shao, Y., Perler, F. B., Protein splicing: an analysis of the branched intermediate and its resolution by succinimide formation. *EMBO J,* **1994,** *13* (23), 5517-5522.

279. Chong, S., Shao, Y., Paulus, H., Benner, J., Perler, F. B., Xu, M. Q., Protein splicing involving the Saccharomyces cerevisiae VMA intein. The steps in the splicing pathway, side reactions leading to protein cleavage, and establishment of an in vitro splicing system. *J Biol Chem,* **1996,** *271* (36), 22159-22168.

280. Xu, M. Q., Perler, F. B., The mechanism of protein splicing and its modulation by mutation. *EMBO J,* **1996,** *15* (19), 5146-5153.

281. Romanelli, A., Shekhtman, A., Cowburn, D., Muir, T. W., Semisynthesis of a segmental isotopically labeled protein splicing precursor: NMR evidence for an unusual peptide bond at the N-extein-intein junction. *P Natl Acad Sci USA,* **2004,** *101* (17), 6397-6402.

282. Poland, B. W., Xu, M. Q., Quiocho, F. A., Structural insights into the protein splicing mechanism of PI-SceI. *J Biol Chem,* **2000,** *275* (22), 16408-16413.

283. Dearden, A. K., Callahan, B., Roey, P. V., Li, Z., Kumar, U., Belfort, M., Nayak, S. K., A conserved threonine spring-loads precursor for intein splicing. *Protein Sci,* **2013,** *22* (5), 557-563.

284. Shingledecker, K., Jiang, S., Paulus, H., Reactivity of the cysteine residues in the protein splicing active center of the Mycobacterium tuberculosis RecA intein. *Arch Biochem Biophys,* **2000,** *375* (1), 138-144.

285. Dawson, P. E., Muir, T. W., Clark-Lewis, I., Kent, S. B., Synthesis of proteins by native chemical ligation. *Science,* **1994,** *266* (5186), 776-779.

286. Xu, M. Q., Southworth, M. W., Mersha, F. B., Hornstra, L. J., Perler, F. B., In vitro protein splicing of purified precursor and the identification of a branched intermediate. *Cell,* **1993,** *75* (7), 1371-1377.

287. Liu, Z., Frutos, S., Bick, M. J., Vila-Perello, M., Debelouchina, G. T., Darst, S. A., Muir, T. W., Structure of the branched intermediate in protein splicing. *P Natl Acad Sci USA,* **2014,** *111* (23), 8422-8427.

288. Ding, Y., Xu, M. Q., Ghosh, I., Chen, X., Ferrandon, S., Lesage, G., Rao, Z., Crystal structure of a mini-intein reveals a conserved catalytic module involved in side

chain cyclization of asparagine during protein splicing. *J Biol Chem,* **2003,** *278* (40), 39133-39142.

289. Scott, C. P., Abel-Santos, E., Jones, A. D., Benkovic, S. J., Structural requirements for the biosynthesis of backbone cyclic peptide libraries. *Chem Biol,* **2001,** *8* (8), 801-815.

290. Nichols, N. M., Evans, T. C., Jr., Mutational analysis of protein splicing, cleavage, and self-association reactions mediated by the naturally split Ssp DnaE intein. *Biochemistry,* **2004,** *43* (31), 10265-10276.

291. Evans, T. C., Martin, D., Kolly, R., Panne, D., Sun, L., Ghosh, I., Chen, L. X., Benner, J., Liu, X. Q., Xu, M. Q., Protein trans-splicing and cyclization by a naturally split intein from the dnaE gene of Synechocystis species PCC6803. *J Biol Chem,* **2000,** *275* (13), 9091-9094.

292. Abel-Santos, E., Scott, C. P., Benkovic, S. J., Use of inteins for the in vivo production of stable cyclic peptide libraries in e. coli. *Methods Mol Biol,* **2003,** *205*, 281-294.

293. Naumann, T. A., Savinov, S. N., Benkovic, S. J., Engineering an affinity tag for genetically encoded cyclic peptides. *Biotechnol Bioeng,* **2005,** *92* (7), 820-830.

294. Merrifield, R. B., Solid phase peptide synthesis. I. The synthesis of a tetrapeptide. *J Am Chem Soc,* **1963,** *85* (14), 2149-2154.

295. Merrifield, B., Solid phase synthesis. *Science,* **1986,** *232* (4748), 341-347.

296. Yan, R., Rychlik, W., Etchison, D., Rhoads, R. E., Amino acid sequence of the human protein synthesis initiation factor eIF-4 gamma. *J Biol Chem,* **1992,** *267* (32), 23226-23231.

297. Bushell, M., Poncet, D., Marissen, W. E., Flotow, H., Lloyd, R. E., Clemens, M. J., Morley, S. J., Cleavage of polypeptide chain initiation factor eIF4GI during apoptosis in lymphoma cells: characterisation of an internal fragment generated by caspase-3-mediated cleavage. *Cell Death Differ,* **2000,** *7* (7), 628-636.

298. Hinton, T. M., Coldwell, M. J., Carpenter, G. A., Morley, S. J., Pain, V. M., Functional analysis of individual binding activities of the scaffold protein eIF4G. *J Biol Chem,* **2007,** *282* (3), 1695-1708.

299. Morino, S., Imataka, H., Svitkin, Y. V., Pestova, T. V., Sonenberg, N., Eukaryotic translation initiation factor 4E (eIF4E) binding site and the middle one-third of eIF4GI constitute the core domain for cap-dependent translation, and the C-terminal one-third functions as a modulatory region. *Mol Cell Biol,* **2000,** *20* (2), 468-477.

300. Byrd, M. P., Zamora, M., Lloyd, R. E., Generation of multiple isoforms of eukaryotic translation initiation factor 4GI by use of alternate translation initiation codons. *Mol Cell Biol,* **2002,** *22* (13), 4499-4511.

301. Safaee, N., Kozlov, G., Noronha, A. M., Xie, J., Wilds, C. J., Gehring, K., Interdomain allostery promotes assembly of the poly(A) mRNA complex with PABP and eIF4G. *Mol Cell,* **2012,** *48* (3), 375-386.

302. Korneeva, N. L., Lamphear, B. J., Hennigan, F. L., Merrick, W. C., Rhoads, R. E., Characterization of the two eIF4A-binding sites on human eIF4G-1. *J Biol Chem,* **2001,** *276* (4), 2872-2879.

303. Cuesta, R., Xi, Q., Schneider, R. J., Adenovirus-specific translation by displacement of kinase Mnk1 from cap-initiation complex eIF4F. *EMBO J,* **2000,** *19* (13), 3465-3474.

304. Morino, S., Hazama, H., Ozaki, M., Teraoka, Y., Shibata, S., Doi, M., Ueda, H., Ishida, T., Uesugi, S., Analysis of the mRNA cap-binding ability of human eukaryotic initiation factor-4E by use of recombinant wild-type and mutant forms. *Eur J Biochem,* **1996,** *239* (3), 597-601.

305. Papadopoulos, E., Jenni, S., Kabha, E., Takrouri, K. J., Yi, T., Salvi, N., Luna, R. E., Gavathiotis, E., Mahalingam, P., Arthanari, H., Rodriguez-Mias, R., Yefidoff-Freedman, R., Aktas, B. H., Chorev, M., Halperin, J. A., Wagner, G., Structure of the eukaryotic translation initiation factor eIF4E in complex with 4EGI-1 reveals an allosteric mechanism for dissociating eIF4G. *P Natl Acad Sci USA,* **2014,** *111* (31), E3187-3195.

306. Rychlik, W., Domier, L. L., Gardner, P. R., Hellmann, G. M., Rhoads, R. E., Amino acid sequence of the mRNA cap-binding protein from human tissues. *P Natl Acad Sci USA,* **1987,** *84* (4), 945-949.

307. Saiki, R. K., Gelfand, D. H., Stoffel, S., Scharf, S. J., Higuchi, R., Horn, G. T., Mullis, K. B., Erlich, H. A., Primer-directed enzymatic amplification of DNA with a thermostable DNA polymerase. *Science,* **1988,** *239* (4839), 487-491.

308. Higuchi, R., Krummel, B., Saiki, R. K., A general method of in vitro preparation and specific mutagenesis of DNA fragments: study of protein and DNA interactions. *Nucleic Acids Res,* **1988,** *16* (15), 7351-7367.

309. Miyashita, S., Shirako, Y., Chromosomal integration of a binding domain:bait gene into yeast enhances detection in the two-hybrid system. *J Microbiol Methods,* **2008,** *73* (2), 179-184.

310. Biswas, T., Aihara, H., Radman-Livaja, M., Filman, D., Landy, A., Ellenberger, T., A structural basis for allosteric control of DNA recombination by lambda integrase. *Nature,* **2005,** *435* (7045), 1059-1066.

311. Stalker, D. M., Kolter, R., Helinski, D. R., Plasmid R6K DNA replication. I. Complete nucleotide sequence of an autonomously replicating segment. *J Mol Biol,* **1982,** *161* (1), 33-43.

312. Greener, A., Filutowicz, M. S., McEachern, M. J., Helinski, D. R., N-terminal truncated forms of the bifunctional pi initiation protein express negative activity on plasmid R6K replication. *Mol Gen Genet,* **1990,** *224* (1), 24-32.

313. Yagil, E., Dolev, S., Oberto, J., Kislev, N., Ramaiah, N., Weisberg, R. A., Determinants of site-specific recombination in the lambdoid coliphage HK022. An evolutionary change in specificity. *J Mol Biol,* **1989,** *207* (4), 695-717.

314. Nagaraja, R., Weisberg, R. A., Specificity determinants in the attachment sites of bacteriophages HK022 and lambda. *J Bacteriol,* **1990,** *172* (11), 6540-6550.

315. Holliday, R., A mechanism for gene conversion in fungi. *Genet Res,* **2007,** *89* (5), 285-307.

316. Walz, A., Pirrotta, V., Sequence of the PR promoter of phage lambda. *Nature,* **1975,** *254* (5496), 118-121.

317. Villaverde, A., Benito, A., Viaplana, E., Cubarsi, R., Fine regulation of cI857-controlled gene expression in continuous culture of recombinant Escherichia coli by temperature. *Appl Environ Microbiol,* **1993,** *59* (10), 3485-3487.

318. Phillips, G. J., New cloning vectors with temperature-sensitive replication. *Plasmid,* **1999,** *41* (1), 78-81.

319. Hasunuma, K., Sekiguchi, M., Replication of plasmid pSC101 in Escherichia coli K12: requirement for dnaA function. *Mol Gen Genet,* **1977,** *154* (3), 225-230.

320. Manen, D., Caro, L., The replication of plasmid pSC101. *Mol Microbiol,* **1991,** *5* (2), 233-237.

321. Tavassoli, A., Benkovic, S. J., Genetically selected cyclic-peptide inhibitors of AICAR transformylase homodimerization. *Angew Chem Int Edit,* **2005,** *44* (18), 2760-2763.

322. Miller, J., Experiments in molecular genetics. *Cold Spring Harbor Laboratory, Cold Spring Harbor, NY,* **1972**, 73-75.

323. Miranda, E., Forafonov, F., Tavassoli, A., Deciphering interactions used by the influenza virus NS1 protein to silence the host antiviral sensor protein RIG-I using a bacterial reverse two-hybrid system. *Mol Biosyst,* **2011,** *7* (4), 1042-1045.

324. Tavassoli, A., Lu, Q., Gam, J., Pan, H., Benkovic, S. J., Cohen, S. N., Inhibition of HIV budding by a genetically selected cyclic peptide targeting the Gag-TSG101 interaction. *ACS Chem Biol,* **2008,** *3* (12), 757-764.

325. Essers, L., Kunze, R., A sensitive, quick and semi-quantitative LacZ assay for the two-hybrid system. *Trends Genet,* **1996,** *12* (11), 449-450.

326. Chang, A. C., Cohen, S. N., Construction and characterization of amplifiable multicopy DNA cloning vehicles derived from the P15A cryptic miniplasmid. *J Bacteriol,* **1978,** *134* (3), 1141-1156.

327. Selzer, G., Som, T., Itoh, T., Tomizawa, J., The origin of replication of plasmid p15A and comparative studies on the nucleotide sequences around the origin of related plasmids. *Cell,* **1983,** *32* (1), 119-129.

328. Tavassoli, A., Benkovic, S. J., Split-intein mediated circular ligation used in the synthesis of cyclic peptide libraries in E. coli. *Nat Protoc,* **2007,** *2* (5), 1126-1133.

329. Cagnon, C., Valverde, V., Masson, J. M., A new family of sugar-inducible expression vectors for Escherichia coli. *Protein Eng,* **1991,** *4* (7), 843-847.

330. Schleif, R., AraC protein, regulation of the l-arabinose operon in Escherichia coli, and the light switch mechanism of AraC action. *FEMS Microbiol Rev,* **2010,** *34* (5), 779-796.

331. Frankel, A. D., Pabo, C. O., Cellular uptake of the tat protein from human immunodeficiency virus. *Cell,* **1988,** *55* (6), 1189-1193.

332. Green, M., Loewenstein, P. M., Autonomous functional domains of chemically synthesized human immunodeficiency virus tat trans-activator protein. *Cell,* **1988,** *55* (6), 1179-1188.

333. Mitchell, D. J., Kim, D. T., Steinman, L., Fathman, C. G., Rothbard, J. B., Polyarginine enters cells more efficiently than other polycationic homopolymers. *J Pept Res,* **2000,** *56* (5), 318-325.

334. Derossi, D., Joliot, A. H., Chassaing, G., Prochiantz, A., The third helix of the Antennapedia homeodomain translocates through biological membranes. *J Biol Chem,* **1994,** *269* (14), 10444-10450.

335. Dom, G., Shaw-Jackson, C., Matis, C., Bouffioux, O., Picard, J. J., Prochiantz, A., Mingeot-Leclercq, M. P., Brasseur, R., Rezsohazy, R., Cellular uptake of

Antennapedia Penetratin peptides is a two-step process in which phase transfer precedes a tryptophan-dependent translocation. *Nucleic Acids Res,* **2003,** *31* (2), 556-561.

336. Lattig-Tunnemann, G., Prinz, M., Hoffmann, D., Behlke, J., Palm-Apergi, C., Morano, I., Herce, H. D., Cardoso, M. C., Backbone rigidity and static presentation of guanidinium groups increases cellular uptake of arginine-rich cell-penetrating peptides. *Nat Commun,* **2011,** *2*, 453.

337. Qian, Z., Liu, T., Liu, Y. Y., Briesewitz, R., Barrios, A. M., Jhiang, S. M., Pei, D., Efficient delivery of cyclic peptides into mammalian cells with short sequence motifs. *ACS Chem Biol,* **2013,** *8* (2), 423-431.

338. Wender, P. A., Mitchell, D. J., Pattabiraman, K., Pelkey, E. T., Steinman, L., Rothbard, J. B., The design, synthesis, and evaluation of molecules that enable or enhance cellular uptake: peptoid molecular transporters. *P Natl Acad Sci USA,* **2000,** *97* (24), 13003-13008.

339. Fillon, Y. A., Anderson, J. P., Chmielewski, J., Cell penetrating agents based on a polyproline helix scaffold. *J Am Chem Soc,* **2005,** *127* (33), 11798-11803.

340. Mandal, D., Nasrolahi Shirazi, A., Parang, K., Cell-penetrating homochiral cyclic peptides as nuclear-targeting molecular transporters. *Angew Chem Int Edit,* **2011,** *50* (41), 9633-9637.

341. Hu, X., Nguyen, K. T., Jiang, V. C., Lofland, D., Moser, H. E., Pei, D., Macrocyclic inhibitors for peptide deformylase: a structure-activity relationship study of the ring size. *J Med Chem,* **2004,** *47* (20), 4941-4949.

342. Iwai, H., Zuger, S., Jin, J., Tam, P. H., Highly efficient protein trans-splicing by a naturally split DnaE intein from Nostoc punctiforme. *FEBS Lett,* **2006,** *580* (7), 1853-1858.

343. Lockless, S. W., Muir, T. W., Traceless protein splicing utilizing evolved split inteins. *P Natl Acad Sci USA,* **2009,** *106* (27), 10999-11004.

344. Cheriyan, M., Pedamallu, C. S., Tori, K., Perler, F., Faster protein splicing with the Nostoc punctiforme DnaE intein using non-native extein residues. *J Biol Chem,* **2013,** *288* (9), 6202-6211.

345. Carpino, L. A., Han, G. Y., 9-Fluorenylmethoxycarbonyl function, a new base-sensitive amino-protecting group. *J Am Chem Soc,* **1970,** *92* (19), 5748-5749.

346. Carpino, L. A., Han, G. Y., 9-Fluorenylmethoxycarbonyl Amino-Protecting Group. *J Org Chem,* **1972,** *37* (22), 3404-3409.

347. Atherton, E., Fox, H., Harkiss, D., Logan, C. J., Sheppard, R. C., Williams, B. J., A mild procedure for solid phase peptide synthesis: use of fluorenylmethoxycarbonylamino-acids. *J Chem Soc Chem Comm,* **1978,** (13), 537-539.

348. Chang, C. D., Meienhofer, J., Solid-phase peptide synthesis using mild base cleavage of N alpha-fluorenylmethyloxycarbonylamino acids, exemplified by a synthesis of dihydrosomatostatin. *Int J Pept Protein Res,* **1978,** *11* (3), 246-249.

349. Wang, S. S., p-alkoxybenzyl alcohol resin and p-alkoxybenzyloxycarbonylhydrazide resin for solid phase synthesis of protected peptide fragments. *J Am Chem Soc,* **1973,** *95* (4), 1328-1333.

350. Sieber, P., Rimker, B., Protection of carboxamide functions by the trityl residue. Application to peptide synthesis. *Tetrahedron Lett,* **1991,** *32* (6), 739-742.

351. Hess, G. P., Sheehan, J. C., A New Method of Forming Peptide Bonds. *J Am Chem Soc,* **1955,** *77* (4), 1067-1068.

352. Konig, W., Geiger, R., [A new method for synthesis of peptides: activation of the carboxyl group with dicyclohexylcarbodiimide using 1-hydroxybenzotriazoles as additives]. *Chem Ber,* **1970,** *103* (3), 788-798.

353. Carpino, L. A., El-Faham, A., The diisopropylcarbodiimide/ 1-hydroxy-7-azabenzotriazole system: Segment coupling and stepwise peptide assembly. *Tetrahedron,* **1999,** *55* (22), 6813-6830.

354. Kaiser, E., Colescott, R. L., Bossinger, C. D., Cook, P. I., Color test for detection of free terminal amino groups in the solid-phase synthesis of peptides. *Anal Biochem,* **1970,** *34* (2), 595-598.

355. Snyder, S. L., Sobocinski, P. Z., An improved 2,4,6-trinitrobenzenesulfonic acid method for the determination of amines. *Anal Biochem,* **1975,** *64* (1), 284-288.

356. Sarin, V. K., Kent, S. B., Tam, J. P., Merrifield, R. B., Quantitative monitoring of solid-phase peptide synthesis by the ninhydrin reaction. *Anal Biochem,* **1981,** *117* (1), 147-157.

357. Weber, U., Hartter, P., [S-Alkylmercapto groups for protection of the SH-function of cysteine. I. Synthesis and stability of some S-(Alkylmercapto) cysteines]. *Hoppe Seylers Z Physiol Chem,* **1970,** *351* (11), 1384-1388.

358. Eritja, R., Ziehler-Martin, J. P., Walker, P. A., Lee, T. D., Legesse, K., Albericio, F., Kaplan, B. E., On the use of S-t-butylsulphenyl group for protection of cysteine in solid-phase peptide synthesis using Fmoc-amino acids. *Tetrahedron Lett,* **1987,** *43* (12), 2675-2680.

359. Sieber, P., Riniker, B., Protection of Histidine in peptide synthesis: A Reassessment of the trityl group. *Tetrahedron Lett,* **1987,** *28* (48), 6031-6034.

360. Carpino, L. A., Shroff, H., Salvatore, A. T., Mansour, E. S. M. E., Wenschuh, H., Albericio, F., The 2,2,4,6,7-pentamethyldihydrobenzofurazan-5-sulfonyl group (Pbf) as arginine side chain protectant. *Tetrahedron Lett,* **1993,** *34* (49), 7829-7832.

361. Sole, N. A., Barany, G., Optimization of solid-phase synthesis of [Ala8]-dynorphin A. *J Org Chem,* **1992,** *57* (20), 5399-5403.

362. Pearson, D. A., Blanchette, M., Baker, M. L., Guindon, C. A., Trialkylsilanes as scavengers for the trifluoroacetic acid deblocking of protecting groups in peptide synthesis. *Tett Lett,* **1989,** *30* (21), 2739-2742.

363. Mehta, A., Jaouhari, R., Benson, T. J., Douglas, K. T., Improved efficiency and selectivity in peptide synthesis: Use of triethylsilane as a carbocation scavenger in deprotection of t-butyl esters and t-butoxycarbonyl-protected sites. *Tett Lett,* **1992,** *33* (37), 5441-5444.

364. King, D. S., Fields, C. G., Fields, G. B., A cleavage method which minimizes side reactions following Fmoc solid phase peptide synthesis. *Int J Pept Protein Res,* **1990,** *36* (3), 255-266.

365. McCurdy, S. N., The investigation of Fmoc-cysteine derivatives in solid phase peptide synthesis. *Pept Res,* **1989,** *2* (1), 147-152.

366. Lundt, B. F., Johansen, N. L., Volund, A., Markussen, J., Removal of t-butyl and t-butoxycarbonyl protecting groups with trifluoroacetic acid. Mechanisms, biproduct formation and evaluation of scavengers. *Int J Pept Protein Res,* **1978,** *12* (5), 258-268.

367. Albericio, F., van Abel, R., Barany, G., Solid-phase synthesis of peptides with C-terminal asparagine or glutamine. An effective, mild procedure based on N alpha-fluorenylmethyloxycarbonyl (Fmoc) protection and side-chain anchoring to a tris(alkoxy)benzylamide (PAL) handle. *Int J Pept Protein Res,* **1990,** *35* (3), 284-286.

368. Chan, W. C., Bycroft, B. W., Evans, D. J., White, P. D., A novel 4-aminobenzyl ester-based carboxy-protecting group for synthesis of atypical peptides by Fmoc-But solid-phase chemistry. *J Chem Soc Chem Comm,* **1995,** (21), 2209.

369. Cudic, M., Wade, J. D., Otvos, L., Convenient synthesis of a head-to-tail cyclic peptide containing an expanded ring. *Tetrahedron Lett,* **2000,** *41* (23), 4527-4531.

370. Conroy, T., Jolliffe, K. A., Payne, R. J., Efficient use of the Dmab protecting group: applications for the solid-phase synthesis of N-linked glycopeptides. *Org Biomol Chem,* **2009,** *7* (11), 2255-2258.

371. Rink, H., Solid-phase synthesis of protected peptide fragments using a trialkoxy-diphenyl-methylester resin. *Tetrahedron Lett,* **1987,** *28* (33), 3787-3790.

372. Frutos, S., Tulla-Puche, J., Albericio, F., Giralt, E., Chemical Synthesis of 19F-labeled HIV-1 Protease using Fmoc-Chemistry and ChemMatrix Resin. *Int J Pept Res Ther,* **2007,** *13* (1), 221-227.

373. Sheehan, J. C., Cruickshank, P., Boshart, G., Notes- A Convenient Synthesis of Water-Soluble Carbodiimides. *J Org Chem,* **1961,** *26* (7), 2525-2528.

374. Sheehan, J. C., Preston, J., Cruickshank, P. A., A Rapid Synthesis of Oligopeptide Derivatives without Isolation of Intermediates. *J Am Chem Soc,* **1965,** *87* (11), 2492-2493.

375. Carpino, L. A., 1-Hydroxy-7-azabenzotriazole. An efficient peptide coupling additive. *J Am Chem Soc,* **1993,** *115* (10), 4397-4398.

376. Mosmann, T., Rapid colorimetric assay for cellular growth and survival: application to proliferation and cytotoxicity assays. *J Immunol Methods,* **1983,** *65* (1), 55-63.

377. Joseph, P., O'Kernick, C. M., Othumpangat, S., Lei, Y. X., Yuan, B. Z., Ong, T. M., Expression profile of eukaryotic translation factors in human cancer tissues and cell lines. *Mol Carcinog,* **2004,** *40* (3), 171-179.

378. Denizot, F., Lang, R., Rapid colorimetric assay for cell growth and survival. Modifications to the tetrazolium dye procedure giving improved sensitivity and reliability. *J Immunol Methods,* **1986,** *89* (2), 271-277.

379. Carmichael, J., DeGraff, W. G., Gazdar, A. F., Minna, J. D., Mitchell, J. B., Evaluation of a tetrazolium-based semiautomated colorimetric assay: assessment of chemosensitivity testing. *Cancer Res,* **1987,** *47* (4), 936-942.

380. Sieuwerts, A. M., Klijn, J. G., Peters, H. A., Foekens, J. A., The MTT tetrazolium salt assay scrutinized: how to use this assay reliably to measure metabolic activity of cell cultures in vitro for the assessment of growth characteristics, IC50-values and cell survival. *Eur J Clin Chem Clin Biochem,* **1995,** *33* (11), 813-823.

381. Ohlmann, T., Rau, M., Pain, V. M., Morley, S. J., The C-terminal domain of eukaryotic protein synthesis initiation factor (eIF) 4G is sufficient to support cap-independent translation in the absence of eIF4E. *EMBO J,* **1996,** *15* (6), 1371-1382.

382. Wood, K. V., de Wet, J. R., Dewji, N., DeLuca, M., Synthesis of active firefly luciferase by in vitro translation of RNA obtained from adult lanterns. *Biochem Biophys Res Commun,* **1984,** *124* (2), 592-596.

383. Koo, J. A., Schmidt, S. P., Schuster, G. B., Bioluminescence of the firefly: key steps in the formation of the electronically excited state for model systems. *P Natl Acad Sci USA,* **1978,** *75* (1), 30-33.

384. Shimomura, O., Goto, T., Johnson, F. H., Source of oxygen in the CO(2) produced in the bioluminescent oxidation of firefly luciferin. *P Natl Acad Sci USA,* **1977,** *74* (7), 2799-2802.

385. Wannlund, J., DeLuca, M., Stempel, K., Boyer, P. D., Use of 14C-carboxyl-luciferin in determining the mechanism of the firefly luciferase catalyzed reactions. *Biochem Biophys Res Commun,* **1978,** *81* (3), 987-992.

386. Plant, P. J., White, E. H., McElroy, W. D., The decarboxylation of luciferin in firefly bioluminescence. *Biochem Biophys Res Commun,* **1968,** *31* (1), 98-103.

387. Hopkins, T. A., Seliger, H. H., White, E. H., Cass, M. H., The chemiluminescence of firefly luciferin. A model for the bioluminescent reaction and identification of the product excited state. *J Am Chem Soc,* **1967,** *89* (26), 7148-7150.

388. Stone, H., The enzyme catalyzed oxidation of Cypridina luciferin. *Biochem Biophys Res Commun,* **1968,** *31* (3), 386-391.

389. Hori, K., Wampler, J. E., Matthews, J. C., Cormier, M. J., Identification of the product excited states during the chemiluminescent and bioluminescent oxidation of Renilla (sea pansy) luciferin and certain of its analogs. *Biochemistry,* **1973,** *12* (22), 4463-4468.

390. Matthews, J. C., Hori, K., Cormier, M. J., Purification and properties of Renilla reniformis luciferase. *Biochemistry,* **1977,** *16* (1), 85-91.

391. Lorenz, W. W., McCann, R. O., Longiaru, M., Cormier, M. J., Isolation and expression of a cDNA encoding Renilla reniformis luciferase. *P Natl Acad Sci USA,* **1991,** *88* (10), 4438-4442.

392. Hart, R. C., Stempel, K. E., Boyer, P. D., Cormier, M. J., Mechanism of the enzyme-catalyzed bioluminescent oxidation of coelenterate-type luciferin. *Biochem Biophys Res Commun,* **1978,** *81* (3), 980-986.

393. Seliger, H. H., Mc, E. W., Spectral emission and quantum yield of firefly bioluminescence. *Arch Biochem Biophys,* **1960,** *88* (1), 136-141.

394. Stewart, J. D., Cowan, J. L., Perry, L. S., Coldwell, M. J., Proud, C. G., ABC50 mutants modify translation start codon selection. *Biochem J,* **2015,** *467* (2), 217-229.

395. Rogers, S., Wells, R., Rechsteiner, M., Amino acid sequences common to rapidly degraded proteins: the PEST hypothesis. *Science,* **1986,** *234* (4774), 364-368.

396. Byrne, B. J., Davis, M. S., Yamaguchi, J., Bergsma, D. J., Subramanian, K. N., Definition of the simian virus 40 early promoter region and demonstration of a host range bias in the enhancement effect of the simian virus 40 72-base-pair repeat. *P Natl Acad Sci USA,* **1983,** *80* (3), 721-725.

397. McKnight, S. L., The nucleotide sequence and transcript map of the herpes simplex virus thymidine kinase gene. *Nucleic Acids Res,* **1980,** *8* (24), 5949-5964.

398. McKnight, S. L., Gavis, E. R., Expression of the herpes thymidine kinase gene in Xenopus laevis oocytes: an assay for the study of deletion mutants constructed in vitro. *Nucleic Acids Res,* **1980,** *8* (24), 5931-5948.

399. McKnight, S. L., Gavis, E. R., Kingsbury, R., Axel, R., Analysis of transcriptional regulatory signals of the HSV thymidine kinase gene: identification of an upstream control region. *Cell,* **1981,** *25* (2), 385-398.

400. Wagner, M. J., Sharp, J. A., Summers, W. C., Nucleotide sequence of the thymidine kinase gene of herpes simplex virus type 1. *P Natl Acad Sci USA,* **1981,** *78* (3), 1441-1445.

401. Zipser, D., Lipsich, L., Kwoh, J., Mapping functional domains in the promoter region of the herpes thymidine kinase gene. *P Natl Acad Sci USA,* **1981,** *78* (10), 6276-6280.

402. Kozak, M., At least six nucleotides preceding the AUG initiator codon enhance translation in mammalian cells. *J Mol Biol,* **1987,** *196* (4), 947-950.

403. Coldwell, M. J., Mitchell, S. A., Stoneley, M., MacFarlane, M., Willis, A. E., Initiation of Apaf-1 translation by internal ribosome entry. *Oncogene,* **2000,** *19* (7), 899-905.

404. Stoneley, M., Subkhankulova, T., Le Quesne, J. P., Coldwell, M. J., Jopling, C. L., Belsham, G. J., Willis, A. E., Analysis of the c-myc IRES; a potential role for cell-type specific trans-acting factors and the nuclear compartment. *Nucleic Acids Res,* **2000,** *28* (3), 687-694.

405. Mitchell, S. A., Brown, E. C., Coldwell, M. J., Jackson, R. J., Willis, A. E., Protein factor requirements of the Apaf-1 internal ribosome entry segment: roles of

polypyrimidine tract binding protein and upstream of N-ras. *Mol Cell Biol,* **2001,** *21* (10), 3364-3374.

406. Mitchell, S. A., Spriggs, K. A., Coldwell, M. J., Jackson, R. J., Willis, A. E., The Apaf-1 internal ribosome entry segment attains the correct structural conformation for function via interactions with PTB and unr. *Mol Cell,* **2003,** *11* (3), 757-771.

407. Nanbru, C., Lafon, I., Audigier, S., Gensac, M. C., Vagner, S., Huez, G., Prats, A. C., Alternative translation of the proto-oncogene c-myc by an internal ribosome entry site. *J Biol Chem,* **1997,** *272* (51), 32061-32066.

408. Stoneley, M., Paulin, F. E., Le Quesne, J. P., Chappell, S. A., Willis, A. E., C-Myc 5' untranslated region contains an internal ribosome entry segment. *Oncogene,* **1998,** *16* (3), 423-428.

409. Jang, S. K., Krausslich, H. G., Nicklin, M. J., Duke, G. M., Palmenberg, A. C., Wimmer, E., A segment of the 5' nontranslated region of encephalomyocarditis virus RNA directs internal entry of ribosomes during in vitro translation. *J Virol,* **1988,** *62* (8), 2636-2643.

410. Palmenberg, A. C., Kirby, E. M., Janda, M. R., Drake, N. L., Duke, G. M., Potratz, K. F., Collett, M. S., The nucleotide and deduced amino acid sequences of the encephalomyocarditis viral polyprotein coding region. *Nucleic Acids Res,* **1984,** *12* (6), 2969-2985.

411. Pilipenko, E. V., Blinov, V. M., Chernov, B. K., Dmitrieva, T. M., Agol, V. I., Conservation of the secondary structure elements of the 5'-untranslated region of cardio- and aphthovirus RNAs. *Nucleic Acids Res,* **1989,** *17* (14), 5701-5711.

412. Duke, G. M., Hoffman, M. A., Palmenberg, A. C., Sequence and structural elements that contribute to efficient encephalomyocarditis virus RNA translation. *J Virol,* **1992,** *66* (3), 1602-1609.

413. Skern, T., Sommergruber, W., Blaas, D., Gruendler, P., Fraundorfer, F., Pieler, C., Fogy, I., Kuechler, E., Human rhinovirus 2: complete nucleotide sequence and proteolytic processing signals in the capsid protein region. *Nucleic Acids Res,* **1985,** *13* (6), 2111-2126.

414. Borman, A., Jackson, R. J., Initiation of translation of human rhinovirus RNA: mapping the internal ribosome entry site. *Virology,* **1992,** *188* (2), 685-696.

415. Marissen, W. E., Lloyd, R. E., Eukaryotic translation initiation factor 4G is targeted for proteolytic cleavage by caspase 3 during inhibition of translation in apoptotic cells. *Mol Cell Biol,* **1998,** *18* (12), 7565-7574.

416. Spriggs, K. A., Cobbold, L. C., Jopling, C. L., Cooper, R. E., Wilson, L. A., Stoneley, M., Coldwell, M. J., Poncet, D., Shen, Y. C., Morley, S. J., Bushell, M., Willis, A. E., Canonical initiation factor requirements of the Myc family of internal ribosome entry segments. *Mol Cell Biol,* **2009,** *29* (6), 1565-1574.

417. Borman, A., Howell, M. T., Patton, J. G., Jackson, R. J., The involvement of a spliceosome component in internal initiation of human rhinovirus RNA translation. *J Gen Virol,* **1993,** *74* (9), 1775-1788.

418. Jefferies, H. B., Reinhard, C., Kozma, S. C., Thomas, G., Rapamycin selectively represses translation of the "polypyrimidine tract" mRNA family. *P Natl Acad Sci USA,* **1994,** *91* (10), 4441-4445.

419. Beretta, L., Gingras, A. C., Svitkin, Y. V., Hall, M. N., Sonenberg, N., Rapamycin blocks the phosphorylation of 4E-BP1 and inhibits cap-dependent initiation of translation. *EMBO J,* **1996,** *15* (3), 658-664.

420. Choo, A. Y., Yoon, S. O., Kim, S. G., Roux, P. P., Blenis, J., Rapamycin differentially inhibits S6Ks and 4E-BP1 to mediate cell-type-specific repression of mRNA translation. *P Natl Acad Sci USA,* **2008,** *105* (45), 17414-17419.

421. Apsel, B., Blair, J. A., Gonzalez, B., Nazif, T. M., Feldman, M. E., Aizenstein, B., Hoffman, R., Williams, R. L., Shokat, K. M., Knight, Z. A., Targeted polypharmacology: discovery of dual inhibitors of tyrosine and phosphoinositide kinases. *Nat Chem Biol,* **2008,** *4* (11), 691-699.

422. Feldman, M. E., Apsel, B., Uotila, A., Loewith, R., Knight, Z. A., Ruggero, D., Shokat, K. M., Active-site inhibitors of mTOR target rapamycin-resistant outputs of mTORC1 and mTORC2. *PLOS Biol,* **2009,** *7* (2), e38.

423. Moerke, N. J., Aktas, H., Chen, H., Cantel, S., Reibarkh, M. Y., Fahmy, A., Gross, J. D., Degterev, A., Yuan, J., Chorev, M., Halperin, J. A., Wagner, G., Small-molecule inhibition of the interaction between the translation initiation factors eIF4E and eIF4G. *Cell,* **2007,** *128* (2), 257-267.

424. Baliga, B. S., Pronczuk, A. W., Munro, H. N., Mechanism of cycloheximide inhibition of protein synthesis in a cell-free system prepared from rat liver. *J Biol Chem,* **1969,** *244* (16), 4480-4489.

425. Obrig, T. G., Culp, W. J., McKeehan, W. L., Hardesty, B., The mechanism by which cycloheximide and related glutarimide antibiotics inhibit peptide synthesis on reticulocyte ribosomes. *J Biol Chem,* **1971,** *246* (1), 174-181.

426. Schneider-Poetsch, T., Ju, J., Eyler, D. E., Dang, Y., Bhat, S., Merrick, W. C., Green, R., Shen, B., Liu, J. O., Inhibition of eukaryotic translation elongation by cycloheximide and lactimidomycin. *Nat Chem Biol,* **2010,** *6* (3), 209-217.

427. Wong, W. L., Brostrom, M. A., Kuznetsov, G., Gmitter-Yellen, D., Brostrom, C. O., Inhibition of protein synthesis and early protein processing by thapsigargin in cultured cells. *Biochem J,* **1993,** *289* (1), 71-79.

428. Thastrup, O., Cullen, P. J., Drobak, B. K., Hanley, M. R., Dawson, A. P., Thapsigargin, a tumor promoter, discharges intracellular Ca2+ stores by specific inhibition of the endoplasmic reticulum Ca2(+)-ATPase. *P Natl Acad Sci USA,* **1990,** *87* (7), 2466-2470.

429. Aktas, H., Fluckiger, R., Acosta, J. A., Savage, J. M., Palakurthi, S. S., Halperin, J. A., Depletion of intracellular Ca2+ stores, phosphorylation of eIF2alpha, and sustained inhibition of translation initiation mediate the anticancer effects of clotrimazole. *P Natl Acad Sci USA,* **1998,** *95* (14), 8280-8285.

430. Stead, R. L., Proud, C. G., Rapamycin enhances eIF4E phosphorylation by activating MAP kinase-interacting kinase 2a (Mnk2a). *FEBS Lett,* **2013,** *587* (16), 2623-2628.

431. Wang, X., Yue, P., Chan, C. B., Ye, K., Ueda, T., Watanabe-Fukunaga, R., Fukunaga, R., Fu, H., Khuri, F. R., Sun, S. Y., Inhibition of mammalian target of rapamycin induces phosphatidylinositol 3-kinase-dependent and Mnk-mediated eukaryotic translation initiation factor 4E phosphorylation. *Mol Cell Biol,* **2007,** *27* (21), 7405-7413.

432. Morenkova, S. A., Incorporation of S35-methionine into insulin. *Nature,* **1966,** *209* (5026), 917.

433. Pollard, J. W., The in vivo isotopic labeling of proteins for polyacrylamide gel electrophoresis. *Methods Mol Biol,* **1994,** *32*, 67-72.

434. Esposito, A. M., Kinzy, T. G., In vivo [35S]-methionine incorporation. *Methods Enzymol,* **2014,** *536*, 55-64.

435. Yefidoff-Freedman, R., Chen, T., Sahoo, R., Chen, L., Wagner, G., Halperin, J. A., Aktas, B. H., Chorev, M., 3-substituted indazoles as configurationally locked 4EGI-1 mimetics and inhibitors of the eIF4E/eIF4G interaction. *Chembiochem,* **2014,** *15* (4), 595-611.

436. Kaiser, C., Dobrikova, E. Y., Bradrick, S. S., Shveygert, M., Herbert, J. T., Gromeier, M., Activation of cap-independent translation by variant eukaryotic initiation factor 4G in vivo. *RNA,* **2008,** *14* (10), 2170-2182.

437. Szczepaniak, S. A., Jemielity, J., Zuberek, J., Kufel, J., Darzynkiewicz, E., Bisphosphonate mRNA cap analog attached to Sepharose for affinity chromatography of decapping enzymes. *Nucl Acid S,* **2008,** (52), 295-296.

438. Sonenberg, N., Rupprecht, K. M., Hecht, S. M., Shatkin, A. J., Eukaryotic mRNA cap binding protein: purification by affinity chromatography on sepharose-coupled m7GDP. *P Natl Acad Sci USA,* **1979,** *76* (9), 4345-4349.

439. Bradford, M. M., A rapid and sensitive method for the quantitation of microgram quantities of protein utilizing the principle of protein-dye binding. *Anal Biochem,* **1976,** *72* (1), 248-254.

440. Mullis, K. B., The unusual origin of the polymerase chain reaction. *Sci Am,* **1990,** *262* (4), 56-61, 64-55.

441. Meselson, M., Yuan, R., DNA restriction enzyme from E. coli. *Nature,* **1968,** *217* (5134), 1110-1114.

442. Aaij, C., Borst, P., The gel electrophoresis of DNA. *Biochim Biophys Acta,* **1972,** *269* (2), 192-200.

443. Sgaramella, V., Ehrlich, S. D., Use of the T4 polynucleotide ligase in the joining of flush-ended DNA segments generated by restriction endonucleases. *Eur J Biochem,* **1978,** *86* (2), 531-537.

444. Bergmans, H. E., van Die, I. M., Hoekstra, W. P., Transformation in Escherichia coli: stages in the process. *J Bacteriol,* **1981,** *146* (2), 564-570.

445. Weber, K., Osborn, M., The reliability of molecular weight determinations by dodecyl sulfate-polyacrylamide gel electrophoresis. *J Biol Chem,* **1969,** *244* (16), 4406-4412.

446. Towbin, H., Staehelin, T., Gordon, J., Electrophoretic Transfer of Proteins from Polyacrylamide Gels to Nitrocellulose Sheets - Procedure and Some Applications. *P Natl Acad Sci USA,* **1979,** *76* (9), 4350-4354.